PREDICTION OF INTERRUPTED CUTTING FORCE SYSTEM USING SOLID MODELING APPROACH

BY

OSCAR EDUARDO RUIZ

Ing. Mec., Universidad de los Andes, 1983
D.Ing., Universidad de los Andes, 1987

THESIS

Submitted in partial fulfillment of the requirements
for the degree of Master of Science in Mechanical Engineering
in the Graduate College of the
University of Illinois at Urbana-Champaign, 1991

Urbana, Illinois

ACKNOWLEDGEMENTS

First, I would first like to thank my advisors, Professors S. G. Kapoor, and R. E. DeVor for their professional advice, guidance, and suggestions throughout the stages of this thesis. I am grateful to them for their understanding, moral support, and encouragement that helped me overcome difficult problems. I also want to thank Professors P. Ferreira, T.C. Tsao, and A. Vakakis who provided me with many invaluable ideas at different levels of this research. Also, I would like to thank General Motors Research Labs. for the funding for this research, but also for the understanding, kindness and help they had for me.

I want to thank thank my friends Kin, Dena, Ricardo, Marisol, Maria Eugenia, Choonkyong, Carlos because they have been good to me. They are my family here.

I want to thank my family, for their support and understanding throughout my graduate years. Their example is invaluable and consitutes a constant source of strength in the most difficult times. Thanks to Papi, Mami and my brothers and sisters who made possible for me to be here.

I want to thank my fellow graduate students for their invaluable help throughout this research. Thanks to them, there was always someone there to answer my questions and help me in my work. Thanks Vijitha, Robert,Vivek, Gu, Giorgio and Mani.

TABLE OF CONTENTS

CHAPTER 1

INTRODUCTION

In manufacturing processes involving material removal one of the key considerations is the preservation of an ideally constant state of contact between the cutting edge and the work piece being machined. Cutting tools such as used in turning, milling, reaming, boring, etc. only succeed when tight geometry, material and thermal considerations are satisfied. Sudden tool failure during cutting is undesirable for several reasons. In the best case failure will produce loss of time and money when the process is interrupted to replace the tool, clean the workpiece, modify the NC program, etc. In the worst case the work could be damaged beyond recovery and/or the machine tool could be affected. Therefore, tool failure is considered as an undesirable phenomenon in metal cutting operations. Although extensive research has been done in this field, a global understanding of it is still far away, and therefore topics related to tool failure continues to be an open field for research.

Although tool failure is related to tool wear, they could be treated as two different phenomena; tool wear refers to the alteration of the tool geometry by gradual loss of its material, as result of the forces, temperature gradients, etc. This allows for a smooth degradation in the quality of the work, increment in the cutting forces, etc, in such a way that tool replacement becomes a decision dictated by quality control standards, and in some cases tool replacement can be delayed until the current work piece is terminated. In contrast, a tool failure represents a sharp change in the geometry of the tool, as result of a sudden loss of material. In these conditions, a tool change is imperative most of the times because, (even in using several cutting teeth as in milling , where the job can be taken by the unfailed teeth) the condition of the failing tooth is unpredictable. It may lead to the damage of the workpiece, the tool, or the machine tool when the chip breaking away from a tool is rubbed against the work piece and the finish is damaged irrespective of the ability of

the other teeth to complete the work in a reasonable way. Tool wear and tool failure are related, in the sense that tool wear alters several variables of the cutting process such as cutting and friction forces and temperature gradients. It also lowers the strength of the tool to resist those changes by introducing failure planes in the material of the tool which ultimately will lead to its chipping off.

Bimetallic cuts have shown to be very harmful to tool life. Reference [18] have reported that by making the tool interact sequentially with two different materials, the number of cycles for the tool to break is less than in the case of only one material, due to the fact that high temperatures and stress regimes, chemical reactions take place in the tool material, thus changing its properties. Also, states of extensive wear open the microstructure of the tool to chemical reactions which depend on the temperature and the chemical affinity of the materials involved.

In studying tool wear and tool failure an obvious concern is the characterization of the cutting forces and their effect on the integrity of the insert. In order to characterize metal cutting processes several lines of research have been pursued in the last forty or fifty years. Chip formation mechanisms have received particular attention since they represent the basis for the characterization of cutting and friction forces, deformation energies, tool and work temperatures, etc [27-31] . This has clear positive effects for the manufacturing industry because it allows for the forecast or simulation of the performance of industrial process variables under real environment conditions. This approach permits researchers to evaluate the feasibility of manufacturing processes, the range of values that process variables (power consumption, forces, currents, voltages, etc) could reach and allows for evaluation of manufacturing alternatives in an economically viable way. This could be achieved without the construction of expensive prototypes in order to simulate the real process. Of course, the efficiency of this approach is measured by how close are the predicted variables to the actual values. A wrong or misleading prediction should be avoided by clearly

establishing the assumptions and limits that supports each model. With the rapid improvement of computers capabilities and the increased sophistication in the needs of industry, more accurate models are both feasible and required. It is demanded that the models conform to the reality for which they have been designed.

In the area of metal cutting models have been developed [28,29,33] to predict the forces that a metal cutting process exerts upon the workpiece, the tool, the set-up, and, ultimately, the machine. At the same time, the response of those elements to these forces has to be evaluated and simulated. For example, the effects of cutting forces on the structure of the machine tool are important because they permit to understand and predict the process variables such as the surface finish, deflections of the machine and workpiece, temperatures, tool wear, etc., which will ultimately govern the quality of the finished piece. These models have been very accurate in the evaluation of those variables, and work is continuously done to extend their capabilities. In particular, metal cutting forces have been a major subject of study for several processes ([29,27,32,30]) to predict the forces in continuous cutting. Continuous cut can be defined as related to plastic deformation of the metal in processes whose parameters (depth of cut, feed, chip load, cutting speed) vary slowly enough to ignore changes in the properties of the material as a result of the slow variation. It can be assumed that those properties are either constant in time and space, or their variation is so smooth that they can be taken as constant for some interval. Since the prediction, control, and monitoring of continuous forces has reached acceptable level of precision, it is possible to use the knowledge gained about the behavior of the process variables in order to make conclusions about the status of the manufacturing operation. For example, monitoring and spectral analysis of force and sound signals allows for the assessment of tool wear.

Tool failure has been specially manifested in entry-exit conditions in metal cutting and several factors have been associated with it by researchers. For example different material

properties dominate the cut when very small portions of it are involved in plastic or elastic deformation and make the work piece unusually stronger in those regions or times.

Another important factor in entry/exit cuts is the sudden change in the state of stresses in the insert in contrast with the continuous cut situation. This "stress reversal" is a phenomenon typical of impact states in which the change in the conditions is so sudden in time and also so sharp in space that a transient state is created inside the bodies and causes stress waves to travel inside them. Tools which are usually designed for working in compression for example are suddenly loaded in tension, and causes the insert to be faced with the danger of failure.

The creation of cyclic thermal stresses as a result of entry/exit cuts and temperature gradients existing between the different zones inside the insert. is considered responsible of tool failure by some researchers,13] .This effect is believed to create the so-called "comb cracks" which communicate with other cracks created by other causes in the insert, producing large weakened regions which fail under loads smaller than the ones forecasted in the insert design stage.

On the other hand, physical/chemical characteristics of the insert material, work material, and the combination of insert/workpiece material play an important role in the failure mechanism [18]. Welded metal accumulation on the cutting edge changes the geometry and the nature of contact in the cut and increases the forces which the tool should stand considerably. Welding of the material is not a function only of the temperatures involved, but also depends on the combination of insert-workpiece materials and their affinity to each other. The importance of the affinity among metals has been demonstrated by keeping constant factors as geometry, feed, depth of cut and speed, and varying the insert / workpiece combination of materials obtaining different results, depending on the capabilities of the insert and geometry to repel build-ups [12,13,14].

One of the most debated issues of body collision in the literature ([1-8]) is the material properties which predominate in entry/exit cuts. This topic is extremely difficult to deal with because those properties depend not only upon the materials involved but also upon the local geometry in the contact zone. The time in which the state of stresses inside the bodies changes is also critical to the properties in certain ranges.

The existence of different material properties such as flow strength in the neighborhood of an entry or exit has been debated for a long time. Researches such as Pekelharing [12,13] dismiss the hypothesis of higher specific cutting forces in the entry/.exit cuts, while other such as Wallen [14] have reported increments in the specific forces in entry/exit cuts, being these increments specially dramatic in the exit stages, although they are reported also for the entry.

Although the reported models of cutting forces have been successful in predicting the static cutting forces, and their dynamic variation due to the changes in the contact area during continuous cuts, they have not addressed the possible existence of different force mechanisms during the entry/exit cuts as a possible cause for tool failure. Also, a link between the geometry of the tool and insert and these entry/exit forces has not been intended for configurations different from orthogonal cuts.

In order to pursue the effort of understanding the interaction between the workpiece and tool, the particular topics of tool engagement/disengagement are dealt with in this thesis As indicated above, this aspect of metal cutting process has dramatic effects on tool life. Since many factors influence the tool failure patterns, the exploration of their effects presents a vast field of research. This thesis concentrates on the geometrical aspects of tool engagement/disengagement, since it represents an important factor in the mechanisms of tool failure.

The specific objective of the thesis is to characterize the fly cutting face milling forces produced in tool entry/exit and correlate them to the geometries of the cutter, insert, and their relative positions in the time of the tool entry/exit. The work covered in the thesis is organized as follows:

Chapter 2 presents a literature review of the proposed research. Topics such as material properties, geometric considerations, computer graphics and finite element applications reported in the literature are discussed. These aspects will be sorted out to explain the main direction of the proposed work.

Chapter 3 formulates an integrated cutting force model, modified to fit the considerations in interrupted cutting. This model considers several important aspects such as contact area growing pattern, force modeling of contact forces, reaction of the control loop of a milling spindle motor to a disturbance in the form of cutting torque applied to the motor in order to estimate the significance of the variations in the cutting velocity, material properties to evaluate the effect of impact on the tool and the work, and the response of the structure to the forces developed, in particular to the sudden increase in the applied force. After considering these factors individually a simplified model which includes the most significant factors will be presented.

A technique to model the contact area history in entry/exit will be presented in Chapter 4. The technique which will be used for modeling is the three-dimensional solid modeling method. The motivation behind this kind of modeling is that it allows flexibility in the description of tools and inserts, and has enough algorithmic power to deal with those descriptions. Information about the actual implementation of the geometry model will be provided in the Chapter. The limitation of the previous approaches is that although the geometry of the tool entry/exit is regarded as critical for the tool life by many researchers, they lack an analytical tool to calculate and display the parameters of that interaction..

The experiments which were run to estimate the forces developed in interrupted cutting are presented in Chapter 5. Continuous cut experiments with the same tools, inserts and cutting conditions were run. The differences between the forces recorded in interrupted cut experiments versus the continuous cut experiments were considered to be coming from two main sources: i) the possible different levels of cutting forces and ii) the dynamic response of the machine tool and workpiece to the sudden application of forces. Experiments directed to assess the forces included by the dynamics are presented.

In Chapter 6 the results of the experimental work and their processing are shown. These results include the fitting of static mechanistic models for the cutters and inserts used, the use of the models and the geometry module for static force predictions, and the procedure for the estimation of the dynamic modes excited by the sudden cutting forces. The dynamic response of the tool / workpiece subsystem to the static models of the cutting forces are also presented.

In Chapter 7 the evaluation of the model fitting, and the comparison between the experimental interrupted cutting forces and the predicted ones by considering the dynamic response to the static forces are covered. Several parameters to express the deviation of the model from the experimental data will be introduced. With the help of the geometry module, several additional parameters will be calculated, with the objective of achieving a quantitative characterization of the cutters and inserts studied.

In Chapter 8 conclusions about the basic assumptions are presented, the results of the model are discussed, and recommendations for further research are given.

CHAPTER 2

LITERATURE REVIEW

The literature survey covers the topics which are related to entry/exit force characterization and its relation to tool failure. The tool entry/exit has been treated as a body collision problem. It is assumed that the tool suffers the same transient effects when it enters/leaves the cut as a body does when its state of motion is suddenly changed by a change in the forces acting upon it. The review concentrates on the literature which helps in understanding the kind of interactions present during the tool engagement stages using energy and momentum considerations as well as the geometry of the colliding bodies and the material behavior during deformation. Several models are identified from the literature which are useful in estimating the forces and classify the impact conditions which predominate at the tool entry/exit and their influence on the material properties. A review of the effect of the tool geometry on the tool life and wear is also covered. The discussion involves geometrical aspects at two levels. The first level considers cutter geometry, which includes rake angles, lead angles, nose radius, diameters, depth of cut and feed, etc. and the second level covers the insert geometry, chamfering, honing, lands in relation to build-up, forces, insert cracking, etc. In the next sections, research relevant to the mechanistic force modeling developed at University of Illinois at Urbana-Champaign is reviewed as antecedent to the present work. Also, in the area of computer simulation, existing research about the application of three dimensional geometry modeling techniques is covered. A geometry / stress analysis using finite element techniques is also reviewed and its effect upon the present research is analyzed. Finally a wrap-up of these different topics will be presented, along with the general line of research that this work will pursue, based on the findings from this chapter.

2.1 Collision of Rigid Bodies

Since it is reasonable to infer that metal deformation mechanisms which act at the entry of the tool into the work are not the ones which act under continuous cutting, the discussion in this section will concentrate on the mechanisms which influence the impact forces and make them different from the steady state cutting forces. The effort will be directed toward understanding the kind of interactions present during the tool engagement stages from a qualitative point of view with the help of the related literature and some preliminary assumptions. The analysis includes energy and momentum considerations as well as geometry and position of the colliding bodies and material behavior during deformation. Several models for the estimation of those forces are presented and a discussion on the facts concerning those models is given. The conditions which predominate at the tool entry/exit stages in metal cutting operations, specifically those which help with the classification of the impact conditions, and the influence of the impact conditions on the properties of the material are examined.

When two bodies collide several phenomena take place, and the relative importance of each one is dependent on the time scale of interest. At very small time scales the predominating phenomenon is a transient stress wave. This has to do with the velocity at which the disturbance caused by the collision travels across the bodies. In order to have that disturbance present in every point of the bodies, both shear stress and longitudinal stress waves must have had enough time to travel some characteristic dimension in the bodies. For example, typical stress wave speeds for steel are [4] 3200 m/s and 5000 m/s for shear stress and tensile/compressive stress respectively.

If the characteristic dimension of the objects is considered to be in the order of D meters, the characteristic time of the shear stress and the tensile compressive stress waves is defined as $T = D/c$ where T is the characteristic time for stress waves to travel the characteristic dimension D, and c is the stress wave velocity.

Under these assumptions the characteristic times of the shear stress and the tensile compressive stress waves are therefore 30 μsec and 30 μsec respectively when the characteristic dimension of the object is 0.1 meter. The preceding results indicate that, in order to study the disturbance flow across the solids we have to concentrate on time scales in the order of microseconds. This decision has an effect not only on the theoretical aspects of the analysis but also influences the measurement devices needed for obtaining the data. However it is important to note here that for engineering applications averaged values of stress states in the bodies are usually considered [3-5]. These are values which arise due to tens and may be hundreds of wave travels and which are more useful when predicting impact responses. The reason for this is that it does not seem worth to concentrate on microscopic time scales when important parameters like impact angles, friction coefficients, velocities, positions, material properties, etc. are represented by a statistical mean rather than a precise deterministic value. As mentioned before, if hundreds of shear and/or longitudinal waves are used, average stress states and times of order of milliseconds should be considered.

Several parameters which could characterize the interaction between two colliding bodies have been developed. One of them examines the magnitudes of the inertial forces when compared with the cohesive forces which are characteristic of the materials involved. This parameter is called "damage number" or "number of Best" and it is defined by [1]:

$$B = \rho v^2 / Y \qquad (2\text{-}1)$$

where: ρ = density of target material

v = impact velocity

Y = mean flow stress

Some ranges of the damage number for which different conditions predominate [3] are:

10^{-5} for quasi-static/elastic conditions

10^{-3} for starting plastic behavior

10^{1} for extensive plastic deformations and,

10^{3} for hypervelocity impact.

Speeds and tool dimensions typical of metal cutting have an approximate damage number of 10^{-4} which appears to fall between the limit of elastic and plastic behaviors. Since the damage number is essentially a comparison between inertial and cohesive forces, it can be argued that on considering only the tool inertia and ignoring the rest of the inertial forces, such as those due to the mass of the drives, motors and slides, the real damage number would more likely represent a plastic condition rather than an elastic one. An independent reasoning shows similar results when the ratio between kinetic energy (KE) of the projectile and the deformation energy (DE) of the target are considered, namely

$$KE/DE = \rho \cdot v^2/(2 \cdot Y) \qquad (2\text{-}2)$$

It is clear that this relation is half the damage number given by equation (2-1). The preceding discussion assumes no deformation occurs in the tool, which is considered to be much harder than the workpiece material.

Parameters such as strain rate which determine the kind of effects that take place in the materials during the impact interval have to be also considered. According to [3] and [4] characteristic times of 10^{-4} sec, strain rates of 10^{2} to 10^{4} /sec, and adiabatic behavior are present in mechanical impact. In this source it is established that the kind of forces involved are inertial forces and in the above strain rate range both elastic and plastic behavior are present.

The extensive literature survey shows that authors have tried to estimate the properties of the target material under high strain rate conditions. The procedure generally used involves impacting a flat semi-infinite solid with projectiles and measuring impacting and rebounding velocities and angles as well as the crater dimensions [1-3]. Based on those measurements, average values for strain rates, strains, and yield pressure are inferred and a re-calculation of the expected values is then done. A good agreement is achieved for crater size, and rebound angles and velocities. A poor one is achieved for contact time, in part because the model seems to be accurate for the entry stage, but not for the rebound part which involves elastic recovery after plastic deformation. It is proposed that tensile/compressive strength properties for a particular strain and strain rate can be inferred from the impacting ball tests.

Simple models which are used to predict the forces present when an object collides in a free impact against a semi infinite solid are shown here [1,3,7]. In these models only the initial (kinetic) energy in the form of momentum is given as an input to the system, and this momentum is changed in the interaction against the workpiece. The assumptions for these models are: constant material resistance force, Y, negligible elastic wave energy dissipative action, plastic tool-work interaction, other system forces are assumed negligible compared to contact forces, adiabatic conditions, and duration of contact longer than the characteristic stress wave travel times.

One of the problems of impact forces analysis is that the identification of the forces themselves is very difficult because in interrupted machining these forces are present along with vibration induced and regular cutting forces. Consequently, the next subsequent step of prediction is also very difficult. In fact, very few of the papers and research reviewed present a way to identify the impact forces present in interrupted cuts.

Another important problem in understanding the impact forces is the identification of the strain rates which predominate, and their variation with time, and space, or position on the

cutting face during the entry stages of the cut.. This identification is pertinent because the properties of the material under high strain rates are different from those under static conditions. An approximate calculation can be made, by applying uni-dimesional stress wave propagation theory [4] which express the strain produced as:

$$\varepsilon = v/c \qquad (2\text{-}3)$$

where ε: strain

v: entry speed (m/sec)

c: elastic stress waves velocity in the material (m/sec)

If the strain value is divided by the time which the tool takes to pass from no engagement to full engagement, the order of magnitude of the strain rate which predominates in this kind of tool-work interaction can be determined.

Once the strain rates are identified, a relation between those strain rates and impact forces must be developed. For this purpose, the assumption that the properties of the material under collisions (highly variable strain rates) are similar to those under controlled strain rate tests is necessary in order to estimate the material properties.

2.2 Geometrical Characterization of Entry-Exit Cuts

In this field there is a classical paper by Kronenberg [9], in which he analyzed the contact in the entry stages between the tool and the workpiece for face milling operations. His work dealt with straight cutting edges, and a workpiece whose entry wall was vertical. For different combinations of feed, depth of cut, axial and radial rake, lead angle and relative position tool axis/entry wall, he developed charts which allowed for obtaining quantitative information about the angle of engagement and point of initial contact and qualitative information about the kind of engagement-disengagement U, T, U or V as shown in Fig

2.1. The sequence of entry-exit of the points in the insert determines the type of entry-exit under consideration. For example if the tool enters the work piece in the order S-T-U-V, it is called a "S engagement". Similar rational applies for other kind of engagements, and disengagements.

An important point of reference [9] is that it presents an experimental evidence which supports the assumption that the rate of development of contact area has definite effects on the tool life, specifically on wear. High rates of change in area with time (dArea/dt, also called "Impact Factor") led to deeper wear in the tool face. An important distinction is evident from this paper in the sense that different criteria apply for tool wear and for tool failure. In general, smaller area rates (called Impact Factor) lead to smaller level of tool wear, as shown in Fig 2.2. However, some configurations of tool-work which have very small characteristic area rates lead to almost certain tool failure in very short times. The reason is that although the area rate is small, it starts in places in which the tool is most vulnerable such as the sharp "S" end of the insert.

In continuation of the Kronenberg's work, a team of Japanese investigators [11] collected statistical data to assess the effect of geometry in tool failure of carbide tools. Several tests were performed in turning while producing interrupted cuts by using a twisted slot whose walls have a determined angle with the radial line as shown in Fig. 2.3. This geometry is aimed at testing the four modes of engagement/disengagement combinations proposed by Kronenberg in his paper of 1946 [9].

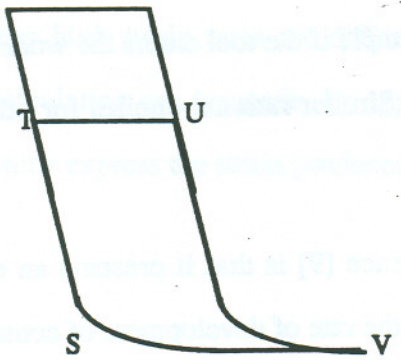

Fig 2.1: Kronenberg's classification of tool points [9].

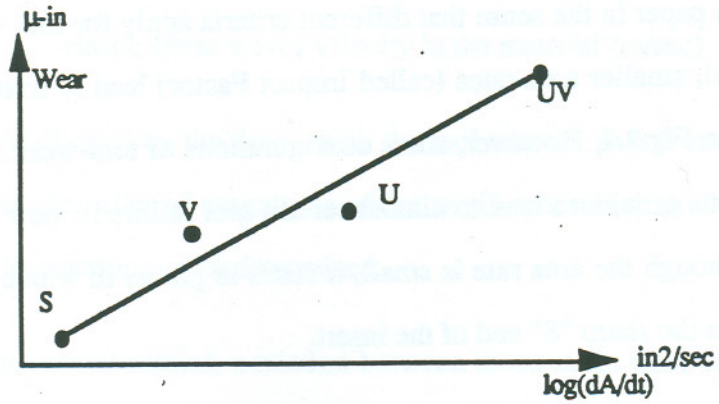

Fig 2.2: Kronenberg's findings of relation Wear/Impact Factor [9].

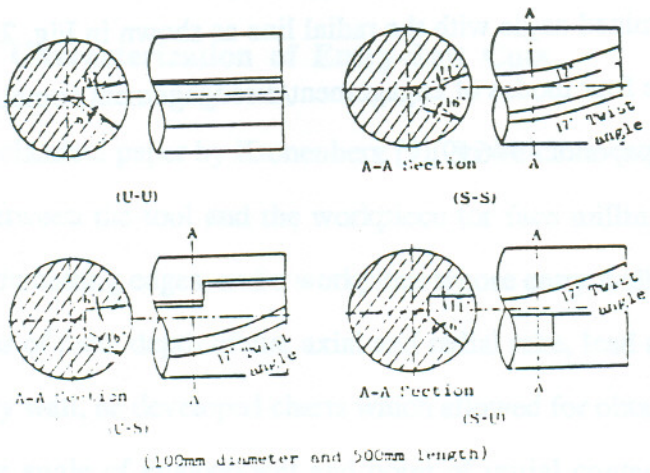

Fig 2.3: Assai's workpiece ([11]).

The combinations of engagement/disengagement are shown in the Fig 2.4. The part of the insert which is actually engaged in the cut is shown, the vertex close to the nose is the "S", the one on the lead edge is "T", the one deep inside the insert is "U" and the one in the relief edge is the "V" point.

The authors in reference [11] used a negative tool holder with -6° back rake, 6° relief angle, 15° lead angle, square regular P20 carbide inserts and TiC tool C, 1350 Hv hardness. The workpiece was plain carbon steel. The cutting conditions were constant depth of cut (0.5mm), cutting speed in the range of 0 to 200 m/min (0-660 fpm) and feed in the range 0-0.5 mm (0-0.020in). Besides measuring the forces by a strain gauge dynamometer, the cutting temperature was recorded using a synchroscope and a high speed camera was used to observe the tool/chip welding phenomena. A plain strain elastic finite element analysis was performed by using the boundary conditions that the high speed camera recorded. The kind of fracture found in this work is called "early fracture" because it appeared in a very short time with no evidence of precracking.

As far as the results of the above work are concerned, there are several findings which are contrary to those commonly found in the literature. One of the findings is that positive geometries, found in this case as S-engagement /disengagement were significantly better in the case of P20 insert, extending the safe zone for the cutting conditions . On the other hand, the TiC insert performed in a very similar way for the geometries used. The P20 is a Tungsten Carbide insert generally used to machine steel, cast steel, malleable cast iron, stainless steel and it is able to stand high feeds and depth of cut, as well as low to high cutting speeds. The TiC class of insert is called "CERMET" and is suitable for light feeds and depths of cut but it is apt for very high cutting speeds and has good wear, thermal and mechanical shock resistance. The difference between the inserts becomes clear on examining Fig 2.5. In the first case a P20 insert is used and found to be very sensitive to the cutting conditions. The contrary is true for the TiC insert, for which the failure rate is

very constant regardless of the differences in engagement/disengagement conditions. The effects of cutting speed and engagement/disengagement on the insert life obtained from the preceding investigation are summarized below.

Cutting Speed effect: For the P20 insert and for a given entry/exit, feed and depth of cut conditions, speed has the effect of increasing the chances of survival of the insert. It can be observed that for higher speeds the safe zone is extended. In contrast, the TiC insert presents a danger zone in the higher speed neighborhood. This is more in agreement with the results reported by other researchers [13,16] who have found that higher speeds increase the risk of failure and the stress reversal effect.

One explanation to this apparent disagreement is the fact that the build up zone occurs at relatively small feeds and speeds. For the P20 insert the kind of buildup is very much associated with the damage zone. In contrast this zone is not associated with damage for the TiC insert and allows the small feed and speed conditions to be safe for the insert.

Engagement/Disengagement: Again, for the P20 insert the conditions of engagement /disengagement affect the life of the tool in contrast with the TiC insert which shows small differences in this regard. For the P20 insert the conditions of S engagement/disengagement are better than that of U. For the TiC insert, the danger region is located at high speeds-high feeds which represents a no-buildup zone and at low speed-all feeds in U disengagement. The buildup for both inserts is slightly more pronounced in U disengagement.

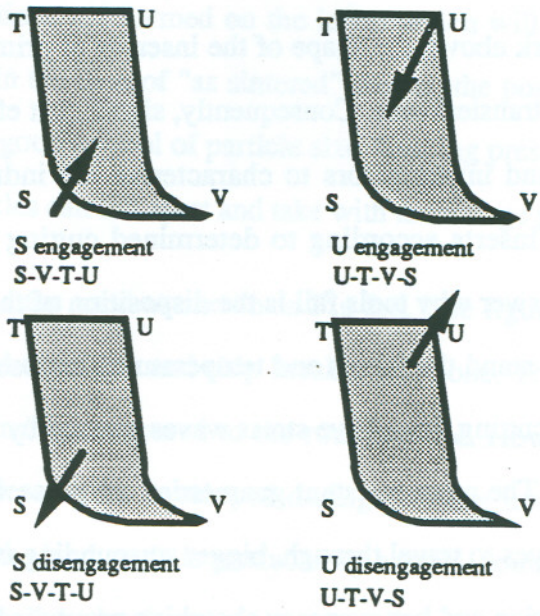

Fig 2.4: Engagement/Disengagement Patterns. (Based on [11])

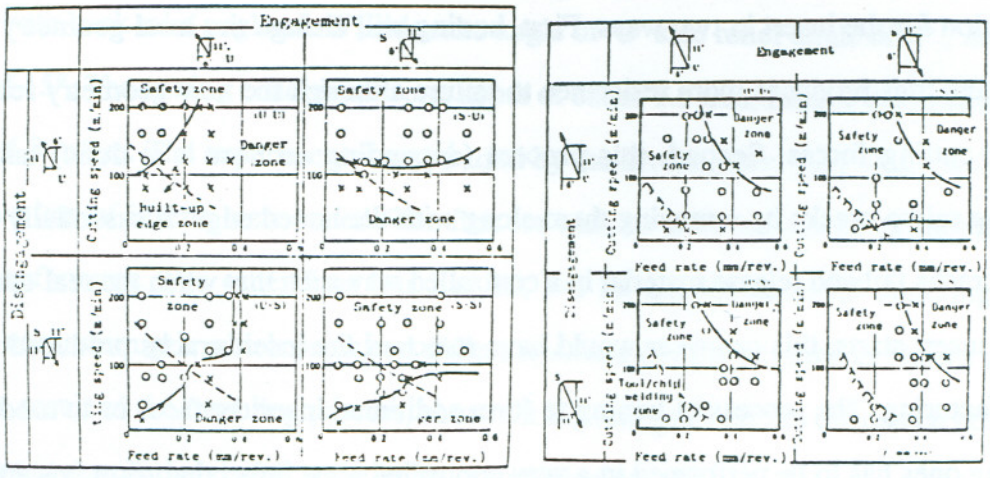

(a) P20 Insert. (b) TiC Insert.

Fig 2.5. P20 vs TiC insert failure regions ([11]).

2.3 Insert Geometry

As discussed in the work above, the shape of the insert is of primary importance for it to withstand the forces in transient cuts. Consequently, significant effort has been exerted by insert manufacturers and investigators to characterize the industrial processes which produce the strongest inserts according to determined cutting conditions. One of the identified reasons to answer why tools fail is the disposition of the material and the shape of the insert which can stand the forces and temperatures imposed on it. For example, in the case of interrupted cutting, impulsive stress waves, caused by the entry/exit conditions travel along the insert. The more resistant geometries are those which present the bigger path length to those waves to travel through, bigger surrounding material support, stronger point of tool/work collision and better energy absorbing properties. This last condition is in contradiction with the desired resistance to progressive wear which requires harder and frequently more brittle materials.

Another considerations along with the macro-geometry of the insert is the presence of micro cracks after the fabrication of the insert [15]. Depending on the process there is a probability that cracks exist in or close to the cutting edge. Honing has been used as a protection for the insert in two ways. First, honing will change the local geometry of the insert and thus produces more resistance to failure although the new geometry results in higher cutting forces. Second, this process (depending on how it is done) takes the existing micro-cracks by removing them along with the honed edge. It essentially makes those cracks fail and release material in a controlled way such that when the real operation of the insert starts, this pre-wear would have removed the insert cracks produced during manufacturing. The process of honing to form additional insert surfaces or to modify the existing ones has to be performed in a very controlled way. Several approaches are used. For example the cutting edge could be ground but care has to be taken with respect to: the amount of force to be applied to the insert being ground, the size of the abrasive, and the

direction of the wheel rotation in relation with the cutting edge. If the ground operation is too harsh, large aberrations are formed on the insert which will produce fracture at the conditions of real cut. In the case of "as sintered" inserts, the possibility of failure exists because, in spite of the good control of particle size, forming pressure, distribution, etc of this process, loose particles can fall apart and take with them large parts of the material.

Several hones and lands are used as shown in Fig 2.6. The figures correspond to sharp edge, hone, K land, land and hone and chip breaker and hone. The K land insert may be more expensive if ground as compared to the rounded one. However, in large quantity manufacturing this angles can be developed during pressing instead of the grinding to achieve smaller costs.If the land angle is produced by a mold, honing is used almost all the times. On the other hand, if the land angle is ground, a small honing is used on a frequent basis [15].

In relation to the removal of insert defects before industrial use experimental work has been carried out [18] to statistically correlate the existence and the magnitude of the radius between the flank and the rake faces of the insert with the tool life in interrupted turning. The experiment was run with SNGN 120408 ISO norm P10 inserts mounted on a tool holder with back rake angle of -6°, side rake angle of -6° side relief angle of 6° , and lead angle of 15°. The cutting conditions were: depth of cut of 1.5 mm, feed of 0.4 mm/rev and speed of 3 m/sec. The experimental set up used by the investigators [18] is shown in Fig 2.7. Five lots of inserts were tested. The first lot with no prior treatment, as supplied by the manufacturer. The other four lots had 12, 24, 36 and 60 hours of tumbling with electro-corundum grit which produced different values of radii r1,r2,r3 as shown in Fig 2.7. The result of the tumbling process, shown in Fig 2.8, presents the difference between the insert as supplied and after some hours of tumbling process.

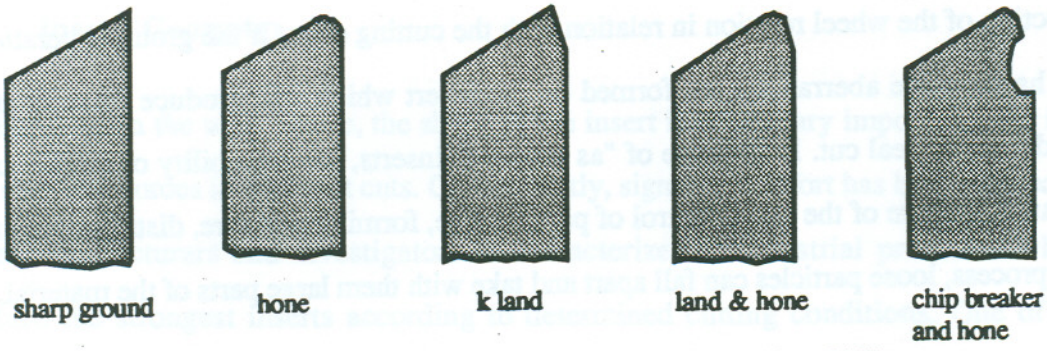

Fig 2.6: Different dispositions of land and honing [15].

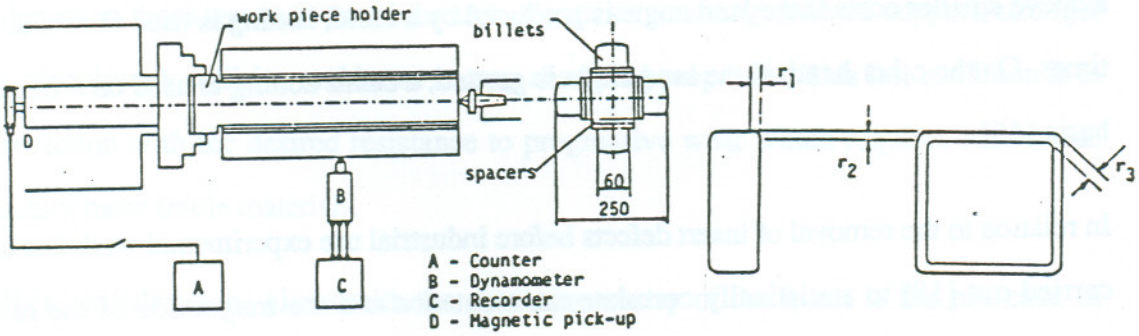

Fig 2.7. Turning Interrupted Cut set up ([18]).

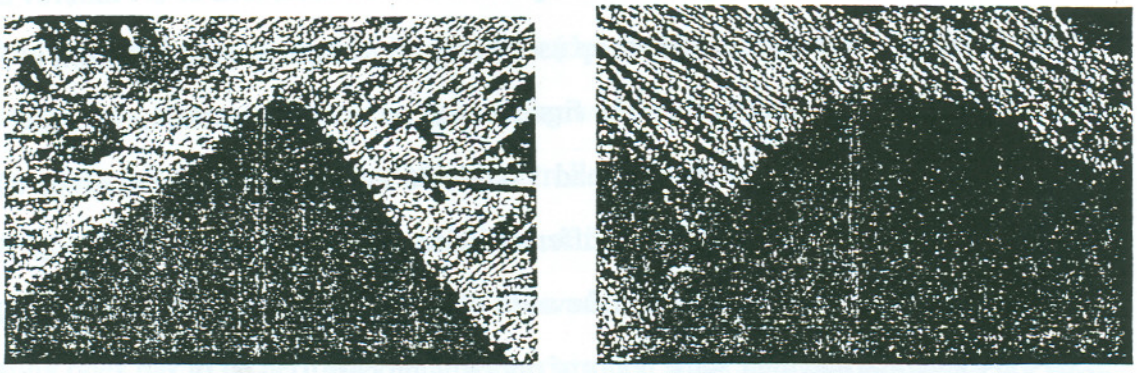

Photo 1 : Replica showing edge profile for insert as supplied. (200 x)

Photo 2 : Replica showing edge profile for insert after 60 hours of tumbling. (200x)

Fig 2.8. Result of tumbling process on the insert ([18).

The results of the tests showed that the expected value of the insert life before failure was maximum for 24 hours of tumbling. The insert lives for 36 and 60 hours of tumbling were below that of the 24 hours, demonstrating that the benefit of pre-wearing is confined to a range beyond which the tumbling process removes the micro-cracks present on the edge plus some more material, thus decreasing the life of the tool.

Swedish investigators [14] did additional work in interrupted metal cutting. The purpose of their work was to evaluate the forces present at intermittent cutting at small feeds. The experiment was run with the modified Charpy machine shown in Fig 2.9, which had an orthogonal tool installed on the extreme end of the hammer. The objective of the experiment was the evaluation of the forces under small chip loads in intermittent cutting, and also the characterization of dead zones in front of the insert, which have strong influence on the forces, tool failure, and surface finish depending on the type of build-up which was predominant for a particular type of tool and workpiece material.

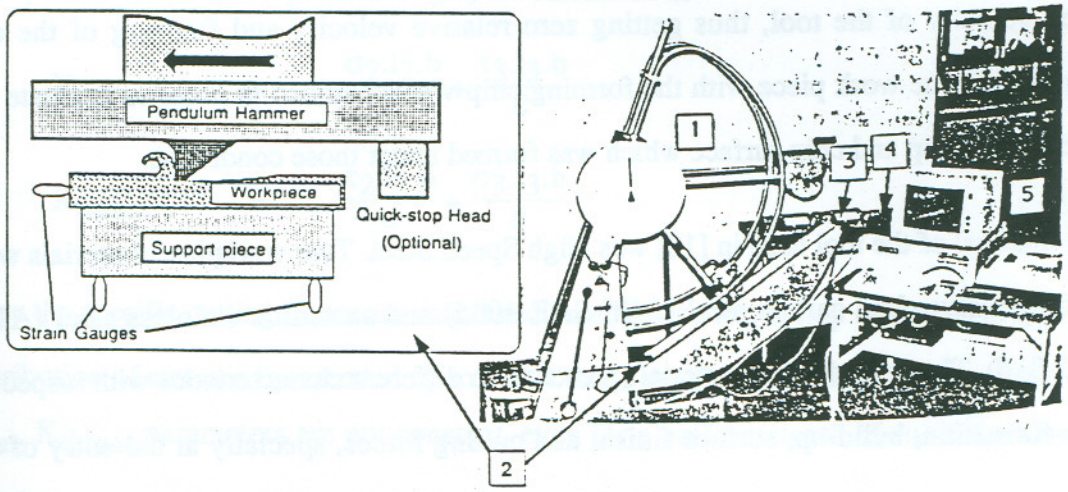

Fig 2.9. Experimental Set Up by Wallen ([14])

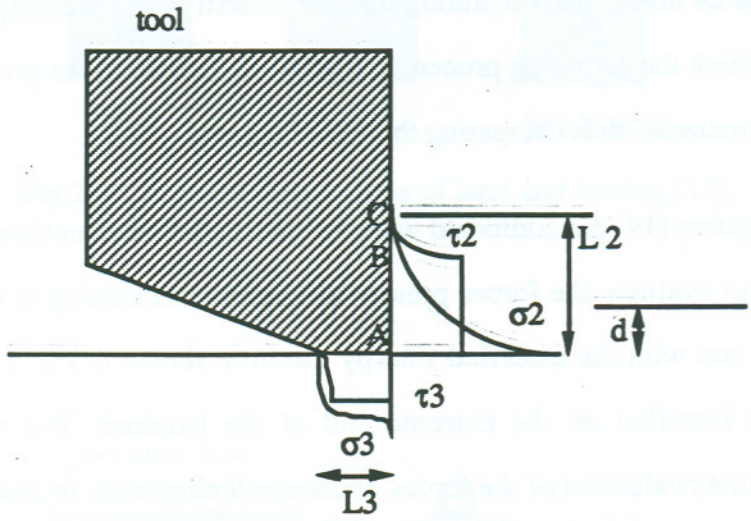

Fig 2.10: Distribution of stresses in orthogonal cut. [14].

For the purpose of dead zone study the pendulum was equipped with a quick stop mechanism in order to suddenly accelerate the workpiece in the middle of the cut up to the same velocity of the tool, thus getting zero relative velocity and freezing of the cut. Afterwards, the work piece with the forming chip was examined in order to evaluate the kind of build-up and chip surface which was formed under those conditions.

The material of the tool used in [18] was High Speed Steel. Two workpiece materials were used, namely: plain carbon steel (AISI-SAE 1045) and austenitic stainless steel (AISI-SAE-316). These workpiece materials present two different characteristics with respect to chip formation, build-up, surface finish, and cutting forces, specially at the entry of the cut.

By observing the experimental set-up, it is evident that two measurements are available for each chip thickness; one is at the entry, and the other is at the exit of the cut. The cutting and thrust forces are approximated by the following equations:

$$F_{cut} = \sigma_2.l_2.b + \tau_3.l_3.b \quad (2.8)$$

$$F_{thrust} = \tau_2.l_2.b + \sigma_3.l_3.b \quad (2\text{-}4)$$

The notation as exemplified in Fig 2.10 is defined as follows:

τ_2 = flow shear stress on rake face τ_3= flow shear stress on relief face

σ_2= normal flow stress on rake face σ_3=normal flow stress on relief face

l_2 = chip-tool contact length in rake face

l_3 = workpiece-tool contact on relief face

d = uncut chip thickness (also called here depth of cut or feed).

b = unit width of the tool

The specific forces (force per unit length) are calculated as

$$K_{cut} = \frac{\sigma_2.l_2.b}{d} + \frac{\tau_3.l_3.b}{d} \quad (2\text{-}5)$$

$$K_{thrust} = \frac{\tau_2.l_2.b}{d} + \frac{\sigma_3.l_3.b}{d} \quad (2\text{-}6)$$

Since the specific cutting forces are calculated based on the uncut chip thickness, d ,and the distribution of stresses is extended up to 3 to 4 times the chip thickness, it is clear that the K_{cut}, K_{thrust} parameters are not constant, even for a uniform depth of cut if the contact length changes.

Figure 2.11 shows the specific cutting forces of a non-chamfered tool for the two materials of [14]. It is observed that the horizontal axis shows that chip thickness was symmetrical about the deepest point in the cut. Although the chip thickness reaches the same values twice, one for the exit and one for the entry the values of specific cutting force were found to be different, as expected from equations (2-5) and (2-6). For the exit condition the effect can be regarded as caused by contact length in the chip. The austenitic stainless steel presents a definite overload in the exit stage as compared with the plain steel. In every case, the exit condition represents an increase in the specific cutting force, and also in the thrust force. For the entry condition, the plain carbon steel shows a small increment in the specific forces while the austenitic presents a decrement. At this point it is important to note that information about the frequency characteristics of the force measurement apparatus was not given and consequently, it is not possible to evaluate the level of accuracy of the entry measurements which usually involve very high frequency signals. As for the effect of velocity, it is observed that the higher the cutting speed the higher are the specific force levels, although the trend doesn't seem to be absolutely consistent.In any case, the trend of high specific forces at the exit stays very consistent.

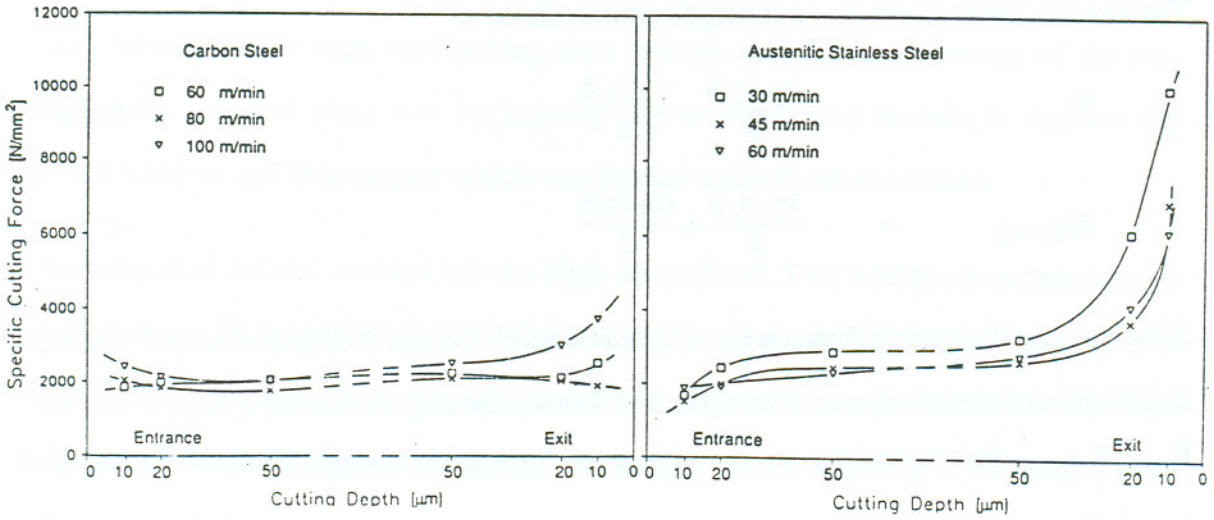

Fig 2.11: Specific cutting force K_{cut} for plain steel and austenitic stainless steel. [14].

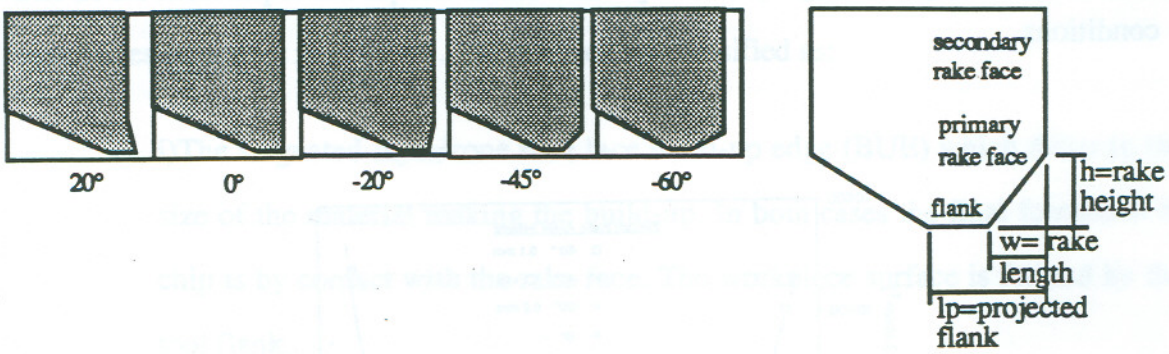

Fig 2.12: Geometry of tool [14]

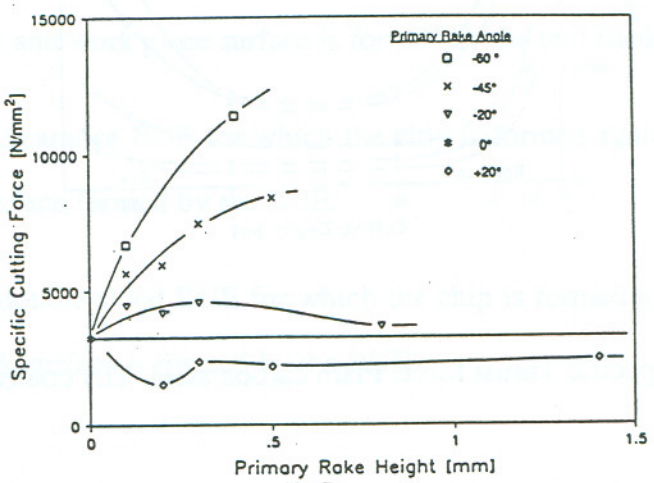

Fig 2.13:. Effect of Rake angle and Primary Rake Height. [14].

The shape of the tool as shown in Fig 2.13 has also an important effect on the cutting coefficients. Blunt tools having primary rake angles of -60° and -25° represent a strong increment of the cutting forces with the increase in primary rake height. For the -20° primary rake angle the force increases to a maximum at about 0.3 mm primary rake height and then decreases beyond that.

An important effect can be observed in Fig 2.14 when, keeping all the other factors constant, the tool is coated with TiN. In this case, the specific forces of the coated insert show a significant increment at the entry stage in comparison with the uncoated tool, but

has kept a similar trend to that of non coated tools for the developed cut and the exit conditions.

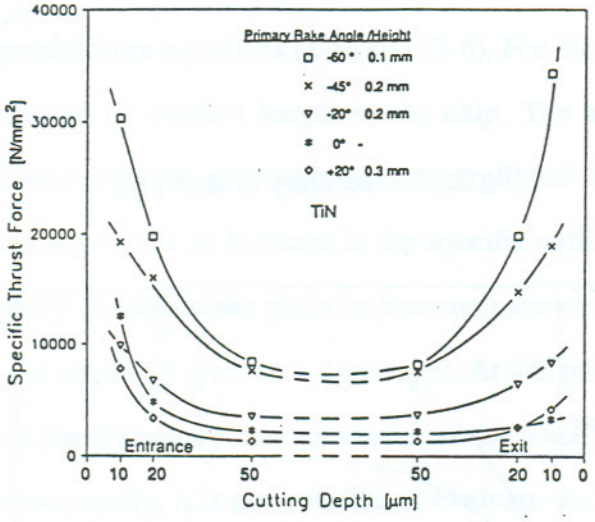

Fig 2.14. Specific Thrust force. Plain carbon steel. TiN coated tool. [14].

Fig 2.15. Characterization of dead zones [14].

One of the most important aspects of the work by Wallen[14] is the characterization of the dead zones presented in Fig 2.15. These zones are classified as:

i)The stagnated layer/zone rake face build-up edge (BUE) which differ in the size of the material making the build-up. In both cases the final formation of chip is by contact with the rake face. The workpiece surface is formed by the tool flank.

ii)The rake BUE or rake face build-Up for which the chip is formed against the build-up and work piece surface is formed by the tool flank

iii)The clearance BUE for which the chip is formed against rake face and the work surface formed by the BUE.

iv)The double sided BUE for which the chip is formed against rake BUE and the work surface is formed by the BUE.

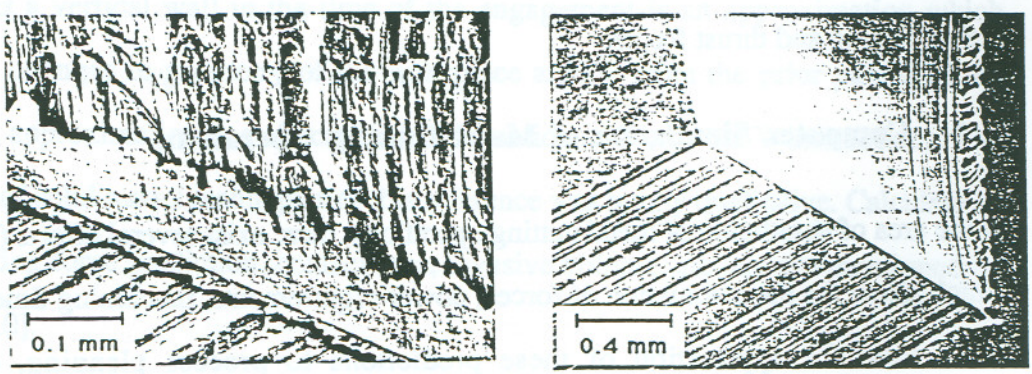

(a) (b)

Fig 2.16. Quick stop results showing chip formation.
a) Left: Plain Carbon Steel. b) Austenitic Steel. [14].

The performance of the two materials (plain carbon steel and austenitic stainless steel) was also analyzed with respect to the kind of chip produced. For the plain carbon steel, the low cutting velocities allowed for the formation of build-up edges (BUE). At high speeds this effect disappeared. As a consequence, the surface finish deteriorates and the back part of the chip becomes highly uneven due to the BUE's. In contrast to plain carbon steel, austenitic steel shows good behavior even at low speeds which allows for obtaining good surface finish, although this is a material much harder and stronger than the plain carbon steel, as shown in Fig 2.16b. The difference in the nature of chip formation is attributed to the element of the tool which forms the chip. In the case of BUE the chip is formed by the build-up or the stagnated zone which presents a random pattern of formation-desintegration as well as a rough surface. In the case of no BUE the chip is formed by the rake face, and thus produces a smooth surface. It is interesting to note also that in the case of double sided BUE and/or clearance BUE the material leaks through the flank face, and produces a rough surface as seen in Fig 2.16a for plain carbon steel.

As a general conclusion from Wallen's work [14] it can be stated that blunt geometries produce higher levels of force. The blunt geometries can arise from negative rake angles, larger flank lengths and/or larger flank heights. In general, larger flank length produces higher cutting and thrust forces.

2.4 Computer Simulation of Metal Cutting Operations

In the area of simulation of metal cutting operations, there exist several efforts ([27-29,32]) which allow for the calculation of forces, power requirements, machining times, etc., and also allow for application of these predictions to process planning, design for manufacturing, etc. Two areas in the force prediction and surface characterization fields are targeted. First, the forces developed on the machine tool and the workpiece can be calculated by considering cutting force coefficients which vary with the geometry of the contact area and the cutting speed. Second, the dynamic models of the structure of the

machine tool have served the purpose of predicting the response of the structure to the forces which is manifested by the variation of the cutting area. The cutting area is changed by the weaviness in the surface caused by the previous passes of the tool and causes a potentially unstable process. Prediction of these phenomena allows for the evaluation of the surface of the workpiece after the cut.

Attempts have been made to characterize the entry-exit conditions in milling [9,10]. As mentioned before, the main objective of reference [9] study was the development of analytical expressions for milling tools . Tables and charts were given to calculate the times of engagement-disengagement for a given insert, tool/work offset, rake angles, lead angles, feeds, and depths of cut. They also permitted knowing the part of the insert which engages first and therefore allowed for the evaluation of the failure patterns.

A geometry module is built by [10] using a solid modeling commercial package, which allows for reconstruction of engagement-disengagement conditions in face milling such as those shown in Fig 2.17. The fact that solid models are used virtually removes the restriction about the edges of the insert which was present in [9]. However, several limitations are still present in the approach of [10]. First, the modeling of the workpiece boundary as a vertical wall in the time of the engagement is an approximation which ignores the changes in geometry of the workpiece arising from the prior passes of the cutter. This approximation has effects in the evaluation of T , U and V interactions. The application of solid model techniques of this reference was purely qualitative. Calculations such as cutting force prediction, contact area, invasive volume, etc. are not mentioned by reference [10].

Additional incursions in the use of computational geometry applied to metal cutting simulations are presented in [53] and [54]. In [53] the entry/exit angles for a given tool path and a workpiece geometry are computed, as well as contact areas. The work is based on 2D geometrical abstractions of the cutter and the workpiece, namely, the cutter is

simulated as a circle, moving in a world of 2D geometric entities (rectangles and circles). By representing the workpiece as a CSG (Constructive Solid Geometry) result of boolean operations on 2D primitives, the program determines which primitives the cutter touches when it is at a given position, and calculates the exit/entry angles and the chip load, assuming that the depth of cut is constant. In this sense, this work is a variation of Gu's work, which uses a 2D boundary representation for the workpiece and cutter, for a variety of cutter geometries.

In [54], a 3D extension of the work in [53] is presented, which is used to predict cutting forces. This prediction allows an adaptive controller to anticipate the changing workpiece, and therefore to change the cutting parameters in order to eliminate force overshoots which would break the tool. Again, in this method, the cutter is thought of as a cylinder traveling through the workpiece, which allows to calculate the boolean intersection of the cutter and the workpiece, thus generating the values for material removal for different positions of the cutter and workpiece. How this voume information is transformed into cutting forces is not explicitly discussed. This step involves the calculation of contact area (chip load) and the determination of the area orientation in order to get the correct force directions.

In the reviewed literature, the application of geometric techniques to the characterization of tool/workpiece interaction has followed two general lines: first, the use of computational geometry in two and three dimensional scenarios is based on the abstraction of the cutter as a circle (2D) or a cylinder (3D). This abstraction is clearly unapropiate if the objective is to characterize process parameters which are function of the instantaneous part/tool geometric relation, specially in the area of tool failure in entry/exit cuts. The inability lies in the fact that the abstraction of the cutter as a cylinder immediately impedes the characterization of insert geometry, rake angles, lead angle, contact area growing patterns, etc. For that purpose, clearly a characterization which accounts for small as well as large geometry is necessary. Second, the attempts made in characterizing small geometry (it means,

accounting for insert and local workpiece geometries) have met important problems: in the case of Kronenberg's work [9], the analytic approach rapidly fails to grasp real world situations such as rounded nose inserts, K land inserts, irregular geometry of the part, etc. On the other hand, the use of solid modeling techniques in that area has allowed to overcome that constraint [10], but still, the aspect of determining which parameters are meaningful to the charaterization of insert/part micro-geometry interaction is open, and so is the quantitative characterization of those parameters.

2.5 Stress Characterization of Entry-Exit Cuts

Several investigators have observed the mechanism of chip formation and detachment in entry and exit conditions while paying special attention to the stress patterns in the work as well as in the insert. Pekelharing [12,13] has provided the base for many of the papers which are related to tool failure in this decade.

The study of Pekelharing deals with early tool fracture as result of interrupted cut. It establishes the fact that the weakest point in this process comes in the exit rather than in the entry stage. In contrast, non-early tool failure (the one occuring after significant service life) is blamed upon all regimes, namely entry, uniform cut and exit conditions.

In [12] a turning test was ran in which a rotary piece is fitted with a circular core of "blades" which allow for the variation of the engagement/disengagement angles between the tool and workpiece. The study is mainly directed to T or U disengagement. This kind of disengagement for a sharp tool is very harmful, and the insert loses the cutting edge in the first or second exits. In this sense, the results presented showed that U or T disengagement conditions were harmful. This agrees with the Asai findings ([11]).

In order to better explain the process of tool failure, Pekelharing [12] took a high speed film photographs of the tool exit. The cut showed several stages when the insert was approaching the exit. In the first place, there existed a positive shear zone in front of the

rake face and a negative shear zone ahead in the cut which bent into the uncut workpiece as shown in Fig 2.19. The positive shear zone is characterized by the fact that compressive stress has developed normal to the shear planes. The negative shear zone below the surface is subjected to a combined regime of shear and tensile stress. As the insert approaches the exit face, this situation grows more critical. This is accompanied by the fact that the contact length between the chip and the insert becomes smaller. Because of the lack of balance in the forces, chip fracture is produced in the proximities of the exit, and it is believed that the chip rotates altogether, breaking away from the insert almost totally. Figure 2.19 is a sequence of frames of the high speed photographies. Figure 2.19a shows that the normal positive shear zone is present, but a negative shear zone has also appeared. It can be observed that deformation occured at the exit wall and that the normally flat work surface has already bent 9° in this particular frame while the contact zone is still 3h (h is the uncut depth of cut). In Fig. 2.19b the situation grows more acute because the deformation of the work surface is bigger, but, more importantly, the contact length has reduced to approximately h. However, it is noticed at this point that there exists still a significant force system acting on the insert.

The rotation of the footed chip can be seen in Fig. 2.19c where a first break away has been produced as shown by a flat portion which makes a 14° angle with the rake face. At this moment, the chip rotation on the rake face is equal to the foot rotation, which means that the foot rotation is responsible for the whole amount of chip rotation.

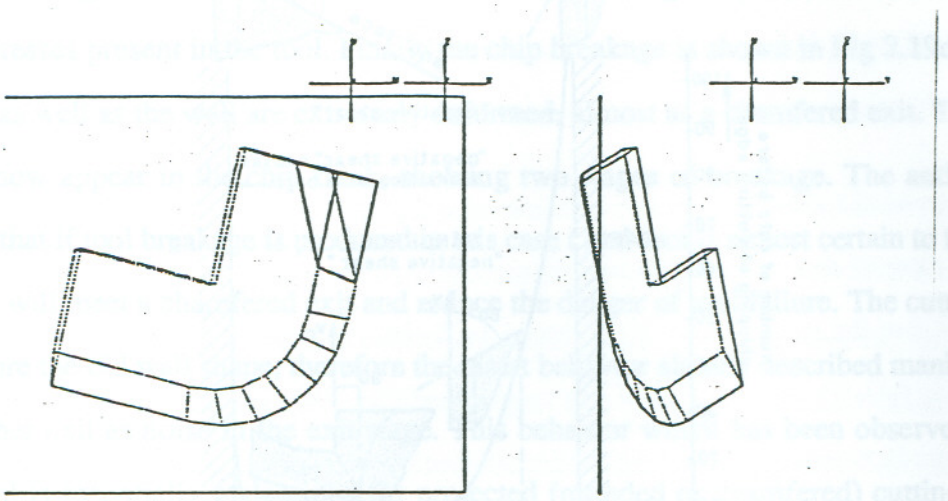

Fig 2.17. Solid Modeling Applied to Entry-Exit Face Milling [10]

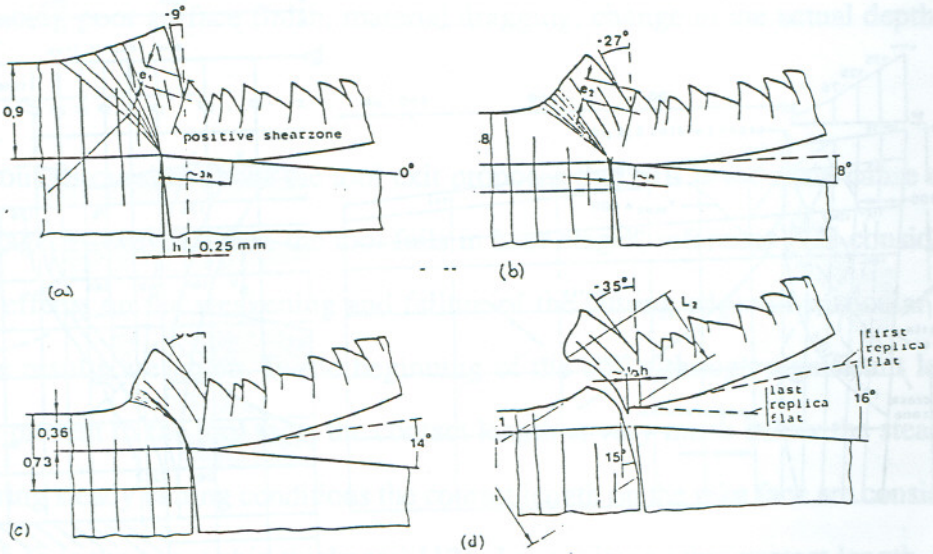

Fig 2.18: Pekelharing's film of footage in tool exit [12].

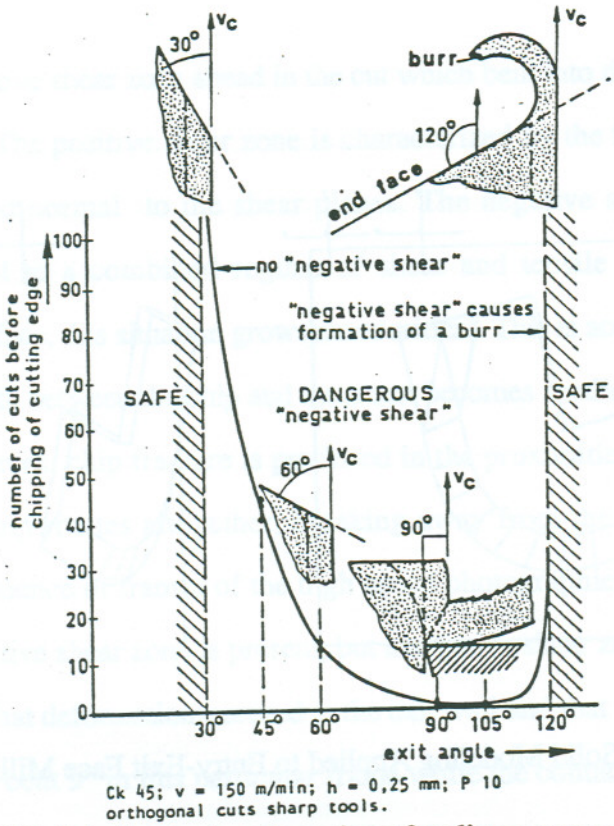

Fig 2.19: Pekelharing's safe regions for disengagement [12].

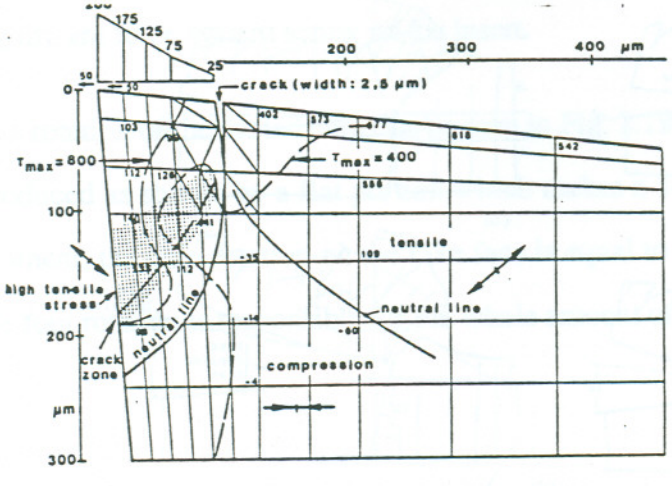

FIGURE 12. Stresses in the cracked tool, are completely changed, and in agreement with tensile cracks as found.

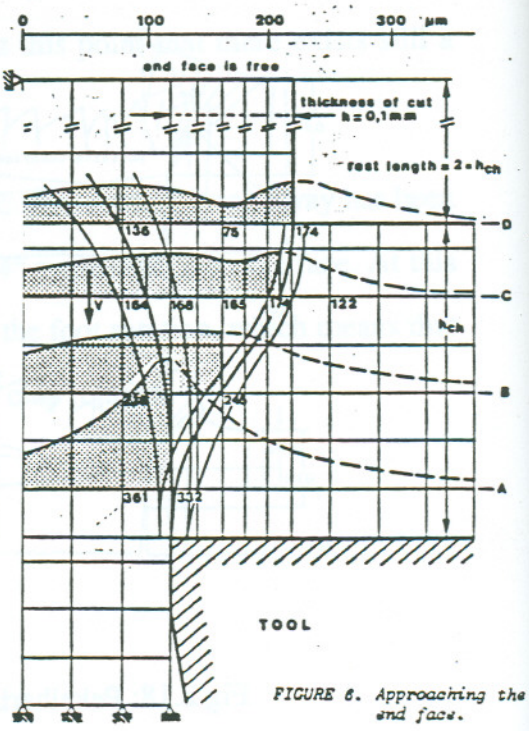

FIGURE 6. Approaching the end face.

Fig 2.20: Stress pattern in a insert close to exit . a) On the Tool. b) On the workpiece[12]

Reference [12] considered that at this point significant forces are still present. These cutting forces are acting on extremely small areas, and contribute to greatly increase the shear and tensile stresses present in the tool. Finally the chip breakage is shown in Fig 2.19d where the chip as well as the wall are extremely deformed, almost as a chamfered exit. Two flat regions now appear in the chip flank, showing two stages of breakage. The author has reported that if tool breakage is produced in this case (and tool is almost certain to fail) its next exit will meet a chamfered exit and reduce the danger of tool failure. The cutter pass will restore the old wall shape, therefore the insert behavior already described manifests at every other exit as noise in the exit stage. This behavior which has been observed for a sharp tool is essentially maintained for protected (rounded or chamfered) cutting edge. However, because of the stronger geometry the insert failure is postponed or in some cases eliminated. The penalty for using chamfered or rounded edge tools is that larger forces, which may lead to larger flank wear are produced. It also raises the the possibility of workpiece material filling the chamfer and leaking between the workpiece and the insert, thus producing poor surface finish, material dragging, change in the actual depth of cut, etc.

The previous discussion about the tool exit proposes that exit is the main cause of early tool breakage. However, when the tool fails in later stages, reference [12] considers that entry has effects on the weakening and failure of the cutting edge. In particular several qualitative results are given. In the beginning of the cut, although significant levels of forces are present in the tool face, the contact length is very much below the steady state value. During steady cutting conditions the contact length on the rake face are considered to be 3h to 4h (h is the uncut chip thickness) [12]. For achieving that contact length, the tool has to be a 10h-50h distance inside the cut. Before the contact length is fully developed, the tool essentially stands full cutting and thrust forces with a very reduced contact length . This period of entry clearly represents a region of risk for the cutting tool. In addition to interrupted cutting, the condition for ending the cut and pulling out the cutter has been

found meaningful with respect to tool failure. It is advised that, in milling for example, the tool be withdrawn after two or three revolutions after the feed is stopped and before turning off the spindle. The tool life may reduce to one third or one quarter of this if the tool is withdrawn under conditions of full feed.

In [13] several mechanisms were considered as responsible for the tool breakage. These include thermal and cutting stresses produced by the foot creation and chip rotation. It was reported that the cases which Kronenberg ranked as most dangerous (e.g. simultaneous contact S-T-U-V) actually lead to the longest tool life. This kind of contradictions shows that the understanding of the tool failure mechanisms are far from being fully understood. Tests were run for orthogonal cutting with sharp tool, with rounded and chamfered tool, and with commercial cutters in order to compare exit performance. The tests were conducted at 80 to 300m/min cutting speed, 0.1 to 0.5mm of depth of cut and used P10 or P30 carbide tools. The immediate conclusion is that sharp tools didn't survive at exit orthogonal cuts.

Test results in Pekelharing ([12,13]) has established the fact that the length of the border between the chip and the work once the footed-chip has been removed is smaller when it is measured in the chip in comparison to when measured in the workpiece. This shows that the dominant mechanism in this case is not brittle fracture but instead there is a heavy plastic deformation which stretches the workpiece side of the cut and compresses the insert side of the cut (L1 vs L2 in Fig 2.18d). The effect of footage is explained and the assessment of the insert rake face is taken to show that although there is damage from the first interchange the damage is relatively small. However, each new exit cut will take away bigger and bigger parts of the insert. The first chipping of the insert occurs at a length on the rake face equivalent to 35% of the depth of cut and, consequently, 65% of the insert still remains intact.

The explanation for this odd behavior is that after the creation of a chamfer the footage is inhibited and thus the failure mechanism is avoided. This is supported by the fact that exit walls other than perpendicular to the cutting velocity as well as deviations from the orthogonal cut seem to increase the chances of survival of the cutter. In this respect, as shown in Fig 2.19 the deviations from 90° of the exit wall produce a safer condition, although they are not very realistic in the practical aspect.

In the case of angles larger than 90°, the tool pushes away rather than cuts the underlying metal, which has no support and bends to form a burr which is undesirable for the finishing of the piece. On the other hand, in case of less than 90° wall angle, the increment in the safe region might be attributed to the fact that the depth of cut diminishes as the tool approaches the exit, making the formerly mentioned effects less notorious. In a similar direction, if the cut is non-orthogonal the cutter will arrive to the exit face by stages, and the chip has another way to flow but the effect of small tool life is still present.

A finite element analysis has been performed to model the shear stresses in the situations of continuous cut as well as exit cut. The modelling is based on an assumption of elastic behavior which of course departs from reality because metal cutting is by definition a plastic deformation process. However, qualitatively the results matched experimental findings in the existence of positive shear in the tool for continuous cut in the proximities of the shear angle which marks the transition between the uncut and the cut chip (see Fig 2.20a). Negative shear stresses show up in the workpiece in the direction ahead of the tool, underneath the new work surface (see Fig 2.20b) for the case of close exit, which coincides with the assumptions drawn from Fig 2.18. It is necessary to mention the fact that the actual values of the loads and inputs to the program were assumptions which are not intended to give a quantitative match but a qualitative one to the observations. Using this kind of analysis the pressure distribution on the rake face is obtained and is found to be approached by a triangular one which is then used to calculate stresses on the tool, as

opposed to the analysis which deals with the work piece state of stresses. This analysis resulted in the highest tensile stress levels near the point in which the failure was found experimentally. Also it shows the division between the compressive and tensile stress regimes inside the insert

As far as the difference between the chamfered and rounded tools is concerned, it is proposed in the reviewed papers [15] that a certain variation in the chamfer dimensions, contrasted with the depth of cut, will produce different effective rake angles, determined by the actual chip flow direction after the cut. This has the effect of producing a fictitious tool tip which is essentially the metal trapped in the corner acting as an extension of the tool. This metal is not welded to the tool and will leave the tool surface with the footed chip when the tool comes out from the cut. If in this case the state of stresses has any relation with the analysis done for a sharp tool, the failure would likely occur exactly in the weakest zone which is the limit between the trapped metal and the insert boundary and thus the tool is released from the stuck metal at at the same time protecting the cutting edge. Pekelharing [13] establishes the fact that no evidence of buildup in the chamfer face was found in any of his experiments, which supports the theory just exposed

The same workpiece was used with the combinations of commercial inserts and cutters. In general, a change of the cutter will not make the situation much better if the sharp insert is used. On the other hand, inserts with chamfer or rounded nose used together with non-orthogonal cutters provide the best performance with respect to this kind of early failure, although they are expected to fail due to other mechanisms.

In the same area of research Loladze [16], a Russian investigator, established some experimental facts which were theoretically treated afterwards by Pekelharing[13] and Ghani [20]. The main purpose of Loladze's work is to study the stress pattern in a tool under conditions of entry (Fig 2.21a), exit (Fig 2.21b) or continuous cutting (Fig 2.21c). For this purpose a series of tests with a tool made of photoelastic material were conducted,

The objective was to identify compression zones, tension zones and neutral zone between them, and also to evaluate the differences in patterns among several processes such as turning, up-milling, down-milling, planning, etc.

The results of the thermoelasticity experiments showed tensile stress in the rake face and compressive stress in the flank surface. The pictures also revealed that the contact length at the engagement and disengagement times was sharply smaller than that of the normal cut. This fact has been found and treated later by other investigators [12]. The highest stresses are shown to be located at 2 to 3 times the uncut depth of cut, and considerably decrease with increasing wedge angle of the tip of the tool, and increase with the increasing depth of cut, This behavior is more noticeable for the tensile stress than for the compressive stress. Since the tensile stress present on the rake face is maximum at the place of failure, it is concluded that higher depths of cut will increase not only the forces on the insert, but also increase the ratio force/area.

Another important point raised by Loladze [16] is the fact that in turning or boring the tool is subject to fluctuating mechanical stresses which don't change sign. This is different from the case of milling where, even in normal cuts, the forces sensed on the tool and insert reverse their sign during one revolution. The author also ran a set of experiments in which it was found that the value of σ_{max} in case of exit in a planning operation reached stress levels between 1.3 to 1.4 times the forces of normal cutting. The exit forces for milling showed an increment of 1.7 times the normal cutting forces.

On the other hand a study of the thermal stresses was made in [16] by making some tentative calculations to obtain the order of magnitude of the stresses created by the effect of alternative cooling and heating of the insert. This tentatives calculations showed that thermal effects are important , and could result in stresses of about 1300 N/mm2, for an insert of tungsten-carbide of 92% WC and 8% Co, and workpieces of carbon steel and nickel based high temperature alloys with transition times of 0.01 sec for changes between

room temperature and 1100°C. It was claimed that this heating and cooling cycles during interrupted cutting causes thermal shocks and cracks. In interrupted turning the temperature gradient is smaller as compared with that of milling and thermal stresses are therefore supposed to be smaller for interrupted turning.

Additional studies made by Ghani [20] are very related to those by Pekelharing in which the emphasis on tool failure in interrupted cutting study is related to exit conditions. It is known that in case of very early tool failure, the exit is very much responsible for the failure. This has been supported by researchers including Kronenberg and Pekelharing. The initial assumption is that the shear angle which in normal conditions points up-ahead of the tool tip (line OA in Fig 2.22) aligns with the velocity vector (line OC in Fig 2.22) in exit conditions and produces piercing of the surface, and it points underneath the new surface (line OC' in Fig 2.22) producing footing, as discussed by Pekelharing.

Ghani [20] ran an interrupted turning test which was aimed at evaluating the effect of work piece exit chamfer geometry (given the angle Θ in Fig 2.22), cutter geometry, insert geometry, speed and material on exit failure. For that purpose the entry was made as smooth as possible and the period between cut was made as short as possible in order to diminish the cooling time after the cut and reduce the effects of heating-cooling of the tool. The tests did not cover the full spectrum of combinations. However, some findings can be extracted from their results.

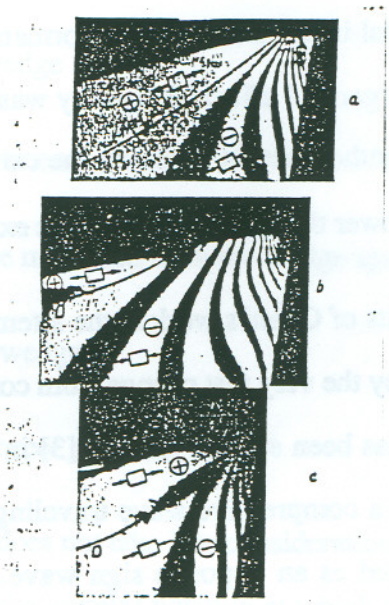

Fig 2.21: Thermoelasticity experiment showing stress patterns.
a)Entry, b)Stationary and c)Exit cuts [16]

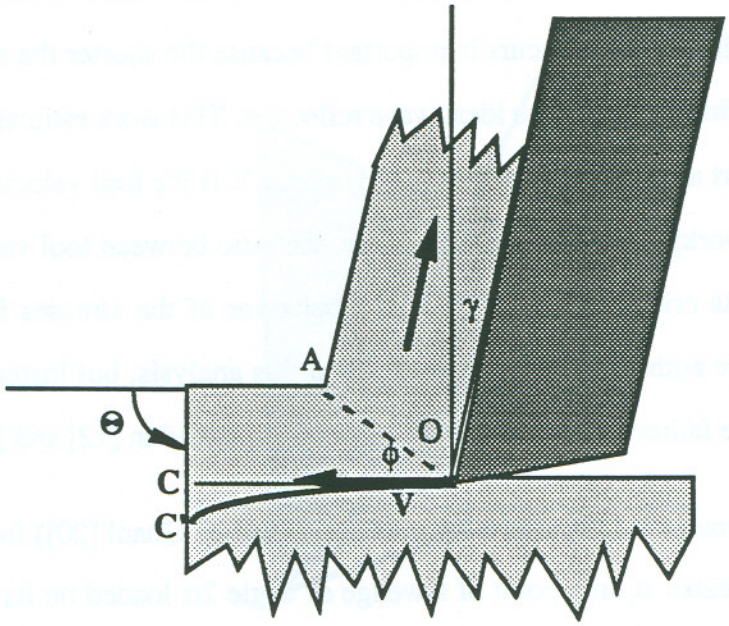

Fig 2.22. Shear Directions OA, OC and OC' for uniform and exit cut ([20]).

It was found that positive geometries were more likely to fail in exit stages. On the other hand keeping other parameters constant, velocity in the neighborhood of 150-175 m/min was found to produce a local increment in the performance of the tool by allowing more exits before failure, but the general effect of velocity was to decrease the number of exits before failure. On keeping other factors constant, the exit angle Θ value has to be as far away from 90° in order to lower the rate of failure at the exit.

One of the interesting results of Ghani's work is the attempt to relate tool failure to stress reversal in the tool caused by the very fast change from compressive to tensile stress in the rake face. Stress reversal has been studied also by [3] in relation with impact dynamics. This study establishes that a compressive wave traveling in a medium will reach a free surface and will be reflected as an opposite sign wave. Thus the wave will turn from compression to tension upon meeting the insert boundary. This kind of switching will go on several times because the wave will travel back and forth inside the body until it exhausts the energy available. In this case, the insert is steadily loaded in compression during normal cut, but this situation is altered when it is released from the cut at exit. The time in which this transition occurs is important because the shorter the time is the closer will the actual behavior reflect the ideal wave reflection. This work estimates the unloading time for the insert as t=OC/V (see Fig 2.22), where V is the tool velocity and OC is the distance to the workpiece exit wall. Obviously, the ratio between tool velocity and stress waves velocity is critical for estimating the behavior of the stresses inside the body. Unfortunately the author did not further develop this analysis, but instead presented the idea of workpiece failure along the line OC' already explained in [12] and [13].

Nakamura & Yamamoto [39] used a formula (also used by Ghani [20]) for calculating the radial normal stresses σ_r in a point of a wedge of angle 2α loaded on its tip by a force P acting at an angle β with the wedge axis of symmetry (see Fig 2.23). This formula is given by:

$$\sigma_r(r,\theta) = \frac{2P}{rb}\left(\frac{\cos\beta\cos\theta}{2\alpha + \sin(2\alpha)} + \frac{\sin\beta\sin\theta}{2\alpha - \sin(2\alpha)}\right) \qquad (2\text{-}7)$$

where α = half of the wedge angle.

β = the angle between the force and the axis of symmetry of the wedge.

r = radial distance measured from the wedge apex.

b = width of the wedge.

P = the applied force.

It can be seen that this equation does not take into consideration the velocity of cut V. Also, no reference is made in [39] to the angular position at which the stresses are evaluated to arrive at the numerical values. It is assumed that they are calculated for $\theta=\alpha$ and r=h/3 which is the place claimed by several authors where the tool is expected to fail more frequently.

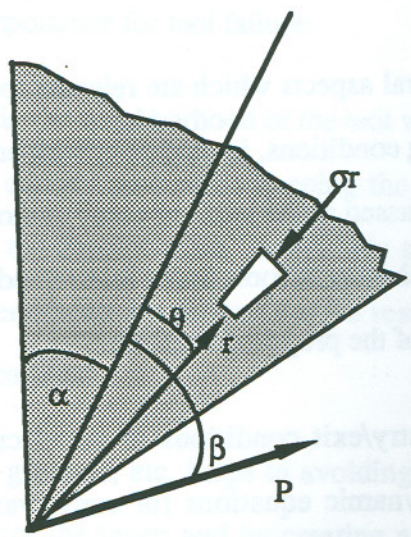

Fig 2.23 Wedged tool abstraction loaded in its vertex.

For austenitic steel the failure is observed regardless of the fact that a foot is formed at exit. For this particular material and insert a very strong tendency to chip welding on the rake face has been reported. This produces subsequent failure in the next entry even in the zone of "safe" entry conditions. In this case, it would be safer to use positive geometries with regard to entry safety, since they allow for less material accumulation. Cast iron seems to be a very advantageous material, since it does not adhere to the insert face, and thus avoids pitting and chipping. From the point of view of stress reversal, cast iron is favorably compared to austenitic steel or low alloy steel whose properties are such that stress reversal reaches levels high enough to break the tool. In conclusion, this work shows that tool failure at entry/exit is dependent on the type of the work materials as follows:

i) For carbon and low alloys steels at low velocities the tool wear is caused by face pitting. At high speeds the mechanism is stress reversal and the failure is caused by chipping.

ii) For stainless steels tool failure is caused by chip adhesion which negatively influences later entries. The failure is chipping

2.6 Summary

As shown above several aspects which are relevant to the reaction of tool and workpiece under transient cutting conditions, in particular with entry/exit cuts have been considered. The aspects were discussed in the work of many authors. Some of the important elements which influence the behavior of tools under interrupted cut are summarized below in order to focus on the scope of the proposed research.

1. In modeling of entry/exit conditions in metal cutting the three important factors considered are: (i) dynamic equations for conservation of momentum, (ii) geometry interaction and, (iii)- material properties.

From these, estimation of the material properties is by far the most difficult task because large of the number of factors involved,in changing the behavior of tools. Among these factors are the chemical affinity between tool/workpiece materials which influence pitting and build-up, temperature effects which change the workpiece strength, and the effect of contact area geometry on material properties.

An effort has been exerted to know the kind of effects present in entry /exit conditions in metal cutting. It has been found from different sources that the deformations are in the elastic-plastic range with strain rates of 10^1-10^4 sec^{-1} and that damage numbers are about 10^{-4} , which allows for estimating contact forces as hydrostatic (neglecting hydrodynamic effects). This estimation also establishes the fact that friction forces are modeled as proportional to the contact normal force and not as a function of the cutting speed as in "drag" coefficients, which are characteristic of hypervelocity impact.

2. The stress analysis performed by Pekelharing, and the other researchers ([16] , [20] , [39]) presents very interesting and plausible conclusions about the nature of failure at exit stages as supported by photographic techniques and thermoelasticity experiments. In this work the following aspects are of importance for tool failure:

(i) Failure of the workpiece in the neighborhood of the exit wall causes some other effects including: reduction in the contact area while keeping the same level of forces, stress reversal phenomena inside the insert which change the state of stresses from compression to tension. These phenomena are difficult to be resisted without causing failure of the tool materials such as carbide.

(ii) The existence of lands, grounds, etc, helps in avoiding the early fracture by eliminating the most sensitive part of the insert and by creating a local (rake) negative geometry which loads the insert in compression rather than in tension. The penalty to pay

for this protection is a significant reduction in tool life as far as wear and non-early damage is concerned.

(iii) The geometry of entry/exit situations is critical for the tool survival. For example entry/exit with the cutting speed vector normal to the workpiece wall produces the highest risk, and angles departing from 90° protect the tool at the price of piercing of the workpiece material.

(iv) The analytical studies reported in the literature are concerned with situations of orthogonal cut in which the cutting speed vector is normal to the workpiece walls. For other cases, the majority of data comes from experimental (statistical) data.

3- There are extremely contradictory reports about the level of forces and the specific force coefficients in the neighborhood of entry/exit positions. Wallen [14] found that the specific force coefficients increase significantly at exit and also at entry under certain conditions such as TiN coating. In contrast, Pekelharing [12] dismissed the role of forces as the main causes of tool failure, preferring the theory of workpiece failure as a cause of early tool failure. This uncertainty extends also to the role of cutting speed in tool failure. The work by Asai [11] shows that depending on the tool material, higher speeds may harm the tool (TiC insert) while in other cases higher speeds represent the safe zone for the insert under any engagement / disengagement conditions (P20 insert). Kronenberg, for example, found that higher area derivatives (dA/dt) are associated with more tool wear.

4- Until now, one of the aspects which promises to constitute an important point in the study of entry/exit interaction is the geometrical modeling aspect. However, this aspect has not been fully exploited owing to the fact that the geometry in this case is extremely involved and difficult to be handled by closed form equations. The computational 3D modeling attempts in this direction have a handicap because they don't give any

quantitative figure for evaluating the impact factors. Parameters like Contact Area, Area Derivative, S-T-U-V interaction are not assessed and evaluated.

This is the reason for devoting an important portion of this thesis to develop a module which allows for the 3D description of insert and workpiece geometry, and for the particular attention given to the entry and exit interaction between insert and workpiece for turning and fly cutting face milling. This module will be used to expand the idea by Kronenberg and Asai with respect to the influence of S-T-U-V interaction on tool life.

Although this literature survey has intended to be as extensive as possible, many more references exist which have not been mentioned here. Only the ones which represent an important result, or those which enclose many others have been included. In this respect, the works by Pekelharing and by Wallen have shown to be very valuable. Other authors whose contribution is central to this work are Kronenberg, Asai and Johnson.

The main objectives of this thesis are:

1- Evaluation of the cutting forces in entry/exit cuts. In particular, it is intended to analyze the source of variation of the cutting forces as compared to the ones registered in continuous cuts.

2.- Evaluation of the effect of insert, tool and workpiece geometry in the cutting forces in entry/exit. Although the several attempts made in this direction covered cases such as orthogonal geometries and straight side inserts, they have not covered the effect of the geometries used in manufacture, such as K lands, rounded corner (nos radius), different rake and lead angles, etc.

In order to fulfill the above objectives, a series of interrupted cut tests will be run using cast iron as the workpiece material, in such a way that the entry/exit conditions represent the most critical conditions reported in the surveyed literature. Cuts with the velocity

normal to the entry/exit workpiece walls will be performed. The cutting forces during these experiments will be recorded, and compared with the static (uniform cut) forces for the same cut/insert. This comparison is expected to tell whether the entry/exit forces present a significant deviation from the static cutting forces. Since the tests will be run for different cutter and insert geometries, the effect of these factor upon the forces will be assessed.

Since the geometrical part seems to be a key part in the analysis of tool failure in interrupted cuts, a 3D geometry module will be developed in order to be able to analyze, correlate and quantify the role of the different geometrical parameters in the prediction of cutting forces in entry/exit cuts.

CHAPTER 3

FORCE MODEL FOR INTERRUPTED CUT

This chapter presents a general force model for the characterization of entry/exit cutting forces. The proposed model consists of four modules. Each of the four modules will be analyzed and its significance will be discussed. Based on this analysis a simplified force model for the entry/exit cutting forces will be developed.

3.1. A General Model for Interrupted Cuts

The proposed general model assumes that the tool entry/exit cutting forces are similar in nature to those present when two bodies (tool and workpiece) collide in space. The contact forces result in changes in the kinematics of the bodies as well as in their material properties (yield strength, hardness,etc). Shape is also changed if permanent deformation is produced. A change in position directly affects the area of contact between the tool and the workpiece and leads to a change in the forces. The change in velocity causes a change in the material properties which in turn affects the cutting pressure coefficients that are used in force models.

The overall entry/exit force characterization model is divided into four modules: a) prediction of forces, b) determination of changes in positions and velocities, c) computation of instantaneous chip area, and d) determination of the change in material properties as result of the rate of application of loads and velocity changes.

A diagram of the proposed model is depicted in Fig 3.1. Module 1 calculates the contact forces based on the material properties (cutting force coefficients) and the contact area. Once the forces are determined, their effect on the position and velocity of the tool and workpiece are established in Module 2.

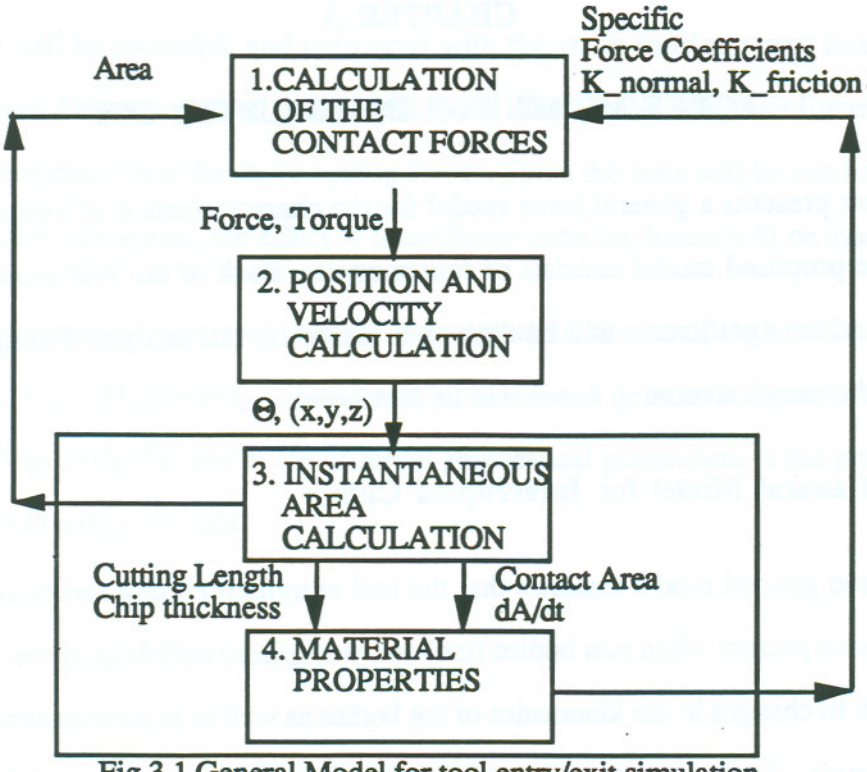

Fig 3.1 General Model for tool entry/exit simulation.

The relative positions of the tool and workpiece determine the contact area between them. Module 3 provides the necessary geometric information and computes the instantaneous contact area. Based on the prevailing velocities the rate of change of the contact area between the colliding bodies is also computed in this module. The information about contact area is fed back to Module 1. Module 4 calculates the properties such as strain rate and compressive stress of the material based on the rate of change of area, the cutting length, the chip thickness and other relevant geometric information. Finally, the cutting pressure coefficients are fed back to the force calculation module and the procedure is repeated. A more detailed explanation of each module follows:

3.2 The Force Calculation Module

This module applies the basic assumptions made in solving the problems of colliding bodies, such as the existence of a force normal to the contacting surfaces, and a friction force tangent to them. The friction force accounts for the loss of momentum in the direction tangent to the contact surfaces while the normal force accounts for the loss of momentum in the normal direction as shown in Fig 3.2. This approach has been applied to the analysis of impact between solid bodies by several investigators. However, the difficulty in formulating such a force model is in the determination of the values for the characteristic constant K of the material and the friction coefficient to be used for estimating the normal and friction forces respectively. These coefficients are calculated in some cases based on values found in material properties tables that apply to very specific and controlled conditions, such as elastic deformation, which by definition does not apply to the metal cutting process. The approach used here will be discussed further in the material properties module.

The normal and friction forces arising when an insert is engaged in cutting can be written (in vector form) as:

$$\mathbf{Fn} = K.An.\mathbf{n} \qquad (3\text{-}1)$$

$$\mathbf{Ff} = \mu . Fn . \mathbf{Vf}$$

$$= \mu . K . An . \mathbf{Vf}$$

$$= Kf . An . \mathbf{Vf} . \qquad (3\text{-}2)$$

where:

Fn, Ff are the vectors representing the normal and friction contact forces

n	is the unit vector normal to the insert face.
Vf:	is unit Vector representing the direction of Ff
Fn, Ff	are the scalar values of the normal and friction forces
An	is the scalar representing the normal area to the insert
μ	is the friction coefficient, and
Kn,Kf	are the scalar force normal and friction coefficient.

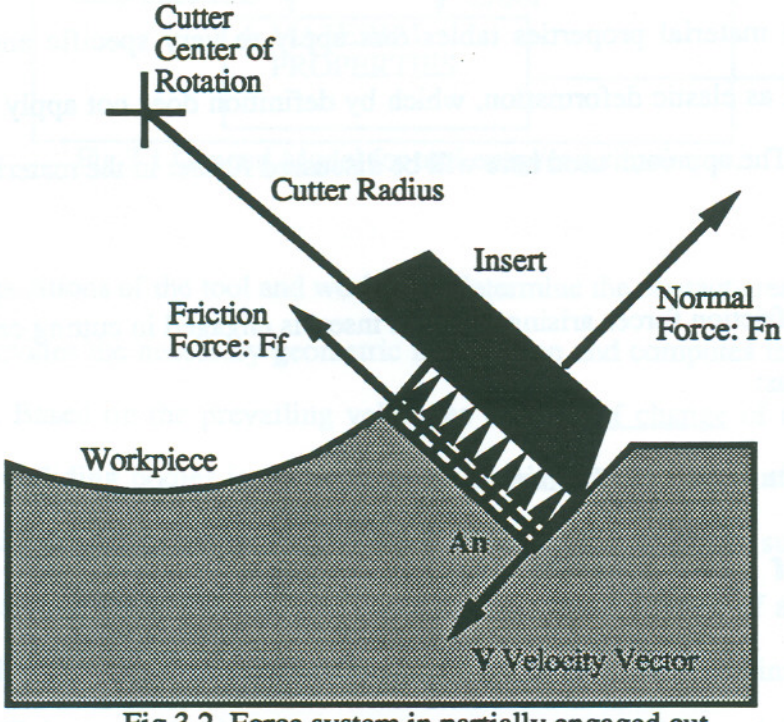

Fig 3.2. Force system in partially engaged cut.

At this point the discussion refers to a generic solids which collide; the **n** vector is normal to the contacting surfaces, the friction force vector **Vf** is in the direction of relative slipping of the bodies. As it can be seen, this analysis is similar to the mechanistic modeling which has so far proven to be useful for continuous cuts. However, the objective of the present

work is to assess the force coefficients Kn, Kf which are applicable to entry/exit regions in the cutting process (In order to keep a nomenclature uniform with [27-29,32] Kn,Kf will be referred to as Kc, Kt from now on).

It is important to note that the contact forces scheme proposed above is a more generalized form of the mechanistic model. This is evident from the mechanistic model approach reported by Fu [30] which is based on the calculation of the two coefficients, Kc and Kt. These coefficients are considered to be the specific cutting pressures for a given tool/workpiece material and tool geometry. When multiplied by the chip contact area they give the cutting and thrust (or friction) forces, Fc and Ft, i.e:

cutting force $\quad Fc = Kc \cdot At \cdot vc \quad (3\text{-}3)$

thrust force $\quad Ft = Kt \cdot At \cdot vt \quad (3\text{-}4)$

where Kt,Kc are the Thrust and Cutting Force Coefficients

vc it the unit vector in the direction of insert velocity

vt it the unit vector coplanar with the rake face, and

At it the chip contact Area in the direction of insert velocity

The direction for the cutting force (for face milling it is the same tangential force) is clearly defined, while the direction of the thrust force is ambiguous. The reason for this ambiguity is due to the fact that although it is known that the thrust force acts in the rake plane, its exact direction actually depends upon the direction of the chip flow on this face. If it is assumed that this direction is normal to the cutting edge in oblique cuts, then, a continuously changing cutting edge (in the nose radius, for example) presents many elementary cutting edges, whose normal direction lying in the rake face constitutes the flow

direction of each elementary chip. In this thesis an approach similar to that is adopted for predicting the direction (vt) and the magnitude (Ft) of the thrust force Ft. The form of the equation that will be used is:

$$|Ft| = Kt(\bar{\bar{tc}}) * At \qquad (3\text{-}5)$$

$$vt = \frac{Ft}{Ft} = \frac{1}{L}\int_{\lambda=0}^{\lambda=L} f(\lambda)\, d\lambda \qquad (3\text{-}6)$$

where Kt is a function of $\bar{\bar{tc}}$, the average chip thickness, defined as

$$\bar{\bar{tc}} = At/L$$

where

L	=	cutting length
At	=	Area in the direction of insert velocity
$f(\lambda)$	=	vector representing the local chip flow direction at a particular position λ on the cutting edge.
vt	=	direction of the thrust force.

These two equations mean that the magnitude of the thrust force is to be calculated as the contact Area times the Kt coefficient, and its direction vt as the average of the unit vectors $f(\lambda)$ normal to the cutting edge and contained in the rake plane as shown in Fig 3.3. For this interpretation it is assumed that the force is uniformly distributed along the cutting edge.

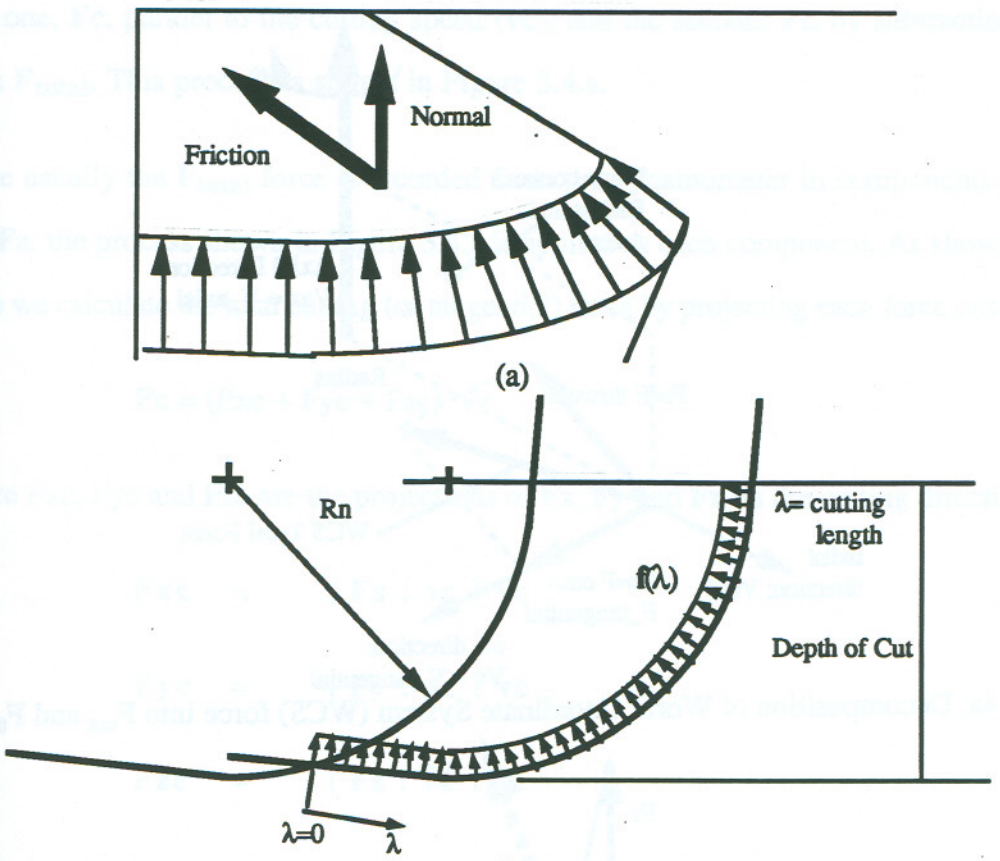

Fig. 3.3. a) Variation of chip flow direction along the cutting length in a K-land insert.
b) f(λ) : the local chip flow direction as function of the position along the cutting edge.

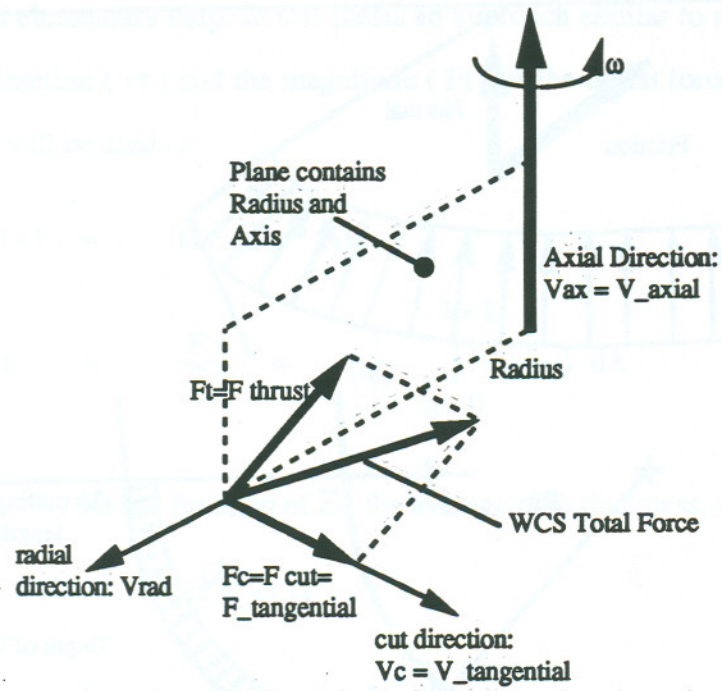

Fig. 3.4a. Decomposition of World Coordinate System (WCS) force into F_{cut} and F_{thrust}.

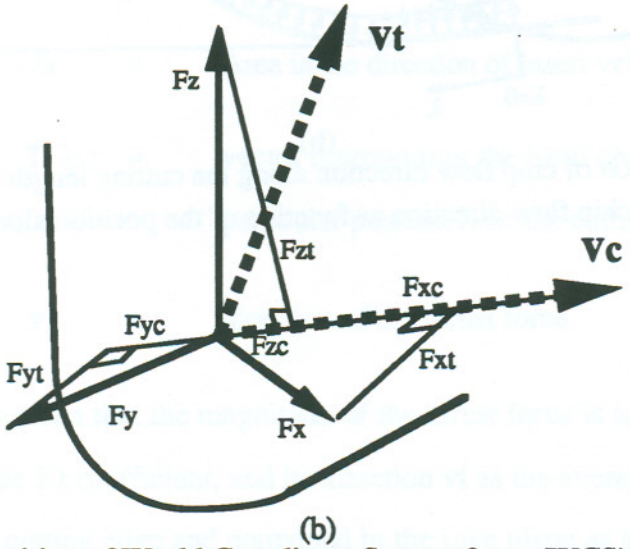

(b)

Fig. 3.4b. Decomposition of World Coordinate System force (WCS) by components Fx, Fy, and Fz into F_{cut} and F_{thrust}.

In order to evaluate the merits of the model it is necessary to find the relation between the forces in the Tool Coordinate System (TCS), **Fc**, **Ft**, and the (measurable) forces in the World Coordinate System (WCS) $\mathbf{F_{total}}$. In order to obtain the **Fc,Ft** forces from the WCS forces it is necessary to decompose the WCS force $\mathbf{F_{total}}$ into two directions: The

first one, **Fc**, paralel to the cutting speed (**vc**), and the second, **Ft**, by subtraction of **Fc** from $\mathbf{F_{total}}$. This process is shown in Figure 3.4.a.

Since usually the $\mathbf{F_{total}}$ force is recorded from the dynamometer in components **Fx**, **Fy**, and **Fz**, the process shown in Figure 3.4.a is applied to each component. As shown in Fig 3.4.b we calculate the total cutting (or tangential) force by projecting each force onto **vc**:

$$\mathbf{Fc} = (\mathbf{Fxc} + \mathbf{Fyc} + \mathbf{Fzc})\ \mathbf{vc} \qquad (3\text{-}7)$$

where Fxc, Fyc and Fzc are the projections of **Fx**, **Fy** and **Fz** on the cutting direction **vc**:

$$\mathbf{Fxc} = (\mathbf{Fx} \cdot \mathbf{vc})\ \mathbf{vc}$$

$$\mathbf{Fyc} = (\mathbf{Fy} \cdot \mathbf{vc})\ \mathbf{vc}$$

$$\mathbf{Fzc} = (\mathbf{Fz} \cdot \mathbf{vc})\ \mathbf{vc}$$

Once the projections in the cutting (tangential direction) are known, the components of the forces in the thrust direction can be calculated as:

$$\mathbf{Fxt} = \mathbf{Fx} - \mathbf{Fxc}$$

$$\mathbf{Fyt} = \mathbf{Fy} - \mathbf{Fyc}$$

$$\mathbf{Fzt} = \mathbf{Fz} - \mathbf{Fzc} \qquad (3\text{-}8)$$

$$\mathbf{Ft} = \mathbf{Fxt} + \mathbf{Fyt} + \mathbf{Fzt} \qquad (3\text{-}9)$$

The vectors **Fxt**, **Fyt** and **Fzt** are perpendicular to the **vc** vector by construction. The plane which contains those vectors is formed by the axis **Vax** of the tool and a radial vector **Vrad** which points from the center of the cutter to the insert (as shown in Fig 3.4a).

By using **Vrad** and **Vax** the thrust force can be further decomposed into radial and axial directions:

$$\mathbf{Frad} = (\mathbf{Ft} \cdot \mathbf{Vrad})\,\mathbf{Vrad} \quad (3\text{-}10)$$

$$\mathbf{Fax} = (\mathbf{Ft} \cdot \mathbf{Vax})\,\mathbf{Vax} \quad (3\text{-}11)$$

The experimental chip flow direction can be expressed as

$$\mathbf{vt} = \mathbf{Ft} / |\mathbf{Ft}| \quad (3\text{-}12)$$

The decompositions of the forces measured in the World Coordinate System into tangential, radial and axial forces assume that the vectors in the direction of the cutting speed **vc** , the radial direction **Vrad** and the axial direction **Vax** are known. In general, the decomposition of forces is much easier if 3D vectors are used instead of computing the transformations with direct trigonometry calculations.

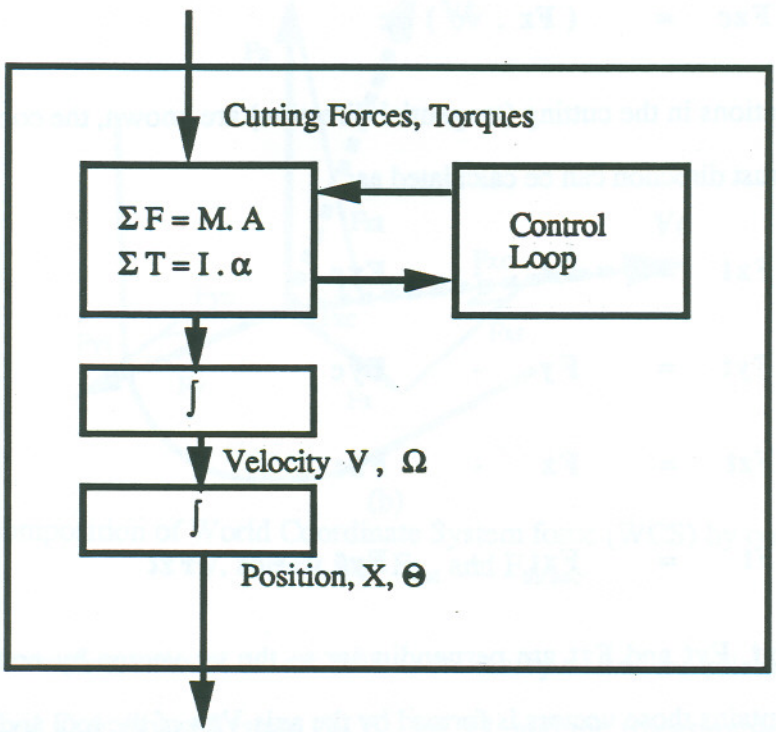

Fig 3.5. Module 2 expansion. Balance of forces acting upon the tool/workpiece system.

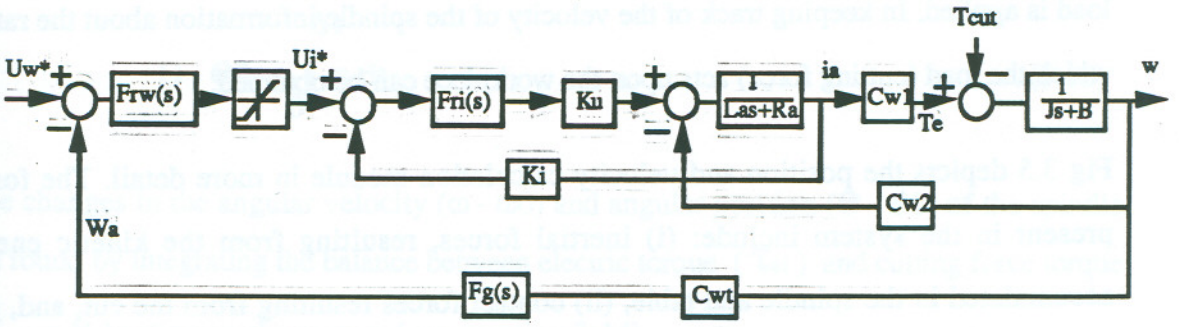

Fig 3.6. Control loop of the face milling spindle drive.

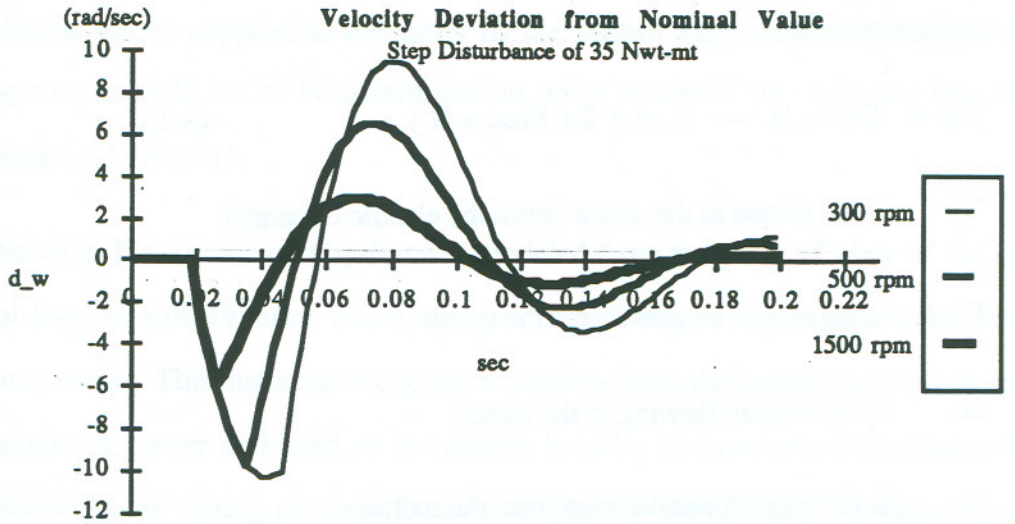

Fig. 3.7. Deviation from steady state speed by effect of disturbance.

3.3 Position and Velocity Calculation Module

This module calculates the balance of forces acting on the bodies (i.e. tool spindle and workpiece attached to the slide table) which participate in the collision during cutting. Some simplifications are made by assuming that the change in the linear momentum of the slide is negligible. The approximation follows from considering the slide as having a very large mass, and/or being driven by a very powerful motor. This simplification implies that Newton equations have to be integrated for the spindle only. The need for accurately knowing the effect of the contact forces on the velocity of the spindle arises from the fact that material properties such as yield stress are frequently dependent on the rate at which the

load is applied. In keeping track of the velocity of the spindle information about the rate at which the load (cutting force) acts upon the workpiece can be obtained.

Fig 3.5 depicts the position and velocity calculation module in more detail. The forces present in the system include: (i) inertial forces, resulting from the kinetic energy accumulated in the spindle and table, (ii) contact forces resulting from the cut, and, (iii) external (electric) forces coming from the control loop of the machine tool. The balance of forces can be written as:

$$\tau_{el} = Cw1 \,.\, Ia = I \,.\, \alpha + \Sigma (\mathbf{Fcut} \times \mathbf{R}) \qquad (3\text{-}13)$$

with τ_{el} is the torque to the motor (from the electric circuitry)

Cw1 is the torque constant form the motor

Ia is the current flowing to the motor

α is the angular acceleration from the motor

R is the radius of application of each cutting force

I is the inertia of the motor-spindle-tool ensemble.

Fcut is the cutting force

The preceding ecuation means the electric torque is spent in two ways: (i) for increasing the velocity of the spindle and (ii) for overcoming the cutting forces. It is assumed that the loss of energy to friction is small compared to the cutting force and inertial force terms.

Aas mentioned earlier the changes in the speed of the table are neglected:

$$\omega - \omega 0 = \frac{1}{I} \int_0^{\Delta t} (\tau_{el} - S (\mathbf{F_{cut}} \times \mathbf{R})) \, dt \qquad (3\text{-}14)$$

$$\Theta - \Theta 0 = \int_0^{\Delta t} \omega \, dt \qquad (3\text{-}15)$$

The changes in the angular velocity ($\omega - \omega 0$) and angular position ($\Theta - \Theta 0$) of the spindle are found by integrating the balance between electric torque (τ_{el}) and cutting force torque ($F_{cut} \times R$) acting on the system (see equation 3-14).

The electric torque supplied to the motor by the control loop which is dependent on the cutting torque itself has to be determined in order to obtain ($\omega - \omega 0$) and ($\Theta - \Theta 0$) in equations 3-14 and 3-15.

As shown in Fig 3.6 the cutting force is modeled from the point of view of the spindle control loop as a disturbance which changes the velocity of the spindle away from the reference setting. This disturbance triggers a response from the control loop which changes the amount of power delivered to the system in order to overcome the additional load represented by the cutting process . In order to quantify the effect of this disturbance it is necessary to model the control loop of the motor as shown in Fig 3.6.

In the block diagram the following notation is used:

$$\omega = \omega_{actual} - \omega_{steady\_state} \qquad (3\text{-}16)$$

$$Uw^* = \Omega_{command} - \omega_{steady\_state} \qquad (3\text{-}17)$$

It is of interest to study the effect of the cutting torque T_{cut} on the angular velocity ω. The transfer function (based on the paramters shown in Table 3-1) from T_{cut} to ω is calculated as:

$$\frac{\omega}{T_{cut}} = \frac{-(1+Fa.Fri.Ki.Ku)}{(sJ+B)(1+Fa.Fri.Ki.Ku) + (Fg.Frw.Fri.Fa.Cw1.Cwt.Ku) + (Fa.Cw1.Cw2)} \qquad (3\text{-}18)$$

If the cutting forces are known, the evolution of the angular velocity can be calculated by using the transfer function in equation (3-18) which includes the torque balance equation (3-13) and the effect of the action taken by the control loop of the motor to keep the velocity constant.

In this way the velocity and position of the spindle for any existing electrical or cutting force configuration can be calculated without resorting to the approximation which assumes that the only forces acting during the entry/exit conditions are the contact forces.

3.4 Instantaneous Contact Area Calculation Module

The methods for computing the chip area proposed by Endres [28] and Radulescu [33] present some limitations when applied to entry/exit cuts. Their approach to calculate the instantaneous chip area considers the effects of the dynamics on the deflections of the machine, the tool and the workpiece which affect the effective feed and depth of cut and cause variations in the contact area. These methods do not account for the case of entry/exit cuts where the tool is partially engaged with the workpiece. The entry/exit cutting problem is very significant to the the proposed research for the following reasons:

Table 3.1. Motor Drive Parameters

Name of Components	Parameters	Constants	Transfer Functions
Equivalent DC Brushless Spindle Drive Fa(s)	B J L_a R_a	0.02158 kgm^2/s 0.04041 kgm^2 0.0063 H 0.45 W	$\frac{1}{Js+B}$ $Fa(s)=\frac{1}{Las+Ra}$
Torque Constant	Cw1	0.91 Nm/A	
Back e.m.f.	Cw2	0.91 Vs/rad	
Tacho Gain	Cwt	0.0286 Vs	
Tachometer	T_g	0.0004 s	$Fg(s)=\frac{1}{Tg\ s\ +\ 1}$

Dynamic Fg(s)			
Velocity Loop Controller Frw(s)	Kpw Kiw	2.805 V/V 241.0 s^{-1}	$Frw(s)=\frac{Kpws+Kiw}{s}$
Current Feedback	K_i	0.05 V/A	
Cur. Loop Gain	K_u	13.0 V/V	
Current Loop Controller Fri(s)	Kpi Kii	240. V/V 1200000.s^{-1}	$Fri(s)=\frac{Kpis+Kii}{s}$
Current Limit	Ia(max)	50 A	

1. Recall that the instantaneous average chip thickness $\bar{t}c$ for fully engaged cut is computed using:

$$\bar{t}c = Ac / lc \qquad (3\text{-}19)$$

where $\bar{t}c$ is the average chip thickness, Ac is the contact Area measured in the rake face and lc is the cutting length.

In some cases of partial engagement of the tool with the workpiece the computation of $\bar{t}c$ using equation 3-19 causes some numerical difficulties. For example in the case of a "U" engagement tool condition (see Fig 2.1; Kronenberg's classification of engagement/disengagement) the part of the tool which first enters the workpiece is located on the rake face, not along the cutting edge. This produces zero cutting length and a finite value of contact area; making $\bar{t}c$ infinitely large and, hence, the cutting force coefficients very small. However, this computational aberration is not likely to occur frequently, and most of the cutter-insert-position conditions are not likely to show this kind of behavior.

2. The literature review has indicated that factors such as "bluntness" in the tools, chamfers on the inserts, and engagement-disengagement angles and regions (S-T-U-V) have important effects in the performance of the tool. Up to now, techniques such as finite element analysis have been applied to orthogonal cuts, very simple geometries and fully engaged cuts. It is desirable to have a computational tool which handles a variety of insert

geometries, cutters and workpieces, and which allows for quantitative as well as qualitative analysis of partially engaged cuts.

3. The time derivative of the contact area (dA/dt), can be shown to be related to the strain rate of the material and therefore influences the strength of the material in high speed deformation . A method to quantitatively estimate the evolution of engaged geometry with respect to time is needed.

4. One of the reasons for tool failure in interrupted cuts is the increase in the forces arising from the excitation of the set up and resulting dynamics. The shape of the force history function at the cut transition conveys the information about the frequency content of the force signal, and therefore about the response of the structures of the machine tool and workpiece to the forces. The more abrupt the engagement, or the shorter the engagement-disengagement period the higher the frequencies present in the force signal, and the higher the frequencies excited in the structure of the machine/tool/workpiece.

Based on the above considerations a contact area calculation module is proposed. The module utilizes solid model geometry techniques in order to take into account several important geometrical features, including:

1. shape and dimensions of the insert (chamfers, lands, arbitrarily shaped inserts)

2. orientation (axial and radial rake angles, as well as nominal lead angle).

3. cutter diameter.

4. cutting conditions such as Depth of Cut, feed per tooth (the program will initially consider fly cutting).

5. relative position cutter / workpiece.

The proposed procedure is aimed at providing accurate qualitative as well as quantitative geometrical data (based on type of engagement for example), without resorting to approximations which are present in the current chip area calculation modules developed up to now [28][33].

3.5 Material Properties Evaluation Module

This module (see Fig 3.9) makes use of the information provided by the contact area calculation module (contact area, length derivative of the contact area, cutting length and chip thickness), in order to evaluate the material properties (cutting force coefficients) that are used in the force calculation module. The properties of interest are essentially the flow stress pressure, represented by Kn in eq. 3-2, and the friction force coefficient represented by Kf, or μ in eq. 3-2. Based on those values the model estimates the contact forces present during in the collision of the tool and workpiece and simulates the kinematics of the tool when entering the workpiece.

There are several ways to estimate the Kn, Kf coefficients:

1) If the strain, ε and strain rate $\dot{\varepsilon}$ are known, information from material properties tables [51] can be used to find the flow stress of the workpiece material. It is important to stress the fact that the calculation of the stress using $Sy=f(\varepsilon, \dot{\varepsilon})$ as specified from laboratory tests is a simplification for the following reasons:

i) The values of ε and $\dot{\varepsilon}$ which are present in real machining environments come from conditions such as non-orthogonal cuts, partial engagements, multi-axial load, etc., which depart form the simple situations of steady state orthogonal cut. In spite of this differences many times the values found from orthogonal conditions are comparable in orders of magnitude with the predominant values under non-ideal circumstances.

ii) Strain-Stress experiments are performed under very controlled constant strain rate conditions and moreover they don't include in any way the effect of different combinations of tool/workpiece materials, coatings, etc. According to Fineberg's work [47], in which extensive literature was compiled about material properties estimation, the relation in the plastic stage between uniaxial flow stress and true strain is:

$$\sigma = \sigma 1 \cdot \varepsilon^{n} \qquad (3\text{-}20)$$

where σ = uniaxial flow stress

ε = true strain = ε(shear strain along shear plane, γ)

$\dot{\varepsilon} = \dot{\varepsilon}$(shear velocity Vs, length of shear plane ls)

$\sigma 1 = \sigma 1(T, \dot{\varepsilon})$

$n = n(T, \dot{\varepsilon})$

some authors ([7]) propose specific models for $\sigma 1$ and n;

$$\sigma 1 = a5 + a6 \log 10(\dot{\varepsilon}) \qquad (3\text{-}21)$$

$$n = a7 + a8 (\log 10(\dot{\varepsilon}))^2 + a9 (\log 10(\dot{\varepsilon}))^3 \qquad (3\text{-}22)$$

where a5, a6, a7, a8, a9 are constants which depend on the material. This set of relations holds for orthogonal cut and uniaxial load. Applying the values found in the charts or tables to metal cutting or collision phenomena where conditions are not controlled is risky because the premises for using the values don't hold. This approach of finding material properties presents two disadvantages: first, there exist always difficulty in obtaining the material properties as functions of high strain rates [47] , being difficult enough to calculate the strain rates themselves; second, the constants in equations (3-20) to (3-22) have to be calculated from laboratory experiments or cutting tests in any case.

2. Metal Cutting experiments can be run to find Kn and Kf values by the application of mechanistic models approach. This alternative produces good results for the prediction of the stationary cutting forces as shown in [33][29] but its value in dealing with transient forces is still an open question. In calibrating the mechanistic model for Kn, Kf coefficients, the force readings close to the engagement/disengagement parts are usually disregarded, Only fully engaged tool force readings are considered. This alternative has the advantage of including factors such as combination tool/workpiece materials, insert geometry, etc, but it has the disadvantage that it has to be applied on a case by case basis. If a different material for the workpiece and/or tool is used, or new tool geometries are tried, new tests have to be run in order to obtain estimations for the Kt, Kf coefficients in the new conditions.

The difficulty in estimating parameters like strain rate its effects on change of the properties of the materials requires a simplified module. This simplification will be discussed in section 3.6.2.

3.6 Simplified Force Model

The modules, as discussed above give complete account for the phenomena that occur in the entry/exit cuts. However for the purpose of this research some of these modules may be simplified without significantly affecting the effectiveness of the model in its final form. This section explains the simplifications made to the model.

3.6.1 Simplification of the Position and Velocity Calculation Module

The importance of the servo drive forces and inertial forces as compared to contact forces in the particular case of the spindle in a horizontal milling machine is evaluated in this section. It is necessary to estimate the extent by which the cutting forces affect parameters such as the spindle velocity in interrupted cuts. The change in velocity, in general, has an effect upon material properties, and the objective is to estimate how large is the change and if this

change is significant how much it will affect properties such as flow stress, which is dependent upon strain rate and thus on the velocity of the cut.

With the transfer function as expressed in equation (3-18) the effect of cutting torque on angular velocity can be determined by modeling the cutting force as a disturbance for the control loop of the motor. A cutting torque of 35 Nwt-m (approx 150 lbs tangential force in a 5 in. cutter) is applied to the system as a disturbance to the original setting of the nominal spindle speed. In figure 3.7 the deviation of the velocity signal from the steady state (reference) value due to the cutting torque disturbance is shown for three values of the angular velocity: 300, 500 and 1500 rpm. As can be seen, the variation in the velocity is esentially the same for the three levels, being proportional to the applied torque. The length of the time interval in which the cutting force is applied determines the magnitude in the drop of the spindle speed. Since for 300 rpm the engagement time is longer than for 1500 rpm, the retarding effect of the cutting force in this case is also greater. Additionally, the inertial force is smaller for the 300 rpm case, making the recovery from the disturbance input more difficult. On the other hand, by having a bigger inertial force (as in cases of high velocity) the control loop has to provide smaller control signals. In other words , the inertia itself is able to maintain the levels of velocity nearly at the same levels, without strong demands on the control loop.

Fig 3.8 shows the effect of the cutting torque on the angular velocity (Fig 3.7 deals with the deviation from the steady state value). Again, in the case of higher speeds (1500 rpm) the effects of the shorter disturbance time and the higher inertia levels make the drop in velocity smaller both in absolute and relative terms.The drop in velocities for 300, 500 and 1500 rpm are 32%, 17% and 3% respectively

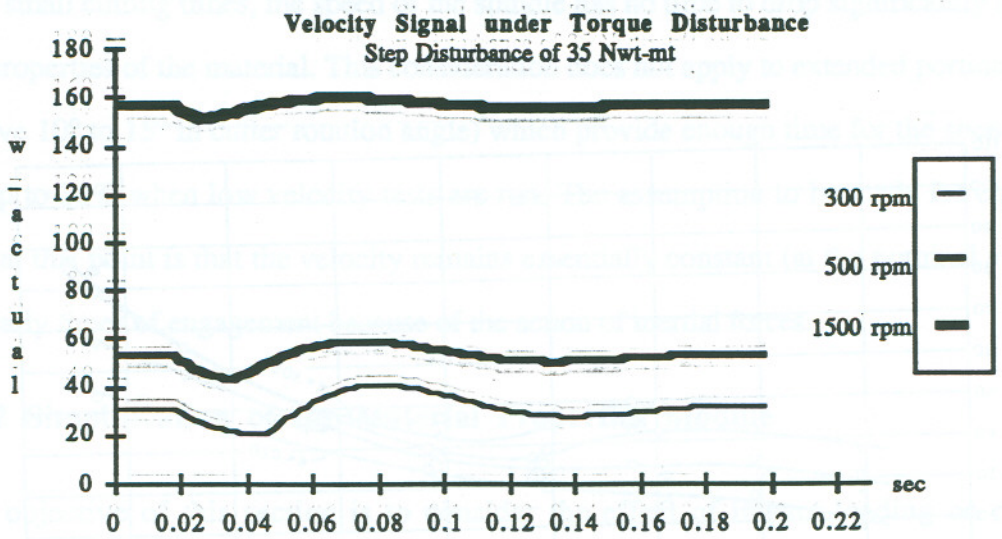

Fig 3.8. Velocity History as affected by a cutting torque disturbance.

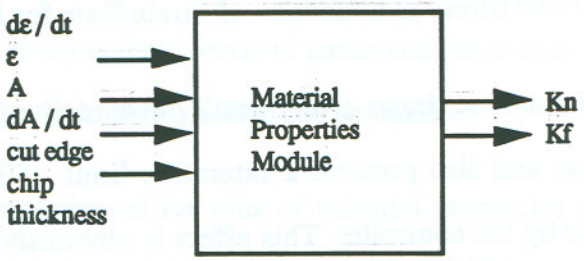

Fig 3.9. Information flow for the Material Properties Module.

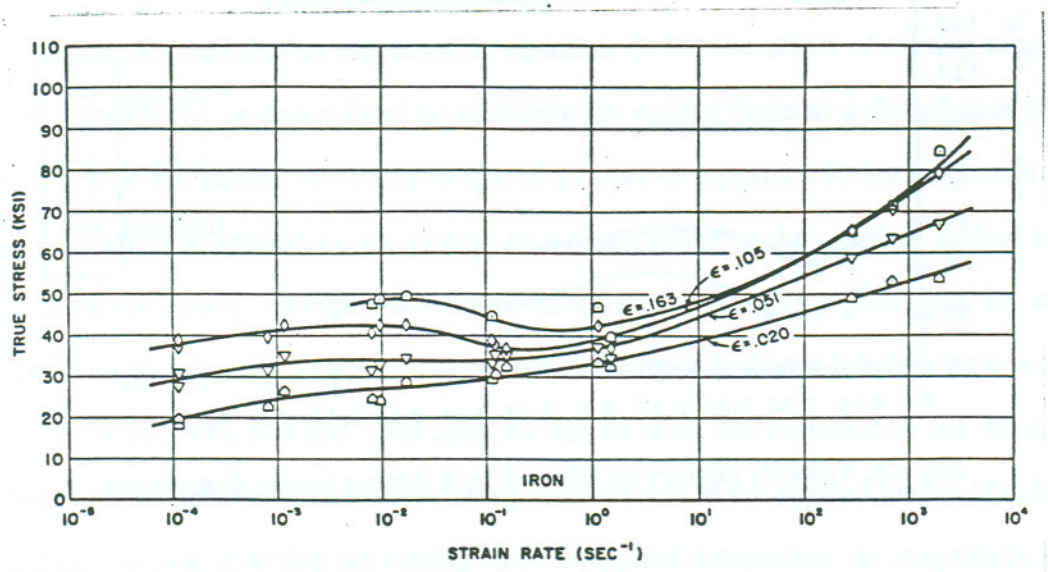

Fig 3.10. Flow Stress as a function of Strain Rate for Iron. [51]

The motor drive of this machine shows a very small power delivery in the linear range, a very long recovery time, and also presents a saturation limit (50 Amps) in the current deliverable to the motor by the controller. This effect is obviously more critical at lower speeds where the cutting forces sometimes are able to stop the spindle.

From this discussion we can conclude that the effect of cutting torque upon velocity variation is not significant in the very early instances of tool entry, although it certainly slows down the spindle at the full engagement stages if the inertial forces are not big enough.This means, we can assume that the properties of the material at the engagement stage is to be the same as those at the nominal cutting speed since the velocity drop is not substantial at the beginning.

Based on this fact, module 2 can be simplified, thus making the existence of external forces (such as electric torque from the motor) insignificant to the determination of cutting forces which are confined to very small portions of the insert trajectory inside the workpiece. For

very small cutting times, the speed of the spindle has no time to drop significantly to affect the properties of the material. This consideration does not apply to extended portions of cut (above 10° to 15° in cutter rotation angle) which provide enough time for the speed to fall by up to 30% when low velocity tests are run. The assumption to be made for entry/exit cuts at this point is that the velocity remains essentially constant (at the nominal value) in the early times of engagement because of the action of inertial forces.

3.6.2 Simplification of the Material Properties Module

The objective of this section is to consider the effect of impact loading on material properties, to establish a set of considerations for that effect, and to decide the way to calculate material properties in the proposed model. The procedure is to use the estimated strain and strain-rates involved in tool engagement/disengagement, for examining the sensitivity of the flow stress to these levels of strain and strain-rate. Based on this, the form of the material properties estimation module can be decided.

Many authors have investigated the area of material properties under shock or impact conditions. It has been estimated that shock is produced if the time of application of the load is of the same order of magnitude or less than the longest natural period of vibration of the piece considered. If the time is greater than that, it is considered as static load. The literature review shows that the properties of materials under impact differ significantly from the static case.

A parameter used to measure the dynamic characteristic of the loading is the strain rate $\dot{e}$. It is defined as the unit deformation per time unit ($\dot{e} = (dl/dt)/lo$). Several authors have published charts and tables which relate the properties of materials at high stress rates with the static properties such as Yield strength, Ultimate Strength, Total elongation, the ratio Yield_strength/Ultimate_Strength, etc. A chart of flow stress as a function of strain and strain rate for cast iron is shown in Fig 3.10. The two problems to be addressed are the

estimation of the order of magnitude of $\dot{\varepsilon}$, and the relation of $\dot{\varepsilon}$ to the material properties of interest. For this purpose an analysis of dimensionless quantities will be used. In order to estimate the order of magnitude of the strain rate a unidirectional stress wave propagation is assumed [4], following Fineberg's approach of the problem as uniaxial load, such that

$$\varepsilon = \frac{v}{c} \cong 0.001 \qquad (3\text{-}23)$$

where ε: strain ([L]/[L])

v: impacting velocity ([L]/[T])

c: compressive stress wave speed ([L]/[T])

The time of engagement for an unfavorable cutting condition[1] is in the order of magnitude[2] of 10^{-3} sec . With this estimate, by using equation (3-23) for ε the value of $\dot{\varepsilon}$ is [10^{-2} - 10^{2}] sec^{-1}. From the chart presented in figure 3.10 for cast iron and the given range of strain rates the flow stress is found to be between 30 and 60 kpsi. On other hand, for a variety of cast irons the maximum static compressive stress is around 1100 Nwt/mm2 (160 kpsi).

From the previous works [33][29] with mechanistic models it has been found that the coefficient for Kn, is of the order of magnitude of 2400 Nwt/mm2 (340 kpsi). This means that the cutting coefficients are much greater than the static compressive strength or any flow stress estimated based on the strain rate.

---

1 Following the literature review results, the velocity vector would be nearly perpendicular to the entry/exit plane of the workpiece.

2 This calculation comes from software 3D_MCUT for a double negative face milling tool rotating at 500 rpm, and entering the work at a plane perpendicular to the cutting speed.

In conclusion it can stated that there is a lack of trustable database of the dynamic compressive strengths, in particular for the material being considered (i.e. cast iron), as well as a lack of an accurate method to estimate $\dot{\varepsilon}$. The approach to be followed in this research is to calibrate a model similar to the Kn, Kf coefficients using the geometrical configurations characteristic of entry/exit cuts.

Module 4 deals with calibrating the coefficients Kt, Kc of the mechanistic model based on the forces measurements of the interrupted cut experiments. The measurement of those forces is another complete topic by itself. The reason for the difficulty in measuring these forces is that sharp transitions carry a strong component of high frequency harmonics, exciting the dynamics of the machine tool, and also of the measurement device (dynamometer) which supports the workpiece. This issue will be dealt with in detail in chapter 5.

3.7 Summary

In this chapter the analysis procedure of colliding bodies has been applied to the tool entry/exit in metal cutting. Simplifications have been made to the initial model mainly in reference to:

1) External forces: It has been shown that in metal cutting applications the inertial forces of the motor-tool ensemble keep the impacting velocity along a time interval long enough after the impact.Also it has been shown that for the particular motor to be used the control loop acts very late, the effect of it being that velocity is essentially kept by inertial effects, not by an injection of power from the control loop. The effect of deceleration by cutting forces and/or dynamics from the control loop are negligible when compared to the inertial forces, which maintain the cutting speed essentially constant.

2) Estimation of material properties: It has been shown that, although there exist plenty of models to calculate flow stress as a function of strain and strain rate for a given material,

this approach has two disadvantages: First, the assumptions for these models are uniaxial loads, unidirectional stress wave propagations and orthogonal cut. Second, they rely on coefficients and parameters which have to be experimentally obtained. Based on these considerations the determination of material properties has been approached as an extension for the mechanistic model by introducing the concept of partial-engagement chip load and chip thickness. The decomposition of the World Coordinate System (WCS) forces into Tool Coordinate System (TCS) forces allows to express the specific force coefficients Kn and Kf as a function of the average chip thickness and cutting velocity.

The analysis of chip removal poses heavy demands on the geometry module. On the other hand, the use of extensive 3D geometry information is shown in the decomposition of the forces between World Coordinate System and Tool Coordinate System as an easy way to achieve those decompositions. It is of interest to be able to express the complex geometries that tools, inserts and workpieces have. It is required that a geometry module be able to express features such as back and side rake angles, lead angle, nose radius, k lands, grounds, chamfers, special contour inserts departing from the traditional rhomboid, square or triangular shapes, instantaneous scene configuration as in relative positions tool-axis/workpiece, angular position of the cutter, direction of the feed, partially engaged cuts and variety of workpiece wall inclinations. Also cutting parameters such as feed, depth of cut and velocity should be fed into the model. .

The advantage of having a 3D geometry module is that extension of concepts such as effective lead angle for inserts such as K land ones with complicated edges and land geometries is very straightforward. The reason for this is that there is no need for approximating 3D situations with their 2D simplifications. Local negative geometries such as the one found in K land inserts are easily included for modeling since the effective lead angle in this case can be evaluated in the space rather than in a plane, rendering the results of force directions directly in three dimensions. Further decomposition of these forces into

World Coordinate System and Tool Coordinate System are immediate. As said before these extensions impose certain requirements upon the geometry module. The way these requirements will be satisfied is treated in Chapter 4, Geometry 3D Model.

CHAPTER 4

GEOMETRY 3D MODEL

Although several factors such as temperature, material properties, vibrations, etc, influence impact forces and tool wear, it has been recognized by several researchers that the geometry of the insert, the workpiece, and their relative positions play an important role in the phenomenon of generation of impact forces. The relative velocity of the bodies (insert and workpiece in this case) also plays a significant role. Apparently, it has to do with the rate at which the contact area develops, and also with the shape and growing patterns of this contact area, as well as the locations on the insert from where it starts (at the beginning of the cut) and ends (at the exit). This chapter discusses a geometric 3D model which takes into account different geometric characteristics of the cutter (insert and tool holder) and the workpiece, and allows to accurately calculate the contact area, its derivative, and evaluates the patterns of area growth on the insert.

For a given geometry of the workpiece, cutter and insert combination, and cutting parameters such as feed per tooth and depth of cut, the model allows the calculation and display of the contact area between the insert and the workpiece, for different angular positions of the cutter. The capabilities of the model are specially directed toward analyzing the partial engagement present during the entry/exit cuts.

The model deals with fly face milling cutting and turning with constant depth of cut. It deals with inserts whose contour can be described as a closed sequence of lines and arcs. Additionally, inserts with negative land (K land) can be specified as long as their land contour is parallel to the external contour of the insert.

Another objective of the 3D modeling of tool / insert / workpiece is to be able to easily transform force and area vectors among several coordinate systems, and to calculate

parameters such as the effective chip flow direction by direct handling of spatial functions without having to recurs to 2D simplifications for these concepts.

As mentioned before, the advantage of developing the 3D geometric model is that the extraction and manipulation of information is easy by applying matrix and vector techniques. On the other hand, the construction and updating of solid models is much more involved than treatment of 2D models.

In the following sections explanations are given as to why several representations for the solid objects are required, what are the main issues dealing with the translation among them, and how the information represented is used to calculate the decomposition of force and area vectors, and evaluation of 3D effective lead direction, etc. Also, geometrical transformations which help to update the objects as the simulation of the tool engagement progresses are presented. The results of the computer implementation of the model are also discussed.

4.1 Overview of the 3D Geometry Module

The geometry module is presented in Fig 4.1. It comprises of two main parts: first, the creation of insert, tool and workpiece representations and second, simulation of cut, object intersection and object update. The INSERT SOLID MODEL CREATION module creates representations for the insert, which are used by the CUTTER SOLID MODEL CREATION module to represent the tool. The tool representation is used to calculate the workpiece object in the WORKPIECE SOLID MODEL CREATION module. These modules belong to the first part of the geometry module. The second part, which is directed to the simulation of cut, places the workpiece and tool objects in the space (INITALIZE SIMULATION module), calculates their intersection (SOLID INTERSECTION) derives the contact area and effective lead direction; calculates the forces (FORCE CALCULATION module) by using the material properties, and updates

the tool object by a rotation angle (TOOL ROTATION module) for the next step of simulation.

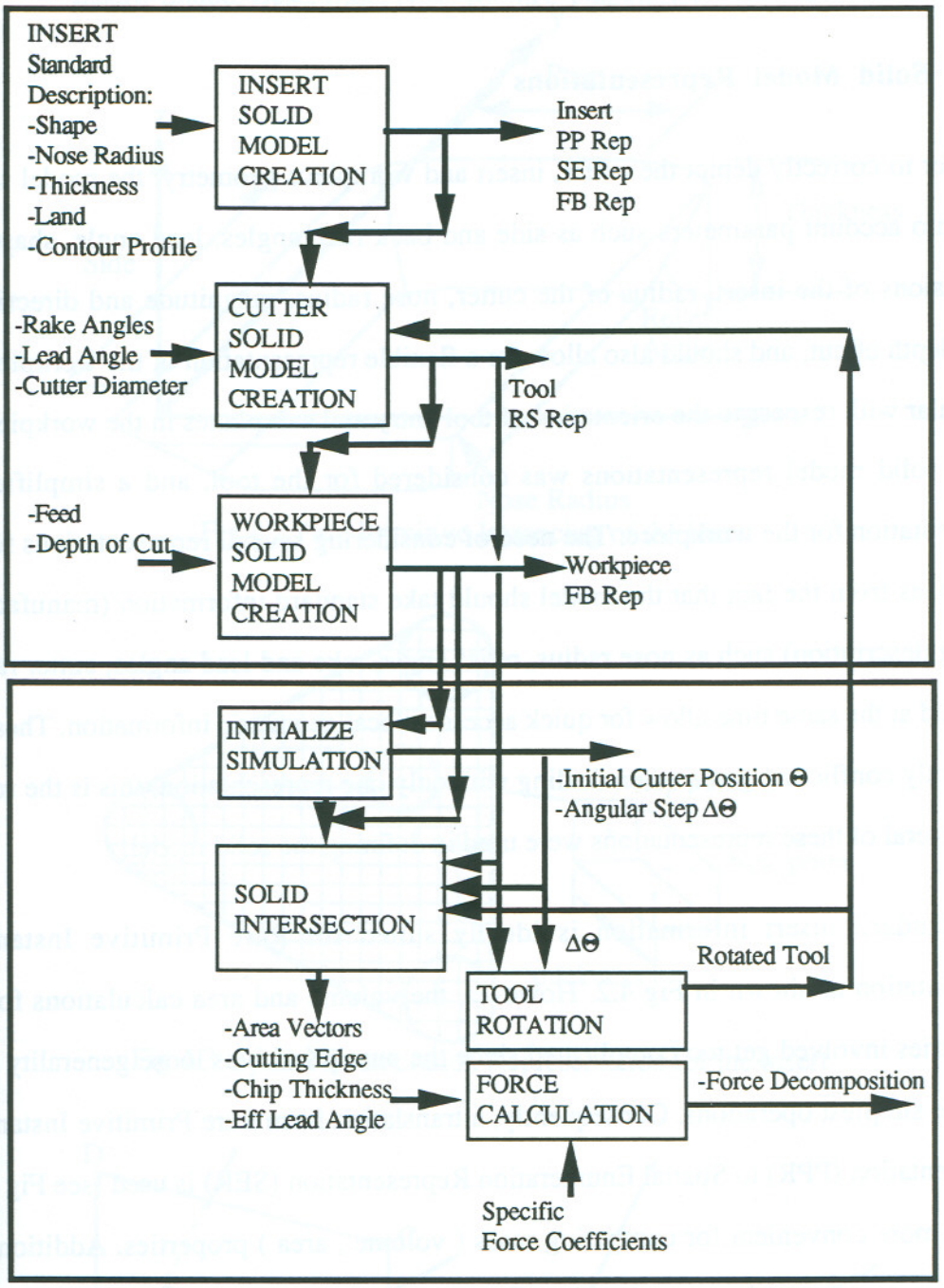

Fig 4.1. Block Diagram of the 3D Geometry Module

In the following sections the geometry aspects of these modules are discussed, starting from the first part which deals with the representation of the objects, and followed by the second part, which deals with the definition of geometry of the simulation parameters. The

FORCE CALCULATION module, which calculates the forces, has been already discussed in Chapter 3.

4.2. Solid Model Representations

In order to correctly depict the cutter, insert and workpiece geometry, the model should take into account parameters such as side and back rake angles, lead angle, shape and dimensions of the insert, radius of the cutter, nose radius, magnitude and direction of feed, depth of cut, and should also allow for a flexible representation of the workpiece, in particular with respect to the orientation of tool entry and exit planes in the workpiece. A set of solid model representations was considered for the tool, and a simplified B-representation for the workpiece. The need of considering several representations for the tool arises from the fact that the model should take standard information (manufacturer catalog description) such as nose radius, relief angle, rake and lead angles, cutter radius, etc. , and at the same time allow for quick access to local geometric information. These are frequently conflicting goals when dealing with only one representation; this is the reason why several of these representations were used in defining the solid model.

The standard insert information is ideally suited for Pure Primitive Instancing representation as shown in Fig 4.2. However, the volume and area calculations for the geometries involved get too complicated since the pure primitives loose generality even with the simplest operations. Consequently, a translation from Pure Primitive Instancing Representation (PPR) to Spatial Enumeration Representation (SER) is used (see Fig 4.3). SER is more convenient for computing mass (volume , area) properties. Additionally, geometric transformations required in this case to express rake and lead angles, cutter radius, feed and depth of cut are straightforward when applied to the points which constitute the cells in the enumeration in contrast to applying them to a whole entities like circles, lines, arcs, angles, etc.

Insert(Shape, Base, Side, Nose Radius, Thickness)

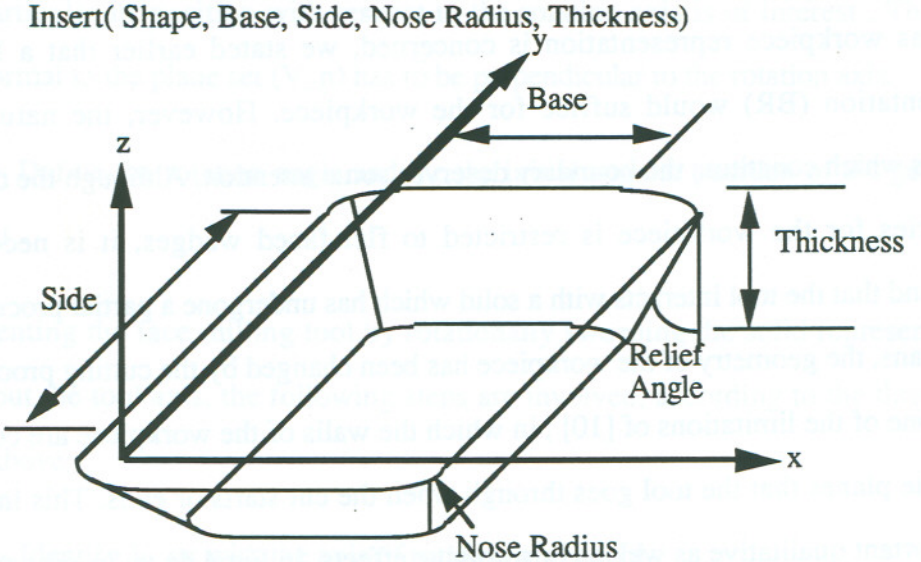

Fig 4.2 Pure Primitive Instancing of the Insert

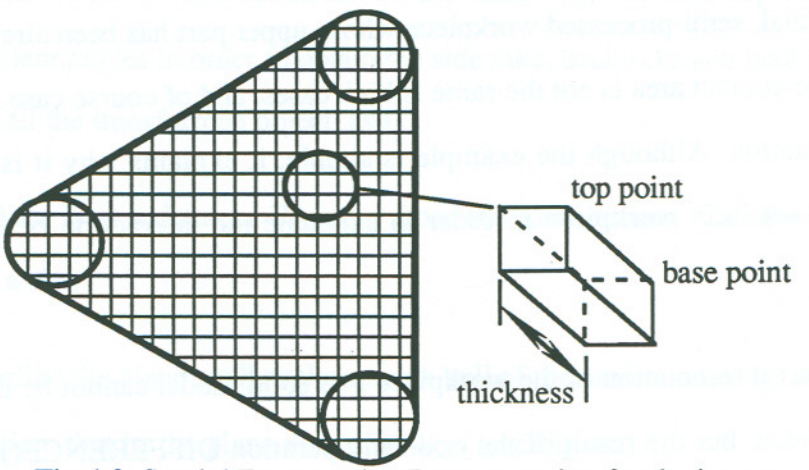

Fig 4.3. Spatial Enumeration Representation for the insert

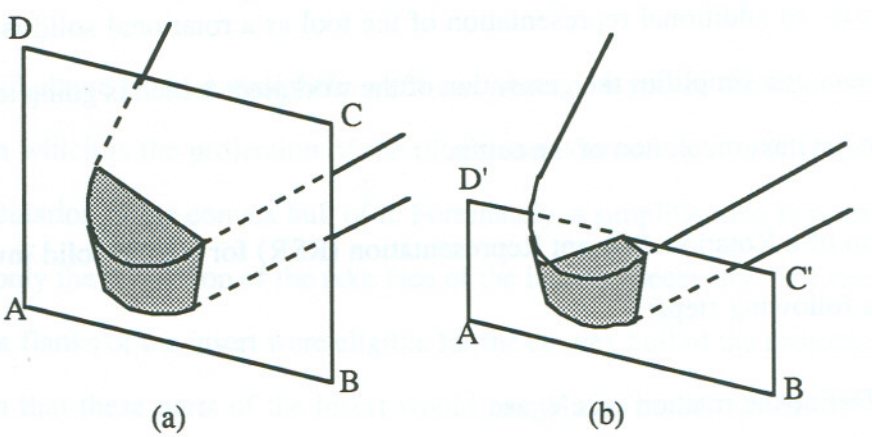

Fig 4.4 .Entry of tool in (a) semi-infinite solid; (b) partially cut solid

As far as workpiece representation is concerned, we stated earlier that a Boundary Representation (BR) would suffice for the workpiece. However, the nature of the elements which constitute the boundary deserves some attention. Although the domain of geometries for the workpiece is restricted to flat faced wedges, it is necessary to understand that the tool interacts with a solid which has undergone a partial process of cut. That means, the geometry of the workpiece has been changed by the cutting process itself. This is one of the limitations of [10] , in which the walls of the workpiece are considered as infinite planes that the tool goes through when the cut starts or ends. This inaccuracy has important qualitative as well as quantitative effects. In Fig 4.4a an insert penetrates a infinite plane ABCD; in 4.4b it penetrates a limited plane ABC'D' which represents the wall of an actual, semi-processed workpiece whose upper part has been already removed. Obviously the contact area is not the same is both cases, and of course case (a) represents an unreal situation. Although the example is simple, it explains why it is necessary to consider the semi-cut workpiece in order to calculate the interaction between the two bodies.

Therefore, the representation of the workpiece as a solid model cannot be the untouched initial workpiece, but the result of the boolean operation DIFFERENCE() between the former workpiece and the solid engendered by the tool in its rotation in the prior passes. Consequently, an additional representation of the tool as a rotational solid is necessary. This representation simplifies the generation of the workpiece which is going to be met by the insert in the next revolution of the cutter.

The creation of a Rotational Swept Representation (RSR) for a solid solid involves (see Fig 4.5) the following steps:

1.- Define the rotation axis V_ax.

2.- Define the plane set S which will be swept in order to form the solid. In particular its position with respect to the rotation axis is of interest . The vector normal to the plane set (V_n) has to be perpendicular to the rotation axis.

3.- Define the rotation angle and the the initial angular position of the generating set.

In representing the face milling tool by rotationally sweeping the solid representing the insert about the tool axis, the following steps are involved, according to the three points outlined above:

1.- Identify V_ax with the axis of rotation of the tool.

2.1- Start with a representation of the insert I_0, tilt this representation by convenient angles in order to obtain the side rake, back rake and lead angles of the tool. Call the transformed object as I_1.

2.2- Place I_1 at a distance R_cutter from the rotation axis. Call the transformed object as I_2 .

2.3- Define the plane set S as the convex hull of the projection of I_2 on the plane of projection, that is, the plane normal to V_n (see Fig 4.5).

3.- Define the swept angle Θ as 360° . Initial angle does not matter in this case.

The point 2.3 above is not a straightforward task since it involves the calculation of the plane region which is the projection of the tilted insert onto the plane of projection, and then the calculation of the convex hull of it. Fortunately, a simplification is possible in this case, since only the projection of the rake face of the insert is necessary. The reason is that if the base or flanks of the insert were eligible for the convex hull of the projection, then, it would mean that these parts of the insert would participate in the cut. Since we are not

considering worn inserts for the generation of the partially cut workpiece, it seems reasonable to assume that only the rake face gets involved in the cut. Since the shape of the rake face in commercial inserts is convex, its projection is convex, and we only have to make the projection operation to get the set S. This reasoning also suggests that a Face Boundary Representation (FBR) of the insert is desirable in order to easily access information regarding particular faces of it. Consequently, this translation from PPR to FBR is necessary.

Given that the curves and lines which constitute the boundaries are not simple curves in the space because of this tilt, it is necessary to decompose them into small segments (see Fig 4.12). This means, taking the FBR and exploding the contours into small line sections in order to approach the tool by the revolution of those lines about the tool axis. In Fig 4.5 it is shown how the contour of the insert is used to define the tool data structure.

From the point of view of the workpiece, the original, prismatic workpiece is affected by the pass of the tool. The boolean operation DIFFERENCE() between the original workpiece and the solid created by the prior passes of the cutter defines the current workpiece that the tool is going to meet in the next pass (See Fig 4.6).

The following sections discuss the inputs for the model (Section 4.2.1), the use of these inputs in the representations and the different representations and their respective features (Section 4.2.2)

4.2.1 Model Inputs

Given the insert, tool and workpiece geometries, and feed and depth of cut, the goal of the model developed is to find, for each angular position of the tool, the contact area between the insert and the workpiece. By extending this capability, the history of area engagement and disengagement as function of the angular position of the insert can be calculated.

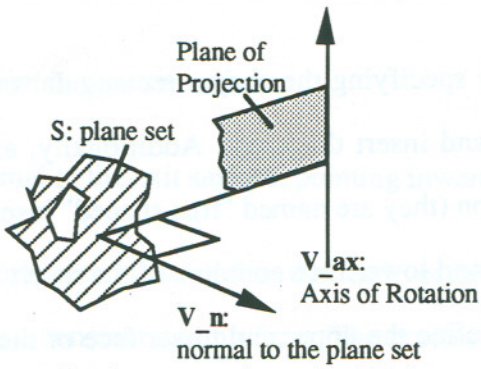

Fig 4.5. Elements for the generation of solids by rotational swept.

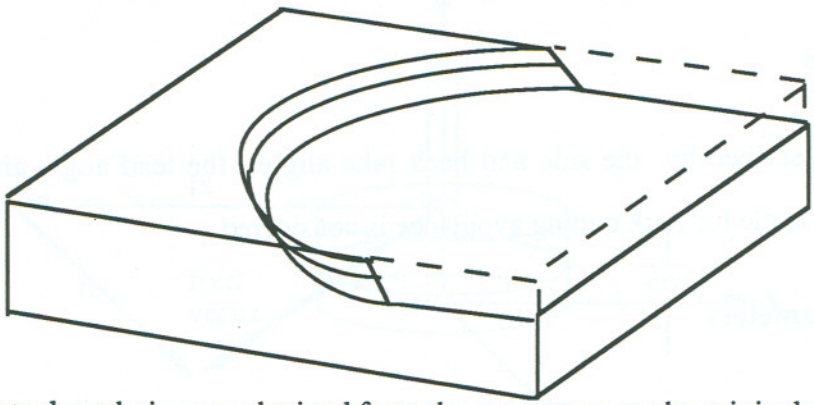

Fig 4.6. Actual workpiece as obtained from the cutter pass on the original workpiece.

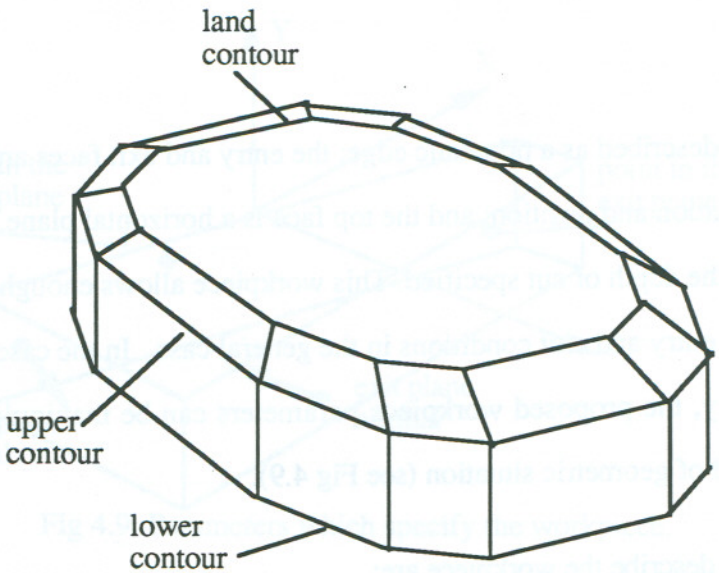

Fig 4.7. Free shaped insert with land and its descriptive contours.

Insert Description

The insert is described by specifying the shape (rectangular or triangular), side length, nose radius, relief angle and insert thickness. Additionally, as there are inserts which don't fit in this classification (they are named "free shaped" inserts), the model allows the specification of the upper and lower face contours of the insert as sequences of lines and arcs in the planes which define the upper and lower face of the insert. In case the insert has a non-flat face (a land on it), the model only considers lands whose contours are parallel to the upper (and lower) contour of the insert. (See Fig 4.7)

Tool Holder

The tool is described by the side and back rake angles, the lead angle and the cutter radius. No tilt angle for back cutting avoidance is considered.

Cutting parameters

The cutting parameters are (see Fig 4.8).feed (described as a vector (fx , fy , fz)) and depth of cut.

Workpiece

The workpiece is described as a prismatic edge; the entry and exit faces are vertical planes of arbitrary orientation and position; and the top face is a horizontal plane, whose position is determined by the depth of cut specified. This workpiece allows enough flexibility as to describe different entry and exit conditions in the general case. In the case of a work with involved geometry, the proposed workpiece parameters can be manipulated in order to approach that kind of geometric situation (see Fig 4.9).

The parameters to describe the workpiece are:

i- An arbitrary point in the entry surface.

ii- The vector normal to the entry surface, pointing inwards to the workpiece.

iii- An arbitrary point in the exit surface.

iv- The vector normal to the exit surface, pointing inwards to the workpiece.

The top surface of the workpiece is parallel to the feed vector, and perpendicular to the tool axis, which produces a constant depth of cut. The precise position of this surface is set depending on the cutter position in order to produce the desired depth of cut.

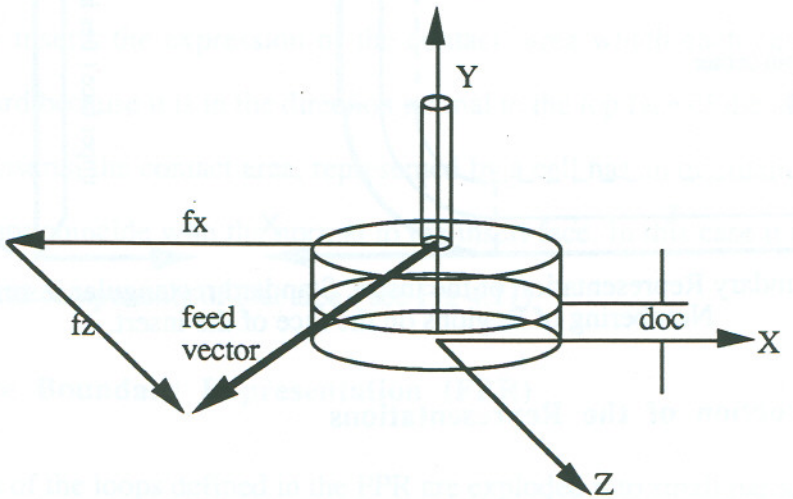

Fig 4.8 Cut parameters FEED and DEPTH OF CUT.

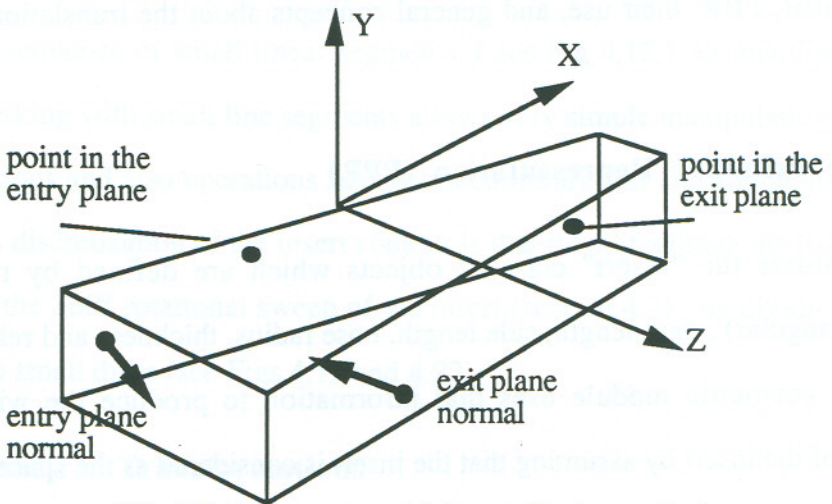

Fig 4.9. Parameters which specify the workpiece.

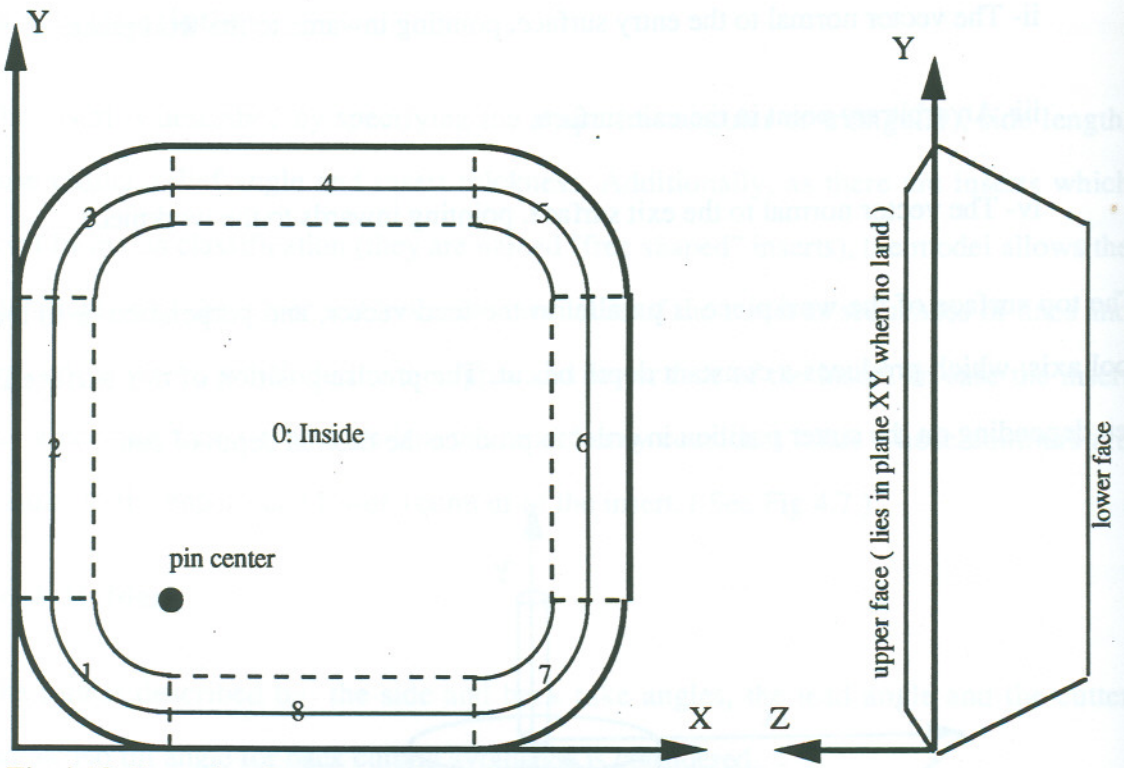

Fig 4.10. Boundary Representation of the insert. Standard rectangular insert with land. Numbering of Regions on the face of the insert.

4.2.2. Construction of the Representations

This section aims at presenting the relation between the different representations used, namely PPR, SER, FBR, their use, and general concepts about the translations among them.

4.2.2.1 Pure Primitive Representation (PPR)

The PPR considers the "insert" class of objects which are defined by the shape (rectangular/triangular) , base length, side length, nose radius, thickness and relief angle. Internally, the geometric module uses that information to produce the wire frame representation of the insert by assuming that the insert is considered as the space between the two flat faces (top and bottom) and a closed sequence of lines and arcs on those faces representing the lateral boundaries. The insert is assumed placed with its working face on

the plane XY (Z=0 unless a land is present) , and the back face shifted by the thickness distance towards the -Z axis. (see Fig 4.10)

4.2.2.2 Spatial Enumeration Representation (SER)

A grid is defined, in which each square cell has the following attributes: one point in the top, one point in the bottom, and a flag which tells if that particular cell of the insert is part of the contact area, in a determined tool / workpiece configuration. An additional mark tells the region in which the cell is included (the regions are labeled as shown in Fig 4.10). For flat face inserts the expression of the contact area which each cell represents is straightforward because it is in the direction normal to the top face of the insert. However, for non flat inserts, the contact area, represented by a cell has an orientation in the space which does not coincide with the normal to the insert face. In this case it is necessary to identify several components of that area (see Fig 4.11)

4.2.2.3 Face Boundary Representation (FBR)

The contours of the loops defined in the PPR are exploded into small parts. For the linear segments this does not represent any approximation; however , we are approaching the arcs as a sequence of small linear segments. (see Fig 4.12.) As mentioned before, the fact of working with small line segments allows very simple manipulations like rotations or translations and also operations like intersections are fast and simple in all sense. The use of this discretization of the insert contour is that it will facilitate the calculation of the tool from the 360° rotational sweep of the insert (section 4.2) , by dividing the resulting toroid into small discs (see Figs 4.13 and 4.22)

4.3. Geometric Transformations

The purpose of this section is to discuss how various inputs regarding the insert, tool holder and cutting conditions are used in the model. These inputs usually describe

standard (manufacturer catalog) information or machining variables, but, in the model they represent geometric transformations (rotations and translations) performed on either the whole objects or on particular parts of them. For example, to simulate the feed, a translation is performed on the whole structure which represents the tool, whereas rake and lead angles are expressed as rotations on a particular part of the tool, namely the insert.

The following sections explain how the 3D geometry module manages information such as rake angles, lead angle, cutter radius, depth of cut and feed and translates this information into geometric transformations applied on the objects defined by the representations discussed in section 4.2.

4.3.1 Interpretation of Rake Angle

For a given geometry of the insert itself, three more parameters are needed to establish the exact position in which the insert is going to cut the workpiece; the back rake (axial rake), the side rake (radial rake) and the lead angle. The first two define the plane which is going to contain the cutting face of the insert; the third one only establishes the position of the cutting edge within that plane. Consequently, if the characterization of the plane in which the cutting face lies is required, it is only necessary to consider the rake angles.

In Fig 4.14 the plane which is going to contain the cutting face of the insert is presented. Positive side and back rakes α_s and α_b are shown where vector $\mathbf{n_1}$ is normal to the rake face. Here it is assumed that the cutting velocity vector of the insert, **V**, is parallel to the **Z** axis. In this discussion **X**,**Y**, and **Z** axis are refereed to as the system in which the insert is defined as in Fig 4.10. The problem to be addressed is to find a set of transformations which will tilt the inset from its position in Fig 4.10 to the position in Fig 4.14, in which its cutting face will have the required rake angles.

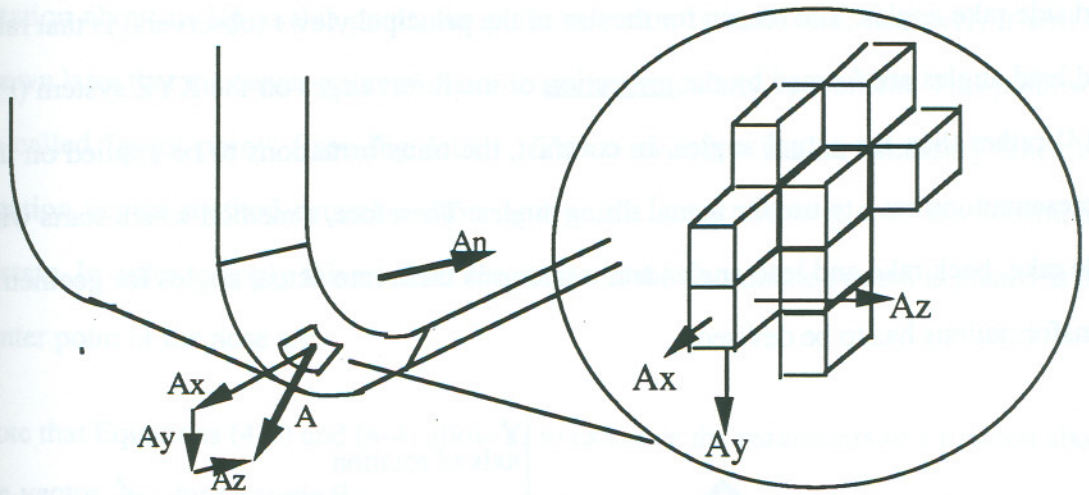

Fig 4.11.Several components of area vector in the case of insert with land. For the flat insert case the component Az turns to be An.

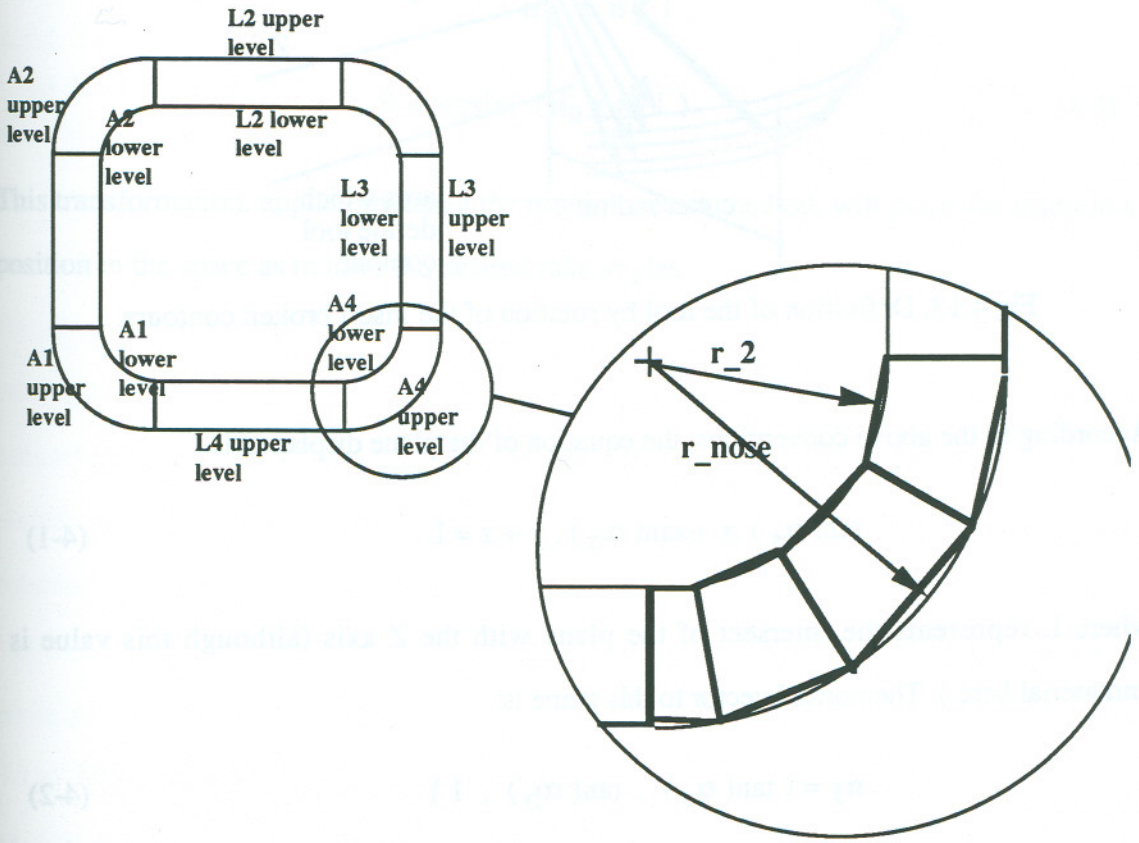

Fig 4.12. Face Boundary Rep and breakdown of it for tool generation

In Figure 4.14 three observers are displayed, meaning that the back rake for example is the angle apparent to the observer labeled "back observer", and so is the case for the lead

and side rake angles. The reason for the use of the principal views (observers) is that rake and lead angles are formed by the projection of the insert edges on the XYZ system (Fig 4.14) rather than the actual angles. In contrast, the transformations to be applied on the representations have to use the actual tilting angles. Therefore, a method which starts with side rake, back rake and lead angles and transforms them into actual angles for geometric transformations has to be devised.

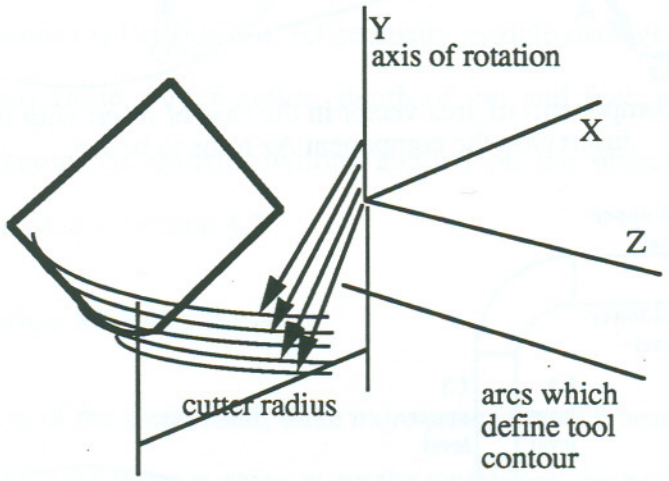

Fig 4.13. Definition of the tool by rotation of the insert broken contours.

According to the above conventions, the equation of the plane displayed is

$$\tan(\alpha_s).x + \tan(\alpha_b).y + z = L \qquad (4\text{-}1)$$

where L represents the intersect of the plane with the Z axis (although this value is unmaterial here). The normal vector to this plane is:

$$\mathbf{n_1} = (\tan(\alpha_s),\ \tan(\alpha_b),\ 1) \qquad (4\text{-}2)$$

The problem now is to find a vector $\hat{\mathbf{e}}_0$ and an angle θ such that the vector $\mathbf{n_0}$ (which represents the normal of the untilted plane), will be rotated on $\mathbf{n_1}$, as would happen if the normals were considered to be attached to the face of the insert. An additional consideration in this case is that it is necessary to "fix" a point on the insert to perform the

rotation about it. Up to this point, the point selection is irrelevant; however, it will be shown later that the center point of the nose arc is particularly convenient. This point will be called "pivot point" (see Fig 4.15). This convention is also necessary since the rotation vector method rotates vectors and points about the origin of the coordinate system. In order to apply this method the origin of the coordinate system is placed at the center point of the nose arc.

Note that Equations (4-3) and (4-4) allow us to calculate the parameters of a rotation about the vector $\hat{e}_0$, by an angle θ :

$$\hat{e}_0 = \frac{\hat{n_0} \times \hat{n_1}}{| \hat{n_0} \times \hat{n_1} |} \qquad (4\text{-}3)$$

$$\theta = \arcsin(| \hat{n_0} \times \hat{n_1} |) \qquad (4\text{-}4)$$

This transformation, applied by using the rotation vector method, will place the insert in a position in the space as to have the desired rake angles.

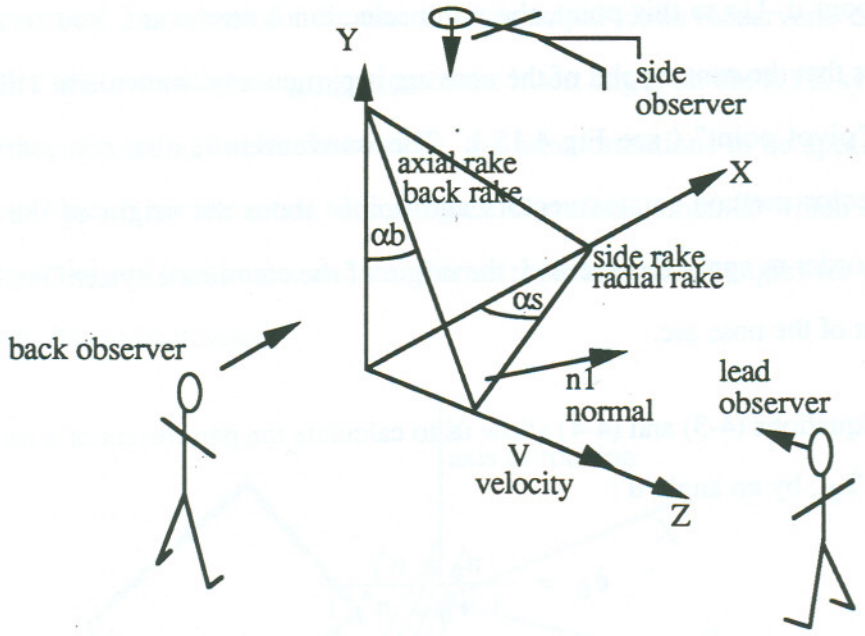

Fig 4.14. Interpretation of rake angles as determining the plane of the cutting face in the insert.

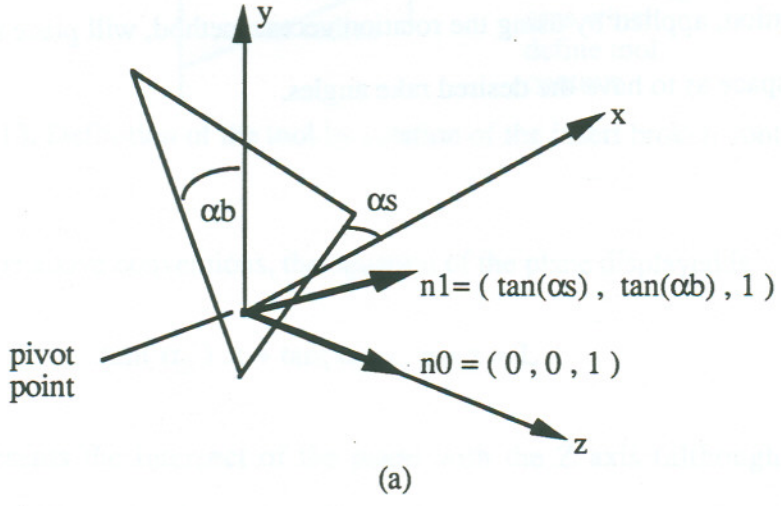

(a)

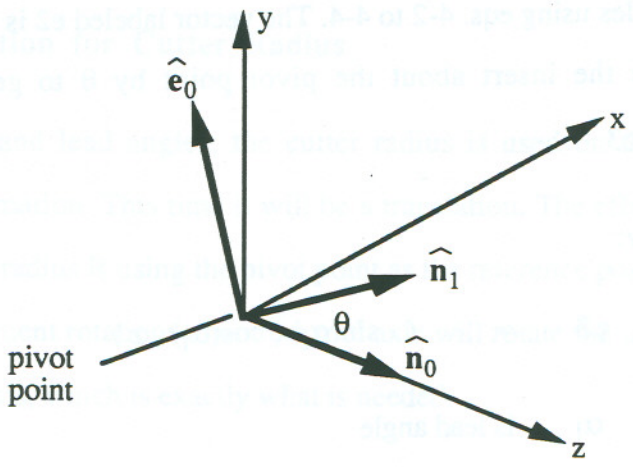

(b)

Fig 4.15. Required change in the normal of the insert to achieve the desired rake angles. (a) Non-normalized vectors. (b) Rotation vector and rotation angle.

4.3.2 Interpretation for Lead Angle

Once the insert is tilted in order to obtain the side and back rake angles, its rake face is on the cutting plane. An additional transformation is necessary to achieve the lead angle. Since the lead angle is the apparent angle presented by the cutting edge to an observer standing in the "lead observer" position (see Fig 4.14), it is necessary to define the cutting edge of the insert. This definition is part of the inputs to the model, and essentially tells which edge of the insert is used to define the nominal lead angle. The problem can be stated as follows (see Fig 4.16): It is desired to use vector **e1**, attached to the insert, as rotation vector, (which guarantees the rake face will remain in the cutting plane). The angle of rotation θ, is such that the lead edge of the insert will arrive at a position where it presents the apparent, nominal lead angle to the observer called "lead observer" in Fig 4.14. However, the rotation angle θ is unknown since the lead angle α_l is an apparent angle measured in the plane perpendicular to the cutting speed while angle θ is measured on the rake plane.

In order to derive the angle θ as function of α_l the cutting edge AB is identified (see Fig 4.17). This cutting edge AB is left in this position when the whole insert is rotated to

achieve the rake angles using eqs. 4-2 to 4-4. The vector labeled **e2** is parallel to AB. It is necessary to rotate the insert about the pivot point by θ to get AB on A'B', or equivalently, **e2** on **e3**.

Vector **e3** is given by:

$$\mathbf{e3} = (- \sin(\alpha_l) , \cos(\alpha_l) , z) \quad (4\text{-}5)$$

where α_l is lead angle (4-6)

on the cutting plane whose equation is

$$\tan(\alpha_s) .x + \tan(\alpha_b) . y + z = 0 \quad (4\text{-}7)$$

it is possible to solve for z in terms of α_s , α_b and α_l :

$$z = \tan(\alpha_s) \sin(\alpha_l) - \tan(\alpha_b)\cos(\alpha_l) \quad (4\text{-}8)$$

The angle θ is the angle between $\hat{\mathbf{e}}_2$ and $\hat{\mathbf{e}}_3$, and the rotation is made by using $\hat{\mathbf{e}}_1$ as a rotation vector. It is clear by construction that $\hat{\mathbf{e}}_2 \times \hat{\mathbf{e}}_3$ is parallel to $\hat{\mathbf{e}}_1$.

4.3.3. Interpretation for Cutter Radius

As with the rake and lead angles, the cutter radius is used on the solid model as a geometric transformation. This time it will be a translation. The effect is to translate the insert by the cutter radius R using the pivot point as the reference position (see Fig 4.18) . In this way, subsequent rotations about the tool axis will rotate the insert at a distance R from the rotation axis, which is exactly what is needed.

4.3.4 Interpretation for Depth of Cut

In order to express the depth of cut, the top plane of the workpiece is set to a DEPTH_OF_CUT distance above the lowest point of the already tilted insert. This operation is specially easy given the representation of the workpiece faces (see Fig 4.8).

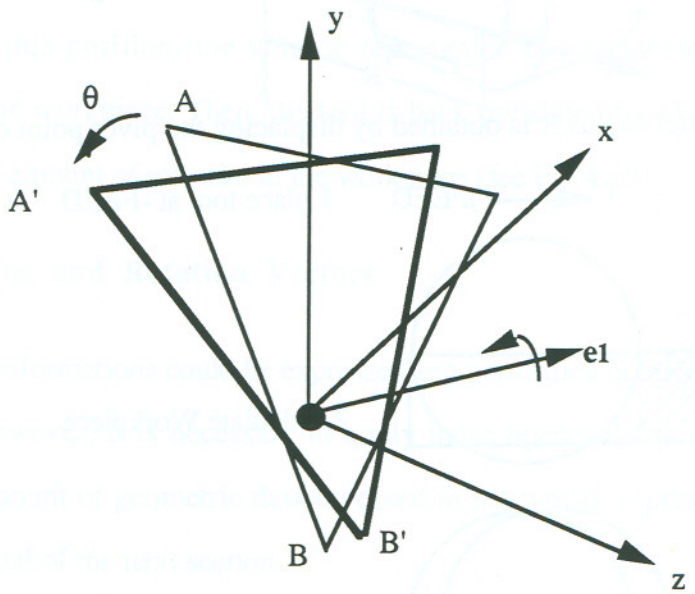

Fig 4.16. Rotation about **e1** by an unknown angle θ to achieve the desired lead angle

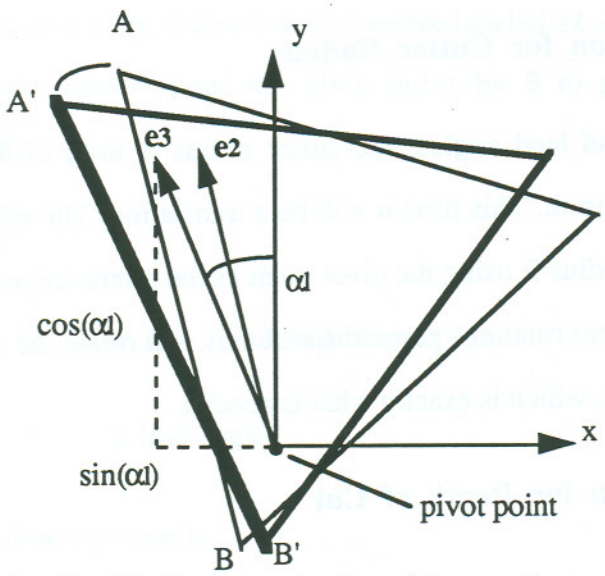

Fig 4.17. Geometry involved in the determination of the rotation angle to generate lead angle αl.

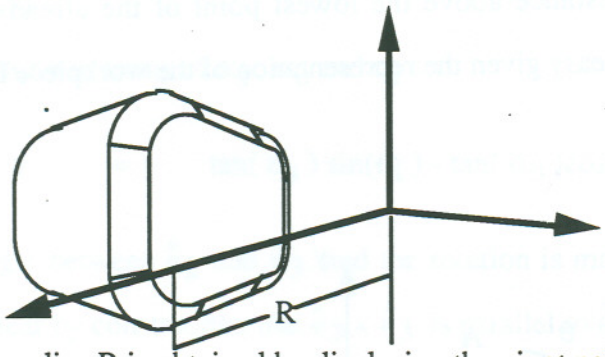

Fig 4.18. Cutter radius R is obtained by displacing the pivot point of the insert.

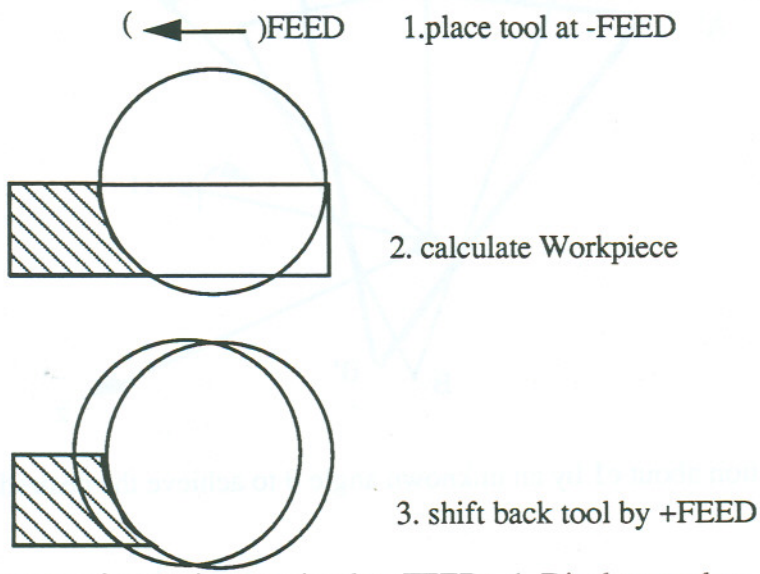

Fig 4.19. Sequence of operations to simulate FEED: -1. Displace tool to -FEED (in Fig FEED is positive to the left). -2. Calculate the difference: (Solid Workpiece - Tool). -3. Re-place Tool at its initial position.

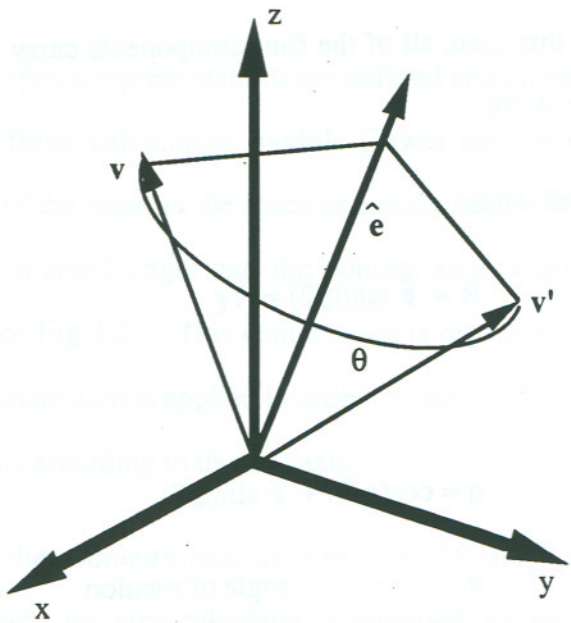

Fig 4.20. Rotation of v to v' about the origin by using rotation vector or quaternion.

4.3.5 Interpretation for Feed

In order to interpret the input FEED, the whole tool object is translated by a distance -FEED. Once in this position, the volume represented by the swept of the insert is subtracted from the workpiece. Then, the tool is back translated by +FEED, such that it will meet the right amount of material in the workpiece (see Fig 4.19).

4.3.1 Quaternions and Rotation Vectors

The preceding transformations could be expressed and performed in different forms on the data structure. However, it is necessary to apply these operations in an efficient way, given the large amount of geometric data involved in the type of representations chosen here. This is the goal of the next section.

The Euler theorem establishes that a displacement of a rigid body with one fixed point can be described as a rotation about some axis in the space. The rotation vector is a vector along this axis, and its magnitude contains information about the rotation angle. The

quaternion is a four component vector; the last three being the components of the axis vector in the space. In this case, all of the four components carry information about the rotation angle. (see Fig. 4.20)

The rotation vector is defined as:

$$R = \hat{e} \tan(q/2) = \hat{e}_f \qquad (4\text{-}9)$$

and the quaternion as:

$$q = \cos(q/2) + \hat{e} \sin(q/2) \qquad (4\text{-}10)$$

where θ = angle of rotation

$\hat{e}$ = rotation axis vector

If transformed by applying the quaternion, the coordinates of $\mathbf{v}$ transformed to $\mathbf{v}'$ are:

$$\mathbf{v}' = \mathbf{v} + 2\, q_0\, (\mathbf{q} \times \mathbf{v}) + 2\, \mathbf{q} \times (\mathbf{q} \times \mathbf{v}) \qquad (4\text{-}11)$$

where q_0 = $\cos(\theta/2)$

for the rotation vector , the coordinates of the transformed point $\mathbf{v}'$ are:

$$\mathbf{v}' = \mathbf{v} + \frac{2\mathbf{R} \times (\mathbf{v} + (\mathbf{R} \times \mathbf{v}))}{1+f^2} \qquad (4\text{-}12)$$

where f = $\tan(\theta/2)$

In the implementation of the geometry model the rotation vector technique was chosen for performing the rotations since it implies 3 cross products compared with 4 for the quaternion.

4.4. Contact Area

Once the tool and workpiece representations are defined and consistent, it is followed by the contact area and force calculation module (lower part of Fig 4.1). The module initializes the position of the insert in the space as outside of the workpiece. Subsequently, the tool is rotated by a small angle and the contact area between the insert and the workpiece is found (see Fig 4.21). This contact area is expressed as a vector, normal to the insert face. A decomposition is applied in order to calculate the area in the radial, axial and tangential directions according to the tool axis.

Since the objective of the geometry module is to find a "history" of the engagement and disengagement processes, the area calculated is recorded, for each position of the tool. These data can easily be translated into Area vs. Time data, by considering the angular velocity of the tool.

This section explains how to determine whether there is tool-work contact for a determined angular position of the cutter and if so, to keep the account of how much area is engaged, and to determine whether a particular position of the tool represents an entry or exit stage or a full engagement. Additionally, once the contact area is calculated, it has to be expressed in several coordinate systems. Translation among them is discussed. The use of this translation between coordinate systems is that it expresses forces and areas decomposed into several systems. For example, force measurements are usually made in World Coordinate System (dynamometer measure), while torque calcuations have to be done in Tool Coordinate System (radial vs tangential directions) ; and, if chip flow direction is required, an additional system, attached to the insert is used, to calculate friction forces. The nature of the 3D model, and the process by which the tool/workpiece relations are calculated, lend themselves to realize transformations between coordinate systems in very easy way by using cross and dot product only.

4.4.1 Contact Area Calculation

For a given angular position of the cutter it is required to determine the contact between insert and workpiece. A contact is realized if any one of the points in the top face of the insert (see Fig 4.3) is inside the workpiece left from the prior pass of the cutter. If a contact is detected, the area associated to the cell making the contact is accumulated. This area is represented by a vector which is not necessarily normal to the rake face (see Fig 4.11, for the case of K lands). Simultaneously, the engaged part of the cutting edge is taken into account for the purposes of average chip thickness calculations and effective lead angle calculations.

In order to distinguish between full and partial engagement, a full engagement is defined as the condition in which all the points in the top surface of the insert which will potentially be engaged in the cut are already engaged. A more detailed explanation in this regard will be given later.

4.4.1.1 Calculation of the Workpiece

By defining the boundary of the insert into small line segments a revolute solid can be defined in a simple manner; by revolving about the tool axis. Each segment engenders a cone trunk. It is assumed that the segments engender a cylinder (see Fig 4.22) whose radius is constant along the (very small) cylinder height.

By applying this definition, the solid representing the tool is essentially formed by a series of closely packed rings. Under the assumption that feed is much smaller as compared to the cutter radius and the angular speed is high, those rings are modeled as circles instead of considering the exact cycloid shape.

When each one of those rings is intersected with the initial wedge-like workpiece, two intersects are obtained in the general case (p1 & p2 of Fig 4-23) ; one for the entry and

other for the exit planes. Joining those intersects there is a circular arc of radius equal to the ring's which caused the intersections. By considering many of those arcs whose extremes are determined by the lateral faces of the workpiece the insert pass on the workpiece is obtained (see Fig 4.23) labeled as p1-p1' and p2-p2'. Thus, the workpiece at some particular point in the computation can be thought of as the data structure resulting from subtracting the tool in a determined position in the space from the initial workpiece (solid block).

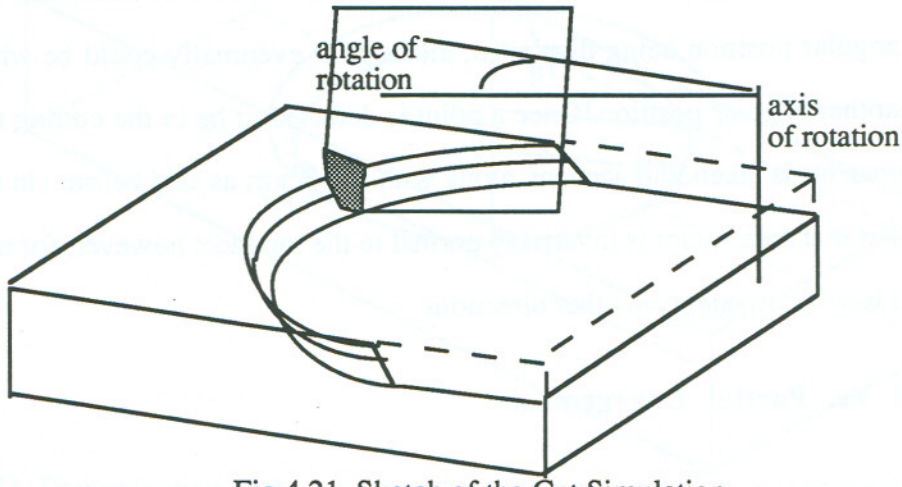

Fig 4.21. Sketch of the Cut Simulation

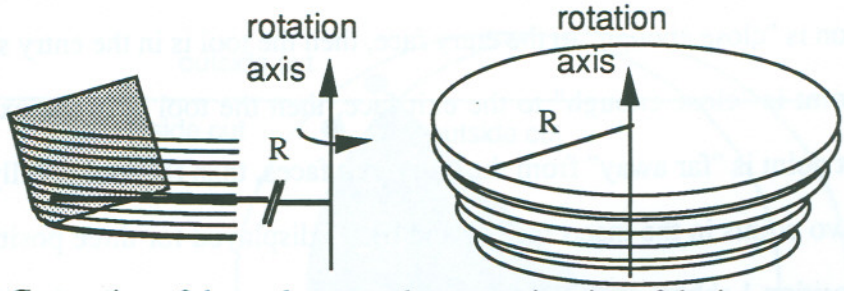

Fig 4.22. Generation of the tool contour by approximation of the insert as a polygon which revolves about the rotation axis.

4.4.1.2 Point Engagement Test

Given a point in the rake face of the insert, it is of interest to know whether or not it is engaged in the cut for a given angular position of the cutter. In other words whether it is "inside" the workpiece (as defined in section 4.4.1.1). The inclusion query tests are

arranged in order of increasing complexity while trying to arrive to an answer for each point in the earliest possible stage (catching the trivial cases first). A point on the top face of the insert represents a contact point if the answer to the following questions is YES:

1-Is it inside the original wedge.

2-Is it "outside" the circular sector labeled as S in Fig 4.24.

In Fig 4.24 three points appear. The one inside the circular sector S is not in the contact area for the angular position being displayed, although it eventually could be when the cutter is in another angular position. Once a point is detected to be in the cutting region, the area it represents is taken into account, along with its vector; as said before , in case of a flat face insert that area vector is invariably normal to the top face; however, for non flat inserts, it will have components in other directions.

4.4.1.2 Full Vs. Partial Engagement

This section explains the algorithm which determines wheter the tool is in a entry, exit or full engagement. If some point in the surface of the insert is found to be engaged in the cut and its position is "close enough" to the entry face, then the tool is in the entry stage. If the contacting point is "close enough" to the exit face, then the tool is in the exit stage. If every contact point is "far away" from the entry/exit faces, then the tool is fully engaged. In Fig 4.25 two points in the insert face (**a** and **b**) are displayed for three positions of the insert. The position 1 shows no engagement since there are no engaged points. In position 2 , both **a2** and **b2** are still out of cut, there exists a point on the surface of the insert which is engaged in cut and is close enough to the entry plane to be considered as contained in the entry wall in the workpiece. In position 3, all points which are found to be engaged are far away from the entry/exit faces. Therefore the tool is considered fully engaged.

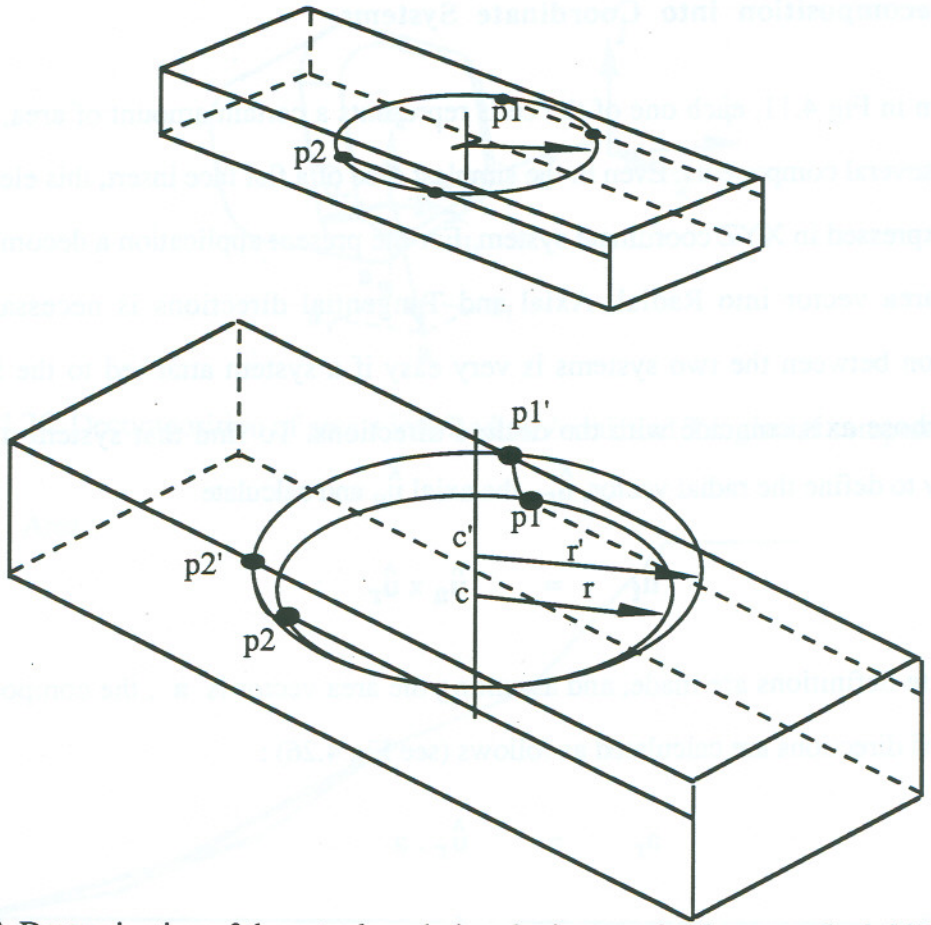

Fig 4.23. Determination of the actual workpiece by intersection between the initial wedge and the rings approaching the tool geometry. Above: Calculation of a pair of points p1 , p2. Below: Extension of the above concept to obtain edges p1-p1' and p2-p2'.

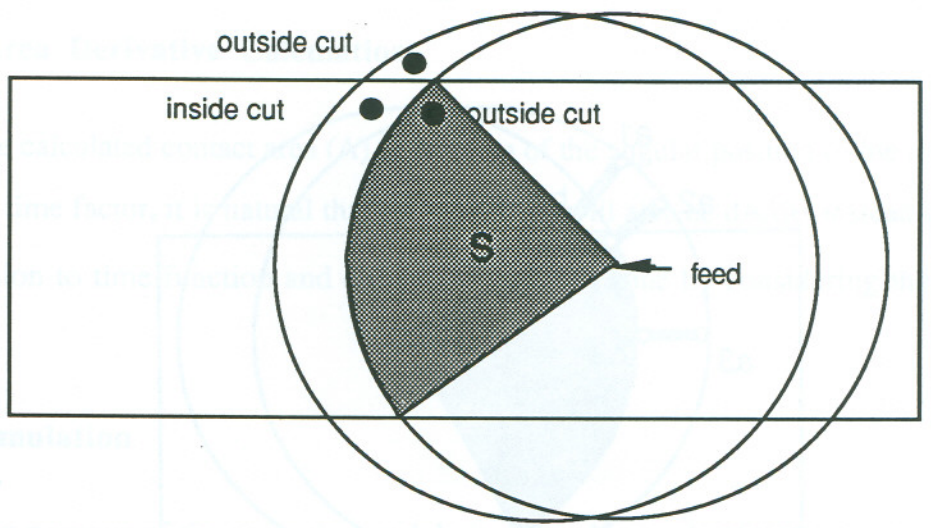

Fig 4.24. Sectors which define engagement/non-engagement for a particular point

4.4.2 Decomposition into Coordinate Systems

As shown in Fig 4.11, each one of the cells represents a certain amount of area, but this area has several components. Even in the simplest case of a flat face insert, this elementary area is expressed in XYZ coordinate system. For the present application a decomposition of that area vector into Radial, Axial and Tangential directions is necessary. The conversion between the two systems is very easy if a system attached to the insert is found, whose axis coincide with the desired directions. To find that system it is only necessary to define the radial vector, $\hat{\mathbf{u}}_r$, the axial $\hat{\mathbf{u}}_a$ and calculate

$$\hat{\mathbf{u}}_t = \hat{\mathbf{u}}_a \times \hat{\mathbf{u}}_r \qquad (4\text{-}13)$$

Once these definitions are made, and assuming the area vector is $\mathbf{a}$, the components in the desired directions are calculated as follows (see Fig 4.26) :

$$a_r = \hat{\mathbf{u}}_r \cdot \mathbf{a} \qquad (4\text{-}14)$$

$$a_t = \hat{\mathbf{u}}_t \cdot \mathbf{a} \qquad (4\text{-}15)$$

$$a_a = \hat{\mathbf{u}}_a \cdot \mathbf{a} \qquad (4\text{-}16)$$

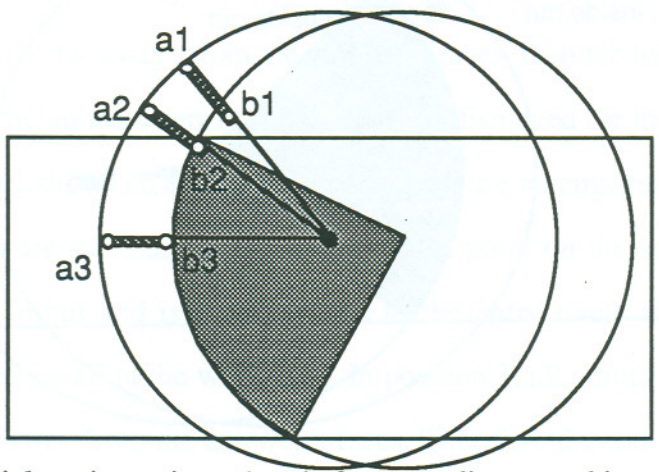

Fig 4.25. Potential cutting points p1 and p2 appear disengaged in position 1 and p2. Complete engagement in position p3.

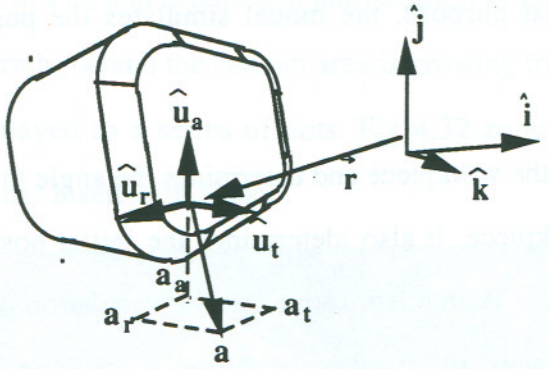

Fig 4.26. Decomposition of area a into Radial, Axial, and Tangential components.

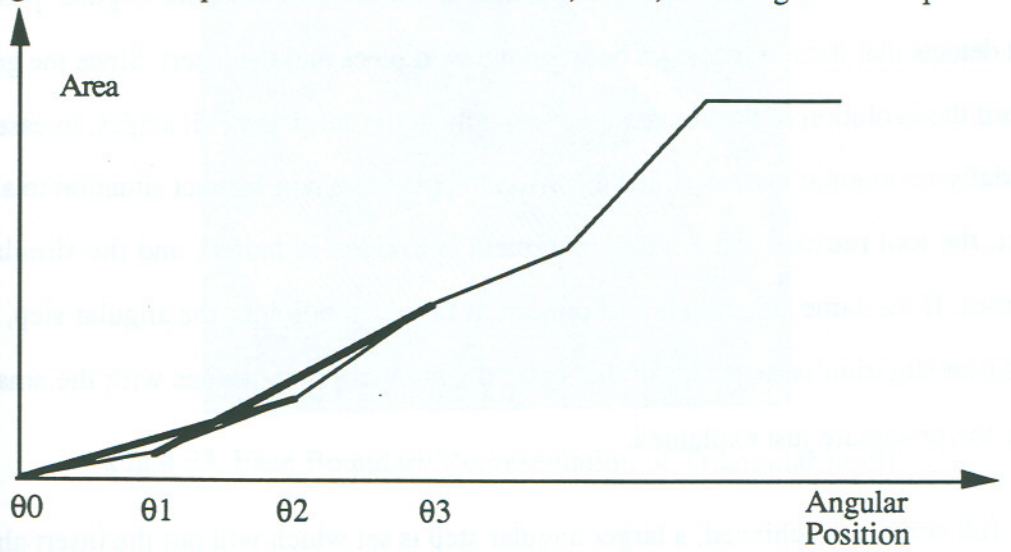

Fig 4.27. Area derivative calculation.

4.4.3 Area Derivative Calculation

Since the calculated contact area (A) is function of the angular position of the tool rather than the time factor, it is natural that the derivative will also be $dA/d\Theta$ instead of dA/dt. Conversion to time function and derivative is easily done by considering the angular velocity.

4.5. Simulation

The main purpose of the geometry module is to be able to simulate the contact area in engagement, disengagement and full cut stages.This section shows that once the geometric

utilities are set for that purpose, the model simulates the pass of the insert on the workpiece.

The model recognizes the workpiece and determines the angle the tool needs to rotate to swap through the workpiece. It also idetermines the initial position of the insert with respect to the workpiece. With this information the simulation proceeds as follows: the geometry module places the tool very close to the workpiece (INITIALIZE SIMULATION in Fig 4.1), but outside it, and starts incrementing its angular position until it detects that there is a contact between the workpiece and the insert. Since the goal is to record the evolution of the contact area specially at the entry and exit stages, in case that the initially set angular increment led the insert to pass from non-contact situation to a full-contact, the tool retreats, the angular increment is divided to halfed, and the simulation reassumes. If the same situation is still present, it further subdivides the angular step, until a transition situation is detected, in this case, the simulation continues with the smallest step by the procedure just explained.

When full contact is achieved, a larger angular step is set which will put the insert almost at the exit, but still in full engagement. Then, the exit transition simulation proceeds in the same form as before for the entry. When it is detected that the insert is completely out of the workpiece, the simulation is stopped. The module calculates the contact area resolved into the Radial, Axial and Tangential Coordinates, the angular position of the cutter, the number of cells involved in the cut in this particular stage, the space orientation of the effective lead direction, and other relevant geometrical information.

Figures 4.28 to 4.32 show different aspects of the insert and tool representation and cut simulation. Fig 4.28 shows a standard triangular insert and Fig 4.29 shows what is called a "free shaped" insert. The later is not a standard rectangular, circular or triangular shaped insert, but instead its contour can be represented by a sequence of lines and arcs (only lines are necessary in this case). Fig 4.30 shows the workpiece as calculated by the model

based on the feed, depth of cut, and orientation and position of the entry and exit planes. Fig 4.31 shows the pattern by which the contact area is growing for the insert of Fig 4.29. The contact area is displayed as a series of dots. Fig 4.32 zooms in the pattern of the growing area of a triangular insert with K land.

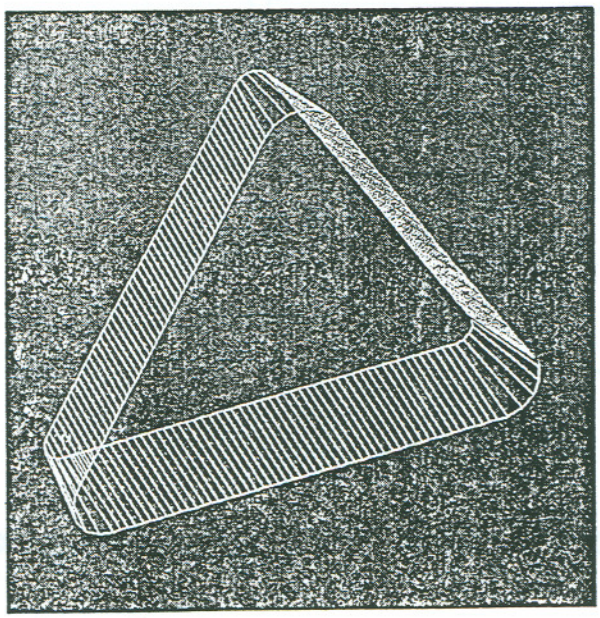

Fig 4.28. Face Boundary Representation of Triangular insert.

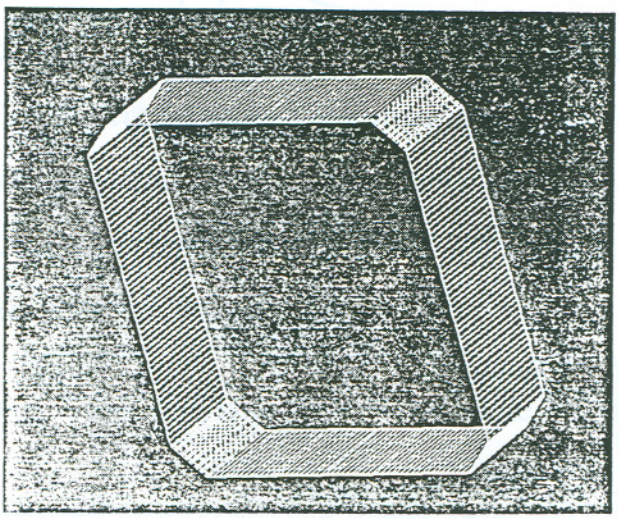

Fig 4.29. Face Boundary Representation of free shaped rectangular insert.

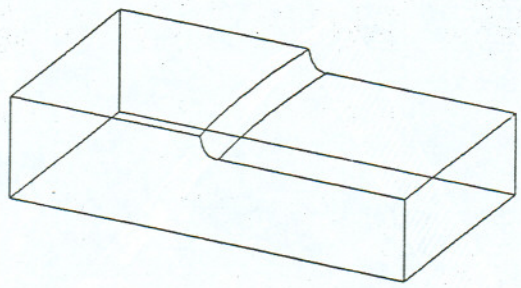

Fig 4.30. Workpiece calculated from depth of cut, feed, entry and exit planes and tool representation.

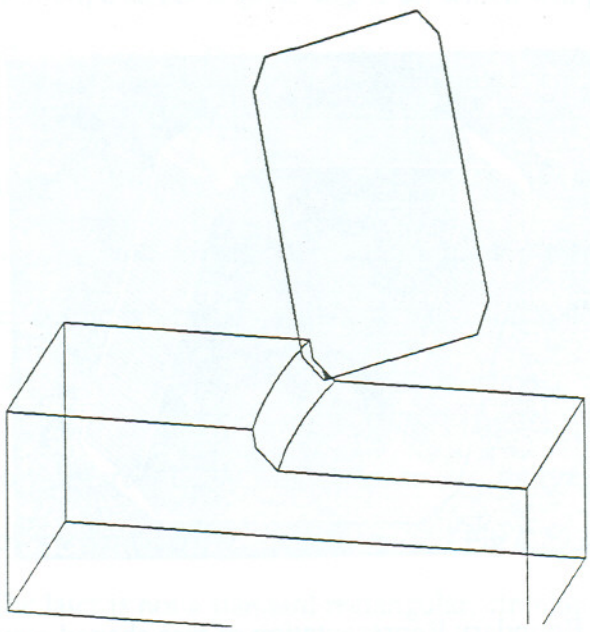

Fig 4.31. Growing contact area pattern for free shaped insert in Fig 4.29 and workpiece in Fig 4.30.

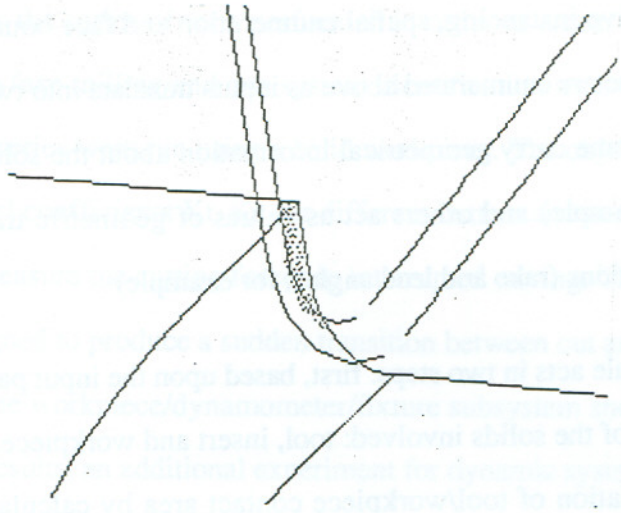

Fig 4.32. Growing contact area pattern for triangular insert with K land and workpiece in Fig 4.30.

4.6 Summary

A 3D Geometry Module has been presented which allows for the calculation of contact area between the tool and workpiece in full as well as in partially engaged cut. The model applies to face milling fly cutting as well as turning operations. It covers essentially any insert whose contour is a closed, coplanar sequence of lines and arcs. It also covers inserts with flat, K lands (no grooves are currently modeled). This model allows for the specification and use of the following parameters:

1.- For the Insert: Shape, land, nose radius, relief angle, thickness, side length.

2.- For the Cutter: back (axial) rake, side (radial) rake, lead angle, cutter diameter. For turning operations large values of the cutter diameter versus narrow workpieces are used.

3.- For the cutting process: Feed, Depth of Cut,

4.- For the workpiece: insert velocity entry and exit angles with respect to the workpiece walls; material properties.

The models used for the module are representations for 3D solids. In this Geometry module pure primitive instancing, spatial enumeration and face boundary representations are used. The parameters enumerated above as inputs translate into two varieties of entities inside the model; some carry geometrical information about the solid represented (insert dimensions, for example) and others act as values of geometric transformations acting upon the representations (rake and lead angles, for example)

The geometric module acts in two steps: first, based upon the input parameters it calculates the representations of the solids involved: tool, insert and workpiece. Second, it performs an angle step simulation of tool/workpiece contact area by calculating the intersection between the solid models representing them. Additional information available includes: conected and non-connected vector contact area, cutting edge, and effective chip flow direction. No approximations are made in regard to the two-dimensionality of the contact area or any other result since all the figures are calculated as vectors in space. By using specific force coefficients the module calculates the cutting forces solved in World Coordinate System and Tool Coordinate System.

Since the stages of entry/exit of the tool are is of special interest, the module chooses a convenient angular step to sweep the cutter thorough the transitional parts, calculating and displaying the patterns of development of contact area for the inserts and cutters covered.

However the model does not handle angular tilt which is commonly used to prevent back cutting. It does not handle multi-insert cutters, and places restrictions on the nature of lands in the inserts already explained above.

CHAPTER 5

DESCRIPTION OF EXPERIMENTAL WORK

This chapter explains the series of tests performed in order to assess the cutting forces in interrupted cuts. Two face milling and one system identification tests were conducted. The first face milling test series were run using a solid workpiece. The objective was to calibrate the mechanistic model coefficients Kt_Kc for different cutters and inserts. The second one was run in order to measure the cutting forces in interrupted cutting. The workpiece for this experiment was designed to produce a sudden transition between cut and no-cut conditions. As the dynamics of the workpiece/dynamometer/fixture subsystem showed its effect in the interrupted cut tests results, an additional experiment for dynamic system identification was conducted in order to synthesize the dynamic modes of this subsystem. In this form the effect of the subsystem dynamics on the results of the interrupted tests could be assessed.

5.1 Milling Experiments

Two sets of face milling experiments were designed. The objective of the first one (continuous cut) was to calibrate the specific force coefficients Kt_Kc for cast iron using different inserts and cutters. A solid workpiece was used in these tests. The second series of tests (interrupted cut), was aimed at measuring the forces produced in entry/exit cuts. This set of experiments used a workpiece which maximizes the sudden transition between cut and no-cut conditions by placing the entry/exit wall of the workpiece normal to the cutting velocity of the insert.

5.1.1 Experiment Set-Up

The experimental set up used for both series of milling experiments is shown in Fig. 5.1. A summary of the specifications of each one of the set up elements is given below.

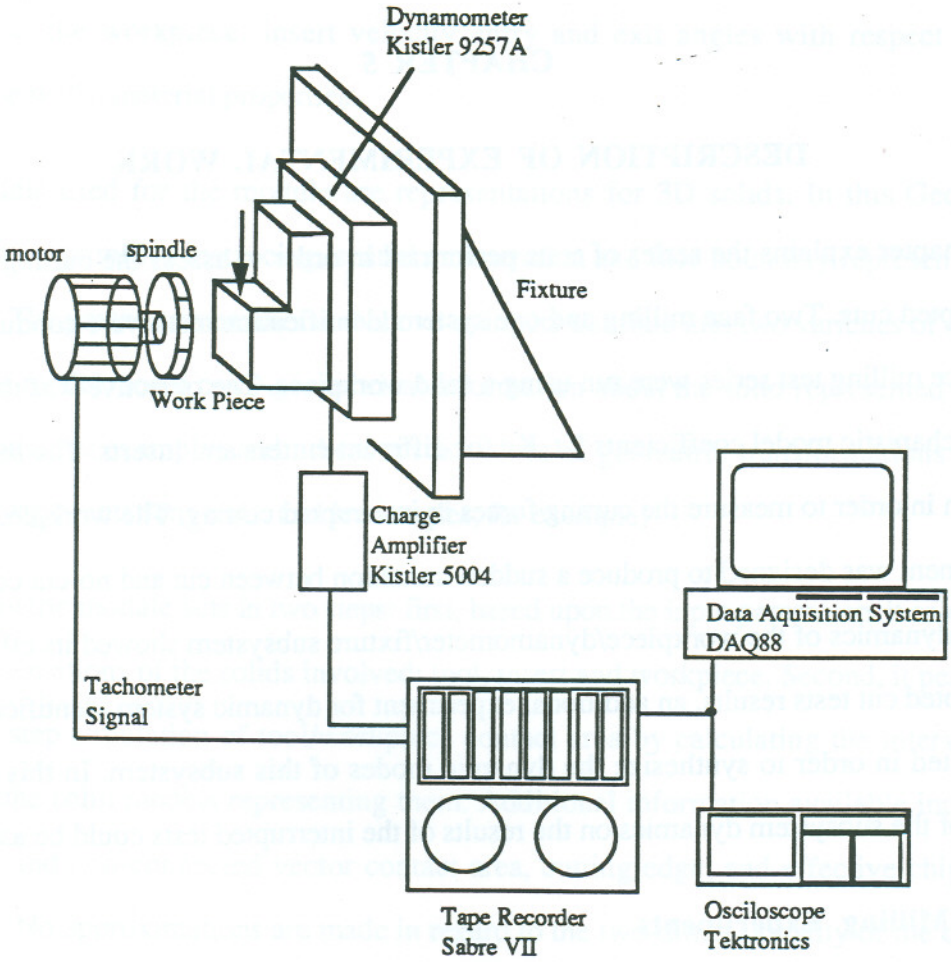

Fig 5.1 Experimental Set-Up for Face Milling Cutting tests.

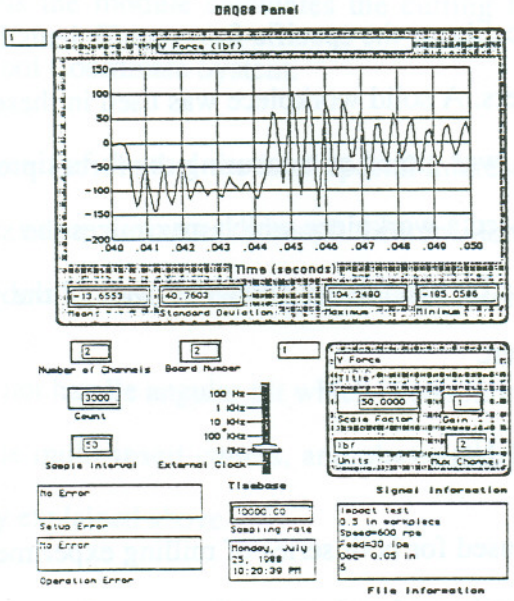

Fig 5.2. Control Panel of Virtual Instrument DAQ88.

The Machine Tool

A slide bed provided by the Ingersoll Milling Co.with the following specifications for its electric drive was used in the cutting tests.:

Motor Drive:	INDRAMAT	Brushless DC servomotor	112-B-0-PD
Servo Controller:	INDRAMAT	TDM-1.2-50-300-W1	
Power Amplifier:	INDRAMAT	TVM-2.1-50-220/300-W1-115/220	

Cutting Force Sensors

A Kistler Dynamometer (9257A) mounter on the fixture, is used to measure the cutting forces in the (X,Y,Z) coordinate system. The dynamometer produces a signal in picoCoulombs that is proportional to the force applied on it.

A Kistler Dual Mode Amplifier (5004) is connected to the Dynamometer. Its role is to convert the charge signal coming from the dynamometer into voltages in the range [-10 +10 V] which can be sampled from a computer board.

Data Collection System

A Sabre Tape Recorder VII 8235 records the force signal coming from the charge amplifier in analog form. This instrument allows the storage of large amounts of data. By playing the data at tape speeds different than recorded, high effective sampling rates can be obtained. The main disadvantage is that the tape is more fragile than disks for effects of long run data storages, and that replaying may become a real problem if the reference place in the tape is lost. In this experiment it was used as a back up device and also to enable high sampling rates when used in connection with the data acquisition system.

The contents of the tape were scanned with a Tektronics Oscilloscope 2025 . It allows the selection of the relevant data from the tape.

A Macintosh based software, LABVIEW™ (from National Instruments) was used to control the sampling and storage of data in the computer. LABVIEW is a Object Oriented Environment for design and assembly of measurement instruments which are software emulated in the computer. Fig 5.2 shows the front panel of the virtual instrument DAQ88 used for this experiment.

Cutting Tools

Fly cutting type experiments were performed. Different cutters and inserts were used. All the inserts are coated with Kennametal coating KC710.

The cutters used are shown in Fig 5.3 and their specifications are listed in table 5.1.

Table 5.1. Cutters for Face Milling Experiment.

Cutter 1	Double Negative KDNR-4-SN4-15CB,	ax.rake=-7°; rad.rake=-7°; lead=15° ; diam=4 in
Cutter 2	Positive KKBR-5-SP4-0-A	ax.rake=5°; rad.rake=0°; lead=1° ; diam=5 in
Cutter 3	Shear KDSR-4-SP4-1CB	ax.rake=5°; rad.rake=-13°; lead=1°; diam=4

The inserts used are shown in Fig 5.4 and their catalog names are listed in table 5.2.

Table 5.2. Inserts for Face Milling Tests.

Regular	SPG-433 KC710
30° double flatted	SPE-43K2 KC710
30° flatted	SPE-43D2R KC710
15° flatted	SPE-43E2R KC710
Negative land	SPG-433T KC 710

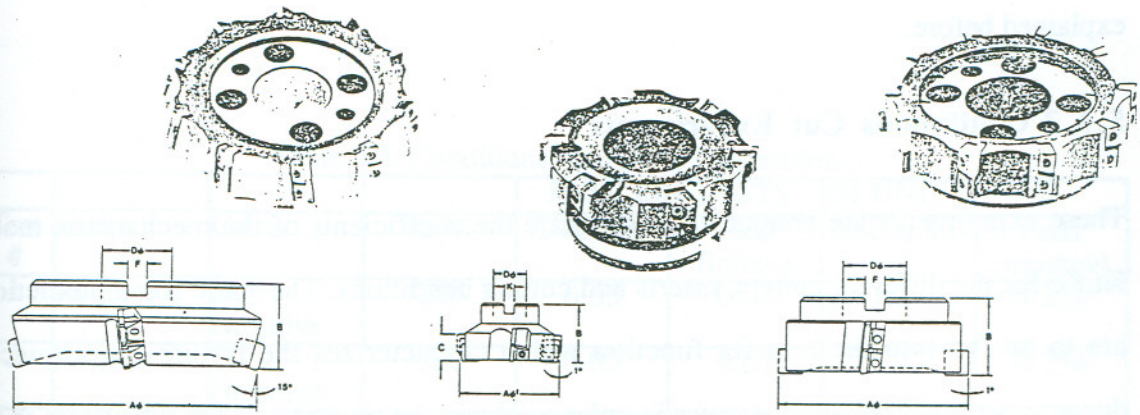

Fig 5.3. Cutters used in the Face Milling tests (Kennametal Co.).

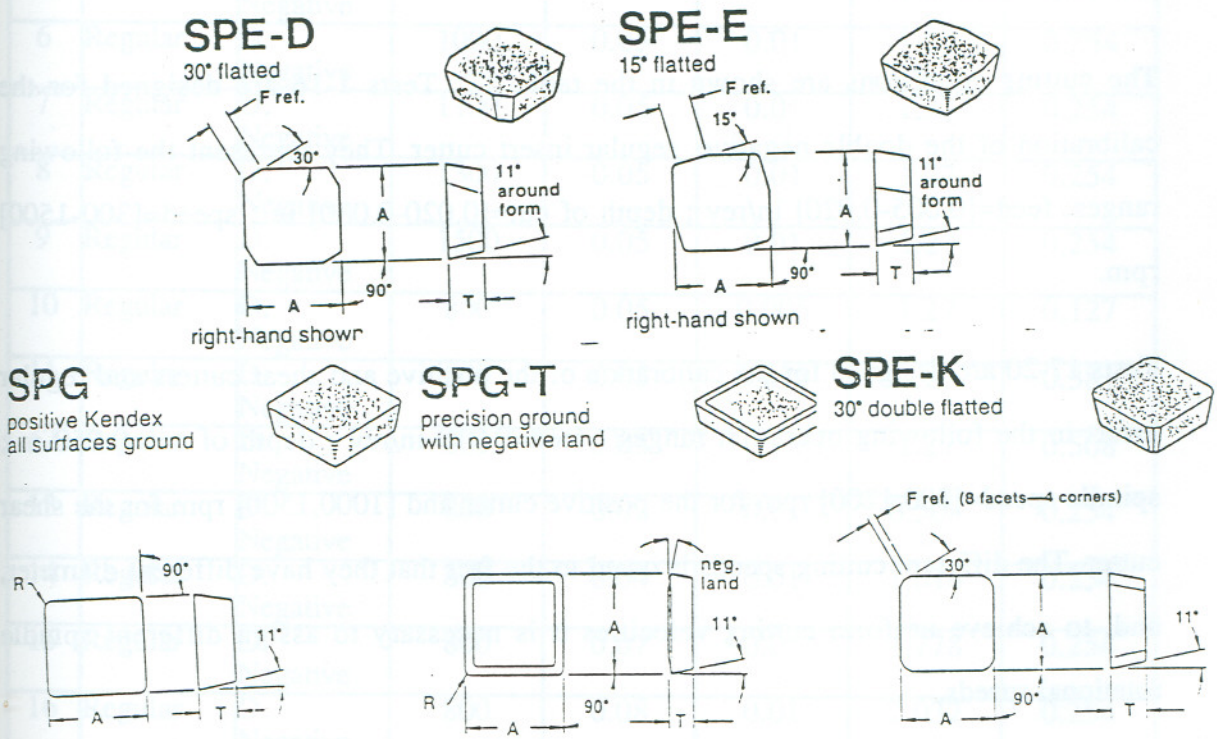

Fig. 5.4. Inserts used in Face Milling tests (Kennametal Co.).

The data collected in the cutting tests included the three cutting forces (feed, axial, and transverse) and the rotational spindle speed. The sampling rate used was 12.5 KHz/channel. In some cases (for interrupted cut tests) the tape recorded was used as explained before.

5.1.3 Continuous Cut Experiments

These experiments are conducted to calibrate the coefficients of the mechanistic model Kt,Kc for the different cutters, inserts and cutting conditions. The static force predictions are to be fed into the transfer function which characterizes the fixture / workpiece / dynamometer subsystem dynamics in order to obtain the response of the subsystem to the static forces.

Cutting Conditions

The cutting conditions are shown in the table 5.3. Tests 1-16 are designed for the calibration of the double negative, regular insert cutter. They represent the following ranges: feed=[0.005-0.020] in/rev ; depth of cut=[0.020-0.080] in ; speed=[300-1500] rpm.

Tests 17-20 are designed for the calibration of the positive and shear cutters and regular insert in the following operation ranges: feed=0.010 in/rev ; depth of cut=0.050 in ; spindle speed=[800,1200] rpm for the positive cutter and [1000,1500] rpm for the shear cutter. The different cutting speeds is owed to the fact that they have different diameter, and, to achieve uniform cutting velocities it is necessary to assign different spindle rotational speeds.

Tests 21-24 are chosen for calibration of 4 different inserts with the double negative cutter in the following operation ranges: feed=0.010 in/rev ; depth of cut=0.050 in ; spindle speed =800 rpm.

Table 5.3. Conditions for Kt_Kc Calibration .

				ENGLISH UNITS		SI UNITS	
Test #	Insert	Cutter	RPM	DoC (in)	Feed (in/rev)	DoC (mm)	Feed (mm/rev)
1	Regular	D. Negative	300	0.05	0.01	1.27	0.254
2	Regular	D. Negative	500	0.05	0.01	1.27	0.254
3	Regular	D. Negative	700	0.05	0.01	1.27	0.254
4	Regular	D. Negative	800	0.05	0.01	1.27	0.254
5	Regular	D. Negative	900	0.05	0.01	1.27	0.254
6	Regular	D. Negative	1000	0.05	0.01	1.27	0.254
7	Regular	D. Negative	1100	0.05	0.01	1.27	0.254
8	Regular	D. Negative	1300	0.05	0.01	1.27	0.254
9	Regular	D. Negative	1500	0.05	0.01	1.27	0.254
10	Regular	D. Negative	800	0.05	0.005	1.27	0.127
11	Regular	D. Negative	800	0.05	0.015	1.27	0.381
12	Regular	D. Negative	800	0.05	0.02	1.27	0.508
13	Regular	D. Negative	800	0.02	0.01	0.508	0.254
14	Regular	D. Negative	800	0.04	0.01	1.016	0.254
15	Regular	D. Negative	800	0.07	0.01	1.778	0.254
16	Regular	D. Negative	800	0.08	0.01	2.032	0.254
17	Regular	Positive	800	0.05	0.01	1.27	0.254
18	Regular	Positive	1200	0.05	0.01	1.27	0.254

19	Regular	Shear	1000	0.05	0.01	1.27	0.254
20	Regular	Shear	1500	0.05	0.01	1.27	0.254
						0	0
21	30° Double Flat	D. Negative	800	0.05	0.01	1.27	0.254
22	30° Flat	D. Negative	800	0.05	0.01	1.27	0.254
23	15° Flat	D. Negative	800	0.05	0.01	1.27	0.254
24	K land	D. Negative	800	0.05	0.01	1.27	0.254

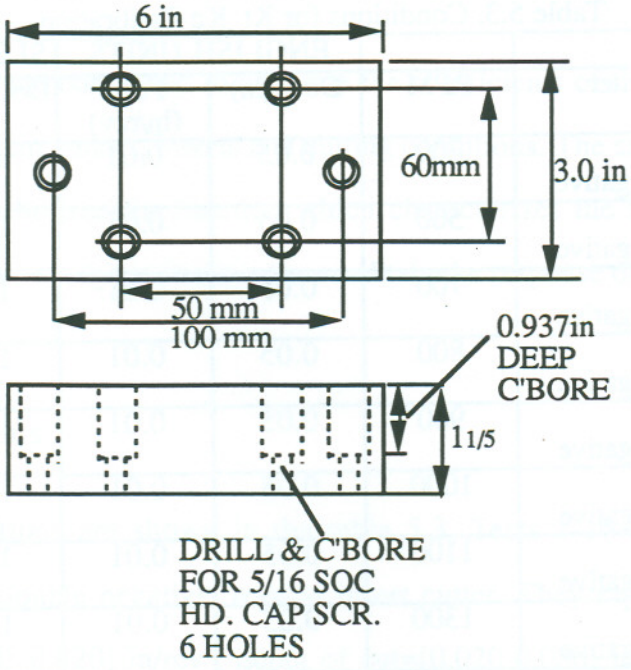

Fig 5.5. Workpiece for the Continuous Cut Calibration Tests.

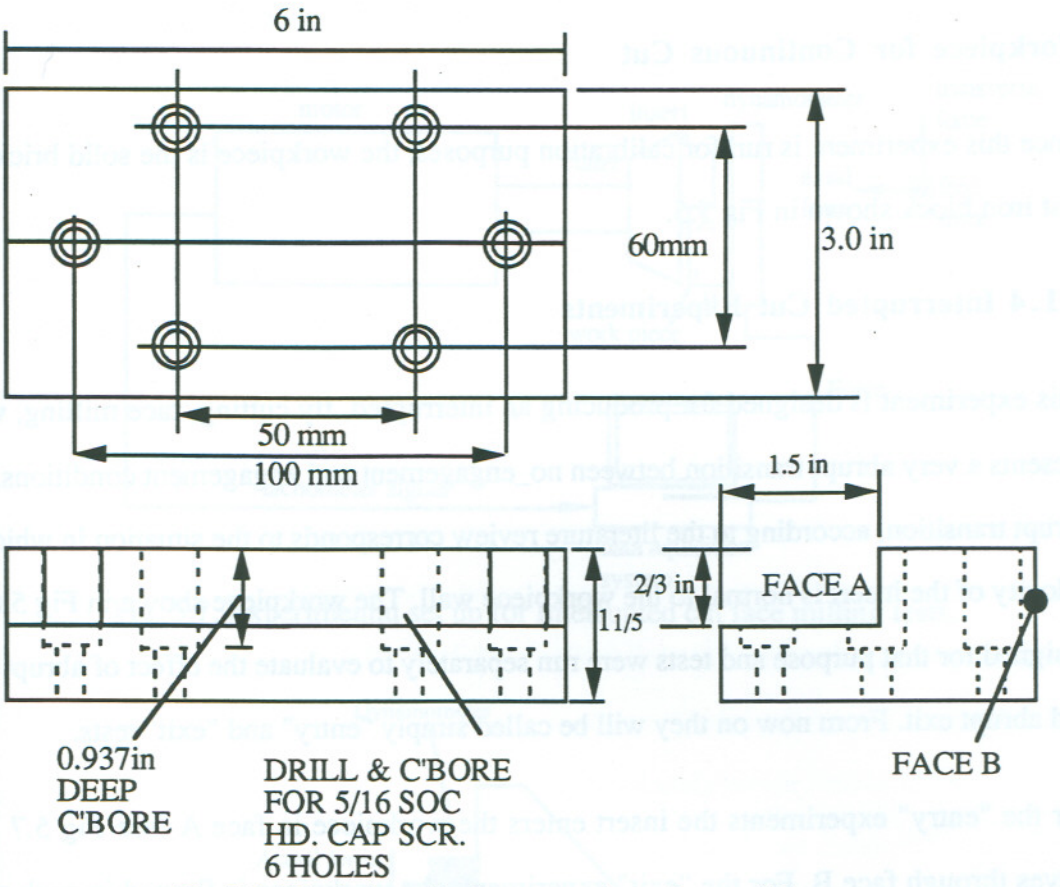

Fig.5.6. Workpiece for Interrupted cut face milling test.

Workpiece for Continuous Cut

Since this experiment is run for calibration purposes, the workpiece is the solid brick-like, cast iron block shown in Fig 5.5.

5.1.4 Interrupted Cut Experiments

This experiment is designed for producing an interrupted, fly cutting, face milling, which presents a very abrupt transition between no_engagement and engagement conditions. This abrupt transition, according to the literature review corresponds to the situation in which the velocity of the insert is normal to the workpiece wall. The workpiece shown in Fig 5.6 was designed for that purpose and tests were run separately to evaluate the effect of abrupt entry and abrupt exit. From now on they will be called simply "entry" and "exit" tests.

For the "entry" experiments the insert enters the workpiece in face A (see Fig 5.7) and leaves through face B. For the "exit" experiments the workpiece is flipped in such a way that the cutter enters through face B and leaves by face A.

Cutting conditions

There are five series of experiments, aimed to evaluate the effect of cutting speed, depth of cut, feed rate, cutter and insert upon the entry exit forces. The experiment series are:

Series 1. Effect of Cutting Velocity

The purpose of this series is to evaluate the effect of cutting velocity on the cutting forces; the other conditions are kept constant at (feed=0.010 in/rev, depth of cut=0.050 in; regular insert, double negative cutter). The conditions are the same as tests 1 to 9 in Table 5.3.

Series 2 Effect of Feed

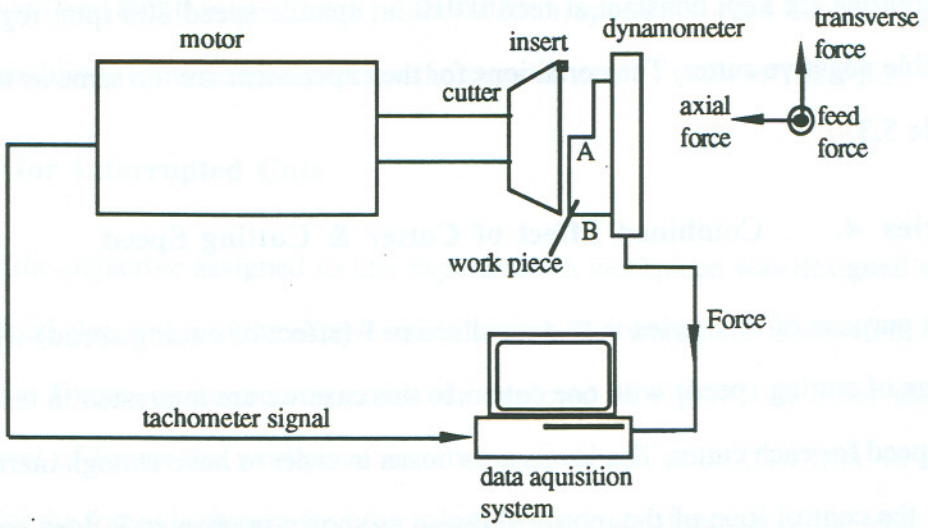

Fig. 5.7. Experimental set up for Interrupted cut face milling tests.

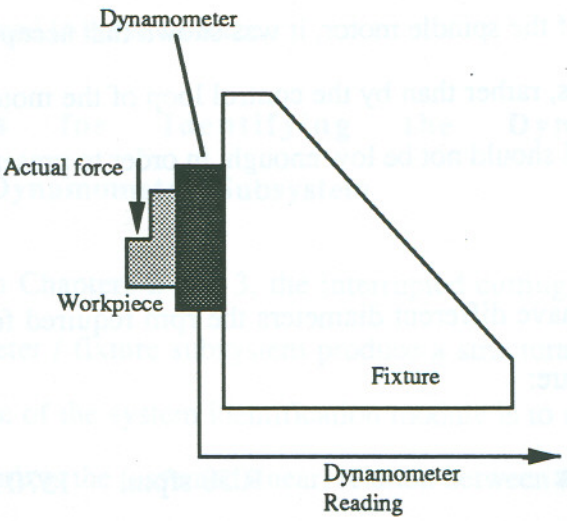

Fig 5.8 . Input/Output variables in the System Identification.

The purpose is to evaluate the effect of feed on the cutting forces; the other conditions are kept constant at a speed of 800 rpm, depth of cut 0.050 in; regular insert, and double negative cutter. The conditions for the experiment are the same as tests 10 to 12 in Table 5.3.

Series 3 Effect of Depth of Cut

The purpose is to evaluate the effect of depth of cut on the cutting forces; the other conditions are kept constant at feed 0.010 in, spindle speed 800 rpm; regular insert and double negative cutter. The conditions for the experiment are the same as tests 13 to 16 in table 5.3.

Series 4. Combined Effect of Cutter & Cutting Speed

The purpose of this series is to extend series 1 (effect of cutting speed) which covered a range of cutting speeds with one cutter. In this case we are interested in testing two levels of speed for each cutter. The levels are chosen in order to have enough inertial forces such that the control loop of the motor, sluggish as shown in chapter 3, does not have to keep the speed under cutting conditions. Recall, by modeling the cutting process as a disturbance for the control loop of the spindle motor, it was shown that acceptable constant speeds are kept by inertial forces, rather than by the control loop of the motor. At the same time, the low level of the speed should not be low enough, in order to present some contrast with the upper level.

Because the cutters have different diameters the rpm required for a given cutting speed vary. The conditions are:

surface cutting Speeds:		1050 sfpm,	1570 sfpm
	for 4 in. cutters:	1000 rpm,	1500 rpm
	for 5 in. cutter:	800 rpm,	1200 rpm

The other conditions are kept constant at feed=0.010 in/rev, depth of cut=0.050 in; regular insert. The conditions for the experiment are the same as tests 17 to 20 in Table 5.3.

Series 5 Effect of Insert

The purpose is to evaluate the effect of insert on the cutting forces; the other conditions are kept constant at (feed 0.010 in/rev, depth of cut 0.050 in, speed 800 rpm, double negative cutter). The conditions for the experiment are the same as tests 21 to 24 in Table 5.3.

Work Piece for Interrupted Cuts

According to the objective assigned to this experiment a workpiece was designed such that it presents maximal abruptness in the entry/exit of the tool. The workpiece is shown in Fig 5.6 and its place in the fixture-dynamometer ensemble depicted in Fig 5.7. In order to produce a significant level of forces the workpiece material was chosen to be Cast Iron. In Fig 5.7 the terminology for the forces is shown; feed force is the force in the direction of the feed; axial force is the force in the direction of the axis of the tool and transverse force is the force perpendicular to the feed force direction and to the axial force.

5.2 Experiments for Identifying the Dynamics of the Fixture/Workpiece/Dynamometer Subsystem

As discussed briefly in Chapters 2 and 3, the interrupted cutting forces applied to the workpiece / dynamometer / fixture subsystem produce a structural response from these members. The objective of the system identification module is to synthesize the transfer function which characterizes the (assumed linear) relation between the actual force applied to the workpiece (see Fig 5.8) and the dynamometer reading. This dynamometer reading is the response of the subsystem to the cutting force. In order to interpret the dynamometer reading in the proper way the dynamic characteristics of the structure have to be known.

The Tested Structure

The fixture/dynamometer/workpiece structure tested is shown in figure 5.8. The input for the system is the actual force applied to the workpiece; the output of it is the dynamometer

reading. At this time we are assuming that the spindle behaves as an infinitely rigid body and therefore its structural response will not be taken into consideration.

5.2.2 Data Collection and Processing Instruments

The instruments used for the system identification are shown in Fig 5.9. In this figure it is important to note that there are two sets of instruments which perform logically separate tasks:

1. Instruments which record/visualize/analyze the data obtained. These include the Tape recorder, the Data Acquisition System in the computer, the Signal Analyzer and the Oscilloscope.

2. Instruments for exciting the system (generate the input excitation) and for quantifying the system response. These include the Impact Hammer and its Power unit, which generate the input force, and the dynamometer and Charge Amplifier which produces the output force readings. In addition, the acceleration in the transverse direction was recorded as well. This signal was recorded because the accelerometer has a frequency range higher than the dynamometer and thus it would produce more reliable signals at higher frequencies. Since the goal is to determine the dynamics of the subsystem, the acceleration signal would provide the same or better information than the dynamometer, which has smaller frequency ranges.

The instruments used in the experiment in addition to the ones already shown in Fig 5.1 are:

1. PCB 208A03 Piezotronics Impact Hammer. It produces a delta function-like force, with the power evenly distributed on a broad range of frequencies, The bandwith of this signal increases with the hardness of the tip used to produce the impact and the lighter the

hammer. The hammer produces a voltage proportional to the force sensed by a piezoelectric crystal fitted in the hammer head.

2. PCB 480A Power Unit for the Impact Hammer. It amplifies and conditions the signal coming from the hammer in order to be sampled from a computer board.

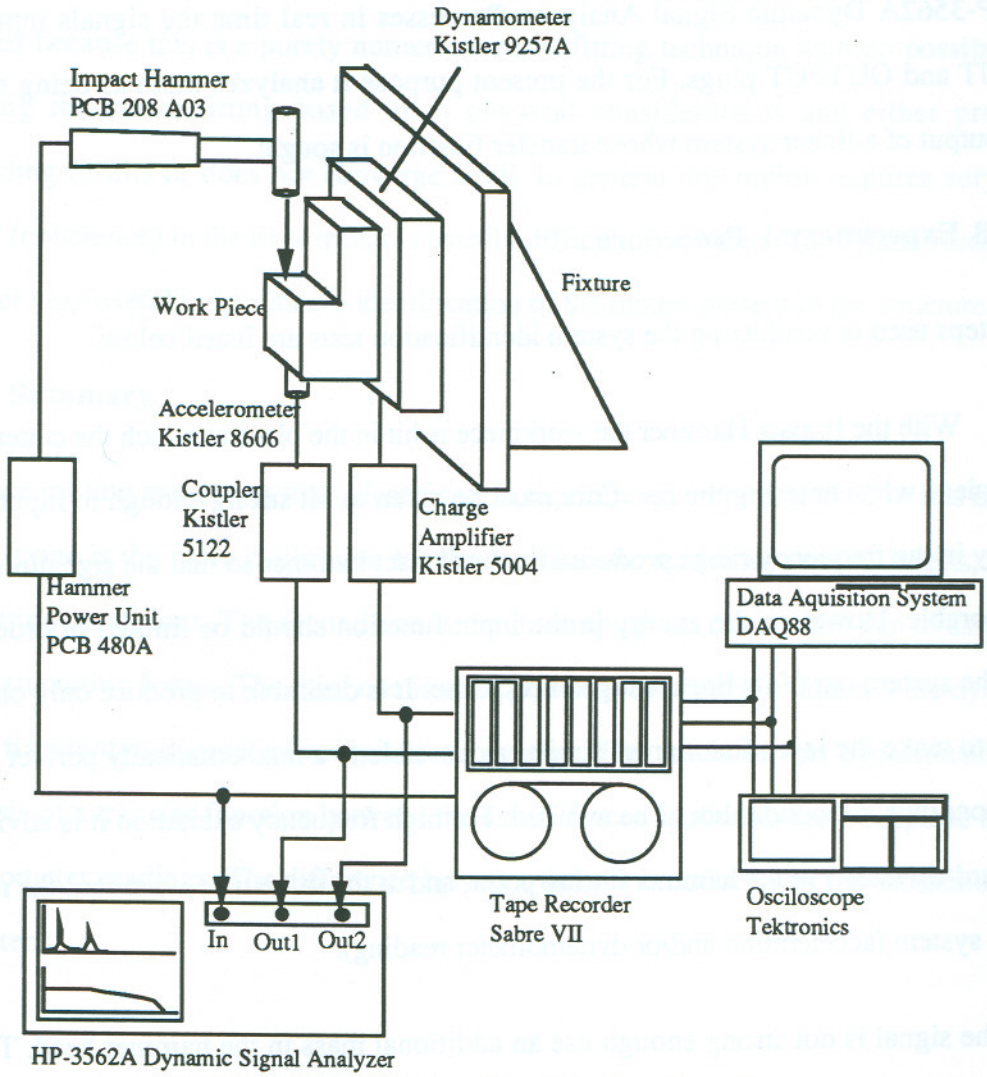

Fig 5.9. Set up of System Identification Experiments.

3. Kistler Accelerometer 8606. This instrument has a resonant frequency of 31 kHz, and sensitivity of 50.15 mV/g with a distortion of 3.4% at 5 kHz. This frequency characteristic is suitable for the range of meaningful frequencies found in the experiment. This aspect is discussed in chapter 6.

4. Kistler Coupler 5122 for the Accelerometer. This instrument provides both the DC power source for the accerelometer and the circuitry which decouples the reading which is emited by the accelerometer from the power source, producing the signal ready for digital adquisition.

5. HP-3562A Dynamic Signal Analyzer. Processes in real time the signals input in the INPUT and OUTPUT plugs. For the present purpose it analyzes them as being the input and output of a linear system whose transfer function is sought.

5.2.3 Experimental Procedure

The steps used in conducting the system identification tests are listed below.

1. With the Impact Hammer the workpiece is hit in the place at which the cutter hits the workpiece when entering the cut. Care must be taken to hit strong enough to input enough energy in the frequency range produced by the impact hammer so that the signal/noise ratio is favorable. However, the energy in the input function should be limited in order not to take the system out of its linear range of response. It is desirable to produce only one hit, in order to make the input function as similar as possible to a mathematically perfect impulse function; thus, rebounds should be avoided. For high frequency excitation it is advisable to use hard-tip (steel) in the hammer hitting point, and at the same time, to record the response of the system (acceleration and/or dynamometer reading).

2. If the signal is not strong enough use an additional mass in the hammer head. This will have the penalty of lowering the natural frequency of the hammer and the range of frequencies it can excite.

3. Record the signal in the tape recorder and / or computer for further analysis.

4. Operating simultaneously with the test, the Signal Analyzer can be used for real time capture and analysis of the input signal (hammer signal) and either one of the two possible

output signals (dynamometer or accelerometer) . It is set in the "AVERAGING" mode in such a way that it will analyze data of several hits, and it is prepared for computing an experimental transfer function based on the Fast Fourier Transform of the Input / Output data. At the end of the number of tests specified for averaging, a curve fitting algorithm can be initiated in order to identify the closed form of the transfer function. This last option was not used because this is a purely numerical curve fitting technique with no possibility of directing the curve fitting based upon physical considerations and either produces misleading results or does not converge at all. In general this option requires very good quality (coherence) in the data which is usually difficult to achieve. The Signal Analyzer is however very useful in qualitative identification of the modes present in the structure.

5.3 Summary

Two face milling and one system identification experiments were described in this chapter. The first one is the force calibration for the mechanistic model for several inserts, cutters and cutting conditions. The second one is the interrupted cut experiment run to assess the entry/exit cutting forces. The third one is an experiment conducted to identify the dynamics of the fixture/dynamometer/workpiece subsystem. The result of this experiment is the synthesis of a transfer function between the actual forces applied to the workpiece and the dynamometer readings. The difference between them is introduced by the vibration of the subsystem.

CHAPTER 6

EXPERIMENTAL RESULTS

In the previous chapters the geometrical aspects of the tool entry/exit force modeling have been discussed and an experimental plan has been presented. The objectives of this chapter are:

1- Discussion of the results of the structural dynamics identification and estimation of transfer function for the fixture/dynamometer/workpiece subsystem For the sake of brevity it will be called "fixture subsystem" from now on.

2- Presentation of the results of the continuous cutting tests and the calibration of the Mechanistic Model.

3- Prediction of the force signatures from the interrupted cut by using the mechanistic model forces and the transfer function from the dynamics identification results.

4- Presentation of the results of the interrupted cut tests

6.1 General Outline of the Data Processing

The experiments of interrupted cut with sharp transition in entry/exit strongly excite the dynamics of the machine tool. This is due to the fact that the sudden engagement / disengagement of the tool with the cut produces a dynamic response in the subsystem formed by the workpiece, the dynamometer and the fixture shown in Fig 6.1. The force signal produced by the dynamometer is the result of this response and therefore does not exactly represent the actual cutting forces. The approach to estimate the transfer function is to assume that the ratio "measured_signal/real_force" conforms to a linear process and then compute the transfer function for this linear process. Once the transfer function is determined, one of the following approaches may be adopted :

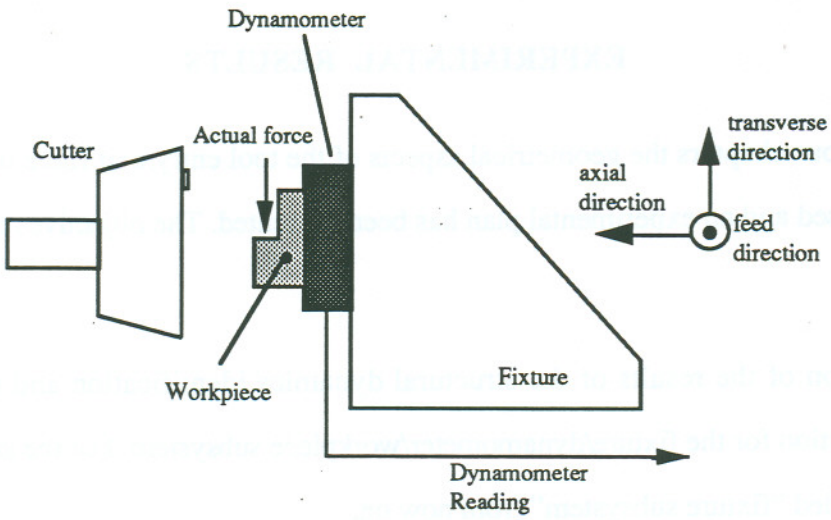

Fig 6.1 Relation between Actual force and Dynamometer Reading.

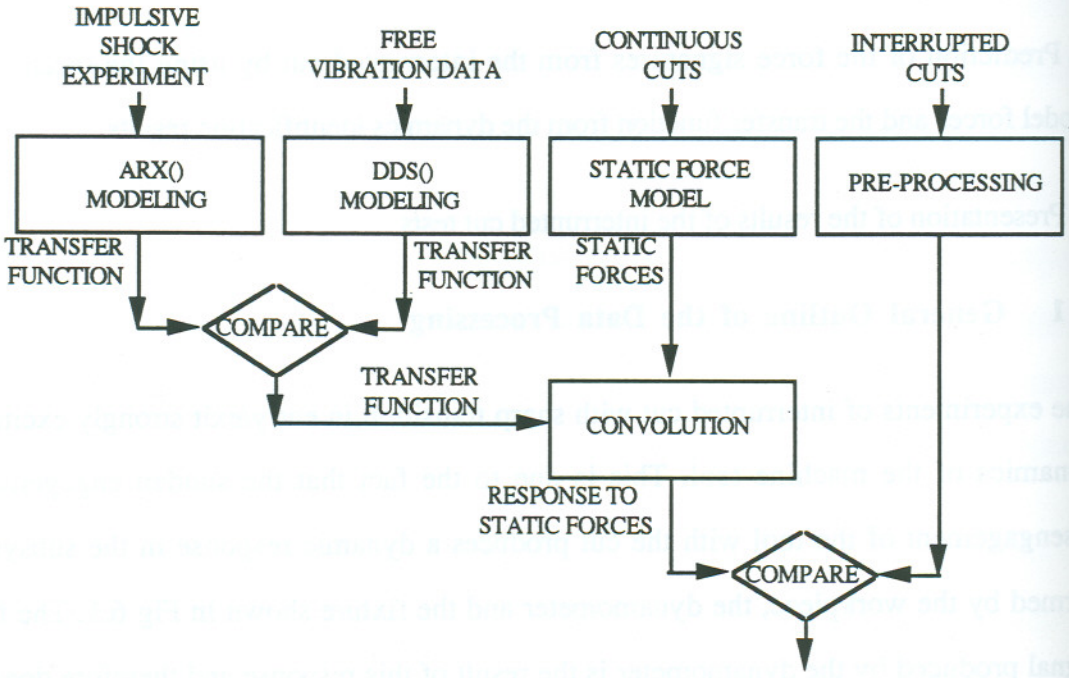

Fig 6.2 General outline of data processing setup.

First, from the measured signal (output) use the transfer function to back-calculate the input (the actual cutting forces) for the system. Second, assume static cutting forces as input, use

the transfer function to calculate the output (dynamometer reading) and compare it with the measured response. Although the first alternative is more elegant from the theoretical point of view, it is difficult to implement because it depends upon the stability of the inverse transfer function to calculate the input of a system based on the output. It is also very sensitive to the quality of the data used to calculate the transfer function, the method; etc. The data processing setup used in this research work can be summarized as shown in Fig 6.2. The procedure requires to:

1- Establish a transfer function between the actual forces applied to the workpiece and the dynamometer readings. This is done by two methods, whose results were compared on the basis of the coherence [25].of the experimental data used. The first method includes the excitation of the structure with an Impact Hammer in order to get the Impulse Response which itself is the transfer function. The second method applies a Dynamic Data analysis [50] to the signal collected when the cutter has just left the cut and the system still vibrates due to the tool exit.

2- Calibrate the static model. In particular, estimate the cutting force coefficients Kf, and Kc. Establish a static model characterization of the cutting forces. In this case a Kt_Kc model based on Fu's algorithm was used. Continuous tests were run with the same conditions (rpm, feed, doc) as the interrupted cutting tests with the purpose of determining a static version of the force model as close as possible to the conditions of the interrupted cuts. The result of this module is the Mechanistic Model calibration for the static forces.

3- Collection and pre-processing of the interrupted cutting forces. Initial pre-processing includes correction for zero offset from the instrument, change from time basis to angle basis where required and units conversion. The change to angle basis is performed because velocity varies too much about the set point during the cut. Consequently any comparison based on time axis for the nominal speed will have meaningless results.

4- Determine the response using Kt_Kc based on static force predictions as inputs to the transfer function. This convolution module predicts the response of the fixture (fixture/dynamometer/workpiece) subsystem to the cutting forces.

5- Comparison of the predicted responses with the experimental data pre-processed as explained in step 3.

6.2 Identification of the Dynamics of the Fixture Subsystem

The purpose of this section is to discuss the experimental procedure followed to obtain the characterization of the dynamics of the fixture subsystem, and to interpret the results obtained from the analysis. Three experiments were run to identify the dynamics of the subsystem. The instrumentation and setup used in these experiments are shown in Fig 6.3. The first two experiments were run by using in impact hammer to excite the dynamics of the system, monitoring at the same time two responses; one from the dynamometer ,and the other form the accelerometer. The third experiment consisted in monitoring the vibration of the system when the cutter leaves the workpiece. A deterministic model was fitted to the data by using Dynamic Data System analysis to find the vibrational modes.

6.2.1 Dynamics Identification Using Impact Hammer Shock

The first two experiments involve the use of an impact hammer to hit the workpiece where the cutter is supposed to be in contact when entering the cut.. In one of them the readings from the dynamometer are considered the response (output force) to the impact hammer force excitation (input force). The objective in this case is to determine the transfer function from the actual cutting forces to the dynamometer readings.

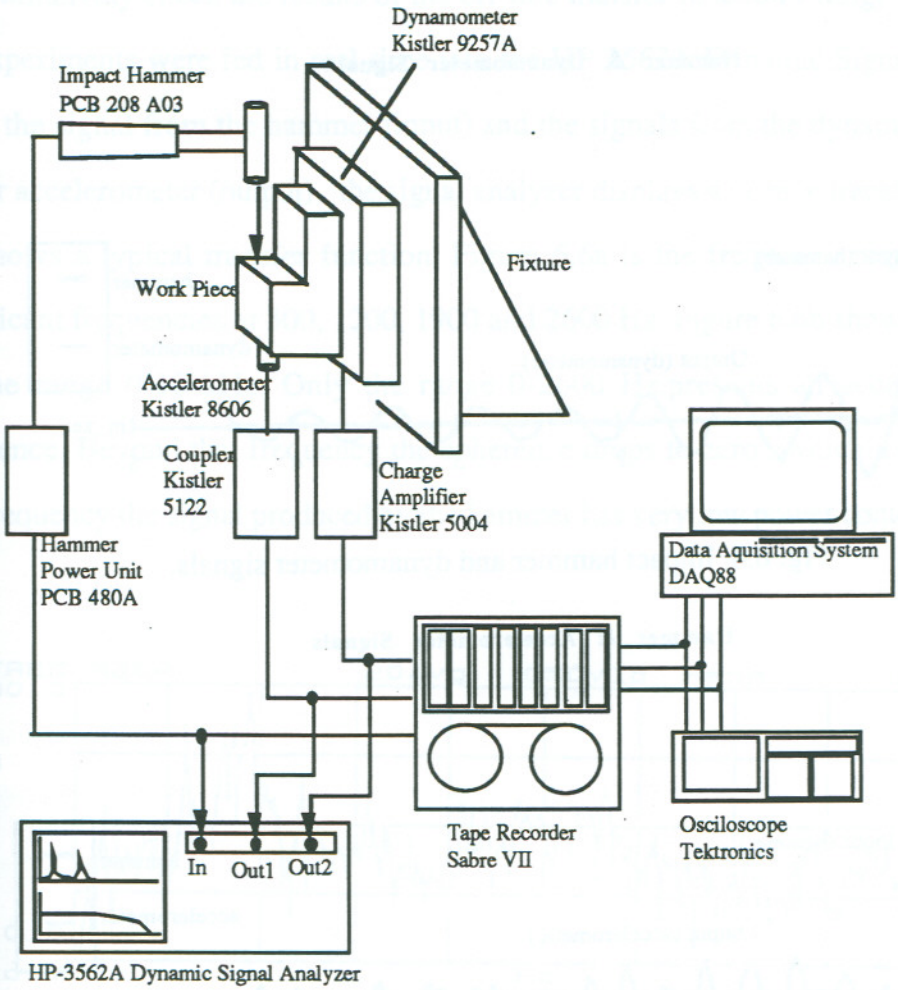

Fig 6.3. Instrumentation and system identification setup.

In the second experiment the readings of an accelerometer (output acceleration) placed in the bottom of the workpiece (as shown in Fig 6.3) are considered the response of the system to the impact hammer (input force) excitation. The objective is to estimate the transfer function between the actual forces to the workpiece and the accelerometer response. The method of processing the data from these experiments consisted of an ARX() model fitting [52], preceded by smoothing and windowing when required.

The impact hammer, dynamometer and accelerometer readings (sampled at a rate of 40000 hz) are shown in Figs 6.4 and 6.5.

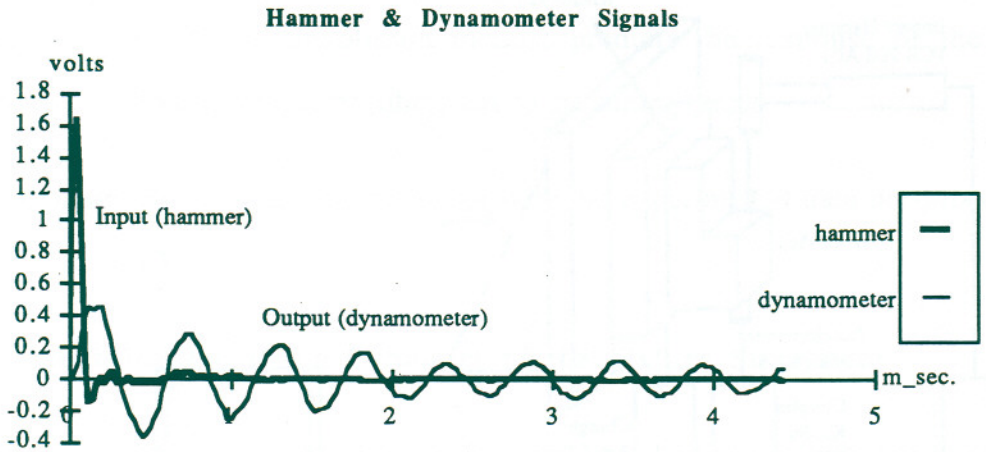

Fig. 6.4. Impact hammer and dynamometer signals.

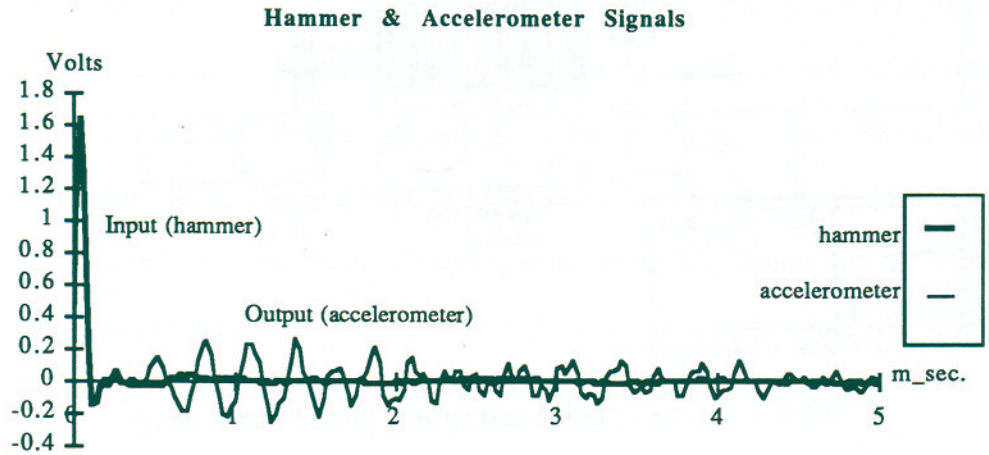

Fig. 6.5. Input Hammer and accelerometer signals.

The coherence between the input and output signals for the second experiment (based on the accelerometer reading) was found to be very low; therefore the transfer function from the impact hammer force to the accelerometer reading could not be adequately estimated In contrast, the signals from the impact hammer and the dynamometer were found better conditioned (by having higher coherence) up to frequencies as high as 2600-3000 Hz. Therefore the discussion will be centered exclusively on the transfer function relating the force signal from the impact hammer to the dynamometer output (force) signal

To qualitatively check the results of the off-line transfer function fitting, the signals from the experiments were fed in real-time into the HP-3562A Dynamic Signal Analyzer. By using the signal from the hammer (input) and the signals from the dynamometer (output) and/or accelerometer (output) , the signal analyzer displays a sample transfer function. Fig 6.6 shows a typical transfer function. Figure 6.6a is the frequency response. It shows significant frequencies at 300, 1200, 1900 and 2600 Hz. Figure 6.6b shows the coherence for the range 0-10 kHz. Only the range 0-2600 Hz.presents an acceptable level of coherence. Beyond that frequency the coherence drops to zero , which means that above that frequency the signal produced by the hammer has very low power content.

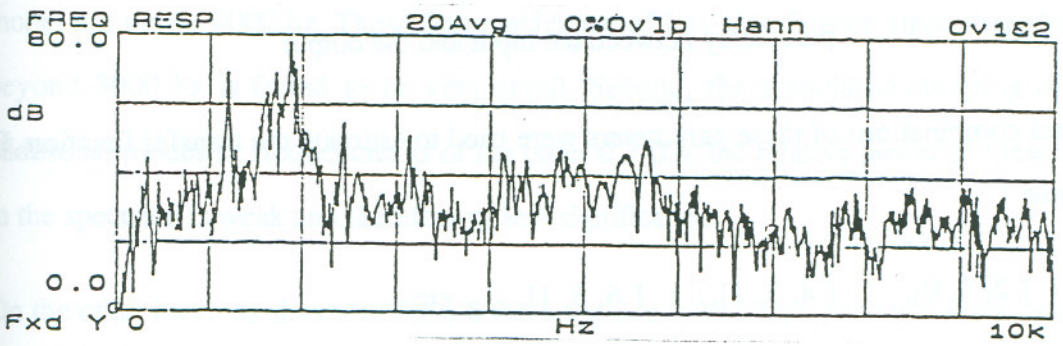

(a)

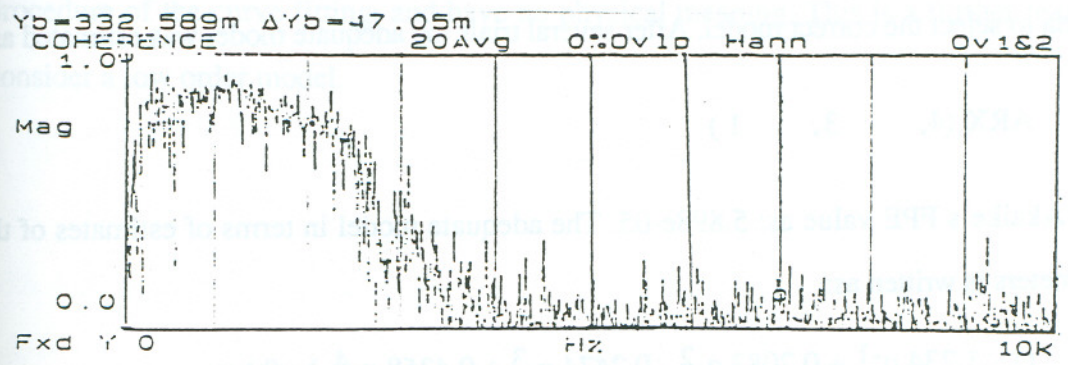

(b)

Fig. 6.6. HP Signal Analyzer synthesis of the Sample transfer function between Impact Hammer signal and the Dynamometer reading.

Model Fitting to Impact Hammer and Dynamometer Force Data

The model for the transfer function estimation was obtained by computing the least square-estimates of the ARX-models. The ARX function is part of Matlab System Identification Toolbox [52]. It estimates the parameters of the ARX model

$$A(q^{-1})\, y(t) = B(q^{-1})\, u(t\text{-}nk) + e(t) \qquad (6\text{-}1)$$

along with the variances for the parameters of the polynomials A(q) and B(q). It assumes e(t) as a white noise. The parameters used for model fitting are:

na	the order of the A(q) polynomial.
nb	the order of the B(q) polynomial.
nk	pure delay between the input and the.output

Several combinations of these parameters were tried to estimate the transfer function. For example

[2, 1, 0], [4, 3, 1], [6, 5, 1], etc.

The adequacy of the model was evaluated by using the Akaike's criteria [50,52]. An stable inverse function ie. stable zeros in the transfer function was also used as an adequacy criteria to select the correct model. After several trials the adequate model was estimated as:

ARX (4, 3, 1)

with Akaike`s FPE value as: 5.898e-05. The adequate model in terms of estimates of the parameters is written as:

$$(1 - 1.234\, q^{-1} + 0.2083\, q^{-2} - 0.2474\, q^{-3} + 0.4358\, q^{-4}\ )\, y(k) =$$

$$q^{-1}\ (\ 0.0829 + 0.0119\, q^{1-} - 0.0356\, q^{-2}\ )\ u(k) + e(k) \qquad (6\text{-}2)$$

The characteristic roots and frequencies are shown in Table 6.1:

Table 6.1. Dynamics of the system derived from Impact Hammer Experiment.

Zeros	Poles:	Natural freq(hz)	Damping
-0.7315	0.9375 ± 0.2714i	1800.5	0.0860
0.5879	-0.3205 ± 0.5957i	7295.4	0.3411
0			

Figure 6.7 shows the response (dynamometer reading) of the system to the input coming from the impact hammer force. The thickest line is the experimental value of the response. The other two lines correspond to the simulated response by using the arx(4,3,1) and arx(2,1,0) models.

It is important to note that in selecting the adequate model, two additional considerations were made. First, the frequencies or modes which appear by increasing the order of the model are above 4000 hz. These frequencies are of less significance since the coherence beyond 3000 hz is found to be very small. Second, the associated damping of these additional modes or frequencies is of the order 0.3-0.6; the relative power of these modes in the spectrum is weak and therefore of less significance.

On the other hand, as shown in Fig 6.8 there appears to be a beat phenomenon although its significance is small. By trying to indefinitely increase the order of the model to match the beat, other frequencies and effects appear in the model which arise purely from the procedure of the curve fitting, and have no physical meaning. This is a further reason to consider a low order model.

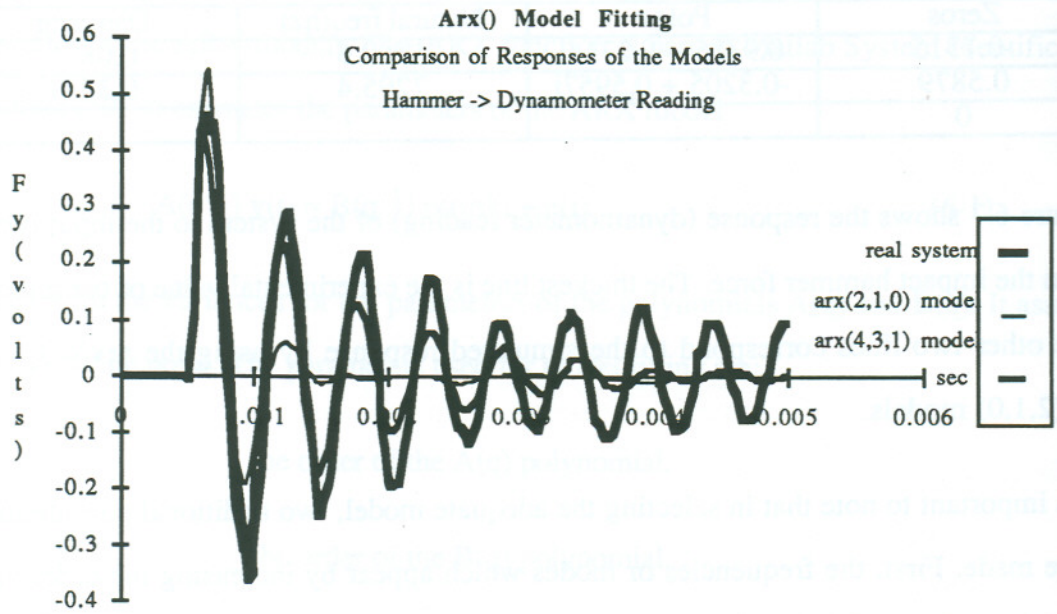

Fig. 6.7. Fitted Models ARX(2,1,0) and ARX(4,3,1) Responses for the Dynamometer/Hammer transfer function.

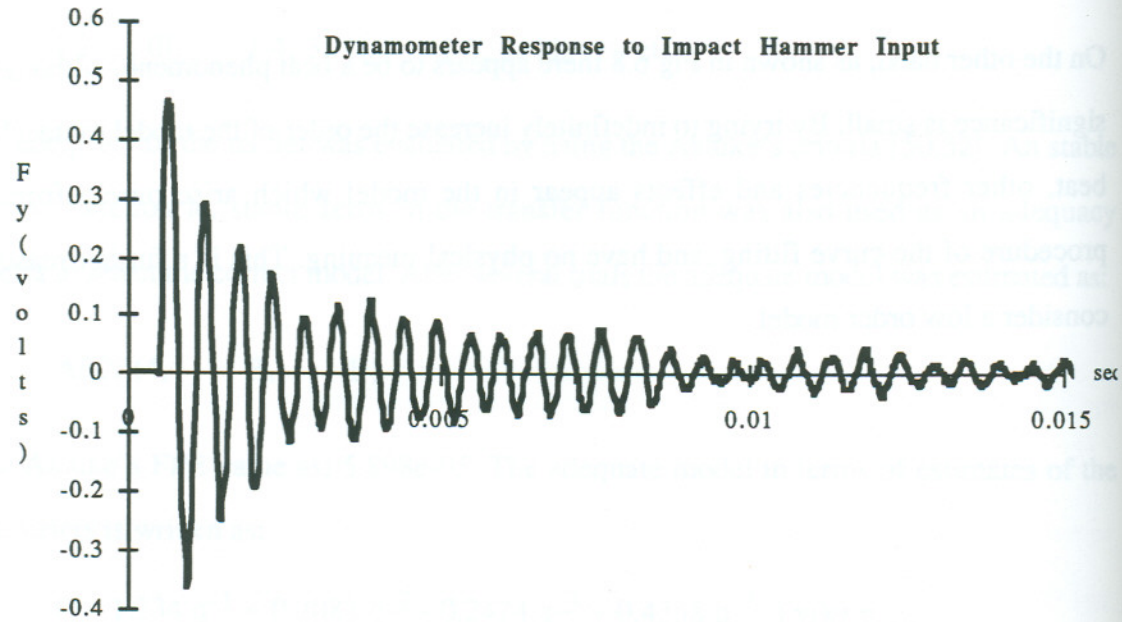

Fig. 6.8. Experimental Response to Impulse Input.

6.2.2 Dynamics Identification Using Free Vibration Test Data

Although the transfer function between the impact hammer signal and the dynamometer output was estimated in the previous section, it was desired to see whether the estimate could be improved by using the force signal when the subsystem is vibrating freely after the cutter has left the workpiece.

Fig 6.9 shows the force response from the fixture subsystem when the tool leaves the cut. This response is thought of as a response produced by releasing a spring from a stretched position in which it is kept by a external force.. In the case of the face milling experiments the system is released from the static transverse force resulting from the cut when the tool exits. Therefore the reaction of the subsystem shown in Fig 6.9 corresponds to the free vibration of a dynamic system after the driving force is withdrawn.

The third experiment for the determination of a transfer function between the applied force to the workpiece and the dynamometer output includes collecting the transverse force readings in actual cut when the cutter leaves the workpiece and the subsystem vibrates freely. A Dynamic Data System analysis [50] is applied to determine the parameters of the deterministic part of the free vibration. These parameters characterize the transfer function between the actual force applied to the workpiece and the dynamometer output.

The ARX() model was fitted to the data shown in Fig. 6.9 (recorded with a sampling rate of 10000 Hz). The actual data and the fitted ARX() model step response are shown in Fig. 6.10. The model fitting for this data showed that a ARX(14,13,1) model was adequate ; with Akaike`s FPE criteria of 12.78. The poles and zeros of the model are shown in Table 6.2. In Fig. 6.11 the poles and zeros of the transfer function are shown. As can be seen all the zeros and poles are stable, and the system therefore stable. The parameters which describe the transfer function are shown in Table 6.3:

Table 6.2. Dynamics of the system derived from free vibration data.

Zeros	Poles	Natural Freq (hz).	Damping
+0.8803 ± 0.1695i	-0.8033 ± 0.4612i	838	0.1454
+0.5626 ± 0.6897i	-0.7991 ± 0.0688i	376	0.9319
+0.0894 ± 0.7684i	+0.8783 ± 0.1561i	333	0.5445
-0.2507 ± 0.7672i	+0.5880 ± 0.6687i	1364	0.1353
-0.8267 ± 0.3936i	+0.3457 ± 0.9073i	1921	0.0244
-0.6658	-0.1470 ± 0.7754i	2233	0.1686
+0.0819	+0.0905 ± 0.6404i	2380	0.2914
0			

Table 6.3. Polynomial for Free Vibration derived Transfer Function.

$A(q^{-1})$	$q^{-1} B(q^{-1})$
1.0000	
-0.3062	1.7056
0.0202	-0.5560
0.7621	-0.3057
-0.4509	0.2074
-0.3403	-0.2534
0.2937	-0.1625
-0.3958	0.1547
-0.0713	-0.5468
0.1697	0.2537
-0.2633	0.0158
0.1812	0.0762
0.1237	0.2298
-0.0024	-0.0194
0.0855	

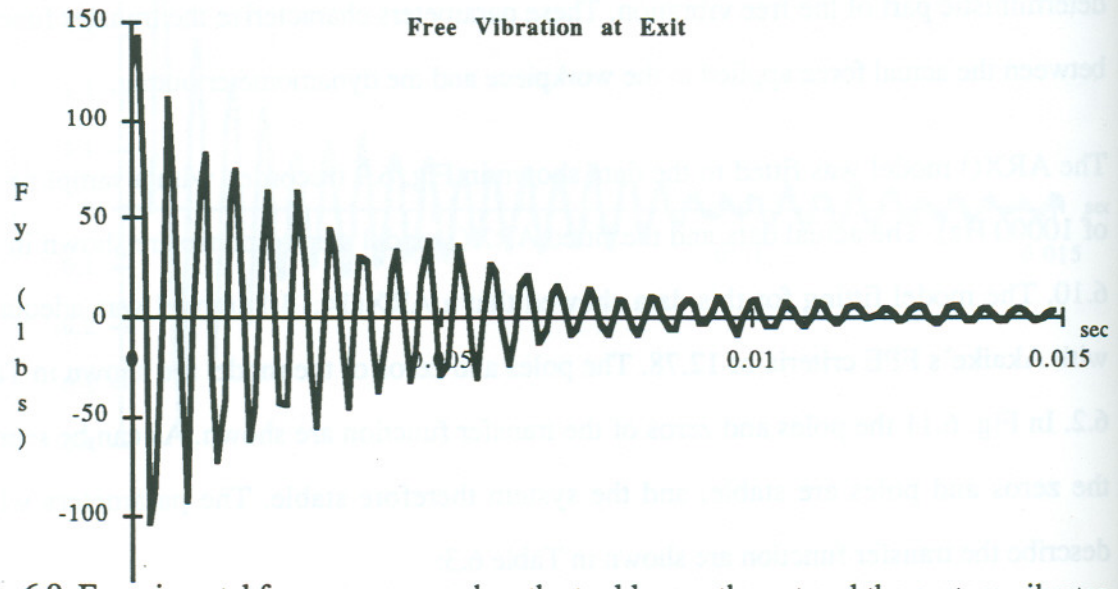

Fig. 6.9. Experimental force response when the tool leaves the cut and the system vibrates freely.

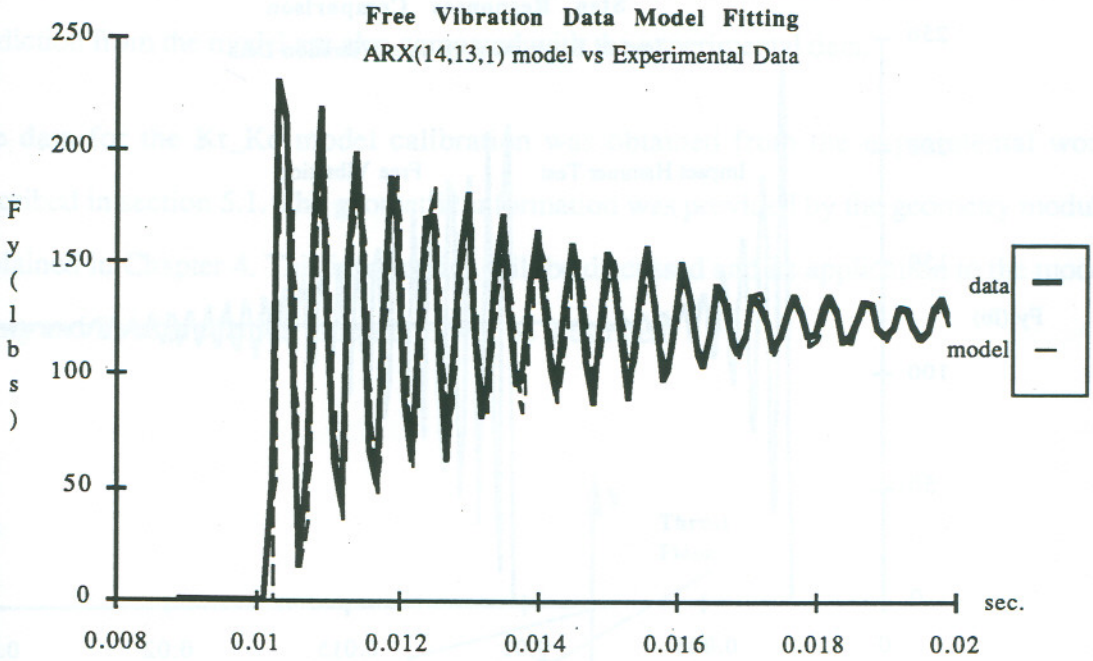

Fig. 6.10. Model fitting for free vibration data.

Fig. 6.12 shows the simulated step responses obtained from the transfer function derived from the impact hammer test and the transfer function derived from the free vibration test data. The free vibration test response shows a much slower decay; due to the fact that its damping coefficient is much lower (0.02 for impact hammer tests vs 0.08 for free vibration data).

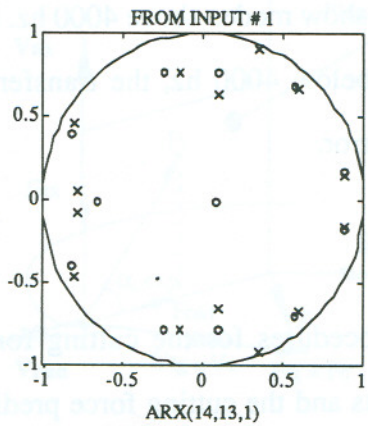

Fig. 6.11. Poles/zeros for the model fitted to the free vibration data.

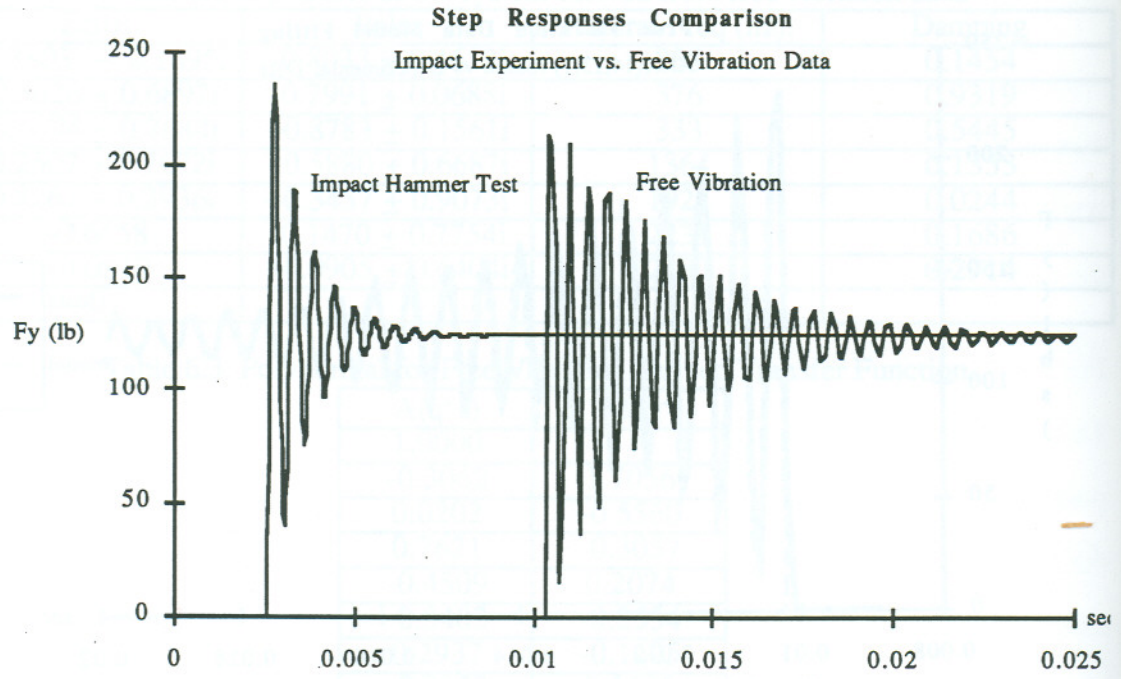

Fig. 6.12 . Comparison between the simulated step responses obtained from the transfer functions derived from the Impact Hammer test data vs the free vibration test data.

Comparing the indicative results of the two transfer functions (free vibration vs impact hammer forces) we select the function obtained from the free vibration test data. The reasons for the selection are: (i) it gives oscillation modes which are more consistent with the experimentally recorded modes (Fig 6.6.a) as obtained from the Signal Analyzer and (ii) the modes obtained from the free vibration test data are below 3000 hz in contrast with the impulse tests results, which show modes above 4000 hz. Since the Impact Hammer and Dynamometer bandwiths are below 4000 hz, the transfer function estimated with the Impact Hammer test data is in error.

6.3 Kt_Kc Model Fitting

This section discusses the procedures for the cutting force model calibration, ie the estimation of Kt,Kc coefficients and the cutting force prediction. Specifically, empirical models are developed for Kt,Kc in terms of cutting velocity and average chip thickness. The geometrical data for the calculation of contact area as function of insert engagement and

cutting edge length is obtained from the geometry models discussed in Chapter 3. The force prediction from the model are also compared with the experimental data.

The data for the Kt_Kc model calibration was obtained from the experimental work described in section 5.1. The geometric information was provided by the geometry module explained in Chapter 4. This information will be discussed and its application to the model fitting and force prediction procedures will be illustrated.

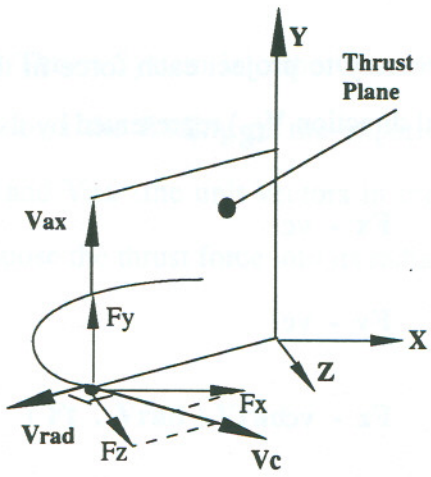

Fig 6.13. Decomposition of World Coordinate System forces into Cut-Thrust System.

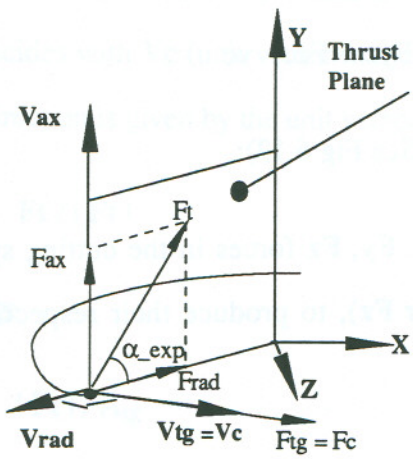

Fig 6.14. Decomposition of Cut-Thrust System into Cutter Coordinate System.

6.3.1 The Kt_Kc Model Fitting Procedure

In Fig 6.13 it is assumed that the three cutting force components expressed in the World Coordinate System , WCS, (Feed=X, Axial=Y, Transverse=Z), are available from an experiment. Since the Kt_Kc model predicts the Cutting and Thrust forces, these forces in WCS are expressed into the Cut_Thrust System (CTS) using the procedure summarized below:

1. Project forces in the WCS into the Cutting speed direction (See Fig 6.13):

For this objective it is necessary to project each force in the WCS in the cutting speed direction (same as tangential direction $\mathbf{V_{tg}}$) represented by the unit vector **vc**:

$$\begin{aligned} Fxc &= \mathbf{Fx} \cdot \mathbf{vc} \\ Fyc &= \mathbf{Fy} \cdot \mathbf{vc} \\ Fzc &= \mathbf{Fz} \cdot \mathbf{vc} \end{aligned} \qquad (6\text{-}3)$$

which are the projections of **Fx**, **Fy** and **Fz** on the tangential direction. Now, the total force in the cutting speed direction can be calculated as:

$$\mathbf{Fc} = (Fxc + Fyc + Fzc)\ \mathbf{vc} \qquad (6\text{-}4)$$

2. Find Thrust Force (See Fig 6.13):

The components of the **Fx**, **Fy**, **Fz** forces in the cutting speed direction are subtracted from each force (**Fx**, **Fy** or **Fz**), to produce their respective components in the thrust plane, as follows:

$$\begin{aligned} \mathbf{Fxt} &= \mathbf{Fx} - \mathbf{Fxc} \\ \mathbf{Fyt} &= \mathbf{Fy} - \mathbf{Fyc} \end{aligned}$$

$$\mathbf{Fzt} = \mathbf{Fz} - \mathbf{Fzc} \qquad (6\text{-}5)$$

Fxt, Fyt and **Fzt** are the projections of **Fx, Fy,** and **Fz** on the thrust tlane. The vectors **Fxt, Fyt** and **Fzt** are perpendicular to the **vc** vector by construction. The plane which contains those vectors is formed by the rotation axis **Vax** of the tool and a radial vector **Vrad** which points from the center of the cutter to the insert (see Fig 6.13). The total thrust force is given by the vector sum:

$$\mathbf{Ft} = \mathbf{Fxt} + \mathbf{Fyt} + \mathbf{Fzt} \qquad (6\text{-}6)$$

3. Decompose the Cut-Thrust System into the Cutter Coordinate System (Radial, Axial, Tangential). This allows the finding of the experimental effective lead angle direction. By using **Vrad** and **Vax** (the unit vectors in the radial and axial directions respectively) we can decompose the thrust force into its radial and axial components (See Fig 6.14):

$$\mathbf{Frad} = (\mathbf{Ft} \cdot \mathbf{Vrad})\,\mathbf{Vrad} \qquad (6\text{-}7)$$

$$\mathbf{Fax} = (\mathbf{Ft} \cdot \mathbf{Vax})\,\mathbf{Vax} \qquad (6\text{-}8)$$

for the force in the tangential direction the decomposition is trivial since **Vtg** (unit vector in the tangential direction) coincides with **Vc** (unit vector in the cutting speed direction). The experimental effective lead direction is given by the unit vector:

$$\mathbf{vt} = \mathbf{Ft} / |\mathbf{Ft}| \qquad (6\text{-}9)$$

4. Calculate Kt,Kc using:

$$Kt = |\mathbf{Ft}| / A_{tg}$$

$$Kc = |\mathbf{Fc}| / A_{tg} \qquad (6\text{-}10)$$

where A_{tg} is the chip area in the tangential direction.

The procedure described above can be applied in different positions of the cutter during the engagement period. This allows having a set of data in the form (v_{cut}, $\bar{tc}$, Kt) and (v_{cut}, $\bar{tc}$), Kc) . This data is used to calculate the Kt,Kc by fitting exponential relations of the following form:

$$Kc = a0 (v_{cut})^{a1} (\bar{tc})^{a2} \quad (6\text{-}11)$$

$$Kt = b0 (v_{cut})^{b1} (\bar{tc})^{b2} \quad (6\text{-}12)$$

where a0, a1, a2, b0, b1 and b2 are the empirical coefficients which allow the prediction of Kt and Kc for a given cutting velocity v_{cut} and the average chip thickness $\bar{tc}$.

6.3.2 Geometrical Information for Model Fitting

As stated in the previous section, as well as in section 3.4, the force model fitting requires the decomposition of the contact area and/or cutting forces for any position of the cutter into tangential, radial and axial directions which correspond to the Tool Coordinate System TCS. Also the cutting length is required for the calculation of the average chip thickness ($\bar{tc}$).

For the purpose of calibration cutting is simulated by using the geometry module described in Chapter 4. The simulation is required to give the following parameters for several positions of the cutting tool during engaged interval:

(i) Angular position of the cutting tooth, (ii) tooth-workpiece engagement status (No engagement / Partial Engagement / Full Engagement), (iii) cutting edge length, (iv) the contact area normal to the rake face (A_n), (v) Decomposition of A_n into the tool coordinate system [A_{tg},A_{rad},A_{ax}] and (vi) Decomposition of A_n in the world coordinate system [A_x,A_y,A_z] .

An example of the simulation results from the geometry module for cutting with Feed=0.02 in/tooth and DOC=0.02 in are shown in Fig.s. 6.15, 6.16 and 6.17. Fig. 6.15a presents the history of the chip area in the feed direction (see Fig. 6.1 for definition of Feed, Transverse and Axial directions) during the cutting period. Note that this area history presents a change of sign for the quantity describing the area in the feed direction. The reason for the change of sign is that for the first part of the cutting period the insert faces in the direction of the feed, while in the second it faces in the opposite direction. The duration of the positive or negative intervals depends on the radial rake of the cutter. Therefore, in general the area profile is not symmetrical. The particular signs in this figure obviously depend on the convention used in defining the WCS; another definition will produce the contrary signs. Fig. 6.15b presents the history of area in the axial direction. The area has the same sign during the whole cut and is negative for this case which corresponds to a cutter with negative axial rake. Fig. 6.15c displays the area corresponding to the transverse direction.

Fig. 6.16 presents the history of cutting edge length and 6.17 presents the history of average chip thickness. Note that there are two peaks in $\bar{\bar{tc}}$, at the beginning and end of the cut, due to the fact that, depending on the engagement/disengagement conditions the lead cutting length may tend to zero faster than the contact area, thus producing a large $\bar{\bar{tc}}$ value ($\bar{\bar{tc}}$ =Area/cutting_length). This is specially true for strongly negative cutters, which engage directly upon the rake face with no initial involvement from the cutting edge.

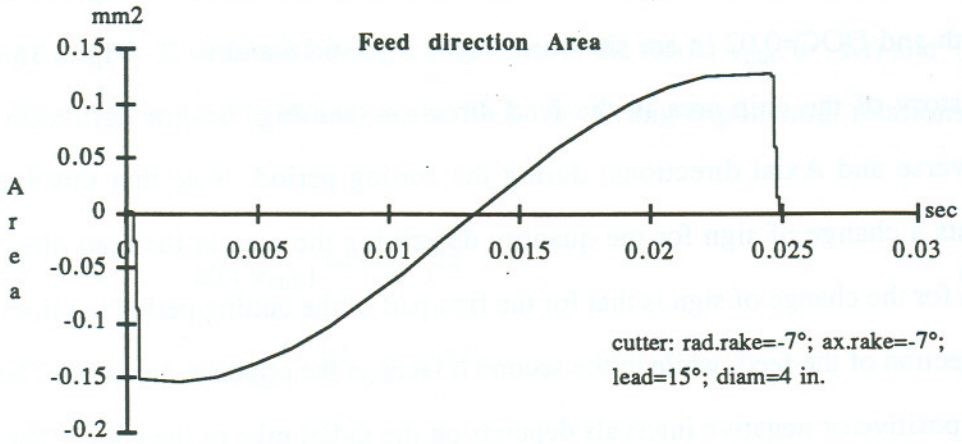

Fig. 6.15a. History of Contact Area in Feed direction. Feed=0.02 in/tooth, doc=0.02 in.

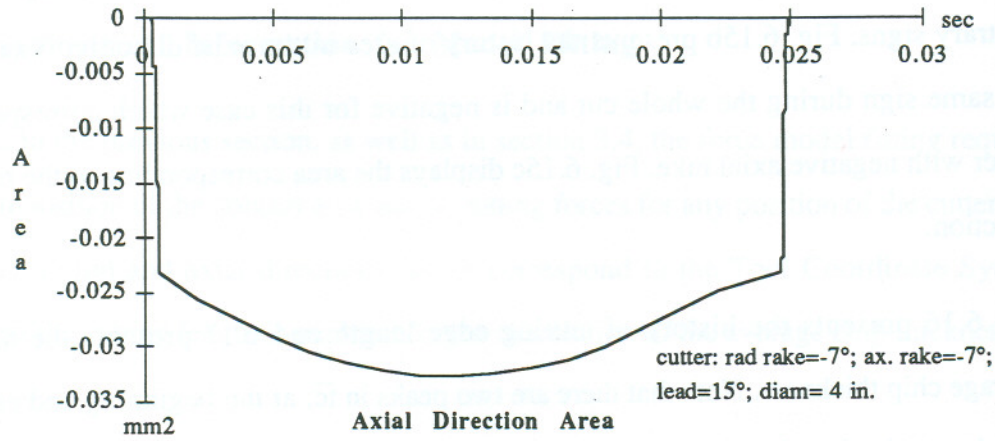

Fig. 6.15b. History of Contact Area in Axial direction. Feed=0.02 in/tooth, doc=0.02 in.

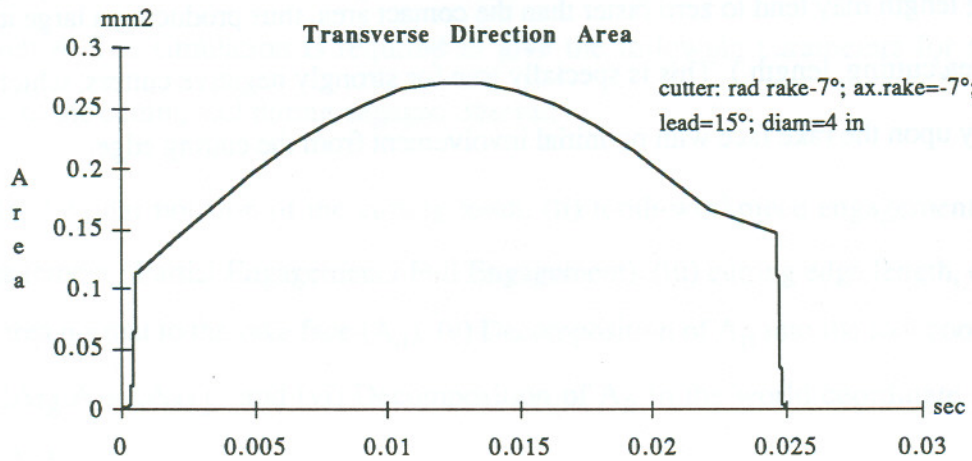

Fig. 6.15c. History of Contact Area in Transverse direction. Feed=0.02 in/tooth, doc=0.02 in.

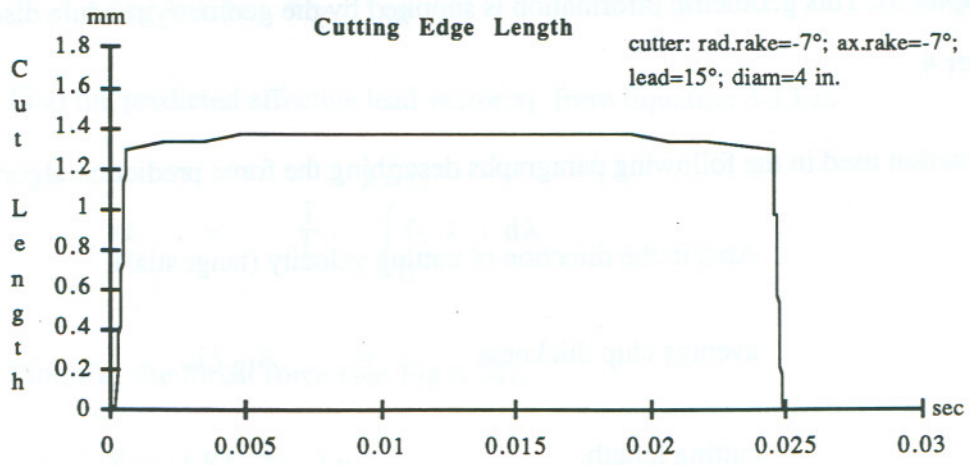

Fig. 6.16. History of Cutting Edge Length. Feed=0.02 in/tooth, doc=0.02 in.

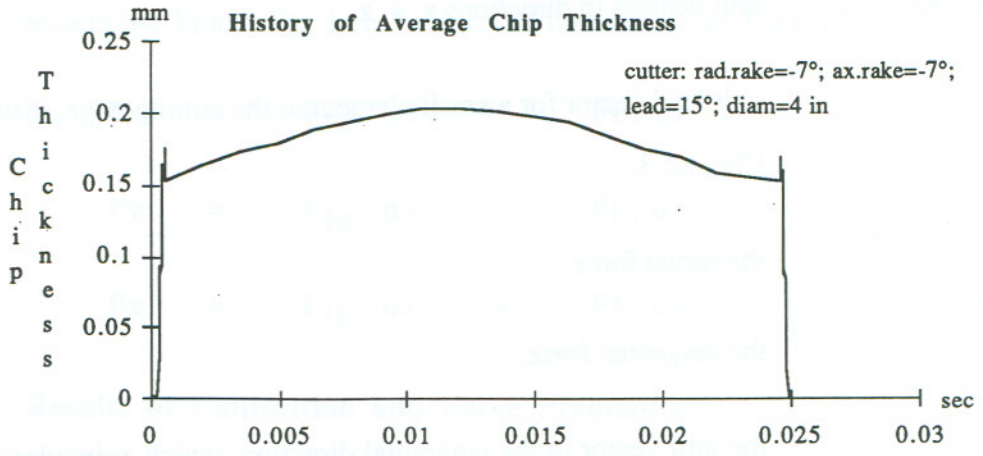

Fig. 6.17. History of Average Chip Thickness. Feed=0.02 in/tooth, doc=0.02 in.

6.3.3 Force Prediction Procedure

Having known the cutting pressure coefficients Kt,Kc in Eqs. 6-11 and 6-12 the force prediction proceeds. For the purpose of force prediction, the following geometric information is needed for any position of the cutter: (i) the decomposition of the contact area into tangential, radial and axial direction (TCS), (ii) the decomposition of the contact area into feed, transverse and axial direction (WCS), (iii) the cutting length so the calculation of the average chip thickness is possible and (iv) the vector which represents the effective lead (calculated from the three-dimensional version of Fu's algorithm, discussed

in Chapter 3). This geometric information is supplied by the geometry module discussed in Chapter 4.

The notation used in the following paragraphs describing the force prediction algorithm is:

A_{tg}	Area in the direction of cutting velocity (tangential).
$\bar{tc}$	average chip thickness = A_{tg} / L.
L	cutting length.
ux, uy, uz	unit vectors in directions x, y, z.
f	unit lead vector for a small element in the cutting edge, discussed in Chapter 3.
Ft	the thrust force.
$\mathbf{F_{tg}}$	the tangential force.
$\mathbf{V_{tg}}$	the unit vector in the tangential direction, which coincides with the cutting velocity vector.
$\mathbf{v_t}$	unit effective lead vector.

The following steps constitute the force prediction algorithm for a given position of the cutter

1. Determine A_{tg}, $\bar{tc}$.

2. With the cutting speed v_{cut} and $\bar{tc}$ determine Kt, Kc using the Equations 6-11 and 6-12.

3. Find $\mathbf{F_{tg}}$ and give it the direction of $\mathbf{V_{tg}}$ (see Fig 6.14).

$$\mathbf{F_{tg}} = (\mathrm{Kc} \,.\, A_{tg})\, \mathbf{V_{tg}} \qquad (6\text{-}13)$$

4. Find the predicted effective lead vector $\mathbf{v_t}$ from Equation 3-13 as

$$\mathbf{vt} = \frac{1}{L} \int_{\lambda=0}^{\lambda=L} \mathbf{f}(\lambda)\, d\lambda \qquad (6\text{-}14)$$

5. Find **Ft** , the thrust force (see Fig 6.14).

$$\mathbf{F_t} = (\mathrm{Kt} \,.\, A_{tg})\, \mathbf{v_t} \qquad (6\text{-}15)$$

6. Decompose **Ft** and **Ftg** into X, Y, and Z directions (see Fig 6.13).

$$\begin{aligned} Fx &= \mathbf{F_{tg} \,.\, ux} + \mathbf{Ft \,.\, ux} \\ Fy &= \mathbf{F_{tg} \,.\, uy} + \mathbf{Ft \,.\, uy} \\ Fz &= \mathbf{F_{tg} \,.\, uz} + \mathbf{Ft \,.\, uz} \end{aligned} \qquad (6\text{-}16)$$

6.3.4 Results of Calibration and Force Prediction

The experimental force data was filtered in order to eliminate frequencies higher than 1000 hz. The Kt, Kc coefficients obtained using the procedure discussed in section 6.3. along with the cutting conditions and average chip thickness are shown in Table 6.4.

Table 6.4. Kt, Kc Data for Double Negative Cutter, Regular Insert

Feed (in)	DoC (in)	rpm	v_{cut} (m/s)	tc (mm)	kc(kg/mm2)	kt(kg/mm2)
0.01	0.05	300	1.6	0.152	236.1	130.9
0.01	0.05	500	2.7	0.152	223.3	124.3
0.01	0.05	700	3.7	0.152	204.2	108.4
0.01	0.05	800	4.3	0.152	204.2	104.2
0.01	0.05	900	4.8	0.152	191.4	90.7
0.01	0.05	1000	5.3	0.152	191.4	93.2
0.01	0.05	1100	5.8	0.152	191.4	104.6
0.01	0.05	1300	6.9	0.152	178.6	94.9

0.01	0.05	1500	8.0	0.152	172.3	88.7
0.01	0.02	800	4.3	0.099	256.9	187.2
0.01	0.04	800	4.3	0.138	211.7	117.5
0.01	0.05	800	4.3	0.152	204.2	104.2
0.01	0.07	800	4.3	0.169	199.6	102.7
0.01	0.08	800	4.3	0.175	215.5	105.9
0.005	0.05	800	4.3	0.076	260.6	161.8
0.01	0.05	800	4.3	0.152	204.2	104.2
0.015	0.05	800	4.3	0.221	186.9	76.9
0.02	0.05	800	4.3	0.287	175.3	69.9

The results of model fitting for different combinations of cutter and insert geometries are given in table 6.5.

Table 6.5 Results of the Kt_Kc Calibration.

Insert	cutter	Range of Conditions.				
		feed (in)	doc (in)	rpm	kc	kt
Reg	D. Neg	0.005 to 0.020	0.020 to 0.080	300 to 800	$150.66\ (\bar{t}c)^{-0.317}\ (v_{cut})^{-0.2}$	$37.344\ (\bar{t}c)^{-0.751}\ (v_{cut})^{-0.252}$
Reg	Pos.	0.01	0.05	800 to 1200	$29.66\ (\bar{t}c)^{-0.952}\ (v_{cut})^{-0.127}$	$3.26\ (\bar{t}c)^{-1.17}\ (v_{cut})^{0.329}$
Reg	Shear	0.01	0.05	1000 to 1500	$87.01\ (\bar{t}c)^{-0.492}\ (v_{cut})^{-0.169}$	$15.97\ (\bar{t}c)^{-1.05}\ (v_{cut})^{-0.212}$
30 D.Flat	D. Neg	0.01	0.05	800	$127.9\ (\bar{t}c)^{-0.304}$	$19.95\ (\bar{t}c)^{-0.764}$
30 Flat	D. Neg	0.01	0.05	800	$104.71\ (\bar{t}c)^{-0.329}$	$22.38\ (\bar{t}c)^{-0.837}$
15 Flat	D. Neg	0.01	0.05	800	$362.2\ (\bar{t}c)^{-0.307}$	$23.22\ (\bar{t}c)^{-0.718}$
Kland	D. Neg	0.01	0.05	800	$40.65\ (\bar{t}c)^{-0.91}$	$11.16\ (\bar{t}c)^{-1.18}$

Figs 6.18, 6.19 and 6.20 show typical results of the cutting force prediction using the procedure discussed in section 6.3.3. Appendix C shows the comparison of measured and predicted force data for various cutting conditions and cutters. It is seen from these plots that the predictions for the transverse and feed directions are quite good. However, the

measured data shows the high frequency fluctuation reflecting the dynamics of the system. More discussion on the comparison of these forces is given in chapter 7.

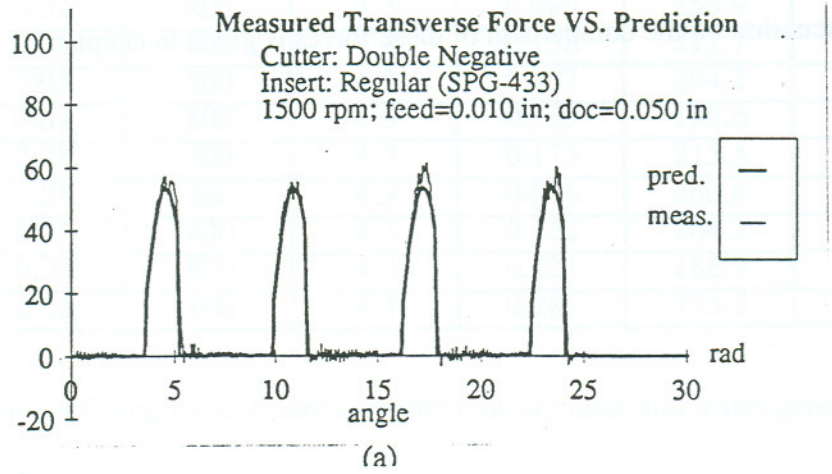

(a)

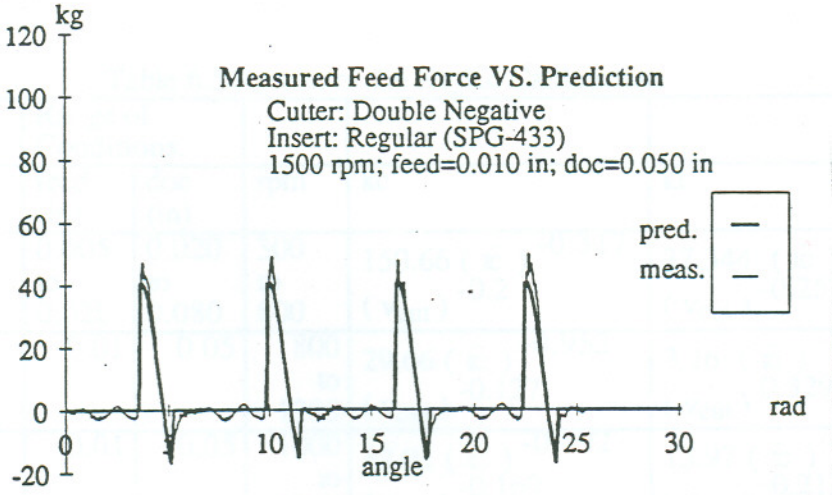

(b)

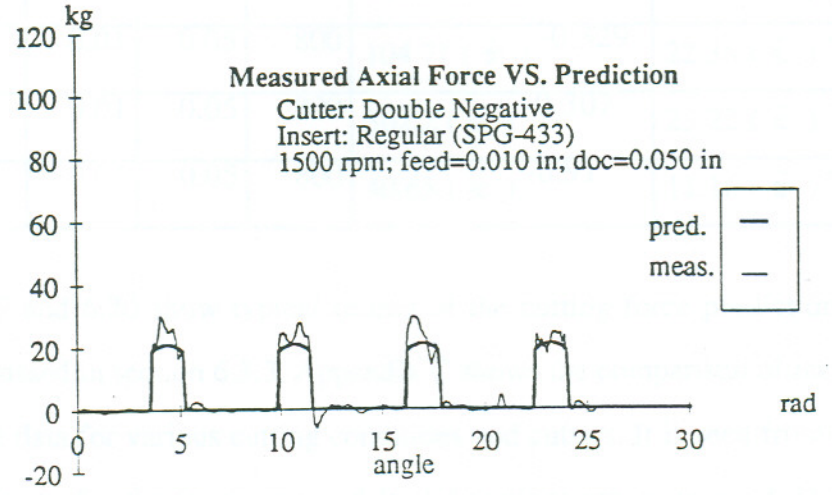

(c)

Fig 6.18. Transverse, Feed and Axial Experimental Force Vs. Predictions for Double Negative Cutter, Regular Insert.

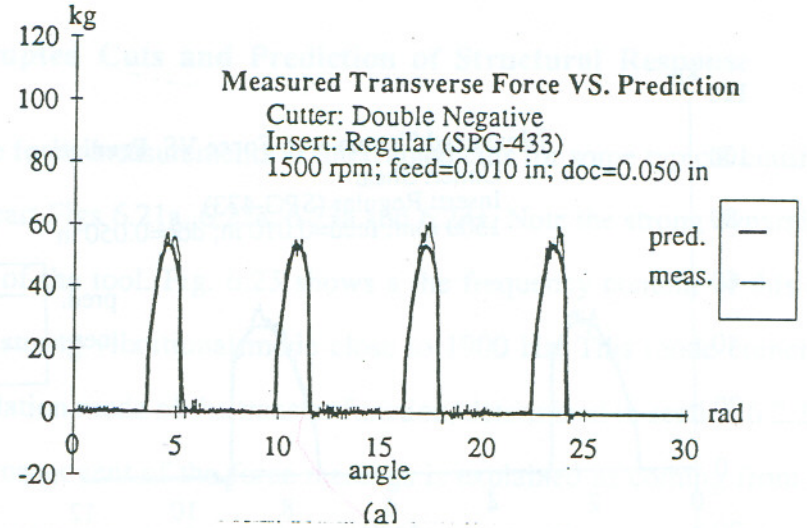

(a)

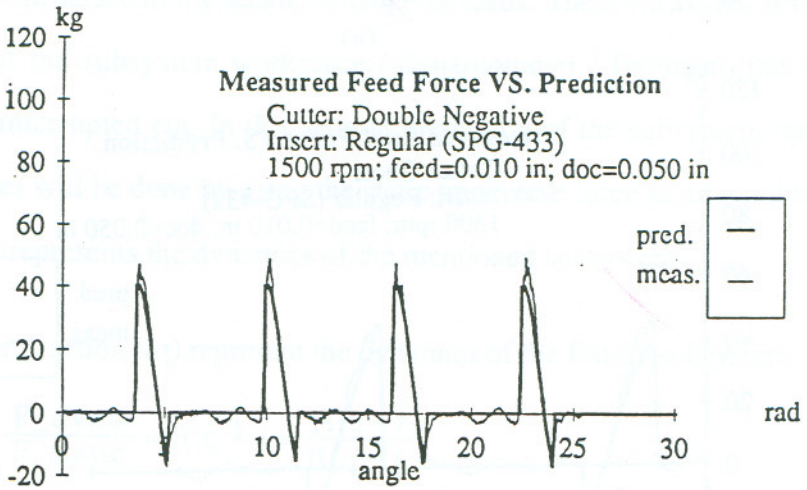

(b)

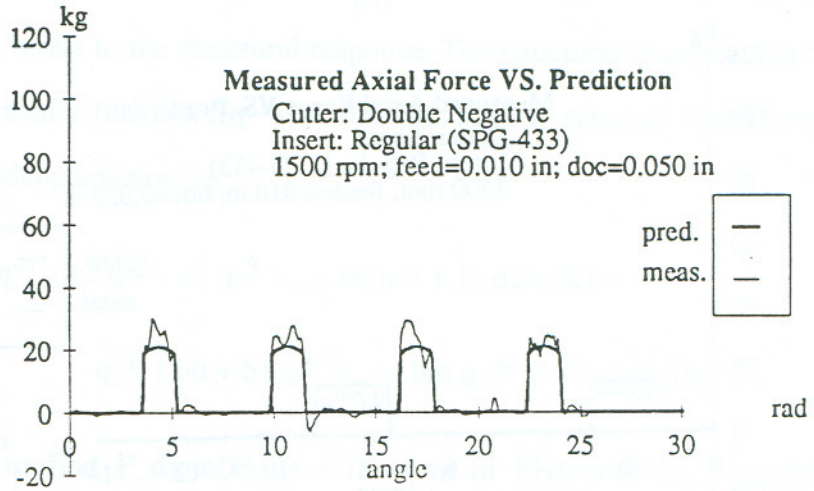

(c)

Fig 6.19. Transverse, Feed and Axial Experimental Force Vs. Predictions for Positive Cutter, Regular insert.

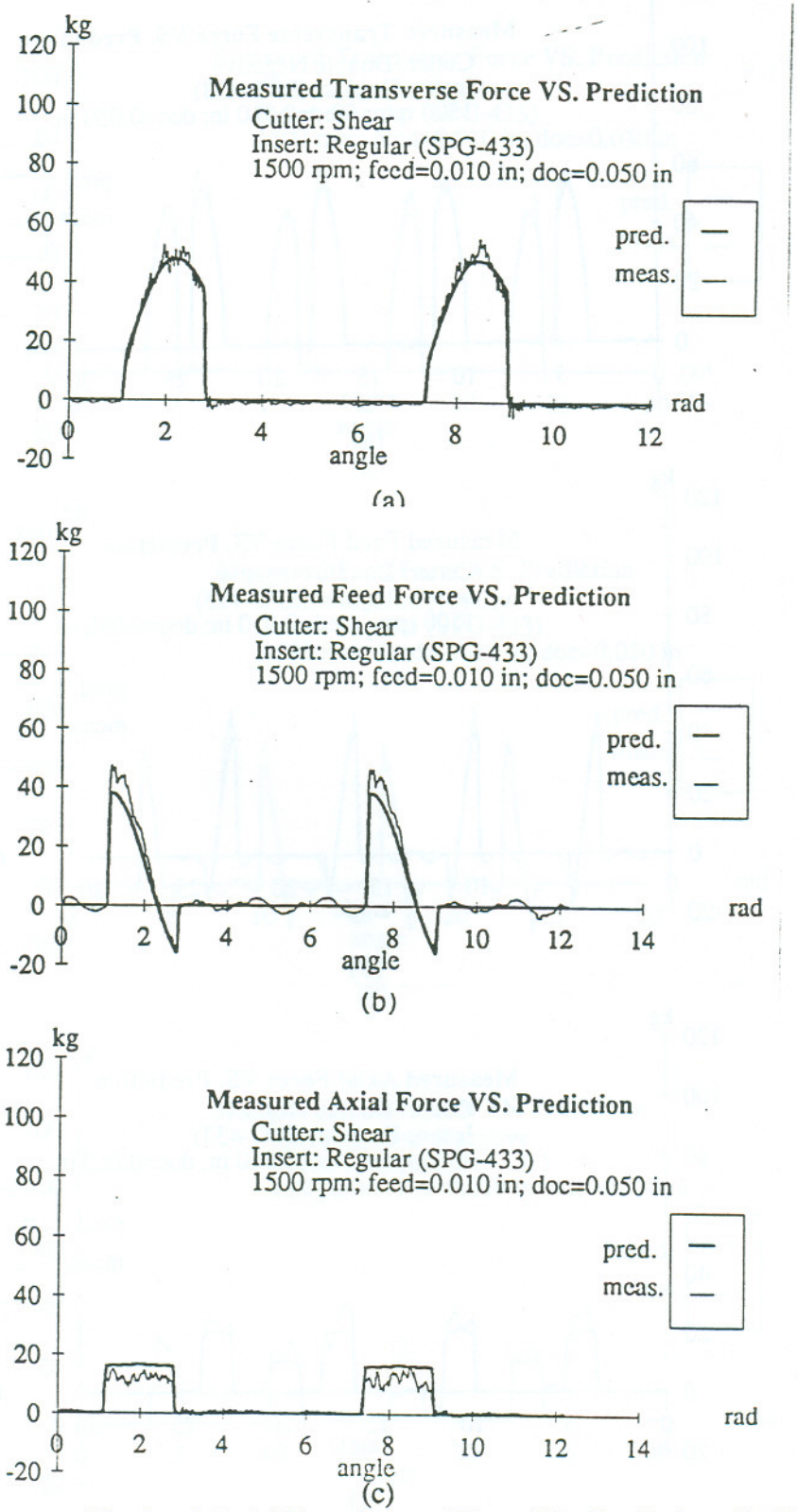

Fig 6.20. Transverse, Feed and Axial Experimental Force Vs. Predictions for Shear Cutter, Regular Insert.

6.4 Interrupted Cuts and Prediction of Structural Response

The transverse force measurements in interrupted cuts for some typical cutting conditions are shown in part Figs 6.21a, 6.22a, 6.23a and 6.24a. Note the strong dynamics caused by the entry/exit of the tool. Fig. 6.25 shows a the frequency content of this dynamics. It shows a very strong vibrational mode close to 1900 Hz. This mode coincides with the principal oscillation mode of the transfer function, determined in section 6.2.2. This shows that a strong component of the force readings is explained as coming from the dynamic response of the structure to the sudden change in loads. These measured forces represent the response of the subsystem workpiece / dynamometer / fixture to the actual forces present in the interrupted cut. In this section prediction of the subsystem response to the transverse forces will be done by using the static transverse force as an input to the transfer function which represents the dynamics of the mentioned subsystem.

Let' the transfer function f(q) represent the dynamics of the fixture subsystem:

$$\frac{F\_dyno}{F\_static} = f(q^{-1}) = \frac{A(q^{-1})}{B(q^{-1})} \qquad (6\text{-}17)$$

where polynomials A(q) and B(q) refer to the transfer function estimated in section 6.2.2 and F_dyno(k) refers to the structural response. The structural response can be found by applying the transfer function $f(q^{-1})$ on the static force F_static(k) found from the Kt_Kc mechanistic model prediction, ie

$$(1 - a1\, q^{-1} - a2\, q^{-2} - a3\, q^{-3} - \ldots\ldots - an\, q^{-n})\ F\_dyno(k) =$$

$$q^{-1}\ (b0 + b1\, q^{1-} + \ldots + bm\, q^{-m})\ F\_static(k) \qquad (6\text{-}18)$$

which allows to find F_dyno(k) as a function of F_dyno(k-1), F_dyno(k-2), and F_static(k-1), F_static(k-2), F_static(k-3), ..etc. such that

$$F\_dyno(k) = (a1 + a2\, q^{-1} - a3\, q^{-2} + \ldots\ldots + an\, q^{-n+1})\ F\_dyno(t\ k-1) +$$

$$q^{-1}\ (\ b0 + b1\ q^{1-} + ... + bm\ q^{-m}\ )\ F\_static(k) \qquad (6\text{-}19)$$

Using the coefficients of the polynomials for $A(q^{-1})$ and $B(q^{-1})$ from table 6.3 the force prediction was modeled. Figs 6.21b, 6.22b, 6.23b and 6.24b show the static force prediction and the corresponding dynamic force response calculated using the transfer function model of the subsystem. Figs 6.21 and 6.22 corresponds to Entry conditions whereas Figs 6.23 and 6.24 correspond to Exit conditions. In these figures the static prediction is shown as a thick line, while the subsystem response is represented by a thin line. It can be seen that there exists a large difference between the forces caused by the cut of the nominal chip area as compared to the disturbance in those forces caused by the sudden entry/exit of the tool. The dynamic prediction in these figures. represents the variation of the cutting forces as a result of the excitation of the subsystem dynamics, which is characterized by the transfer function (6-17) .

The results for the Dynamic Response simulation for several other tests can be found in Appendix C. The discussion of these results will be further presented in Chapter 7, Discussion and Conclusions.

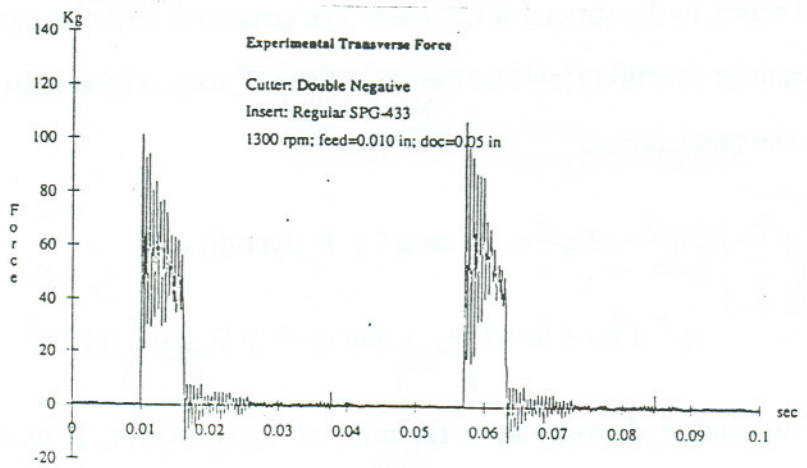

(a)

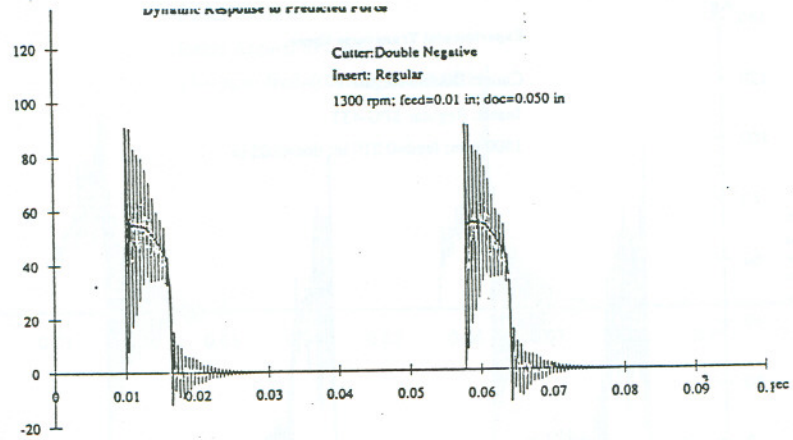

(b)

Fig 6-21 Force signature in Interrupted Cut. Series 1. Entry. 1300 rpm.
(a) Experimental. (b): Prediction by Dynamic response.

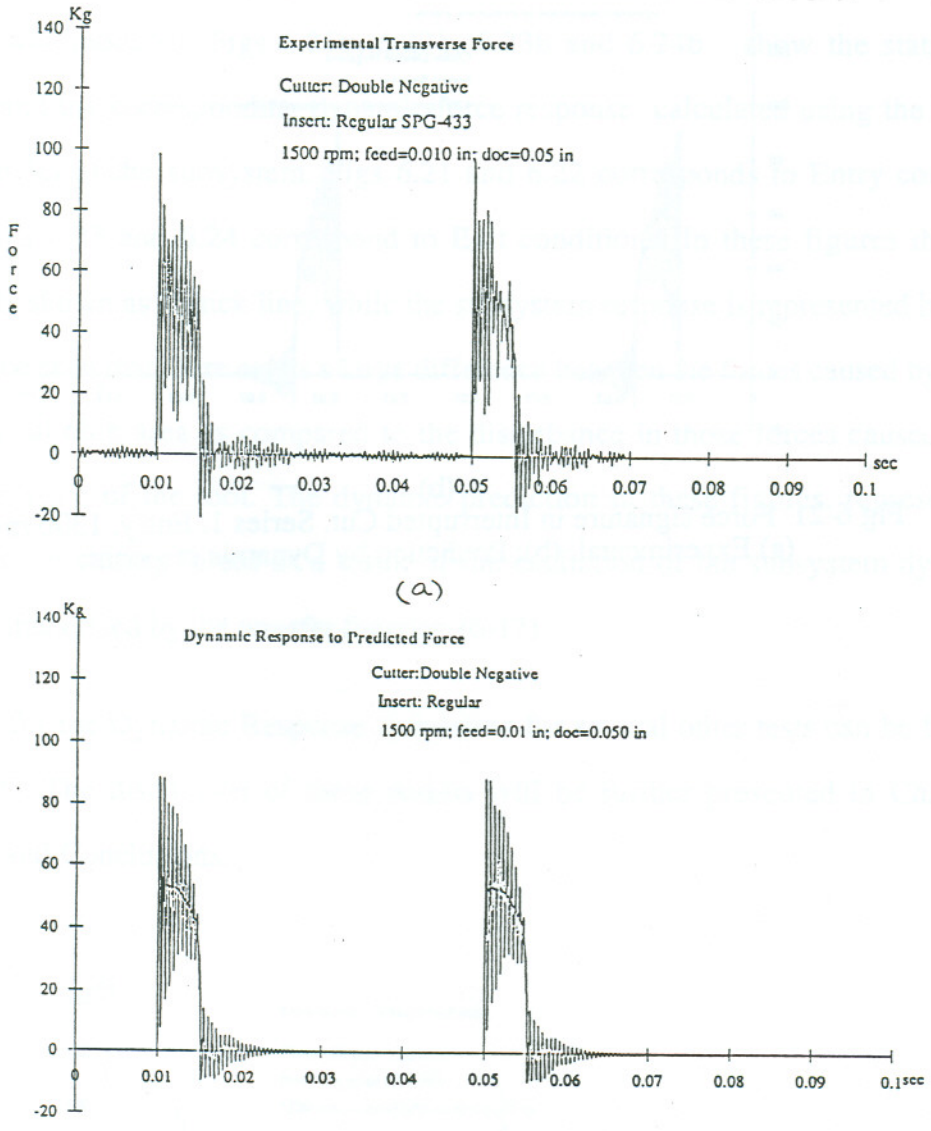

Fig 6-22 Force signature in Interrupted Cut. Series 1. Entry. 1500 rpm.
(a) Experimental. (b): Prediction by Dynamic response.

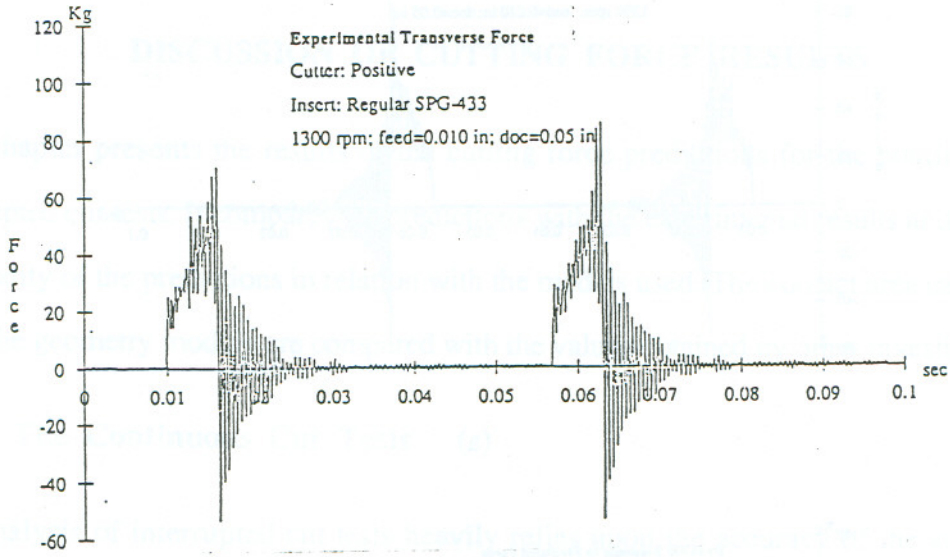

(a)

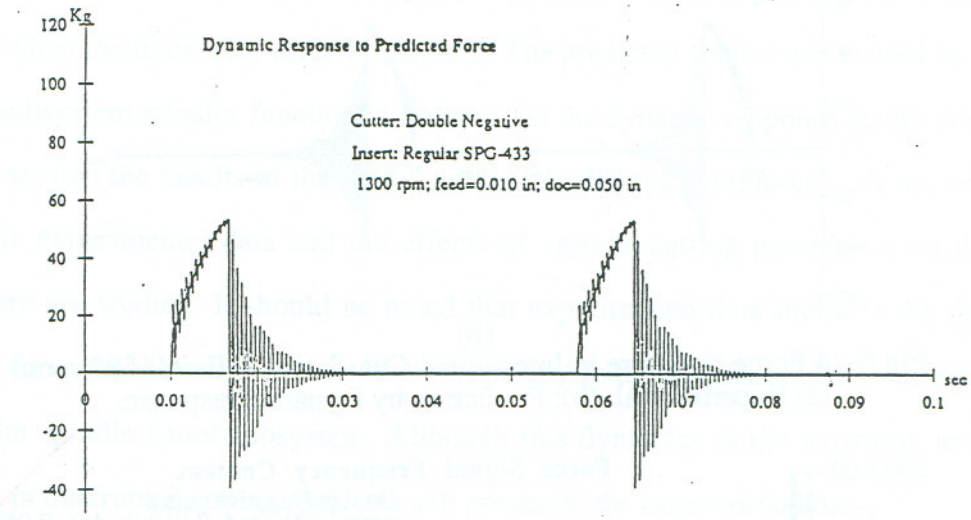

(b)

Fig 6-23 Force signature in Interrupted Cut. Series 1. Exit. 1300 rpm.
(a) Experimental. (b): Prediction by Dynamic response.

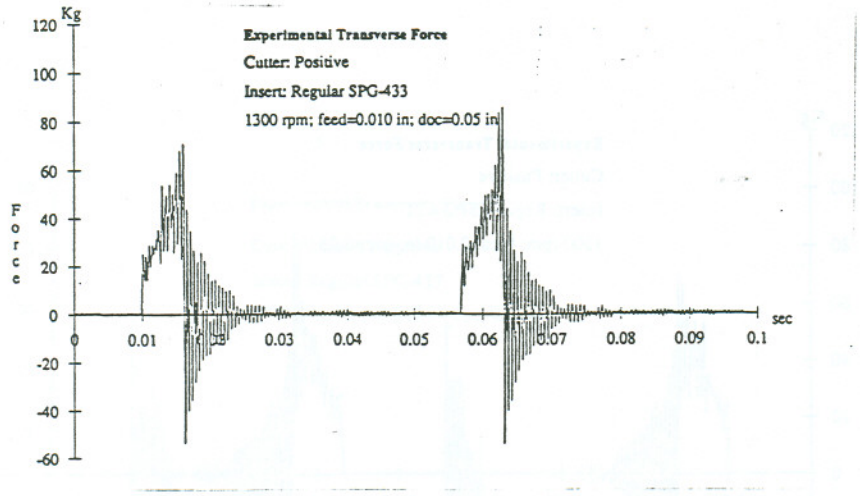

(a)

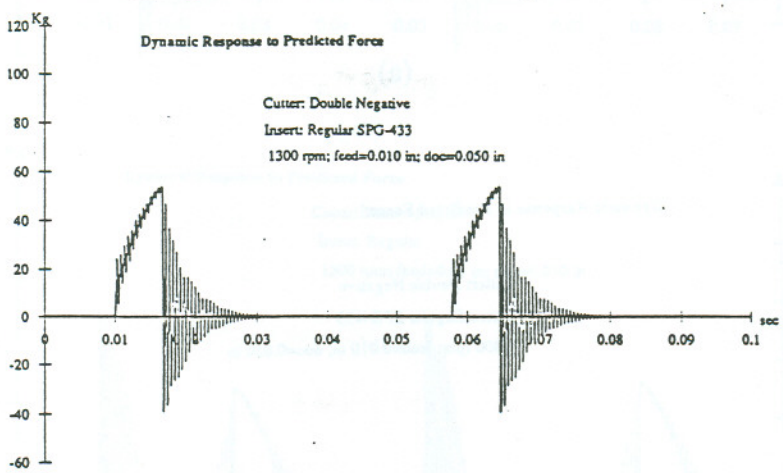

(b)

Fig 6-24 Force signature in Interrupted Cut. Series 1. Exit. 1500 rpm.
(a) Experimental. (b): Prediction by Dynamic response.

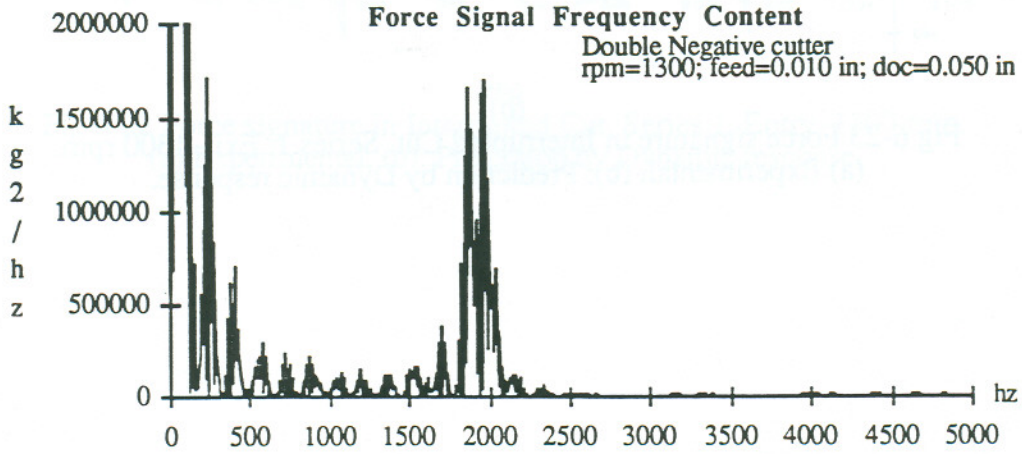

Fig 6.25 . Frequency content of Interrupted cut force signal

CHAPTER 7

DISCUSSION OF CUTTING FORCE RESULTS

This chapter presents the results of the cutting force predictions for the continuous and interrupted cut tests. It compares the predictions with the experimental results and discusses the quality of the predictions in relation with the models used. The contact area calculations from the geometry module are compared with the values obtained by other investigators.

7.1. The Continuous Cut Tests

The analysis of interrupted cut tests heavily relies upon the accuracy of the static force prediction by the Kt_Kc mechanistic model. The transverse force is most relevant to this research since the workpiece was designed to provide a very sharp transition for tool entry or exit when the transverse force is maximal. The predicted static force is used as an input to the subsystem transfer function in order to get the dynamic response of the subsystem. In this section the results of the model predictions for the continuous cuts are compared with the experimental data and the effects of various cutting parameters on the force signature are studied. It should be noted that experimental data includes the dynamics arising form the vibration of the solid workpiece / fixture / dynamometer subsystem and from the spindle / tool subsystem. Although this dynamics is not as strong as the one present in interrupted cutting tests, it is still present in the experimental data.

In the following paragraphs the prediction error is calculated by taking the maximum difference between the predicted and measured data, and normalizing it with respect to the corresponding measured value. A negative error means underestimation of the experimental forces by the model; a positive one means overestimation of the forces by the model.

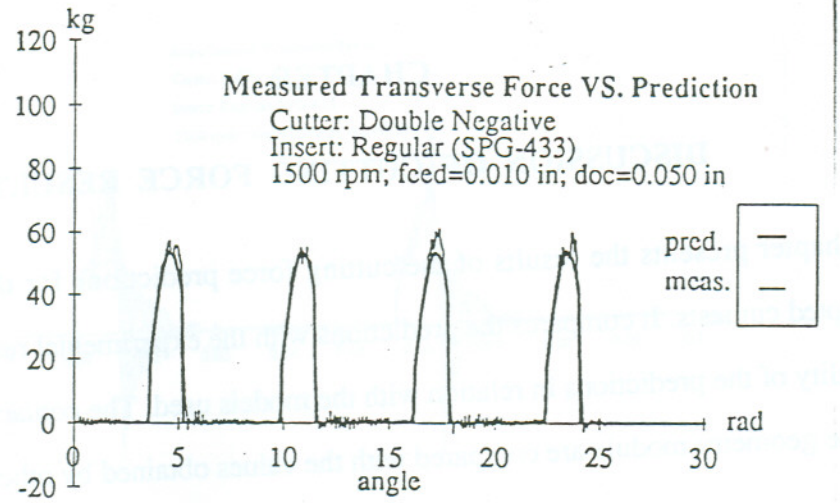

(a)

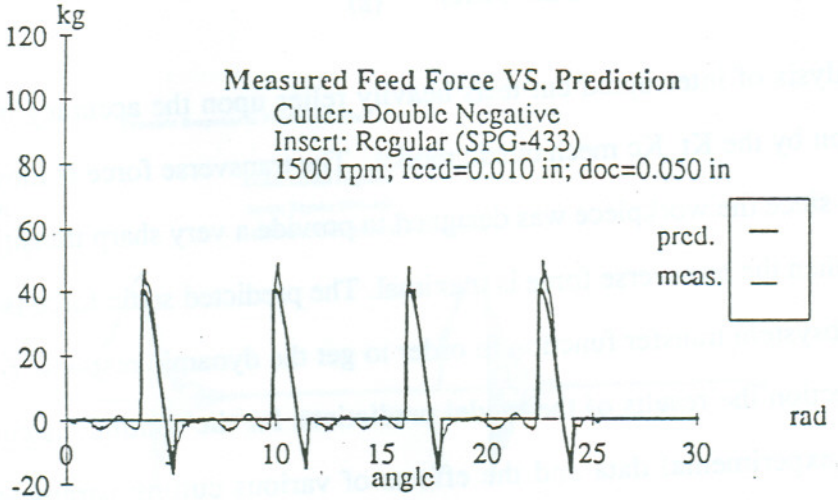

(b)

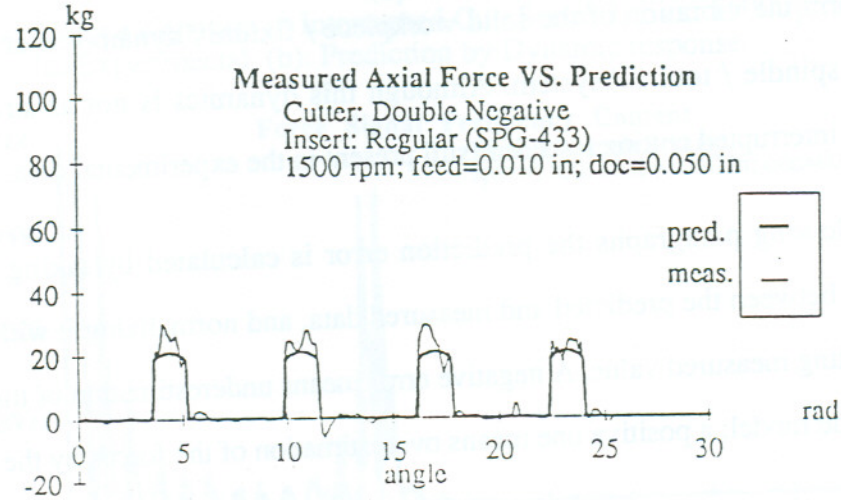

(c)

Fig 7.1 Transverse, Feed and Axial Experimental VS Predicted Forces for Series 1, velocity effect.

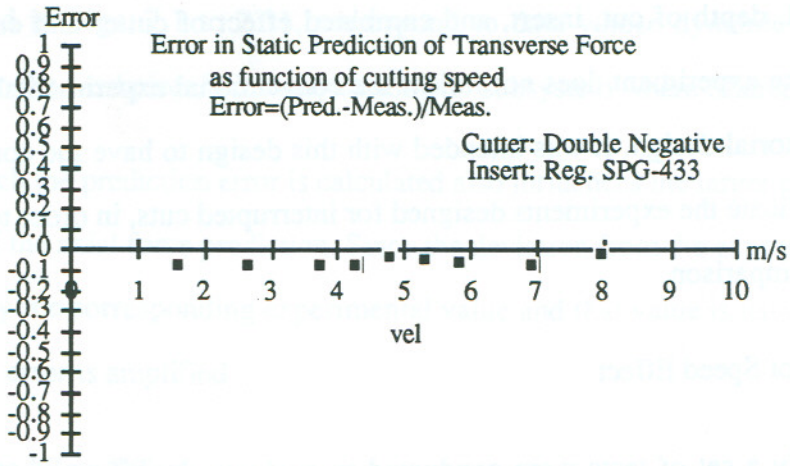

(a)

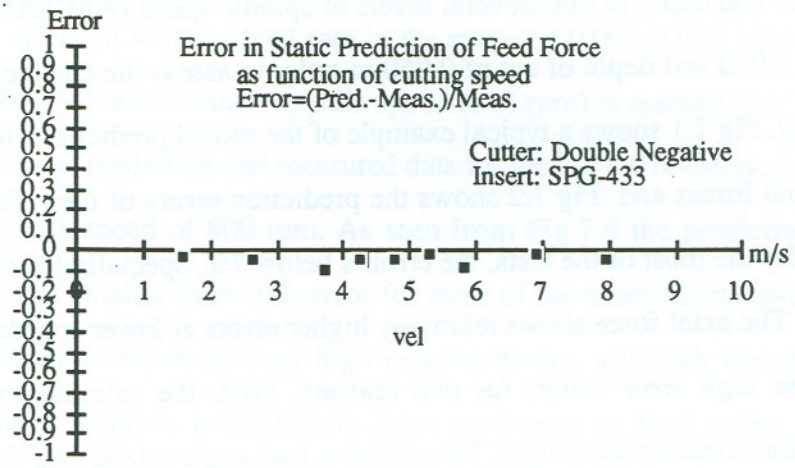

(b)

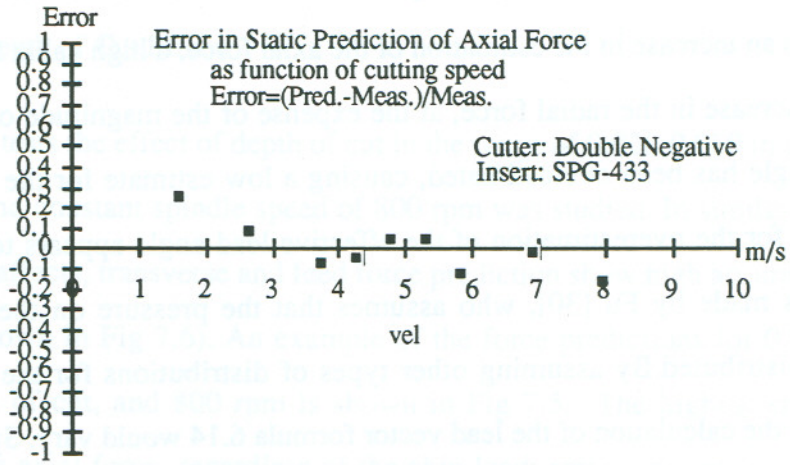

(c)

Fig 7.2. Error in prediction of static forces. Series 1 of continuous cut: Velocity Effect. (a) Transverse Force. (b) Feed Force. (c) Axial Force

Five series of tests were run to evaluate the effect of the following parameters: cutting speed, feed, depth of cut, insert, and combined effect of cutter and cutting speed. The design of the experiment does not follow the conventional experimental design schemes, such as factorial design. It was intended with this design to have the continuous cut tests exactly replicate the experiments designed for interrupted cuts, in order to provide a better basis for comparison.

Assesment of Speed Effect

In this study a set of tests were conducted to evaluate the effect of cutting velocity at constant feed and depth of cut. Several levels of spindle speed (800-1200 rpm) were used at a feed of 0.010 and depth of cut of 0.050 in order to assess the change in cutting forces with velocity. Fig 7.1 shows a typical example of the model predictions for the transverse, feed and axial forces and Fig 7.2 shows the prediction errors of these forces. It has been found that, for the most of the tests, the error is below 7%, specially for the transverse and feed forces. The axial force shows relatively higher errors at lower speeds. The axial force present these high error values for two reasons. First, the calculation of axial forces depends on the effective lead angle. The effective lead angle establishes the direction of the thrust force which is calculated from equation 6-15. A low value of the effective lead angle causes an increase in the estimation of the axial force; a high value for the lead angle causes an increase in the radial force, at the expense of the magnitude of the axial force. The lead angle has been overestimated, causing a low estimate for the axial force. The explanation for the overestimation of the effective lead angle appears to result from the assumptions made by Fu [30], who assumes that the pressure on the cutting edge is uniformly distributed.By assuming other types of distributions for the pressure on the cutting edge the calculation of the lead vector formula 6.14 would vary. Specifically, if the distribution assigns more weight to the cutting pressure in the lower part of the contact area the axial component of the thrust force will increase. Second, the measured forces include

dynamic components while the static forces don't have that component. The measured forces presented in Figs. 7.1 to 7.11, correspond to data whose dynamic components corresponding to the workpiece/fixture/dynamometer subsystem where filtered out.

The way in which the prediction error is calculated also influences the larger error numbers characteristic of the axial force prediction. Since the deviation from the experimental value is normalized by the corresponding experimental value and that value is usually small for axial forces, the error is amplified.

Assesment of Feed Rate Effect

In this case the effect of varying feed rate in the range of 0.005-0.020 in/rev at constant depth of cut (0.050 in) and constant spindle speed (800 rpm) is assesed. Fig 7.3 shows an example of the model prediction and measured data for feed of 0.010 in/rev, depth of cut of 0.050 in.and spindle speed of 800 rpm. As seen from Fig 7.4 the predictions are good, resulting in an error smaller than 10% error for most of the cases for transverse and feed forces. Axial forces however present high relative errors, although the absolute error (prediction-measurement) is not different from transverse or feed cases. It should be noticed that specially at low chip loads, the errors tend to be bigger for any force.

Assesment of Depth of Cut Effect

In this series of tests the effect of depth of cut in the range of 0.020-0.080 in with constant feed of 0.010 and constant spindle speed of 800 rpm was studied. In similarity to cutting speed and feed affects, transverse and feed force prediction show high accuracy (less than 7% error, as shown in Fig 7.6). An example of the force predictions for 0.010 in. feed, 0.080 in. depth of cut, and 800 rpm is shown in Fig 7.5. The highest error, again is recorded for the axial force, regardless of the chip load; errors are constant all over the range of depth of cut.

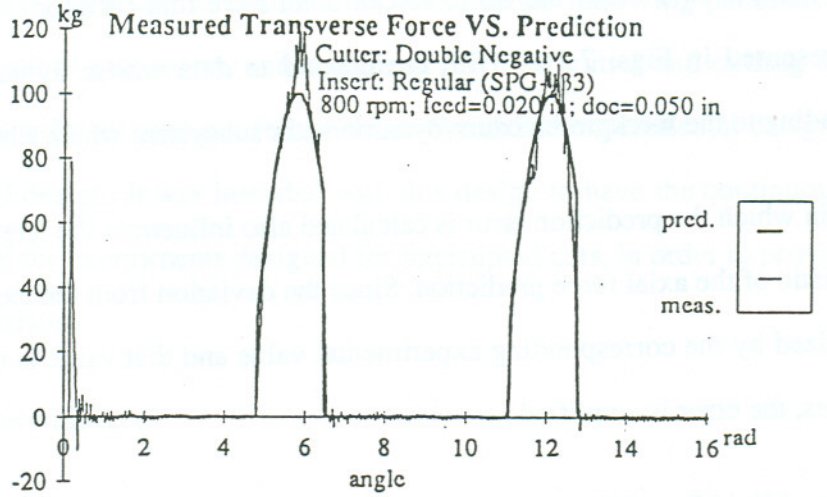

(a)

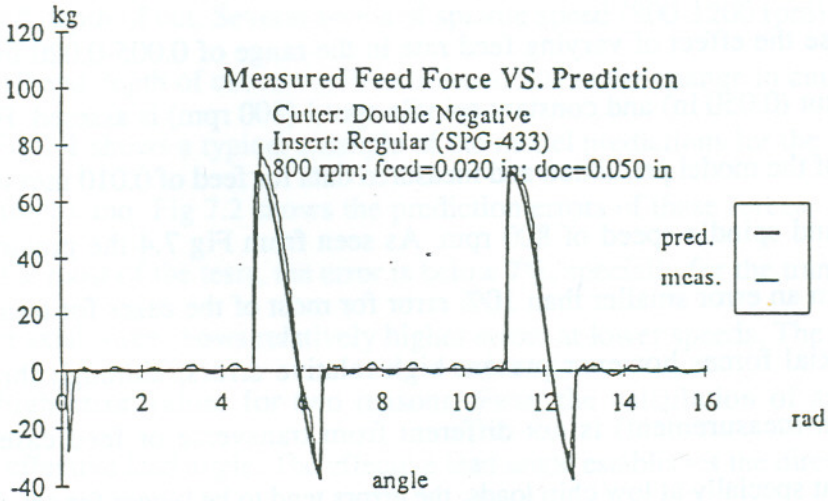

(b)

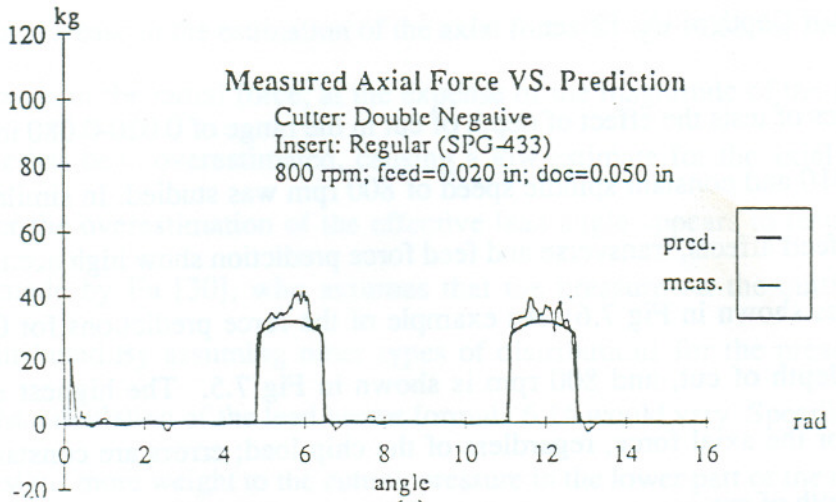

(c)

Fig 7.3 Transverse, Feed and Axial Experimental VS Predicted Forces for Series 2, Feed Effect.

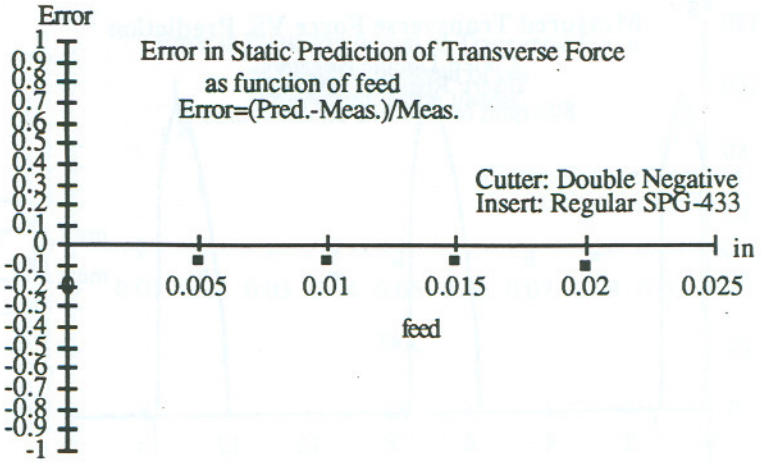

(a)

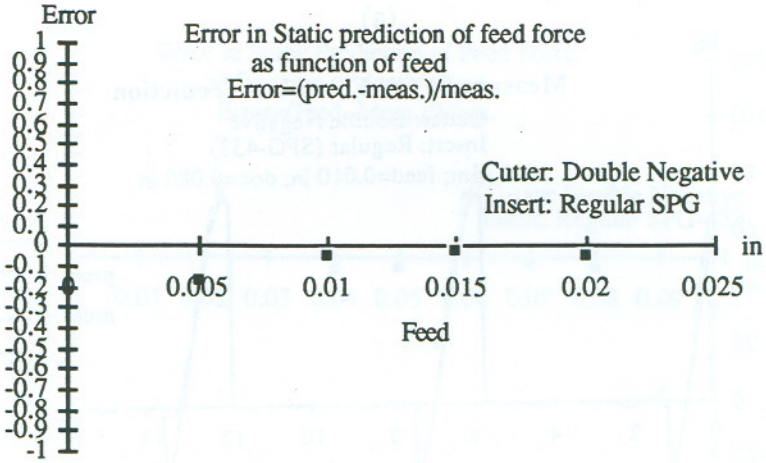

(b)

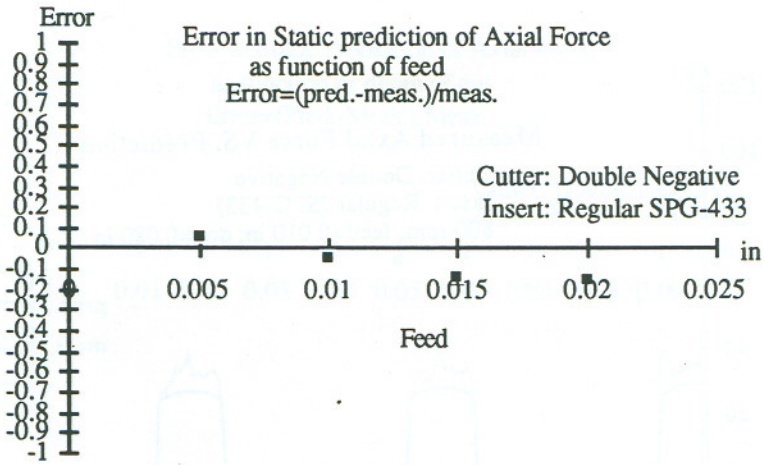

(c)

Fig 7.4. Error in prediction of static forces. Series 2 of continuous cut: Feed Effect.
(a) Transverse Force. (b) Feed Force. (c) Axial Force

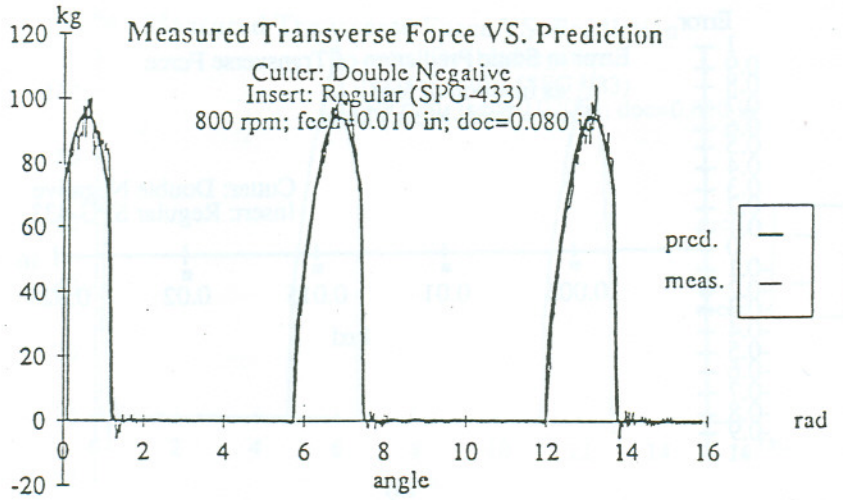

(a)

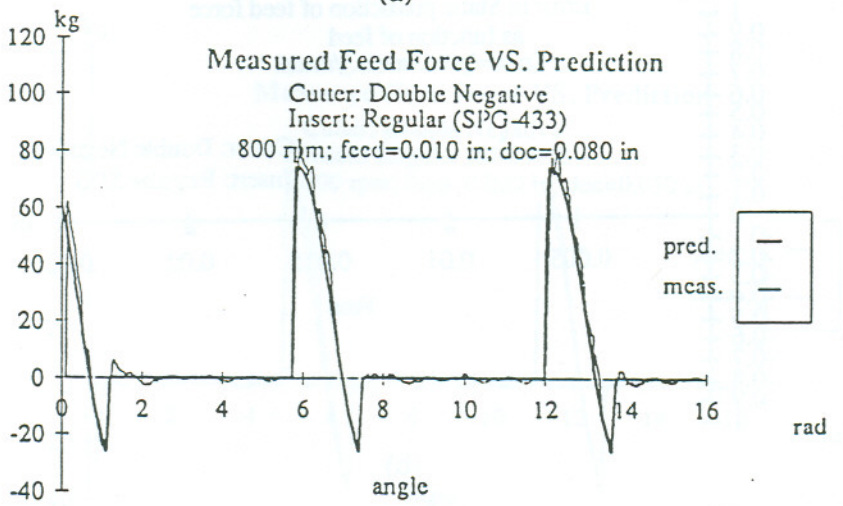

(b)

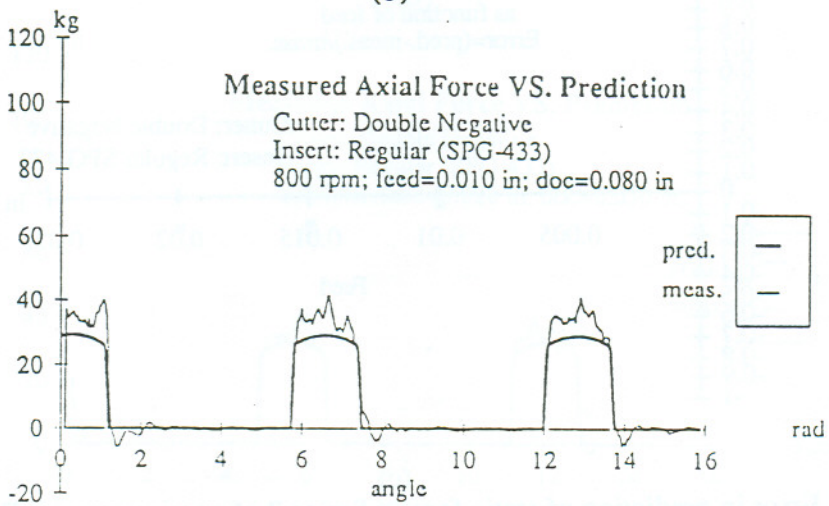

(c)

Fig 7.5 Transverse, Feed and Axial Experimental VS Predicted Forces for Series 3, Depth of Cut Effect.

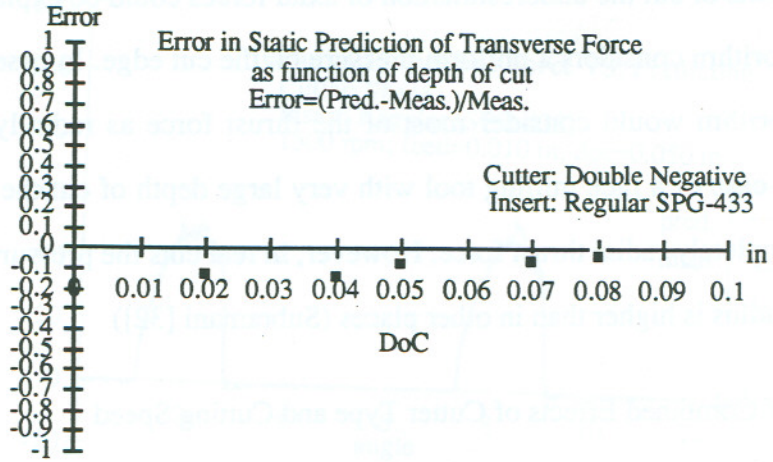

(a)

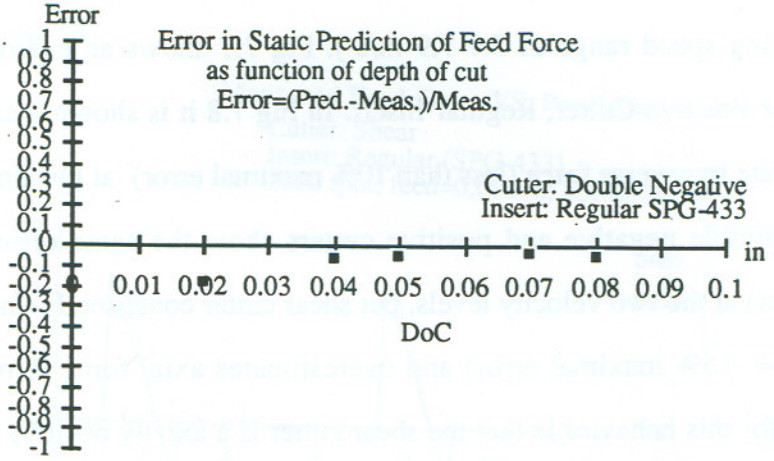

(b)

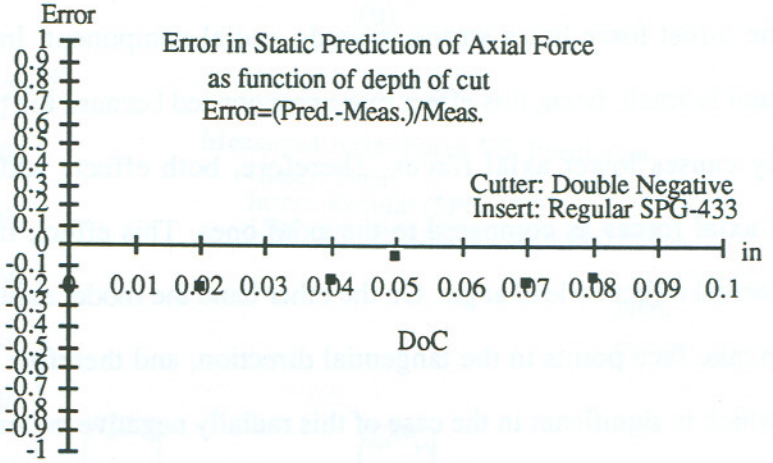

(c)

Fig 7.6. Error in prediction of static forces. Series 3 of continuous cut: Depth of Cut Effect. (a) Transverse Force. (b) Feed Force. (c) Axial Force

For large depths of cut the underestimation of axial forces could be explained by realizing that Fu's algorithm considers a uniform pressure on the cut edge. In case of high depth of cut this algorithm would consider most of the thrust force as radially directed. In the hypothetical case of a face milling tool with very large depth of cut the algorithm would predict a completely radial thrust force. However, in real cuts the pressure on the lower tip of the nose radius is higher than in other places (Subramani [32])

Assesment of Combined Effects of Cutter Type and Cutting Speed

This series of tests are intended to evaluate the effect of the type of cutter and speed (3 cutters , cutting speed range of 5.7-7.9 m/s). Fig 7.7 shows an example of the model prediction for Positive Cutter, Regular Insert. In Fig 7.8 it is shown that the three cutters predict accurate transverse force (less than 10% maximal error) at low and high speed. For feed force, double negative and positive cutters show the same error (less than 10% maximal error) at the two velocity levels, but shear cutter consistently underestimates feed force (error ≈ -15% maximal error) and overestimates axial force (error ≈ +25%). The explanation for this behavior is that the shear cutter is a axially positive cutter (axial rake +5°), but radially negative one (whose radial rake is -13°). Because this strongly negative radial rake the thrust force has a strong inwards, radial component. In comparison, the axial component is small, being this effect more pronounced because the positive axial rake which usually causes lower axial forces. Therefore, both effects add up to lower the experimental axial forces as compared to the axial ones. This effect, in turn produces a lower experimental effective lead angle. On the other hand the model assumes that the force normal to the rake face points in the tangential direction, and therefore ignores its radial component, which is significant in the case of this radially negative cutter. The model does not have a way to include this effect of radial component of the normal force. It will estimate the lead vector in the same way as for double negative cutters, with no consideration to the actual smaller axial forces present.

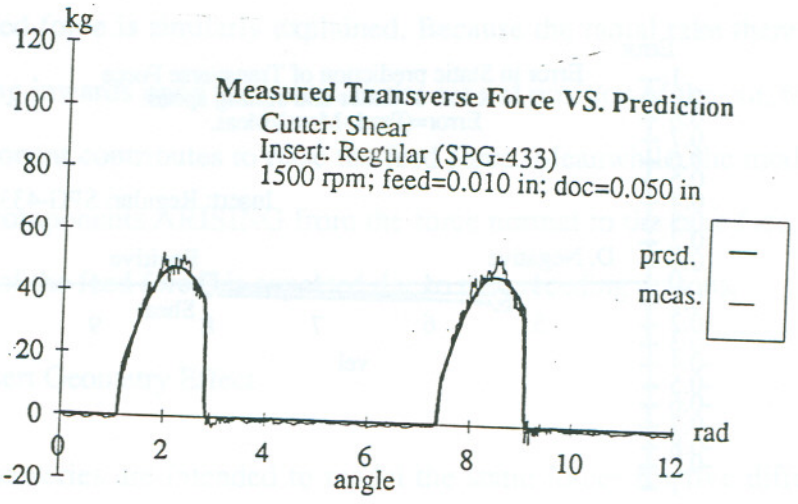

(a)

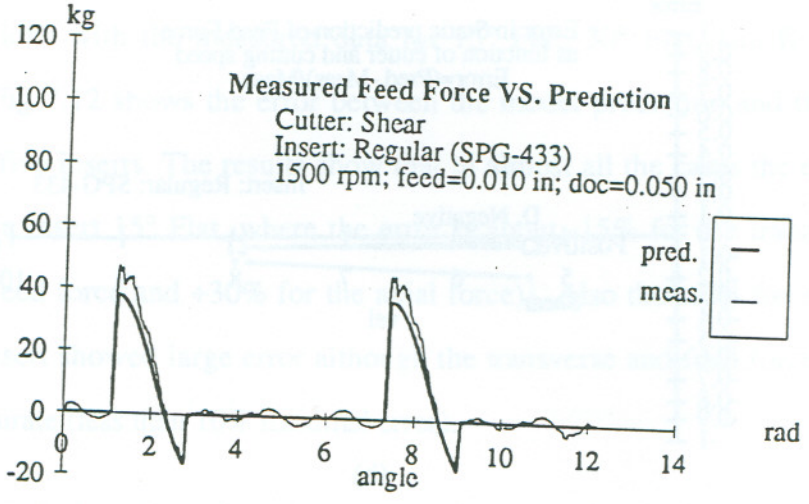

(b)

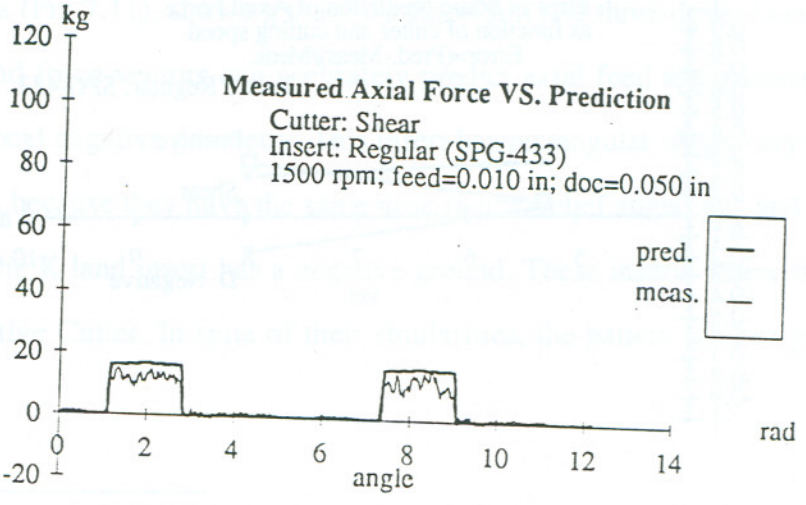

(c)

Fig 7.7 Transverse, Feed and Axial Experimental VS Predicted Forces for Series 4. Cutter X velocity Effect

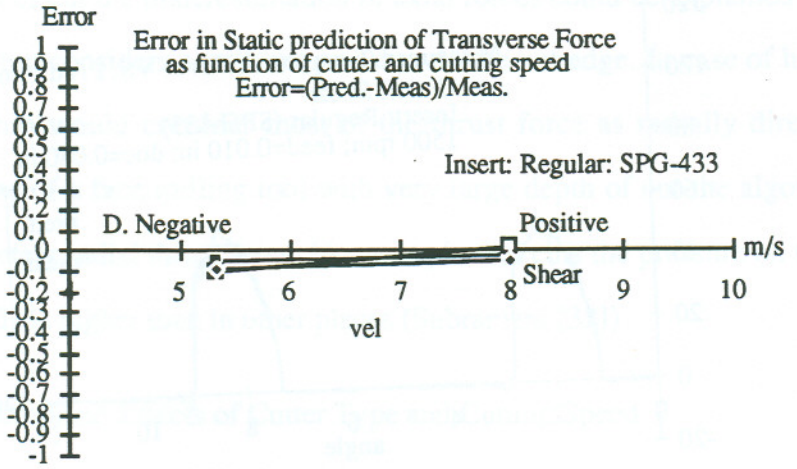

(a)

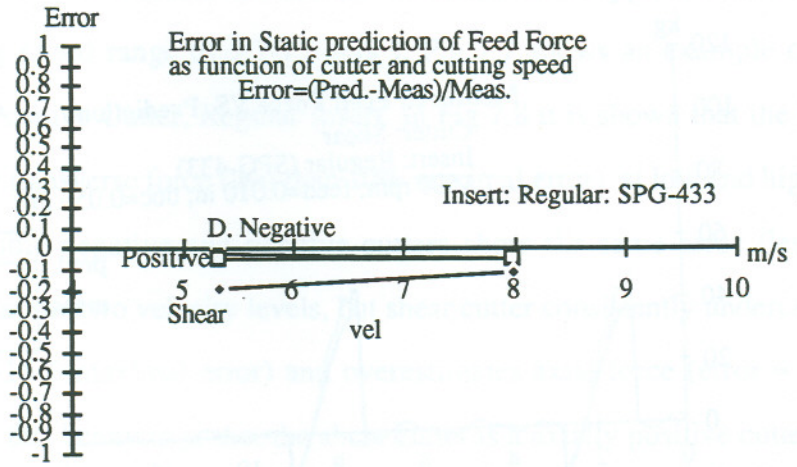

(b)

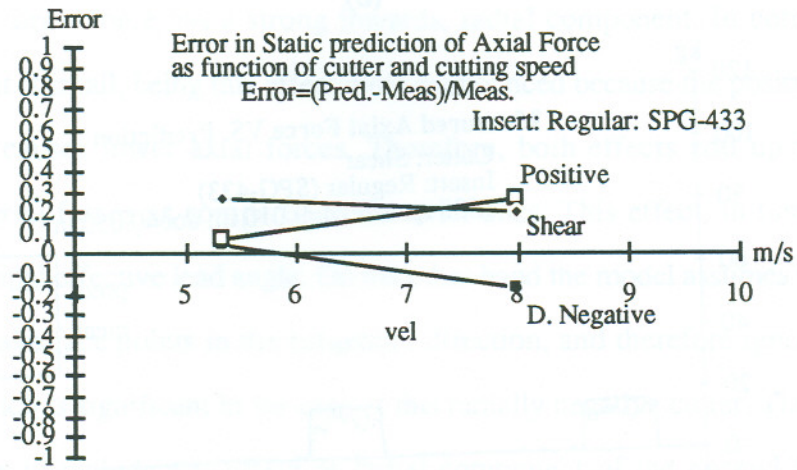

(c)

Fig 7.8. Error in prediction of static forces. Series 4 of continuous cut: Combined Effect of Velocity and Cutter. (a) Transverse Force. (b) Feed Force. (c) Axial Force

The effect on feed force is similarly explained. Because the radial rake there is a strong radial force acting inwards upon the cutter. In the central position of the cut, for example, this radial component contributes to raise the feed force. Meanwhile, the model does not consider radial components ARISING from the force normal to the rake face. Therefore, underestimation of the feed forces is expected due to the preceding reasons.

Assesment of Insert Geometry Effect

The tests in these series are intended to model the static forces for five different insert geometries, with Double Negative cutter. Figs. 7.9, 7.10 and 7.11 show the comparison of model predictions with the measured data for 15° Flat, 30° Flat, and K land inserts respectively. Fig 7.12 shows the error between the model prediction and the measured forces for the five inserts. The results show that in almost all the cases the error is quite low, except the insert 15° Flat, where the error is about -15% for the transverse force, -20% for the feed force and +30% for the axial force)[1]. Also the axial force for the 30° Double Flat insert showed large error although the transverse and feed force predictions were more accurate (less than 10% maximal error).

The K land insert also showed good agreement between the model prediction and the measured data (Fig 7.11), showing that Fu's algorithm and three-dimensional calculation of the area and force vectors can accurately predict axial feed and transverse forces in inserts with local negative geometry. This insert has rectangular shape very similar to the regular insert,.because they have the same nose radius, relief angle, etc, and only differ in the fact that the K land insert has a negative ground. These inserts where tried using the Double Negative Cutter. In spite of their similarities, the pattern of area growth is very

---

1 These values are calculated using the maximal deviation of the predicted force from the measurement. Therefore these values are an inflated value of the error. Probably the average error would be a more significant value.

different for these inserts. Figs 7.1, 7.3 and 7.5 show the force predictions for several different conditions for the regular insert, while Fig 7.11 does so for the K land insert.

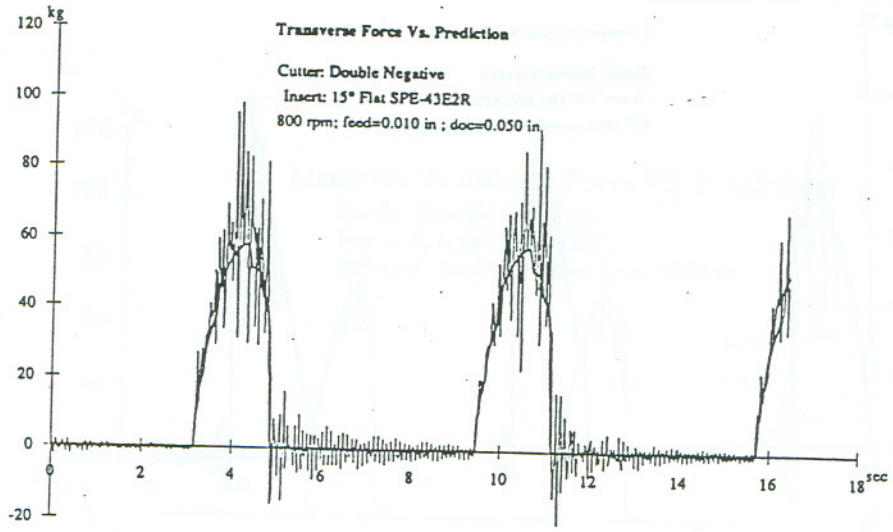

(a)

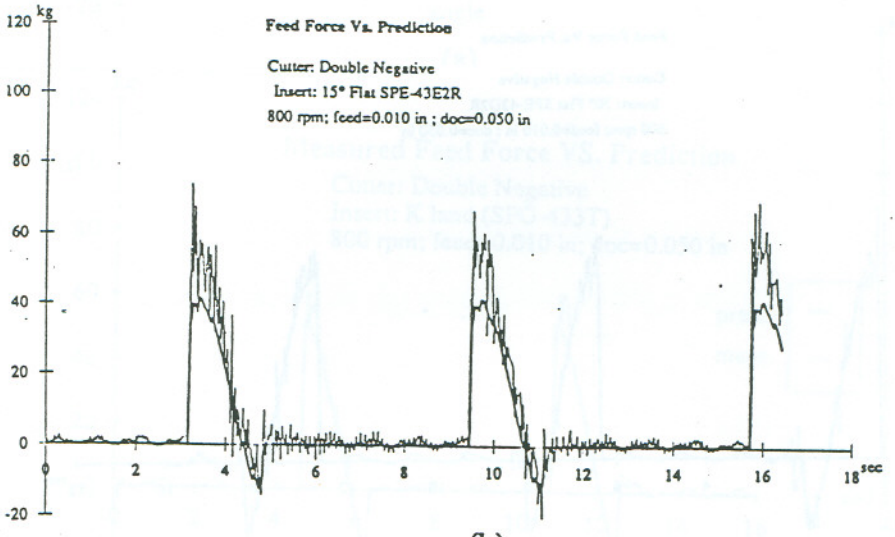

(b)

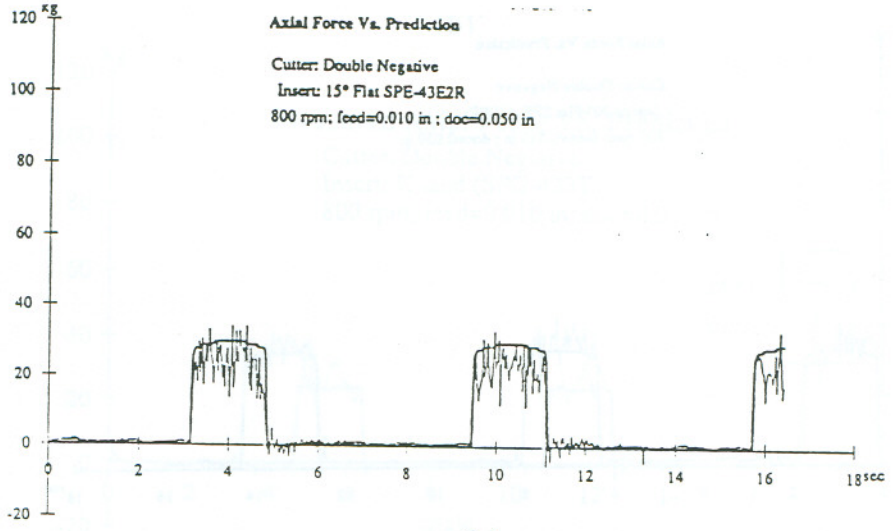

(c)

Fig 7.9 Transverse, Feed and Axial Experimental VS Predicted Forces for Series 5. 15° Flat Insert Effect

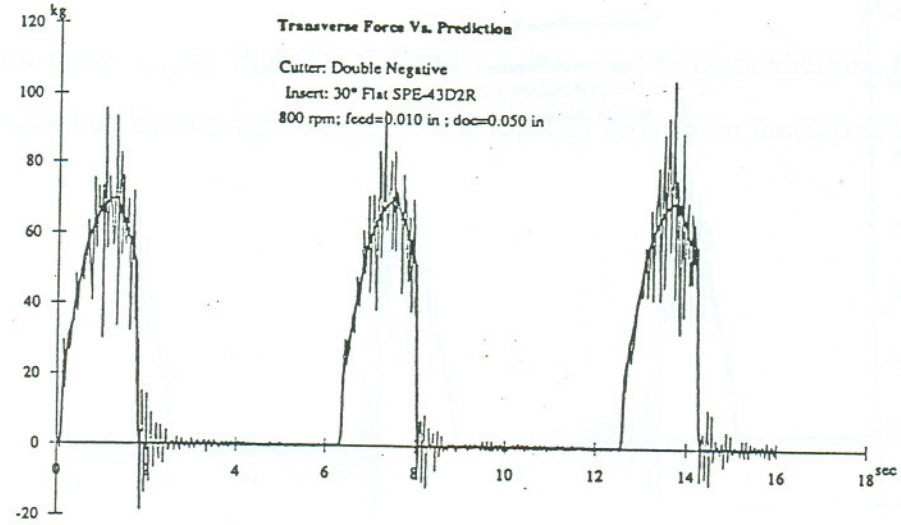

(a)

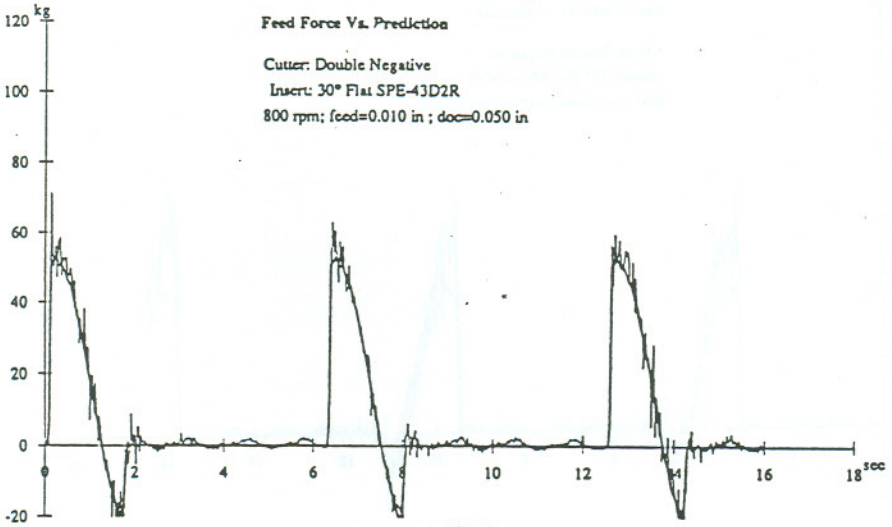

(D)

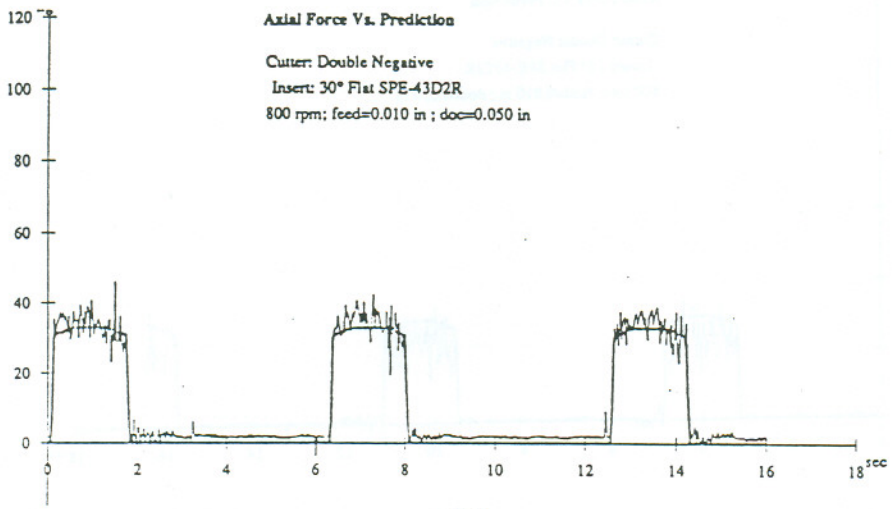

(c)

Fig 7.10 Transverse, Feed and Axial Experimental VS Predicted Forces for Series 5. 30° Flat Insert Effect

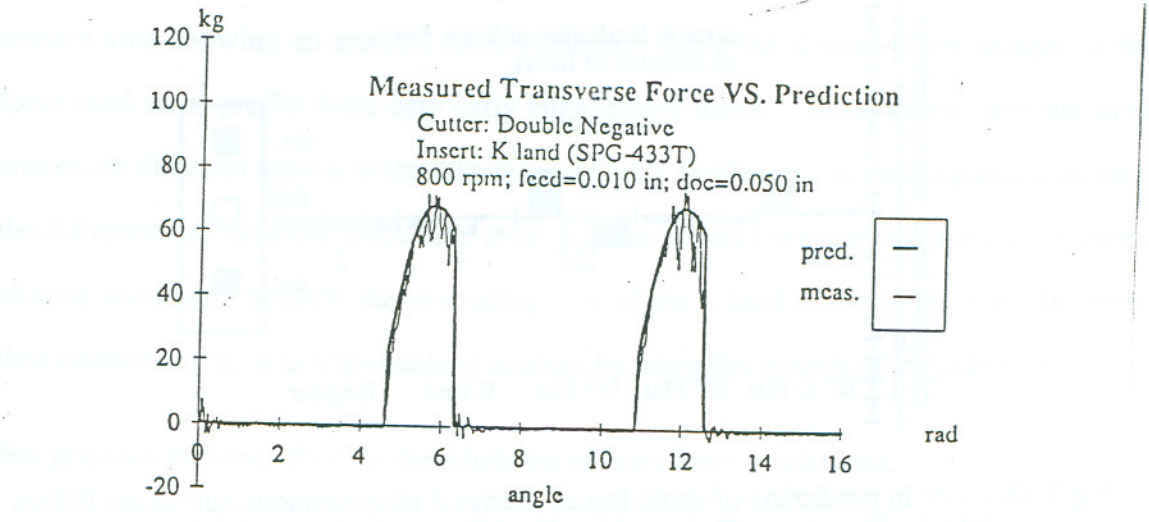

(a)

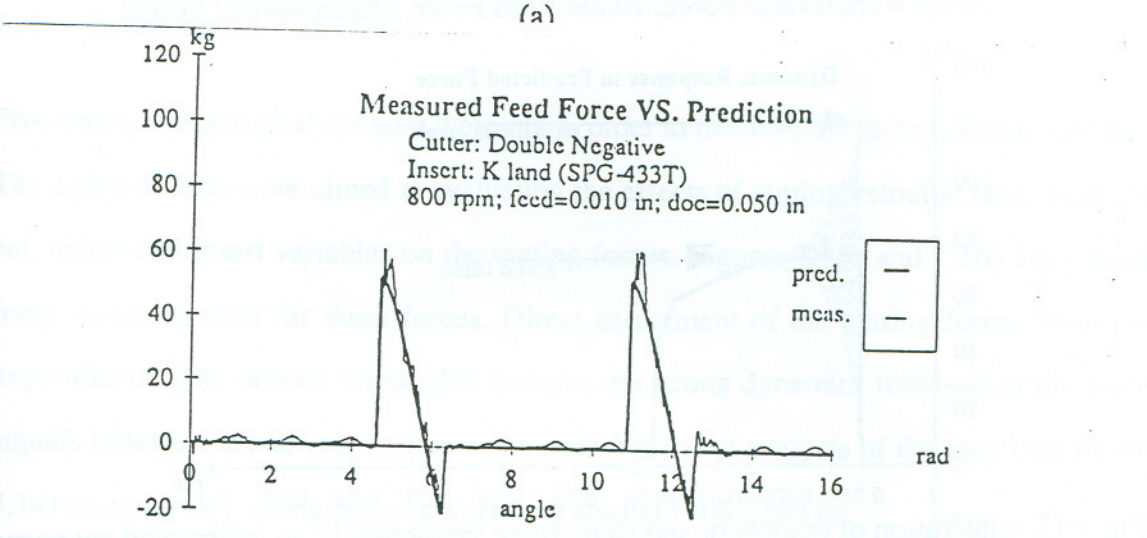

(b)

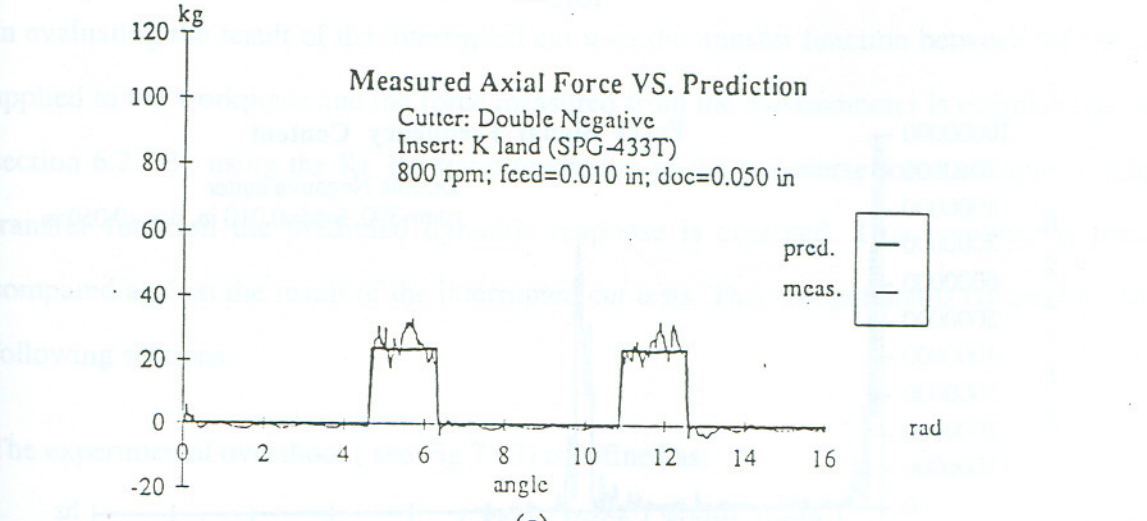

(c)

Fig 7.11 Transverse, Feed and Axial Experimental VS Predicted Forces for Series 5. · Kland Insert Effect

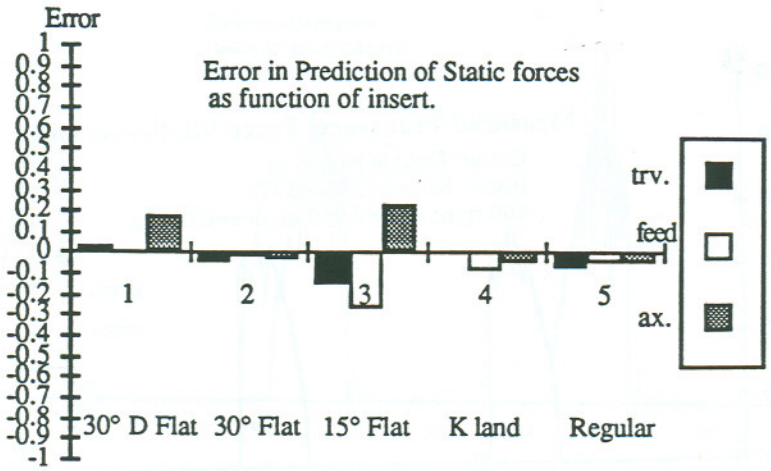

Fig 7.12. Error in prediction of static forces. Series 5 of continuous cut: Insert Effect. (black =Transverse Force, white=Feed Force, shaded=Axial Force)

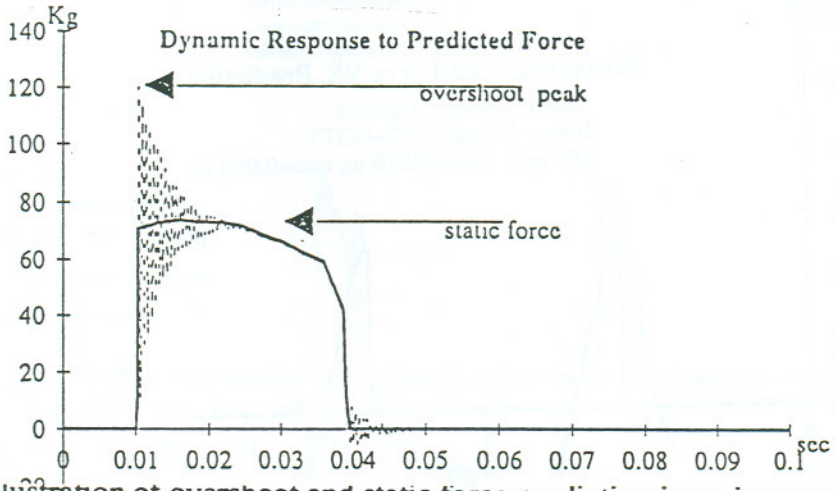

Fig 7.13. Illustration of overshoot and static force prediction in an interrupted cut entry test.

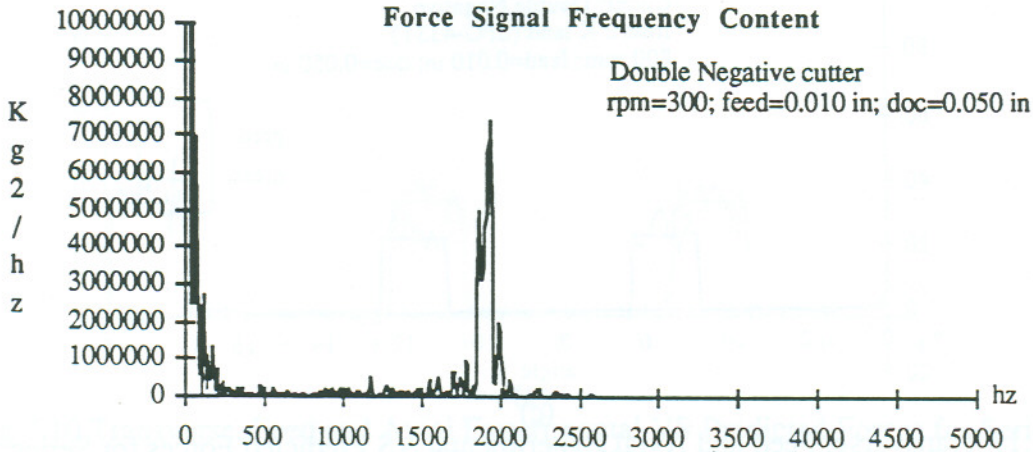

Fig 7.14. Frequency content of the interrupted cut transverse force.

In particular the axial force shows the difference. The regular insert slowly develops the contact area showing an arc-like force signature, while the K land insert presents a flat force (and area) profile from very early engagement times. These inserts have the same area in the direction normal to the rake face, and very similar area in the tangential direction, the difference in the axial force (and area) profiles comes from the fact that the geometry module accurately projects the protruding land of the K land insert on the axial direction, thus considering an area impossible to account by using flat models of the rake face.

See graphics in Appendix C of the whole set of static force predictions.

7.2 Interrupted Cut Tests

Five series of interrupted cut tests were run in order to measure the forces in entry/exit cut. The series of tests were aimed at evaluating the effects of cutting velocity, feed, depth of cut, cutter and insert variables on the cutting forces. Figures 7.15a and 7.16a are typical force measurements for these forces. Direct assessment of the cutting forces from the experimental data proved impossible because the strong dynamics involved in the force signals hides the actual cutting forces present. A spectral analysis of the tests (see figure 7.14) shows a very strong power component around 1900-2100 hz.

In evaluating the result of the interrupted cut tests the transfer function between the force applied to the workpiece and the force measured from the dynamometer is estimated as in section 6.2. By using the Kt_Kc static prediction of the transverse force as input to this transfer function the predicted dynamic response is obtained. This response is then compared against the result of the interrupted cut tests. This comparison is covered in the following sections.

The experimental overshoot (see Fig 7.13) is defined as:

$$\text{overshoot} = \frac{(\text{Peak\_force} - \text{Static\_force})}{\text{Static\_force}} \qquad (7\text{-}1)$$

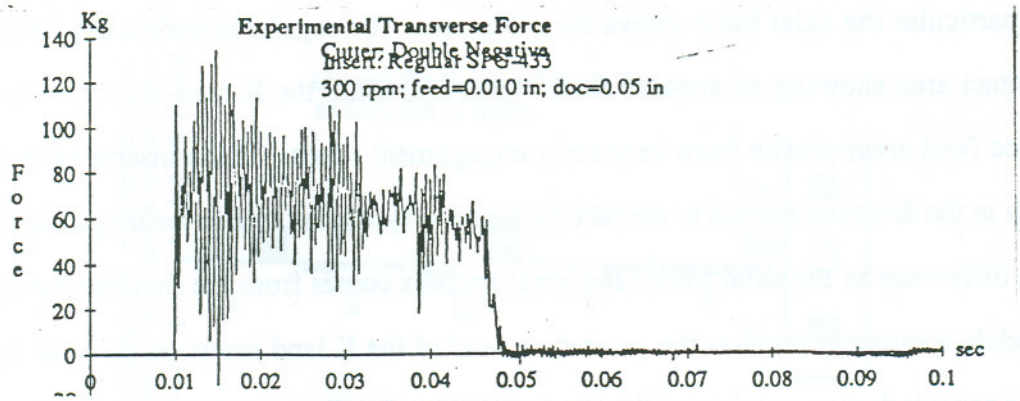

(b) Experimental results

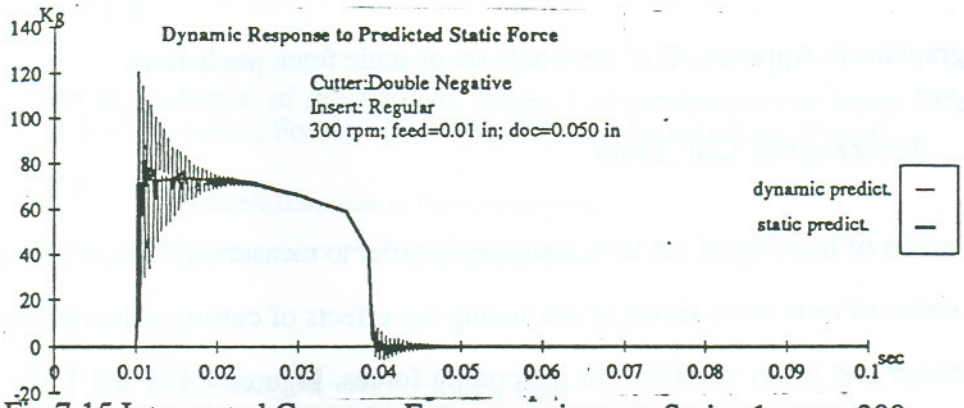

Fig 7.15 Interrupted Cut tests. Entry experiments. Series 1. rpm=300

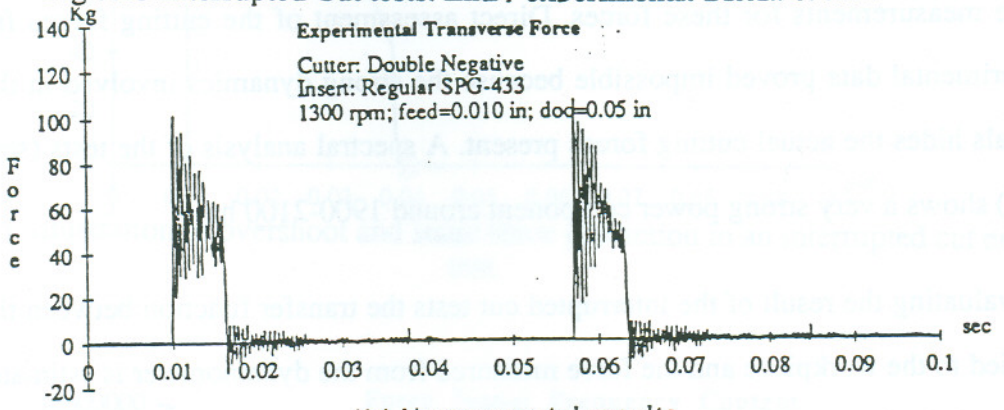

(b) Experimental results

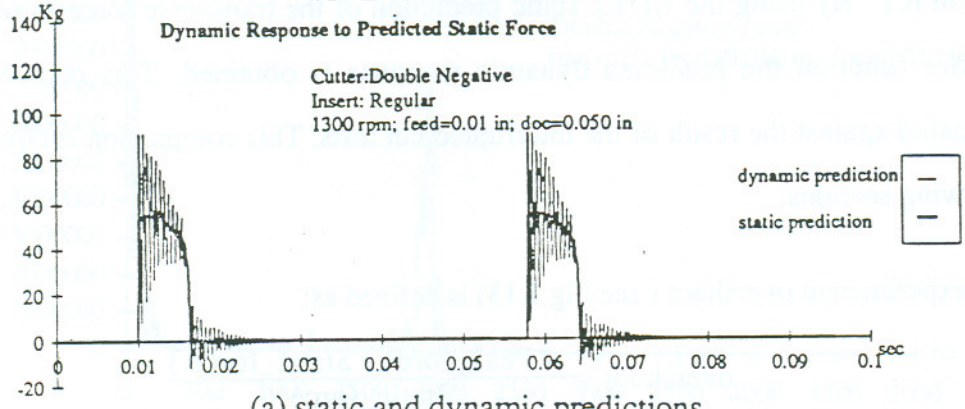

(a) static and dynamic predictions

Fig 7.16 Interrupted Cut tests. Entry experiments. Series 1. rpm=1300

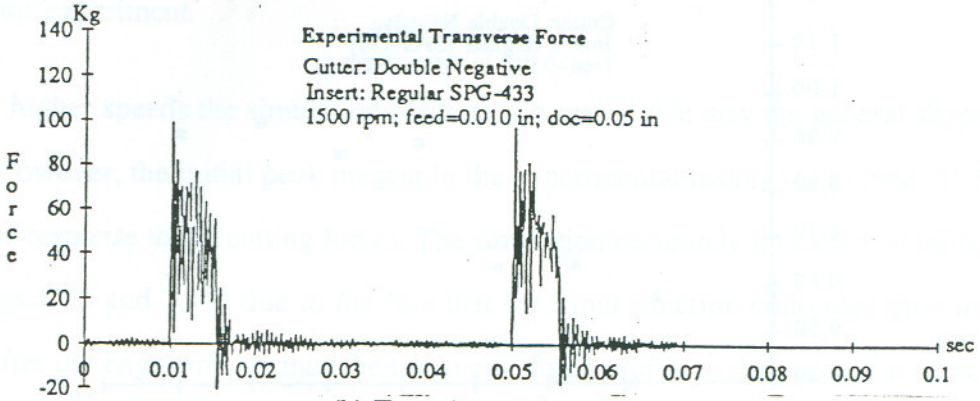

(b) Experimental results

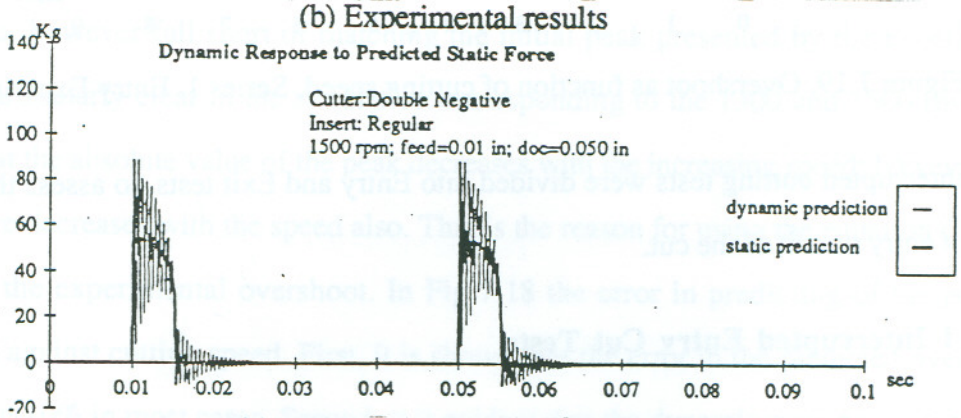

(a) static and dynamic predictions

Fig 7.17 Interrupted Cut tests. Entry experiments. Series 1. rpm=1500

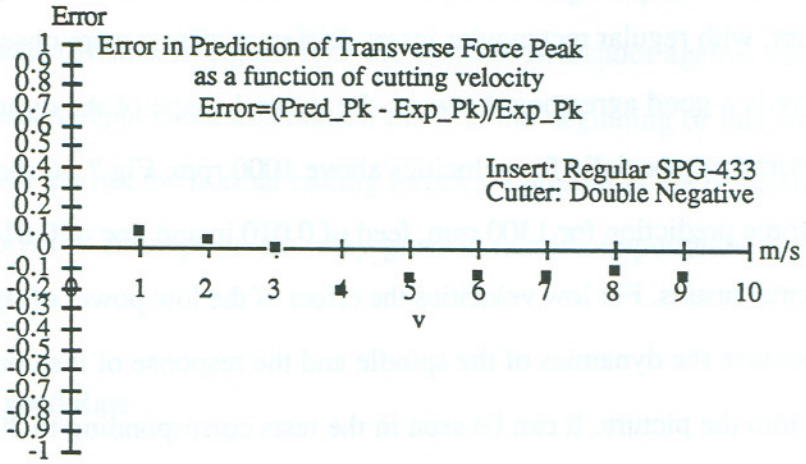

Fig 7.18. Error in Peak Prediction as function of velocity. (doc=0.05"; feed=0.010")

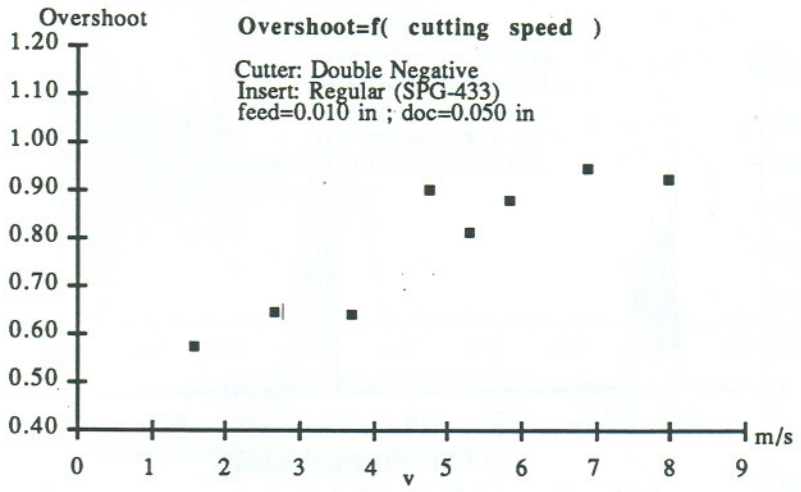

Figure 7.19. Overshoot as function of cutting speed. Series 1. Entry Experiments.

The interrupted cutting tests were divided into Entry and Exit tests, to assess the effect of abrupt entry or exit of the cut.

7.2.1 Interrupted Entry Cut Tests

Assessment of the Speed Effect

As in the continuous cutting tests, this series was run using a 4 in diameter, double negative cutter, with regular rectangular insert. Different effects were observed for this set of tests. There is a good agreement between the general shape of the dynamic simulation and the experiments, specially for velocities above 1000 rpm. Fig 7.16 shows an example of dynamic force prediction for 1300 rpm, feed of 0.010 in and doc of 0.010 in. along with the experimental results. For low velocities the effect of the low power of the motor distorts the results because the dynamics of the spindle and the response of the control loop of the motor come into the picture. It can be seen in the tests corresponding to 300-700 rpm that the simulation predicts the initial peak, but after that point, the effects which dominate the cut are very different (see Fig 7.15). In the experiment the spindle dynamics gets excited and responds to the sudden impact. On the other hand, the spindle decelerates strongly and the low inertial energy accumulated by the effect of velocity is not enough to maintain the

cutting speed. This is the reason for the prediction to show an cutting period shorter than that of the experiment.

For the higher speeds the simulation predicts in a reasonable way the general shape of the wave. However, the initial peak present in the experimental results is not predicted by the dynamic response to the cutting forces. The simulation accurately predicts two initial peaks (see Figs.7.16 and 7.17) due to the fact that the input function continues growing for a while after the engagement since the transverse force profile is skewed to the right. Those two peaks, however fall short of matching the initial peak presented by the experiment. This is particularly clear in the simulation corresponding to the 1300 and 1500 rpm test. Notice that the absolute value of the peak decreases with the increasing speed; however, the static force decreases with the speed also. That is the reason for using the equation (7-1) to calculate the experimental overshoot. In Fig 7.18 the error in predicting of the peak is displayed against cutting speed. First, it is shown that the error in the predicted overshoot is less than 10% in most cases. Second, it is evident that the dynamic response to the static force underestimates the value of the peak, specially as the speed increases. For lower speeds the dynamic simulation overestimates the peak and gives positive errors (prediction is larger than experiment). In figure 7.19 the trend of overshoot against cutting speed is shown. This results support the assumption made at the beginning of this work assuming that forces which are not the normal cutting forces are present at the beginning of the cut, and also supports the assumption that they grow in relative importance as the impacting velocity grows.

Assessment of Feed Rate

In this set of tests the observation made in the past paragraphs about a remaining peak not explained by the dynamic simulation still holds. Otherwise, the simulation follows in reasonable way the general form of the experimental response (see Fig 7.20).

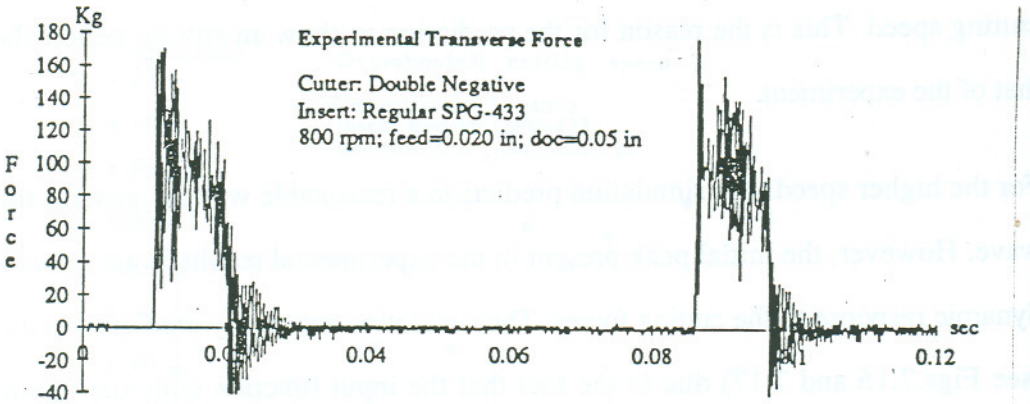

(b) Experimental results

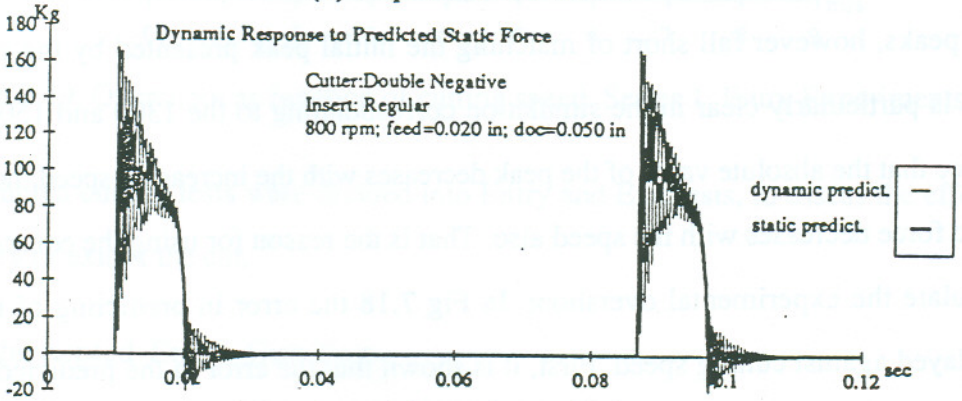

(a) static and dynamic predictions

Fig 7.20 Interrupted Cut tests. Entry experiments. Series 2. feed=0.020 in.

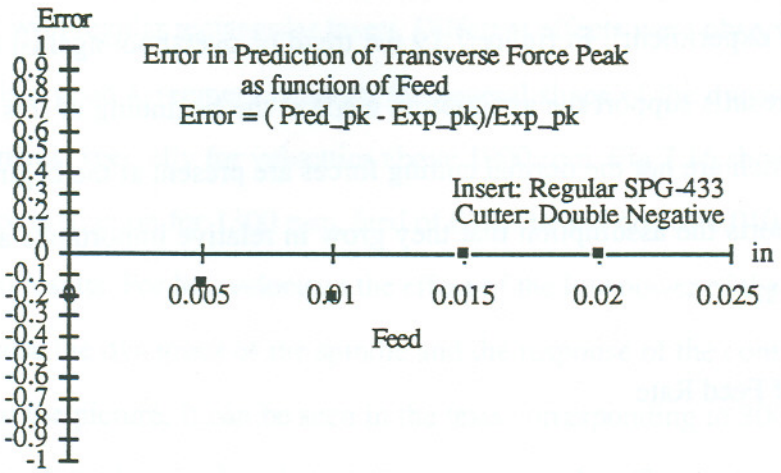

Fig 7.21. Error in Peak Prediction as function of feed.

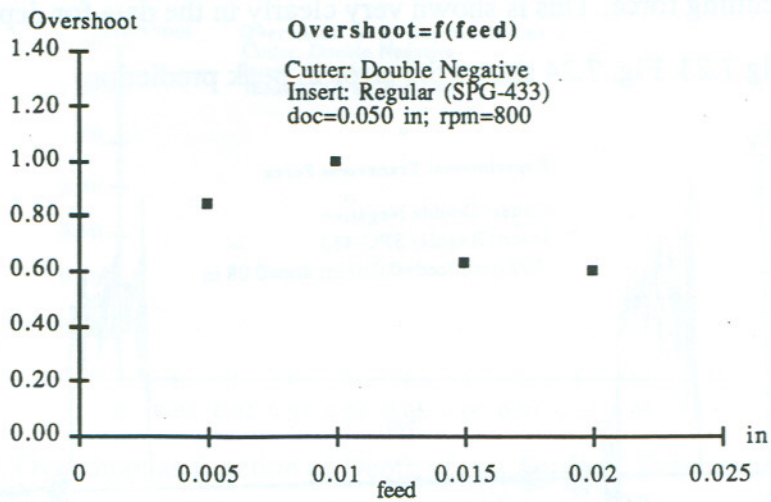

Fig 7.22. Overshoot as function of feed. Series 2. Entry experiments.

In Fig 7.21 the errors in prediction of the initial peak as function of feed are shown to be less than 20% and reaches very low values for the heavier cuts. For light cuts the initial peak prediction falls short of the experimental value. In both cases there are two or three initial peaks, some times increasing given the growing input function, and then the envelope starts decreasing. In this part usually the results differ from the experiment; specially for heavy cuts the process is strongly non-linear. The plots for the feed of 0.020 in show non-linearity similar to the one found in series 1 (speed effect). This occurs because, again, the forces for heavy cuts are big enough to slow down the spindle even if the spindle speed is now 800 rpm. In Fig 7.22 the overshoot as function of feed is shown; the effect, if any, is decreasing.

Assessment of Depth of Cut

In this set of tests the above comments for feed effect apply again. For light cuts (up to doc=0.050 in) the process is reasonably linear. However, for heavy cuts although the simulation correctly predicts the initial peak, the experimental data shows a very strong damping.effect which acts after the engagement is completed Consequently, the simulation matches the engagement overshoot, but its envelope decreases much slower than the

experimental cutting force. This is shown very clearly in the data for depth of cut of 0.080 in.plotted in Fig 7.23. Fig. 7.24 shows the error in peak prediction.

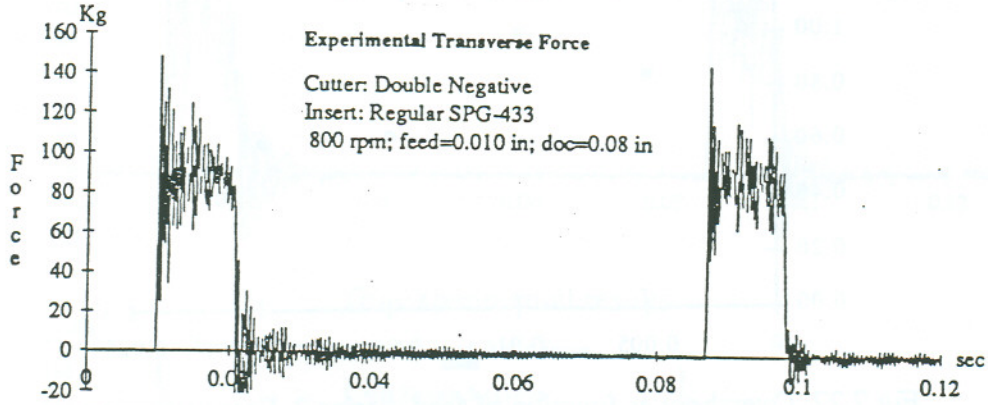

(b) Experimental results

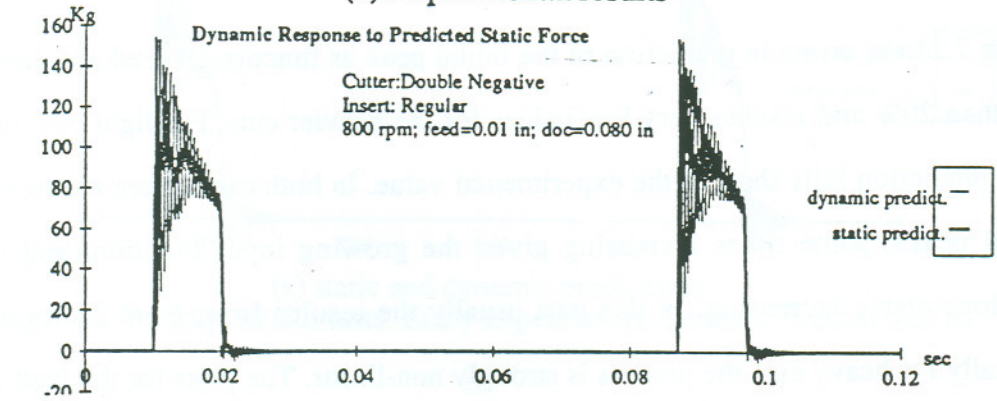

(a) static and dynamic predictions

Fig 7.23 Interrupted Cut tests. Entry experiments. Series 3. DoC=0.080 in.

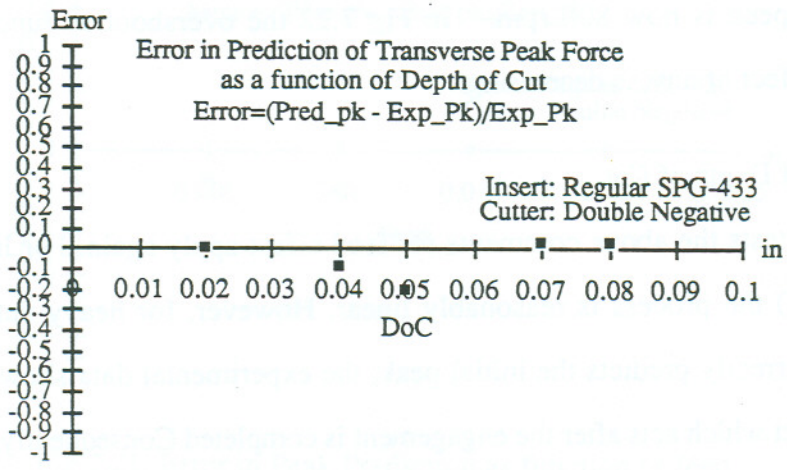

Fig 7.24. Error in Peak Prediction as function of DoC.

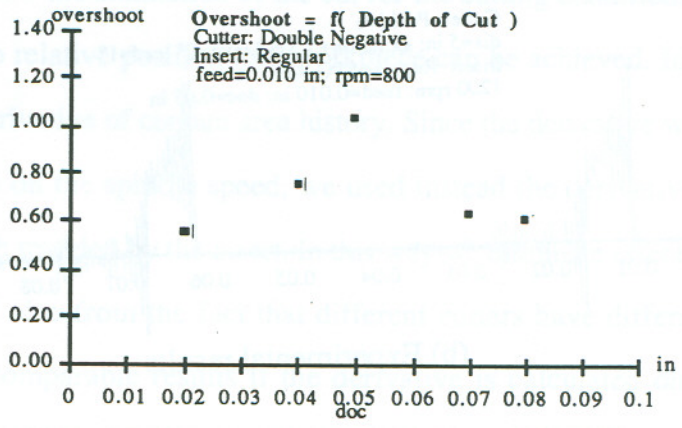

Fig 7.25. Overshoot as function of Depth of cut. Series 3. Entry experiments.

Fig. 7.24 shows a good agreement of the masured and predicted forces for heavier cuts (error less than 5%), but an underestimation of peak force for medium cuts (0.050" doc) which result in errors close to 20%. The variation of overshoot with Depth of Cut is shown in Fig 7.25. As mentioned before, no particular trend is evident. However, it has been observed that for heavier cuts the experimental overshoot also decreases which supports the hypothesis of a non-linear process with different kind of damping effect when entering and when cutting.

Assessement of COmbined Effect of Cutter and Velocity

This group of tests evaluates the combined effect of cutter and cutting velocity. The same procedure for calculating the overshoot is followed. Figures 7.26 and 7.27 show examples of the predictions of dynamic peaks for Positive (at 1200 rpm) and Shear (at 1500 rpm) cutter respectively. In both cases the general shape of the envelope curve is similar to the experimental force reading. In particular, there is good level of accuracy in the prediction of the initial peak(s). Figs. 7.28 presents the error in peak estimation and Fig 7.29 shows the experimental overshoot as function of the area derivative. The use of this parameter to characterize cutters will be discussed: since there is no way to quantitatively classify the cutters, the characterization of them from the point of view of their engagement process will be attempted.

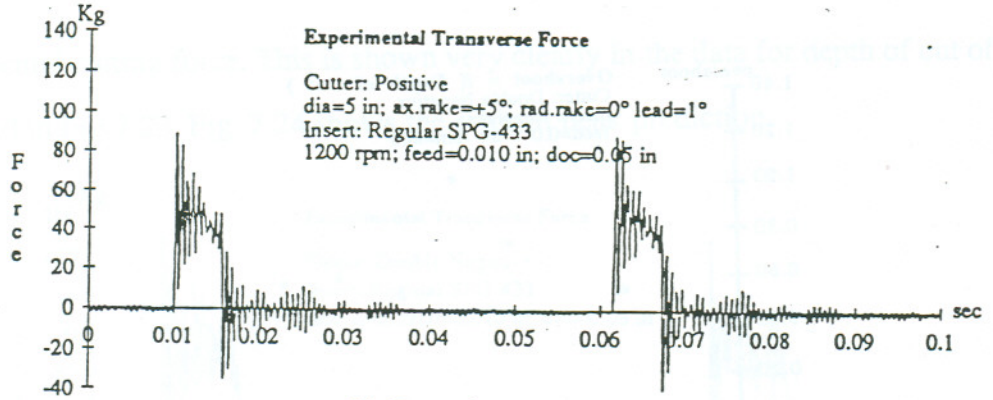

(b) Experimental results

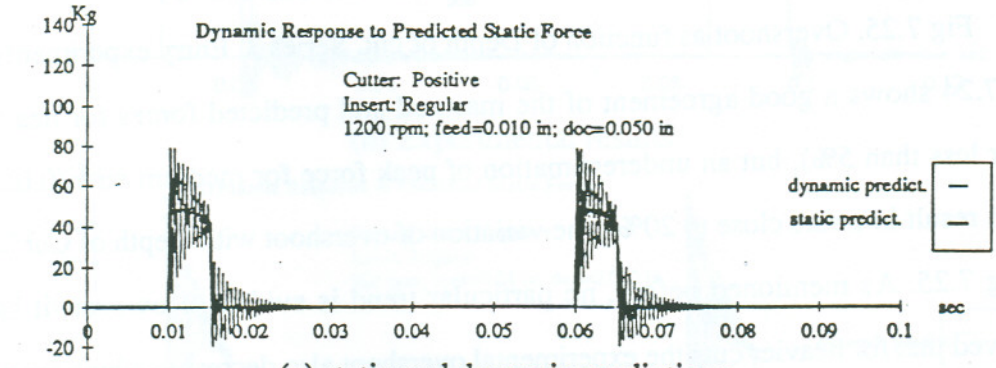

(a) static and dynamic predictions

Fig 7.26 Interrupted Cut tests. Entry experiments. Series 4. Positive Cutter.

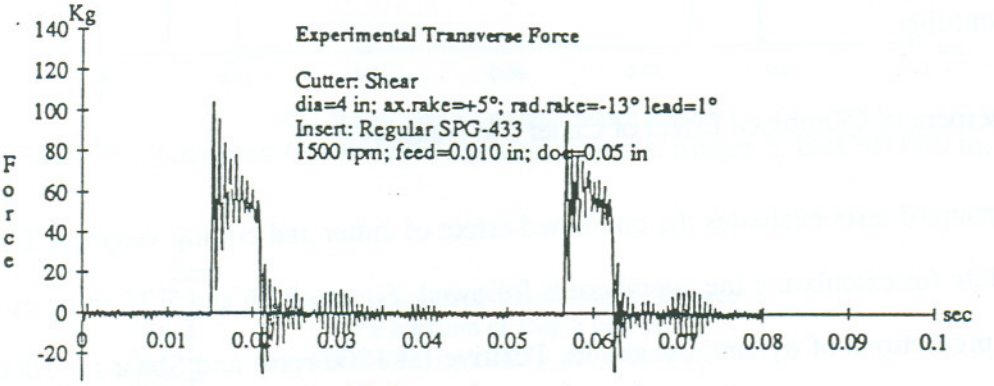

(b) Experimental results

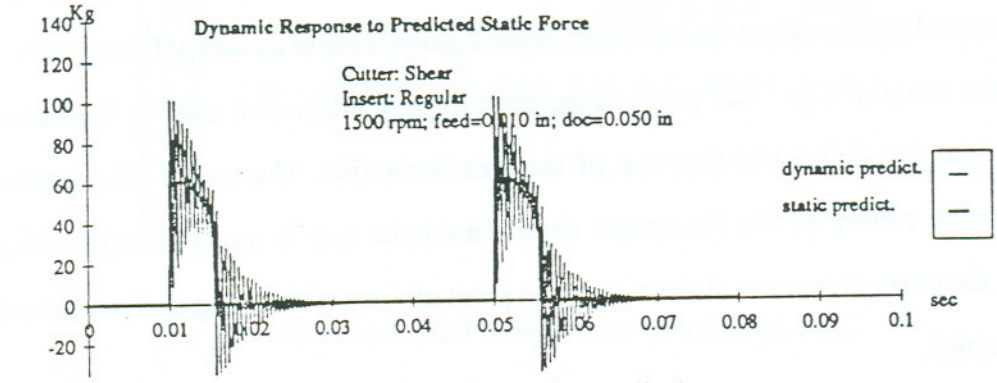

(a) static and dynamic predictions

Fig 7.27 Interrupted Cut tests. Entry experiments. Series 4. Shear Cutter.

By using 3D_MCUT the simulation of the cut for the cutting conditions, cutter and insert geometry, and also relative position tool/workpiece can be achieved. In particular we are interested in the derivative of contact area history. Since the derivative with respect to time obviously depends on the spindle speed, we used instead the derivative of the area with respect to the length traveled by the insert. In this way we eliminate effects coming from the spindle speed, and also from the fact that different cutters have different diameters and would yield non-comparable results if the derivative is calculated on the basis of, for example, angular position. Another consideration is to "normalize" the area derivative with respect to the full area engaged. The reason for this normalization is to keep the "rate of change of area" value independent of the absolute amount of contact area involved. The parameter calculated is then:

$$\Delta A = (1/A_{full}).\frac{dA}{dl} \qquad (7\text{-}2)$$

In Figs 7.30 to 7.32 the area derivative history as produced by 3D_MCUT is shown. The big area spike at entry is seen at the initial parts of the cut. As expected, negative cutters produce the highest area derivative and also the highest cutting forces. The horizontal axis corresponds to the angular position of the cutter.

In Fig 7.33 the result of overshoot as function of cutter and cutting speed is shown; the intention of running the ΔA simulations is to relate the maximal derivative to the information obtained from Fig 7.33. Effectively, it appears that for the Double Negative cutter, which has bigger ΔA parameter, the overshoot is higher at both levels of speed: 1050 sfpm (5.3 m/s) and 1570 sfpm (7 m/s).

For Positive and Shear cutters the result is mixed. The difference in ΔA for them is very small, and obviously other considerations have to be made. However, the parameter ΔA characterizes the cutters indicating that blunt geometries have stronger impact effect than sharp ones. An interesting detail is that the Positive cutter, which shows advantages at low

speeds because it produces small static cutting forces and even smaller overshoots, at higher speeds loses its advantage to negative cutters.

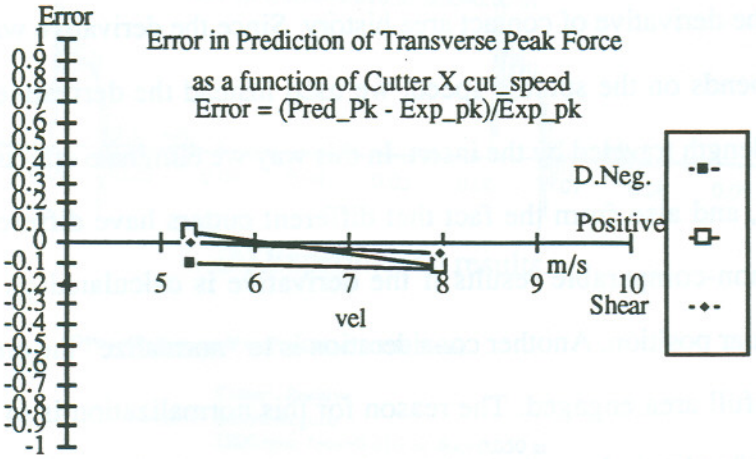

Fig 7.28. Error in Peak Prediction as function of Cutting speed and Cutter. (DoC=0.050"; feed=0.010")

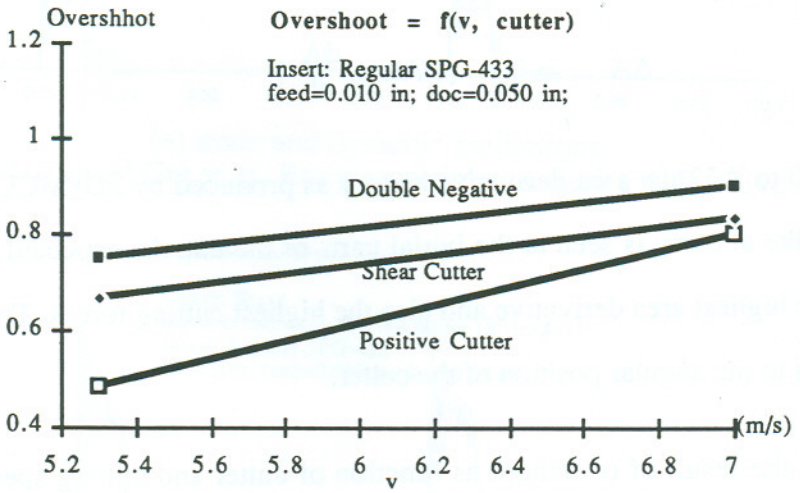

Fig 7.29. Combined effect of cutter and cutting speed on the overshoot. Series 4. Entry Experiments.

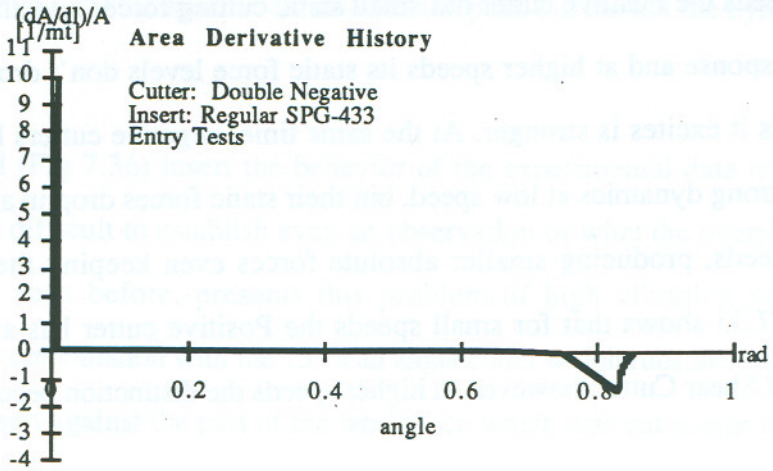

Fig 7.30. Area derivative for Double Negative cutter. Series 4. Entry .

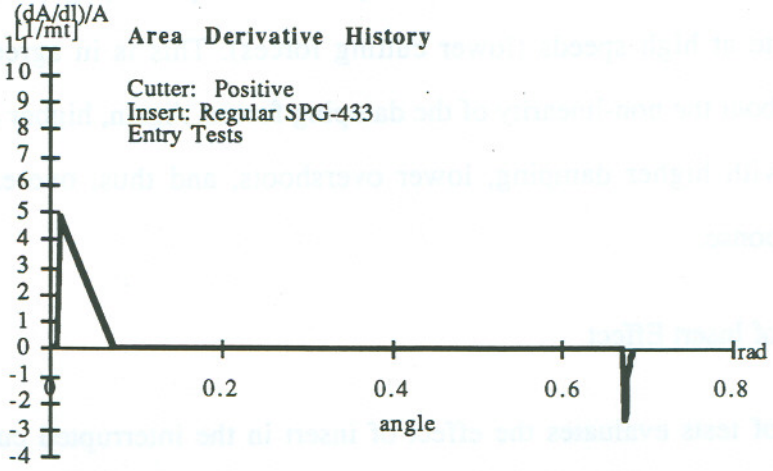

Fig 7.31. Area derivative for Positive cutter. Series 4. Entry .

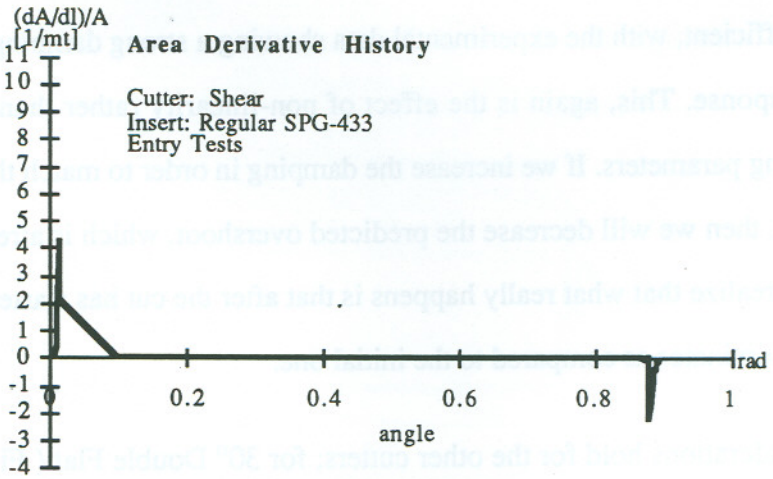

Fig 7.32. Area derivative for Shear cutter. Series 4. Entry .

At lower speeds the Positive cutter has small static cutting forces and also produces small dynamics response and at higher speeds its static force levels don't drop too much , but, the dynamics it excites is stronger. At the same time, negative cutters have higher static forces and strong dynamics at low speed, but their static forces drop in a significant factor at higher speeds, producing smaller absolute forces even keeping the same overshoot levels. Fig 7.33 shows that for small speeds the Positive cutter has an advantage over Negative and Shear Cutter; however, at higher speeds the distinction becomes blurry.

In Fig 7.34 the error in peak prediction is shown for cutters at different cutting speeds. There is a definite trend to overestimate the peak at low speeds (higher cutting forces) and underestimate at high speeds (lower cutting forces). This is in agreement with prior discussion about the non-linearity of the damping forces. Again, higher cutting forces are associated with higher damping, lower overshoots, and thus, overestimation by the dynamic response.

Assessment of Insert Effect

This group of tests evaluates the effect of insert in the interrupted cutting forces. For regular insert (see Fig 7.33) the peak is too high as compared to the predicted dynamic response. The dynamics shown by the experiment differs essentially in the strength of the damping coefficient, with the experimental data showing a strong damping compared to the predicted response. This, again is the effect of non-linearity rather than of estimation of linear damping parameters. If we increase the damping in order to match the fast collapse of the envelope, then we will decrease the predicted overshoot, which is already too low. It is important to realize that what really happens is that after the cut has started a different type of damping dominates as compared to the initial one.

Similar considerations hold for the other cutters; for 30° Double Flat (Fig 7.34) insert the simulation matches the peak and also the dynamics afterwards in a good way. For 30°

Flatted insert (Fig 7.35) the simulation matches the peak but the not the dynamics after the entry.

For 15° Flatted (Fig 7.36) insert the behavior of the experimental data is very erratical, which makes it difficult to establish even an observation of what the overshoot would be. This insert, as seen before, presents this problem of high vibration which could be attributed to the combination with the 15° lead angle cutter which rubs the trailing part of the cutting edge insert against the part of the workpiece which was cut one or two revolutions before.

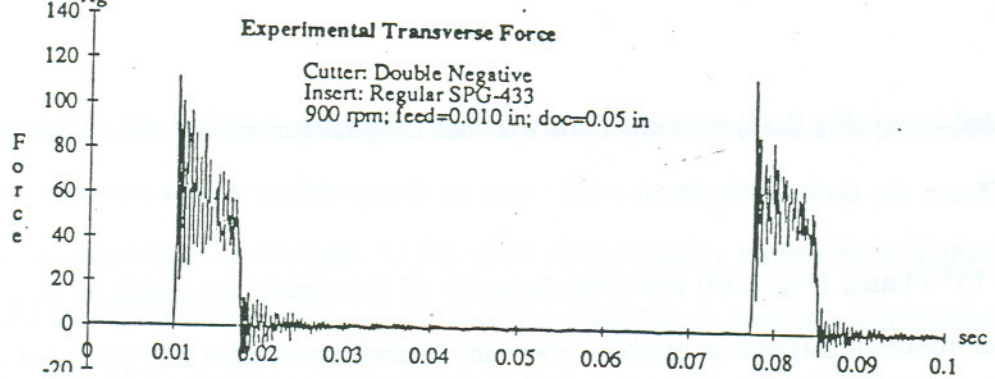

(b) Experimental results

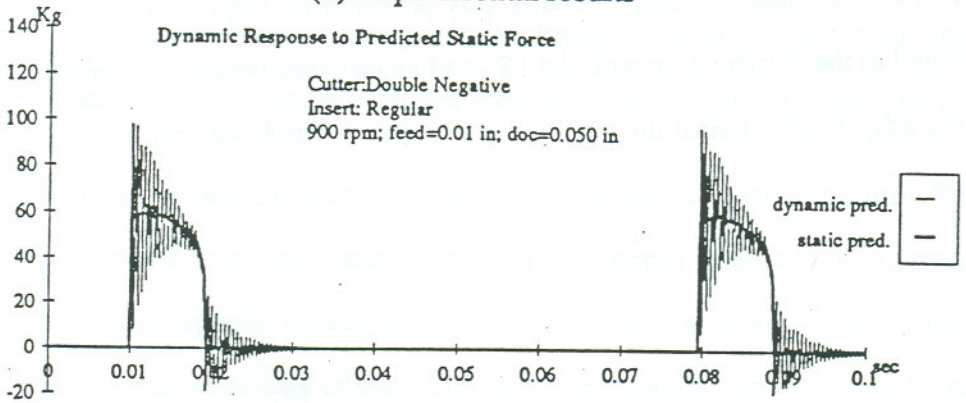

(a) static and dynamic predictions

Fig 7.33 Interrupted Cut tests. Entry experiments. Series 5. Regular Insert.

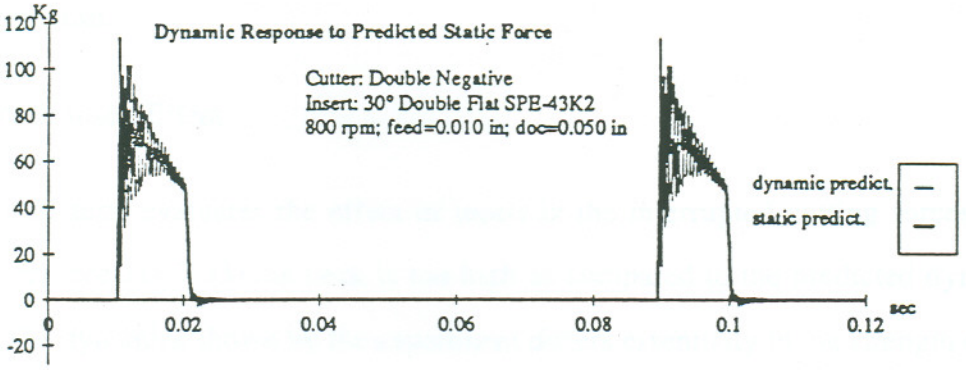

(b) Experimental results

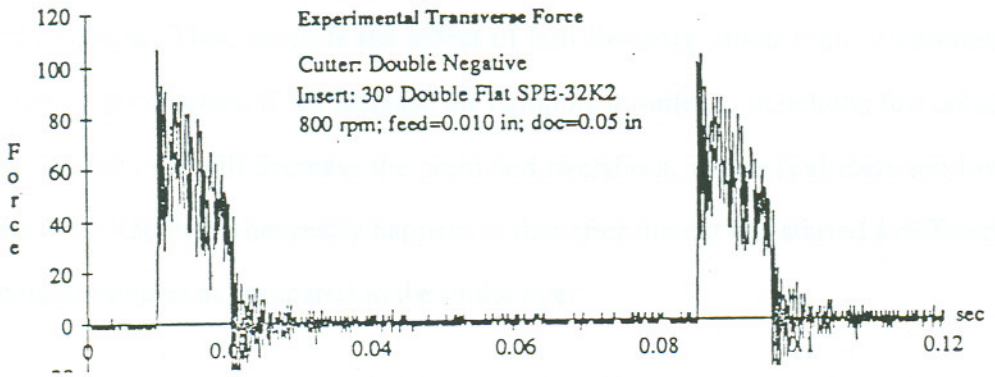

(a) static and dynamic predictions

Fig 7.34 Interrupted Cut tests. Entry experiments. Series 5. 30° Double Flat insert.

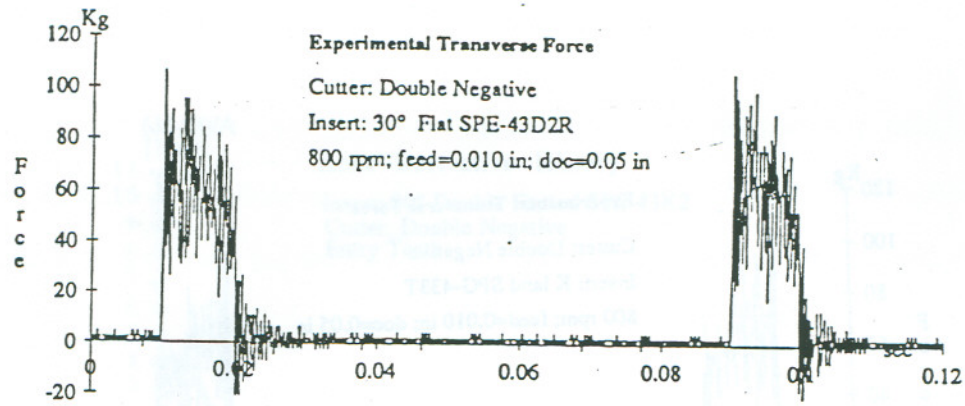

(b) Experimental results

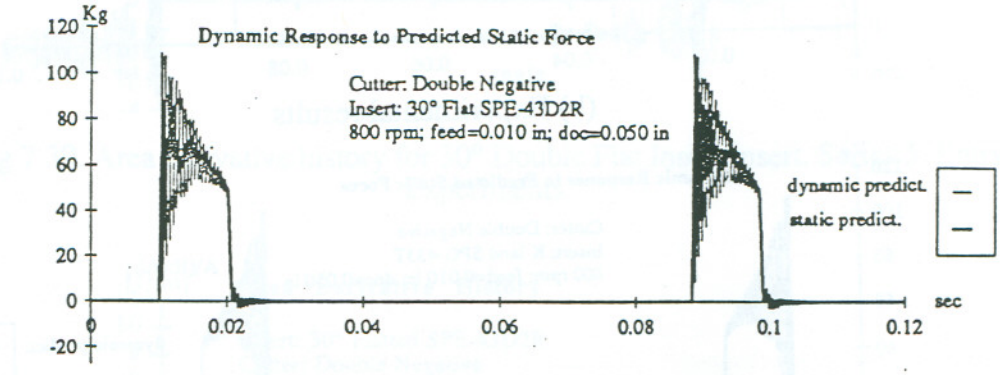

(a) static and dynamic predictions

Fig 7.35 Interrupted Cut tests. Entry experiments. Series 5. 30° Flat insert.

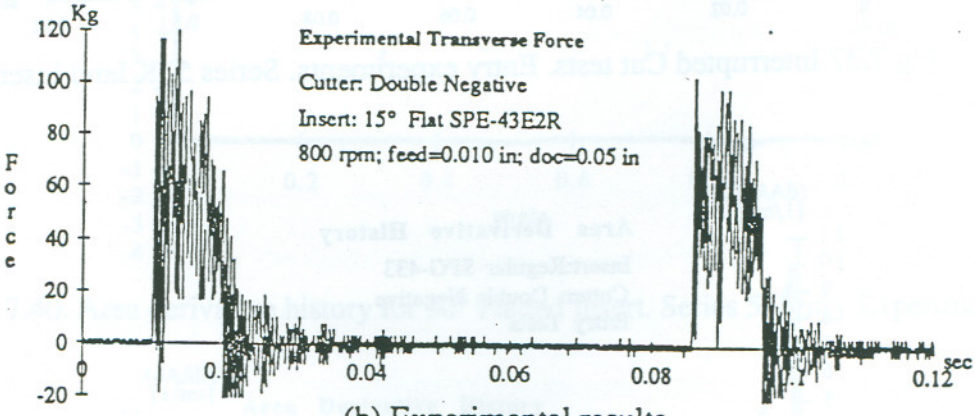

(b) Experimental results

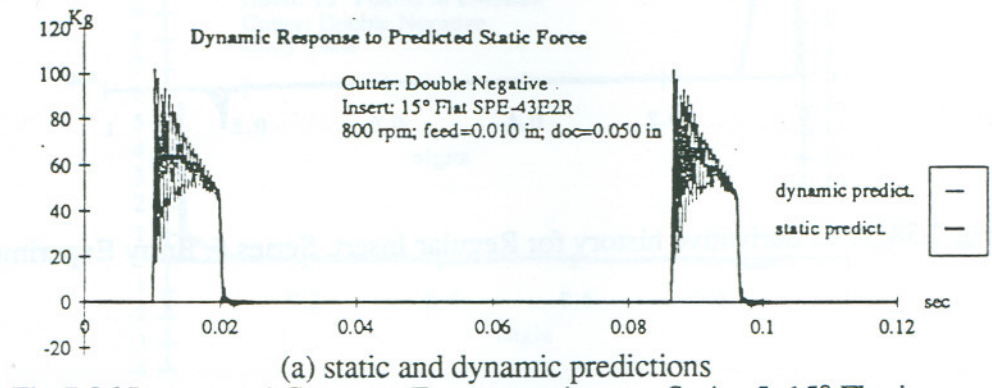

(a) static and dynamic predictions

Fig 7.36 Interrupted Cut tests. Entry experiments. Series 5. 15° Flat insert.

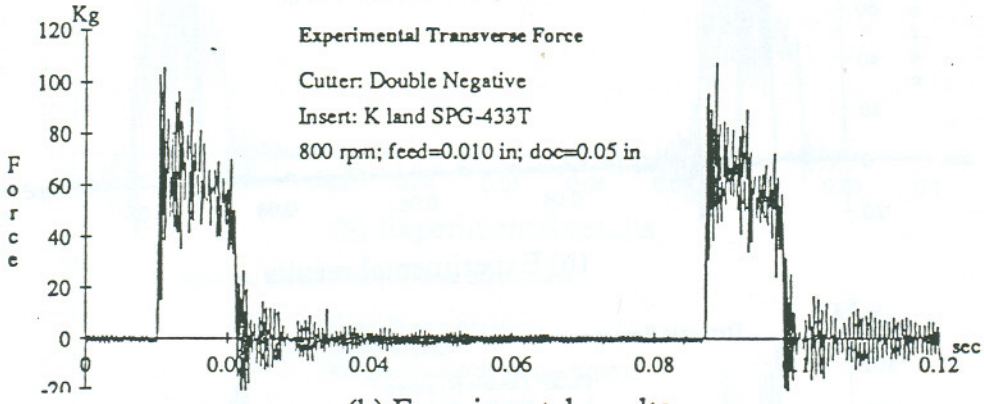

(b) Experimental results

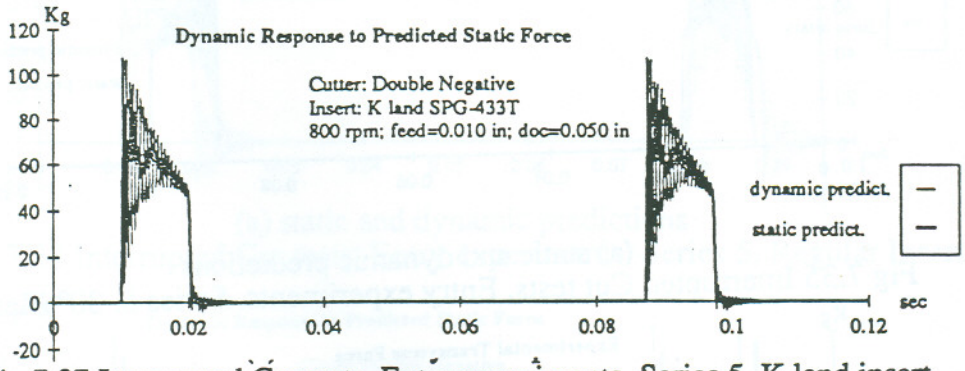

Fig 7.37 Interrupted Cut tests. Entry experiments. Series 5. K land insert.

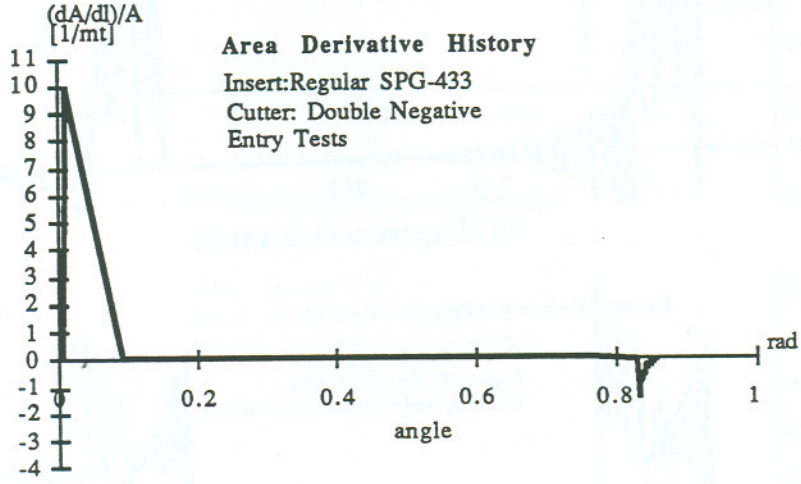

Fig 7.38. Area derivative history for Regular Insert. Series 5. Entry Experiments.

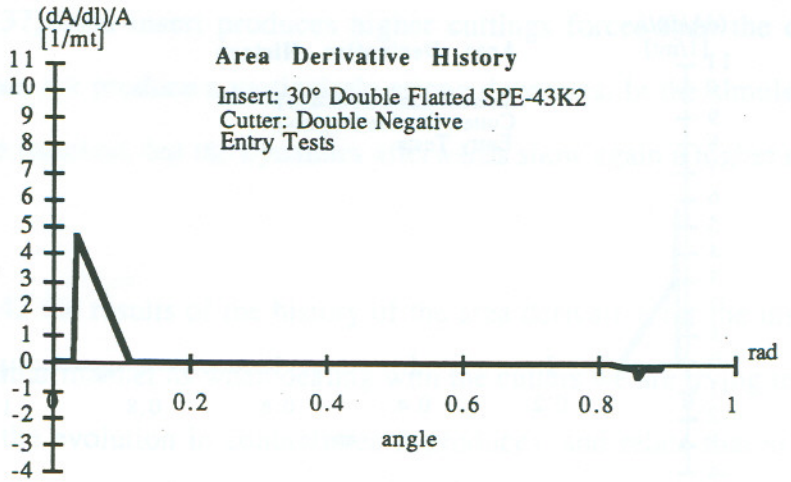

Fig 7.39. Area derivative history for 30° Double Flat Insert Insert. Series 5. Entry Experiments.

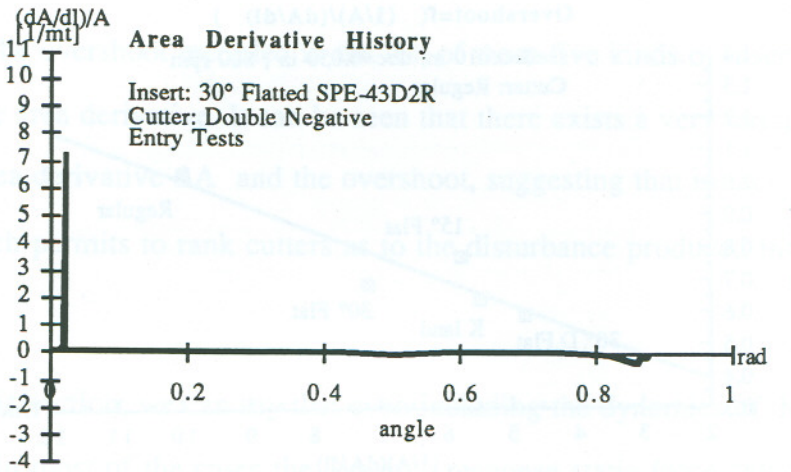

Fig 7.40. Area derivative history for 30° Flatted Insert. Series 5. Entry Experiments.

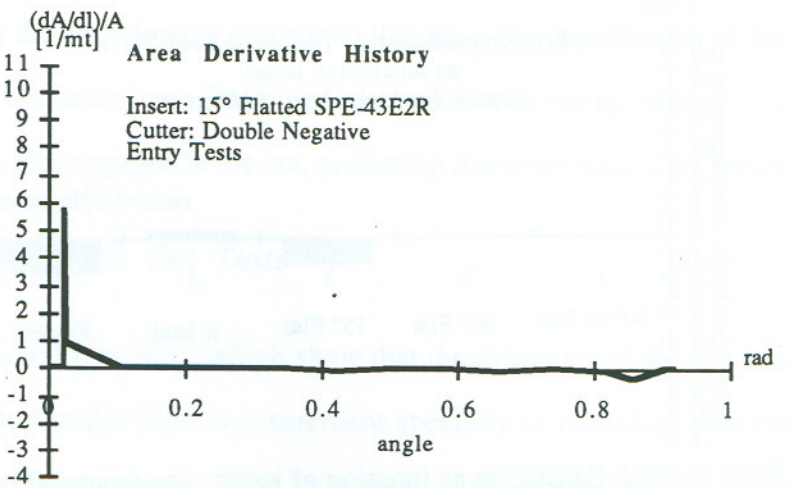

Fig 7.41. Area derivative history for 15° Flatted Insert. Series 5. Entry Experiments.

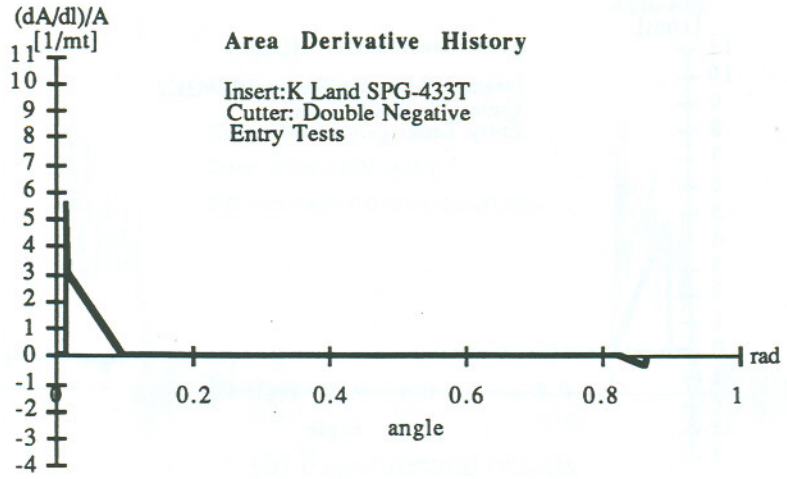

Fig 7.42. Area derivative history for K_land Insert. Series 5. Entry Experiments.

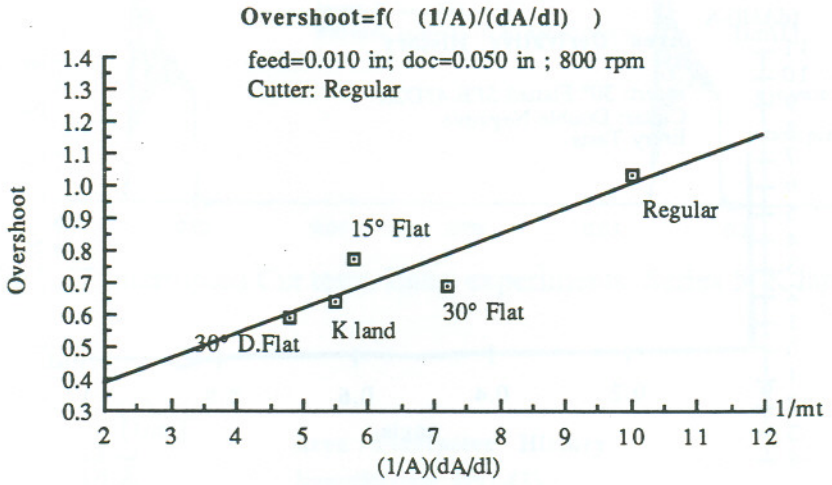

Fig 7.43. Overshoot as a function of Area derivative. Series 5. Entry Experiments.

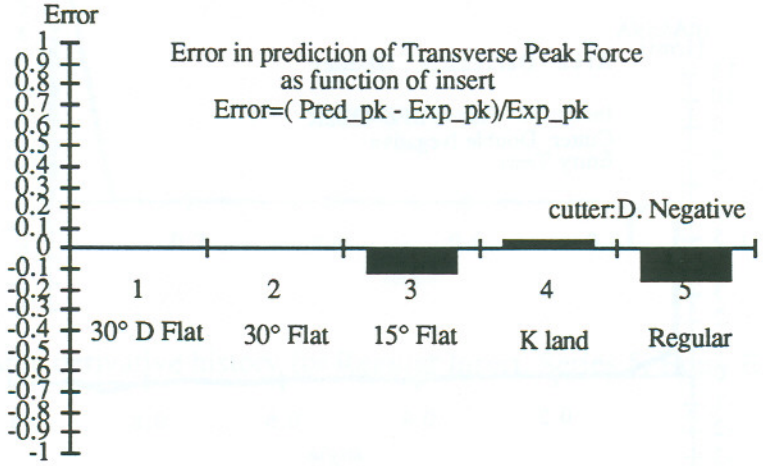

Fig 7.44. Error in Peak Prediction as function of insert type.(rpm=800; DoC=0.050"; feed=0.010")

The K (Fig 7.37) land insert produces higher cuttings forces than the other inserts. However, it does not produce a particularly strong dynamics. In the simulations run the first peaks were matched, but the dynamics afterwards show again a higher damping than projected.

In Figs 7.38-7.42 the results of the history of the area derivative for the inserts tested is shown. In a similar manner as when dealing with the cutters we are trying to characterize each insert by the evolution in contact area it produces, and relate that area derivative parameter to the overshoot observed in the interrupted tests. We attempt the same characterization as for cutters by using the ΔA parameter.

In figure 7.43 the overshoot recorded in the test of these five kinds of insert is shown as related with the area derivative. It can be seen that there exists a very strong correlation between the area derivative ΔA and the overshoot, suggesting that in fact ΔA may be a parameter which permits to rank cutters as to the disturbance produced in the set-up is related.

To conclude this section, we can say that even including the dynamics of the set up into consideration, in most of the cases the dynamic response static force calculation is not enough for explaining the big overshoot at the beginning of the cut. However, it is has been seen along the experiments performed that the main contribution of forces produced by interrupted cut comes from flexibility in the particular set-up, which accounts for very big variations in area engaged in the cut, producing therefore high force levels.

7.2.2 Interrupted Exit Cut Tests

In contrast with the Entry tests, which show that the dynamics of the set-up accounts for a significant portion in the force measurement specially in moderate cuts (feed=0.010 in, doc=0.050 in) at higher speeds (1000-1500 rpm), in the exit interrupted cut tests the result of the simulation and the experiments differ greatly (see Fig 7.45) . For all the simulations

run, the effect of the dynamics disappears gradually, leaving the static signal virtually untouched by the dynamic response. In the experimental result, however, the dynamic instability grows as the tool approaches the exit wall; time in which the cut turns unstable. The explanation for this may be an instability in the damping of the process, or an increase in workpiece fragility as the tool approaches the exit. The second explanation is more in agreement with the work by Pekelharing [12,13] which found that the failure of the workpiece in conditions of exit with a 90° angle is very likely, and that the mechanism of cut is replaced by a crack mode which blows away small parts of the exit edge.

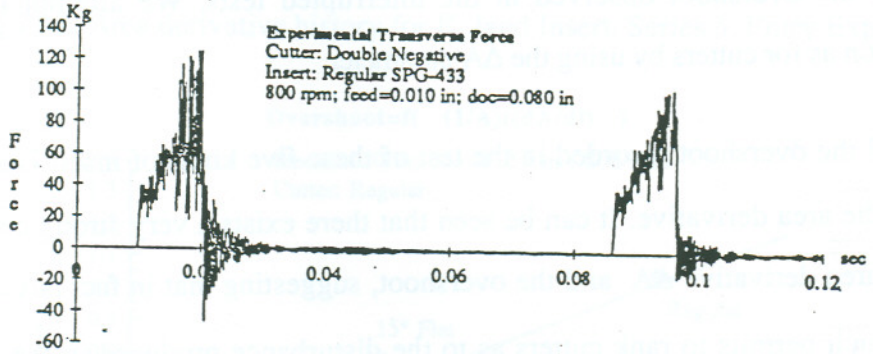

(b) Experimental results

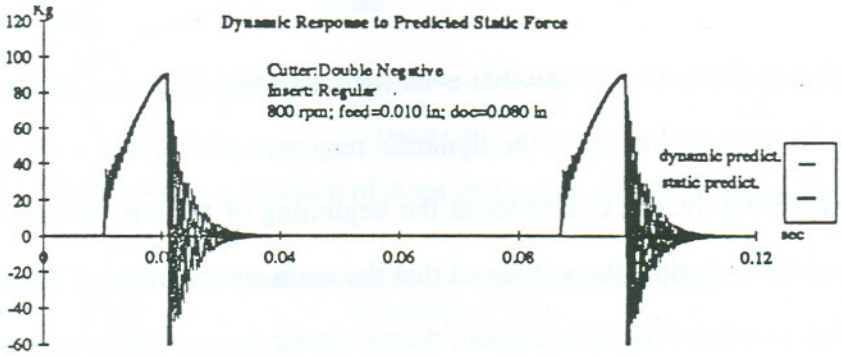

(a) static and dynamic predictions

Fig 7.45. Interrupted Cut. Exit Tests. Regular Insert; Double Negative Cutter.

7.3 Geometry Module.

As mentioned earlier in Chapter 4 the solid model program 3D_MCUT accepts diverse insert and cutter geometries and is useful for simulating interrupted and continuous cut in face milling (fly cutting) and also turning. The new approach is particularly useful in

modeling the cutting forces because the geometry module provides the geometric information in the vector form, thus allowing for straightforward calculations of features such as projected areas, force decompositions, coordinate system transformation, etc. The geometry module can easily be extended for other purposes, such as finite element calculation of stresses and temperature fields in the insert and workpiece since the geometrical information needed to these analysis is already available with the geometry model.

A drawback of the geometry model is the intensive computation involved in examining the cells which make up the insert face. The cell enumeration scheme in representing the insert and workpiece geometries in the computer is quite cumbersome. However for finite element analysis, the model already gives the nodal structure or mesh and therefore there is no further need to generate mesh for the analysis

Table 7.1.

feed (in)	doc (in)	feed (mm)	doc (mm)	Endres'	3D_MCUT	% ERROR
0.01	0.05	0.254	1.27	0.322	0.313	2.7
0.01	0.02	0.254	0.508	0.129	0.125	3.2
0.01	0.04	0.254	1.016	0.258	0.250	2.9
0.01	0.05	0.254	1.27	0.322	0.313	2.7
0.01	0.07	0.254	1.778	0.451	0.441	2.3
0.01	0.08	0.254	2.032	0.516	0.503	2.5
0.005	0.05	0.127	1.27	0.161	0.153	5.0
0.01	0.05	0.254	1.27	0.322	0.313	2.7
0.015	0.05	0.381	1.27	0.482	0.471	2.3
0.02	0.05	0.508	1.27	0.641	0.627	2.1

Table 7.1. Comparison between Endres' formula and 3D_MCUT evaluation of tangential area for Double Negative cutter, Regular insert.

In order to check the accuracy of the area calculation using the 3D_MCUT module the results were compared with the results of Endres [28,29] for different cutting conditions and cutter geometry. The comparison is given in Table 7.1 In general the error between the two methods is less than 5%.

The slight difference between the two areas comes from two sources: (i) Endres' calculation approaches the tangential area as the area measured in the rake face while 3D_MCUT does not make that approximation. (ii) Endres' formula is analytical while 3D_MCUT divides the rake face in small squares and therefore its accuracy depends on the quality of the subdivision.

7.4 Summary

In this chapter the results of the diverse experiments and software were evaluated. In particular the quality of the force model prediction for the static forces and the dynamic response prediction were assessed based on the experimentally measured values obtained in the continuous and interrupted cutting tests respectively. The static feed and transverse cutting forces are accurately predicted by the mechanistic model. The axial force prediction has been found more deviated from the measured values.

In interrupted cutting tests it was found that the predicted dynamic response to the static transverse force is similar to the force measurements in interrupted entry cuts. The agreement between the force measurements and the predicted dynamic forces is good for high cutting speeds, but degrades for low velocities, where the low inertial energy of the spindle motor allows decelerations which affects the measured forces in addition to the subsystem dynamics. For exit cuts the predicted dynamic response to the static forces does not resemble the dynamics shown in the measurements, which indicates that in exit cuts effects different from the dynamic response of the subsystem produce the instability found in the force measurements. More discussion on the results is presented in Chapter 8.

CHAPTER 8

CONCLUSIONS AND RECOMMENDATIONS

The stated objectives of this thesis include:

1. Identification of the nature of the cutting forces present in entry/exit stages of metal cutting through actual machining tests.

2. Development of a mechanistic model for these force if they are found to be significantly different from the static cutting forces

3. Establishment a relationship between the measured process variables (forces and specific cutting forces) and the geometric configurations of the respective cutting conditions.

In order to meet these objectives the following activities have been performed:

1. Design and execution of interrupted cut force tests in face milling, fly cutting. A cast iron workpiece has been designed to produce sharp transitions between cut/no_cut conditions both in entry as well as in exit conditions. The tests were aimed at measuring the effect of variables such as cutting speed, feed, depth of cut and cutter/insert geometries on the interrupted cut forces.

2. Design and execution of continuous cutting tests in face milling, fly cutting. The objective of these tests was to calibrate a mechanistic model for static conditions with end goal of providing a basis of comparison of the test results with the results of interrupted cutting tests mentioned above. Consequently these cutting conditions exactly replicated those in interrupted cutting tests. The only difference was in the geometry of the workpiece. In this case a solid workpiece was used in contrast with the interrupted geometry used for the previous tests.

3. Design and implementation of a geometric module which allows for the flexible modeling of entry/exit as well as continuous cuts for different inserts, cutters, and relative positions between workpiece and tool This module has been developed using solid modeling techniques to take advantage of the power of these techniques in handling complex situations which prevail in entry/exit cuts. A quantitative measure of the form of engagement/disengagement based on the "Impact Factor" defined by Kronenberg [9] was implemented in the module in order to evaluate the abruptness of the transition cut/no_cut conditions. Also, mechanistic modeling of the cutting forces was included in the module following Fu's algorithm for effective lead angle [30] and predictions based on the continuous cut calibrations where made.

4. Estimation of the dynamic characteristics of the subsystem including workpiece, dynamometer and fixture. This dynamic modeling was necessary because the force signal from the interrupted cutting tests included the dynamic response of the subsystem to the sudden application of entry/exit and static cutting forces. By determining the transfer function between the cutting forces applied to the workpiece and the dynamometer reading it was possible to take into consideration the dynamic factor in the forces measured in the interrupted cutting tests.

5. Estimation of the response of the force measuring system to a static force prediction. This response was calculated by feeding the static force predictions made by the geometry/force-prediction module into the transfer function mentioned in point 4. This estimation was then compared with the experimental measurements of interrupted cutting forces. The comparison focussed specially on the accuracy of the prediction of the force peaks in abrupt entry/exit cuts, and on the spectral contents of the force signal. .

Based on the results of the activities described above the conclusions and recommendations of the thesis are listed in sections 8.1 and 8,2 respectively.

8.1 Conclusions

1. The initial peak registered in entry cuts is largely explained by the dynamic response of the workpiece/dynamometer/fixture system to the static forces. For most of the tests the relative error between the predicted dynamic response to static forces and the measurements in interrupted entry cutting tests are below 10%. Although there is a consistent trend of underestimation of the recorded peak by the dynamic predictions, it can be explained by a previous underestimation of the static forces which where used as input to the transfer function representing the dynamics of the subsystem.

2. In entry cuts, although there is a slight trend of increase in the relative peak ((peak force-static force)/static force) with the cutting velocity it is very small for the range of speeds considered (300 rpm to 1500 rpm). It is possible that wider ranges of cutting speeds would give more definite results.

3. The shape of the dynamic oscillations present in the entry force signatures during the interrupted cuts is well approached by the simulated dynamic response form the dynamometer / fixture / workpiece subsystem to the input of static force. This agreement degrades for low cutting speeds. The reason is that at low cutting speeds the cutting forces significantly decrease the angular velocity of the spindle. This causes the control loop of the spindle motor to react trying to increase the velocity. This process of deceleration and late acceleration is reflected in the force signatures as additional dynamics superimposed on the workpiece/dynamometer/fixture dynamics. The quality of the dynamic prediction which does not take into consideration the effect of the dynamics of the spindle/tool subsystem degrades.

4. For abrupt exits, the dynamics detected in the experimental results, specially in the neighborhood of the exit wall is not correctly predicted by convoluting the transfer function of the dynamic subsystem with the input static force. In the first case, the dynamics

increases towards the end of the cut while in the second case the dynamics is mainly observed in the initial times of engagement, and decreases towards the end. The implication of this result is that, unlike entry cuts, the dynamics and instability at the exit are not caused by the sole response of the structure to the cutting forces but by the workpiece material itself which behaves in different ways in the neighborhood of the exit wall. This result confirms the effects reported by Pekelharing [12] which reported workpiece failure in the exit stages.

5. In respect to the relation between geometric parameters and the interrupted force experiments, it was found that for entry cuts, the magnitude of the relative peak is very dependent on the geometry of the cutter, insert and the relative position between the tool and workpiece. More specifically, this relative peak is very dependent on the Impact Factor (defined by Kronenberg as dA/dt, where A is the engaged area). The relative peak as determined from the interrupted cutting tests increases with an increment in the contact area derivative. The area derivative was calculated by using the solid geometry module described before. This module is designed to closely follow the insert engagement/disengagement process both qualitatively as well as quantitatively

8.2 Recommendations

The results of the comparison between dynamic simulation and interrupted cuts showed that the rotational dynamics of the spindle/tool subsystem is important because it changes the shape of the force signature, producing modes of oscillation which are additional to the ones appearing in the dynamic simulation. Inclusion of this subsystem's dynamics should improve the predictions.

In order to continue the line of research in entry/exit forces and the effect in insert failure, two approaches are possible. First, with the help of a set-up whose natural frequency is higher than the current one (2000 hz approx) the existence of higher frequency force

signals could be studied. Second, the evidence in this experiment shows that, unless very-high frequency and magnitude forces are present , the emphasis of further research in the area of insert failure should be shifted to thermal and mechanical stresses. It is believed that the forces themselves are not present in a level that makes the insert fail.Instead, the effect of these stresses on the workpiece and/or the insert create a potential for tool failure. For continuing in this continuing line of research finite element modeling of the thermal and mechanical stresses in the insert is promising.

The three dimensional analysis of geometry in metal cutting has proven to be a powerful qualitative as well as quantitative tool for analysis. It gives the flexibility to model different geometries and conditions of cut. If future research is done in this direction, the emphasis should be on integrating it with finite element techniques which could use the geometric local information provided by the model. Currently these techniques have been applied to very simple local geometries, in orthogonal cuts. Their extension to oblique cuts, with a non-infinite workpiece should prove useful, specially in analyzing tool failure mechanisms.

APPENDIX A.

SPECTRAL ANALYSIS OF INTERRUPTED CUTS.

A.1 This appendix shows some typical Fast Fourier transforms applied to the interrupted cutting tests

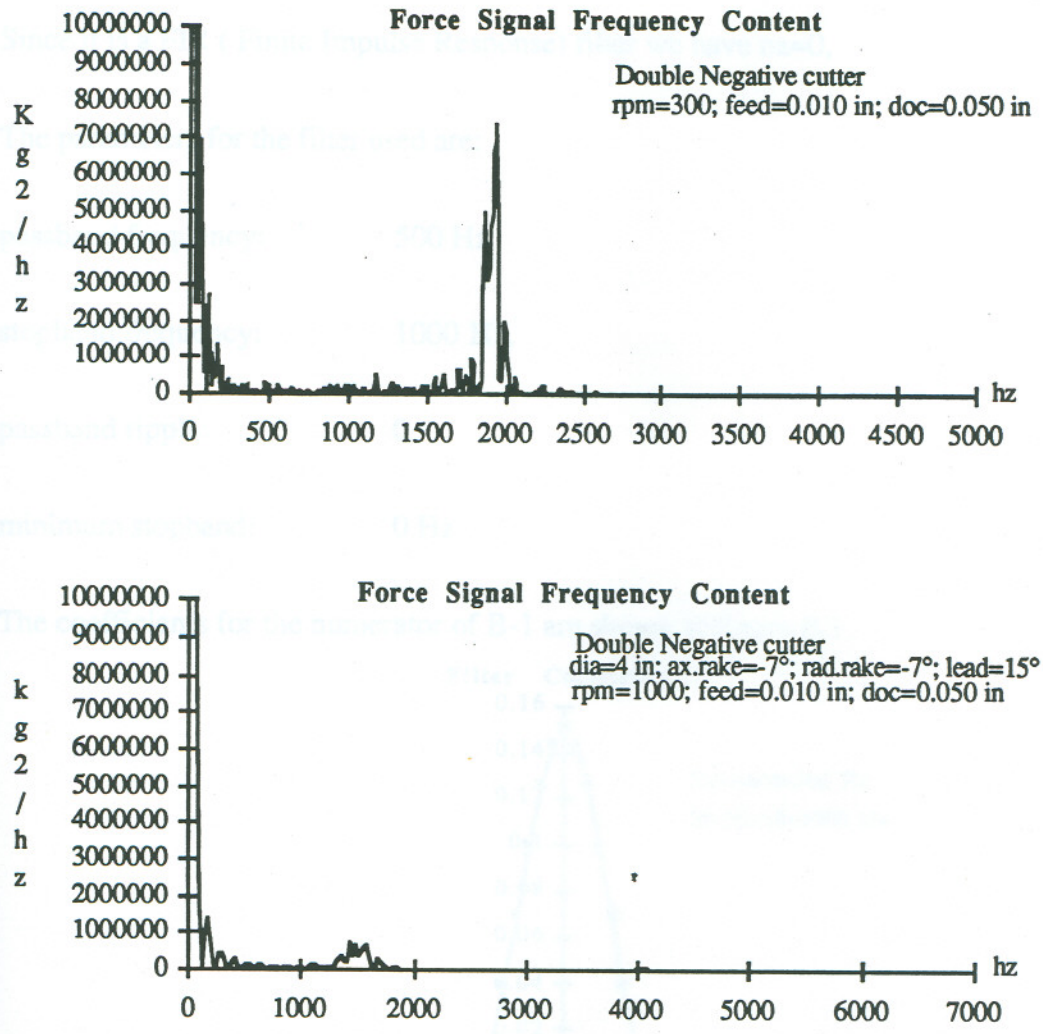

Fig A.1. Frequency Content In two tests of the Series 1, velocity effect. Note the displacement of the dominant peak.as effect of workpiece shortening.

APPENDIX B.

FILTERING

The digital filter used conforms to the general description:

$$Y(z) = \frac{b_1 + b_2 z^{-1} + b_3 z^{-2} + \ldots\ldots + b_{nb+1} z^{-nb}}{1 + a_2 z^{-1} + a_3 z^{-2} + \ldots\ldots + a_{na+1} z^{-na}} X(z) \qquad \text{(B-1)}$$

Since it is a FIR (Finite Impulse Response) filter we have na=0,

The parameters for the filter used are:

passband frequency: 500 Hz

stopband frequency: 1000 Hz.

passband ripple: 0

minimum stopband: 0 Hz

The coefficients for the numerator of B-1 are shown in figure B.1.

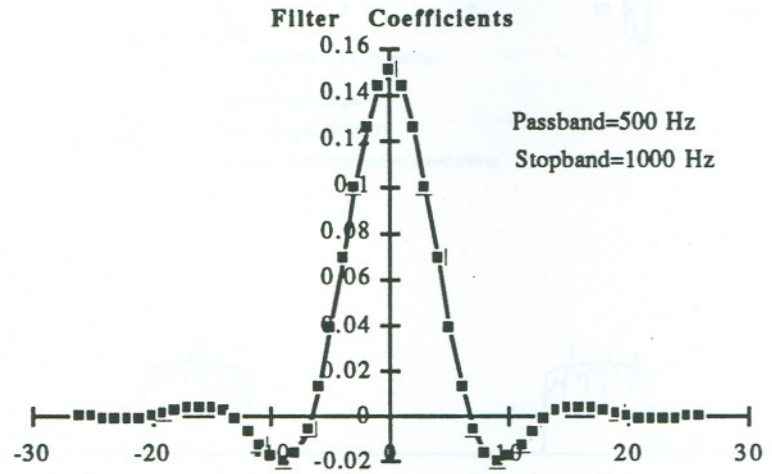

Figure B.1. Filter Weigth Coefficients.

APPENDIX C
CONTINUOUS CUT TESTS. EXPERIMENTS AND PREDICTIONS.

In this appendix the results of the continuous cut tests are shown; Kt_Kc mechanistic model force predictions appear with the experimental data.

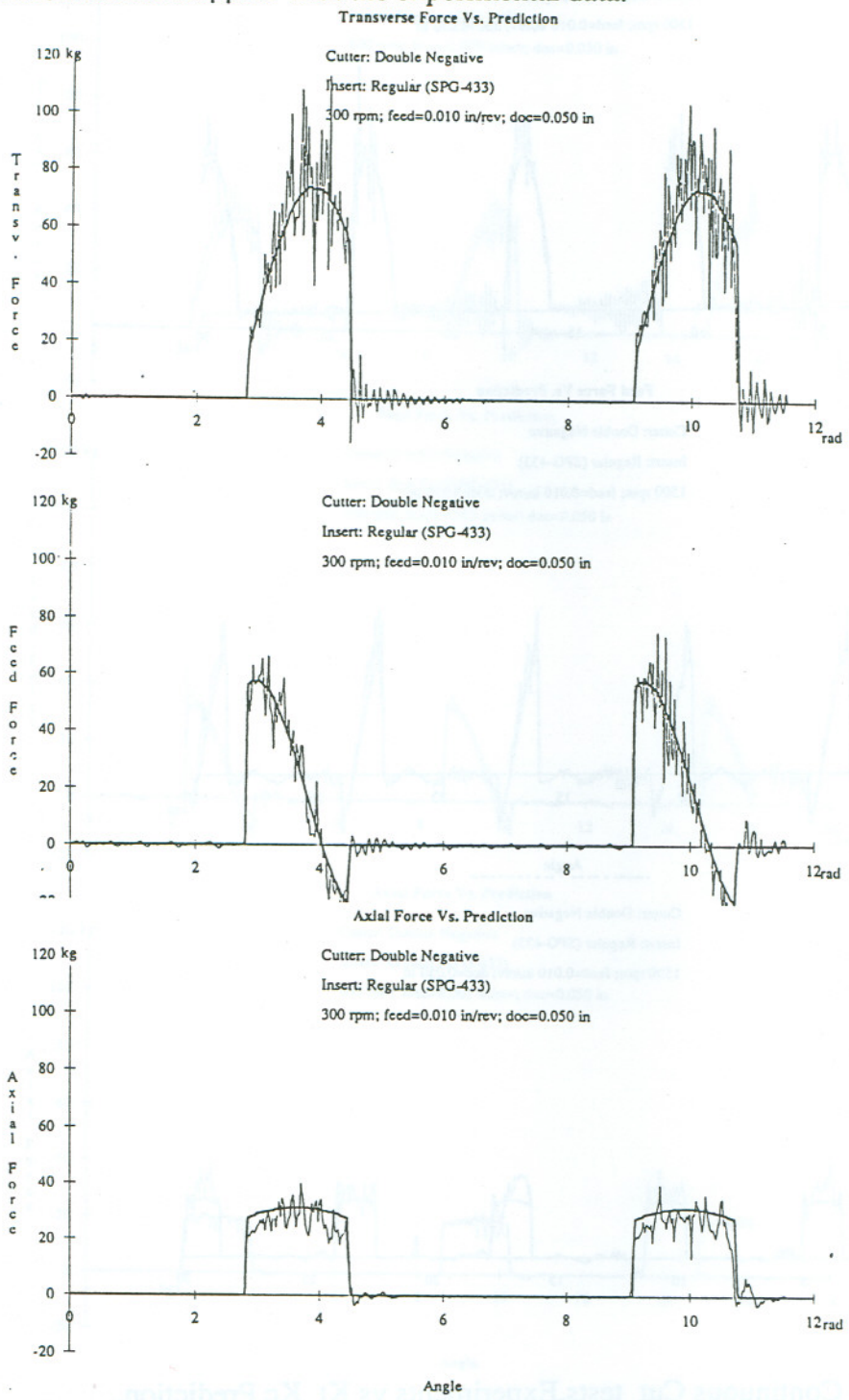

Fig C.1 Continuous Cut tests.Experiments vs Kt_Kc Prediction.
Double Negative Cutter. Regular Insert. 300 rpm; feed=0.010 in ;doc=0.05 in.

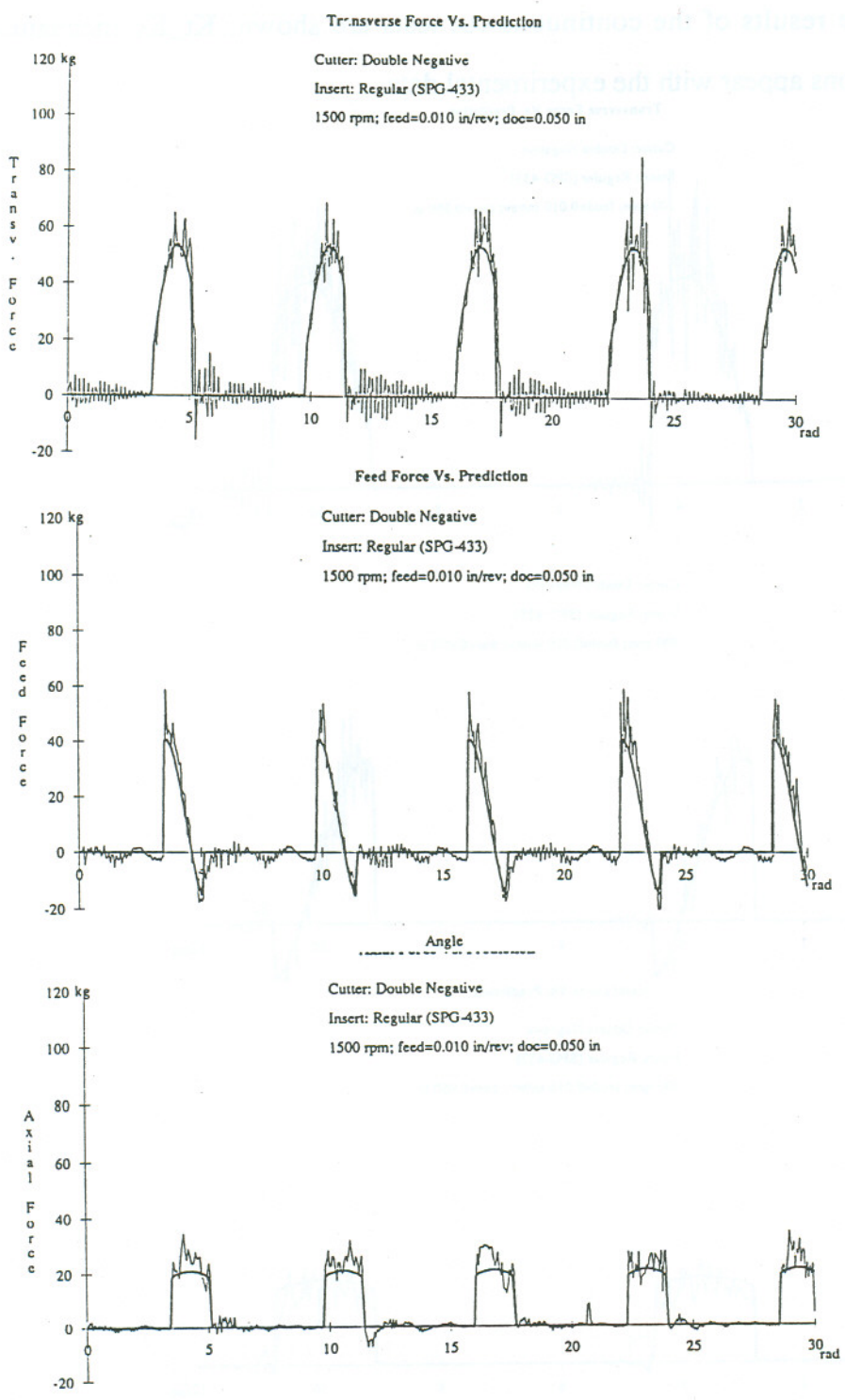

Fig C.2 Continuous Cut tests.Experiments vs Kt_Kc Prediction.
Double Negative Cutter. Regular Insert. 1500 rpm; feed=0.010 in ;doc=0.05 in.

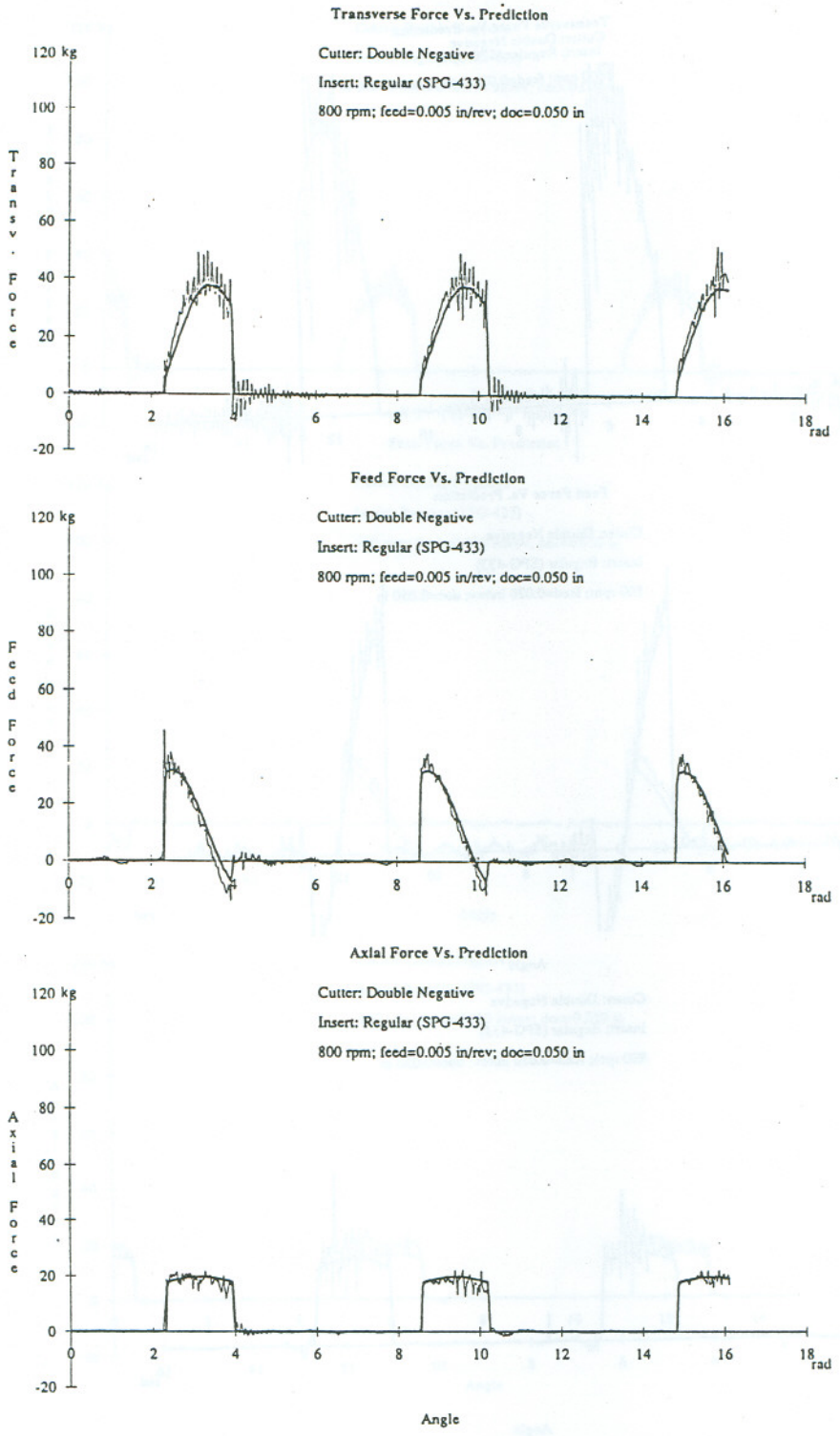

Fig C.3 Continuous Cut tests.Experiments vs Kt_Kc Prediction.
Double Negative Cutter. Regular Insert. 800 rpm; feed=0.005 in ;doc=0.05 in.

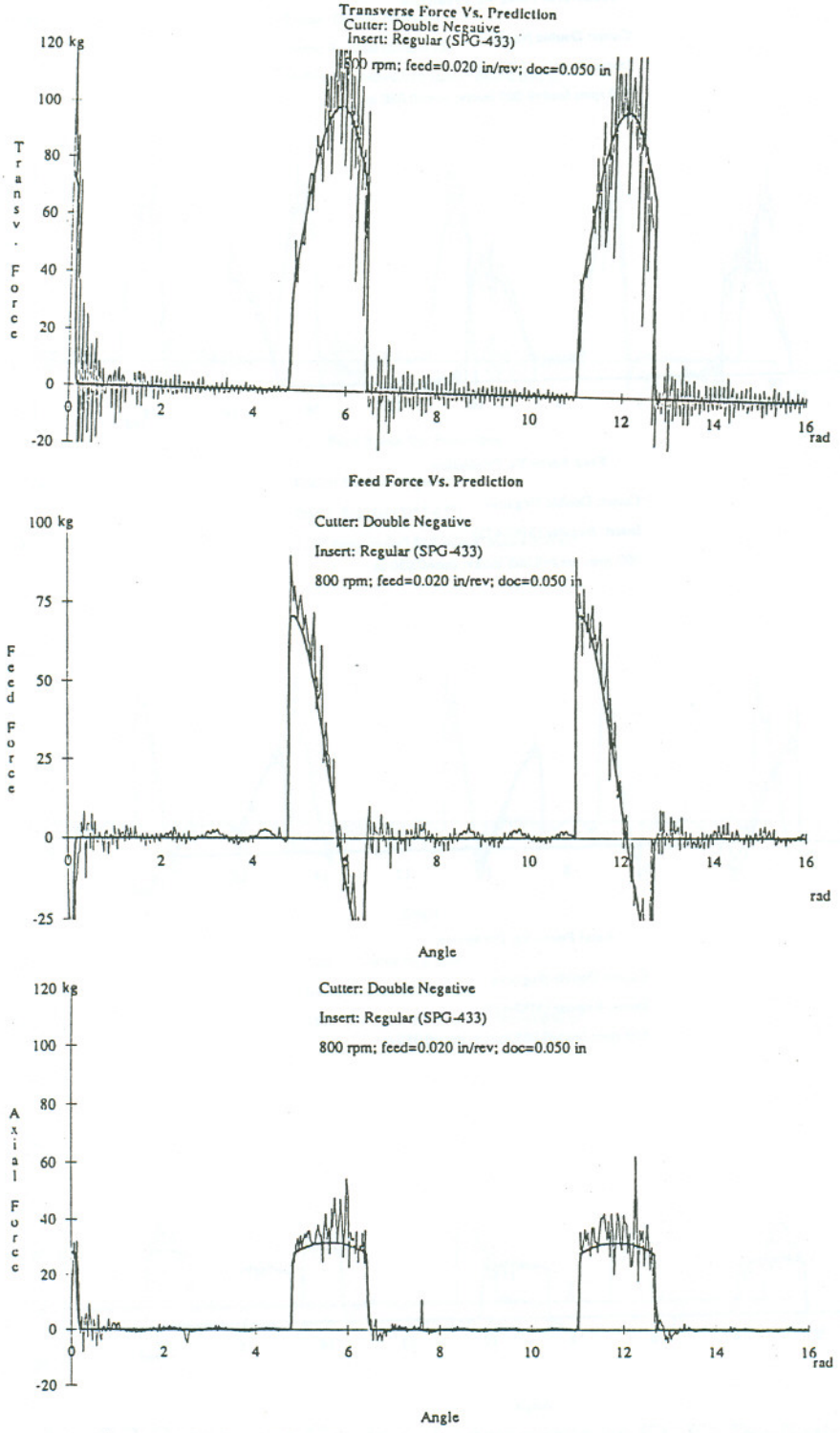

Fig C.4 Continuous Cut tests.Experiments vs Kt_Kc Prediction.
Double Negative Cutter. Regular Insert. 800 rpm; feed=0.020 in ;doc=0.05 in.

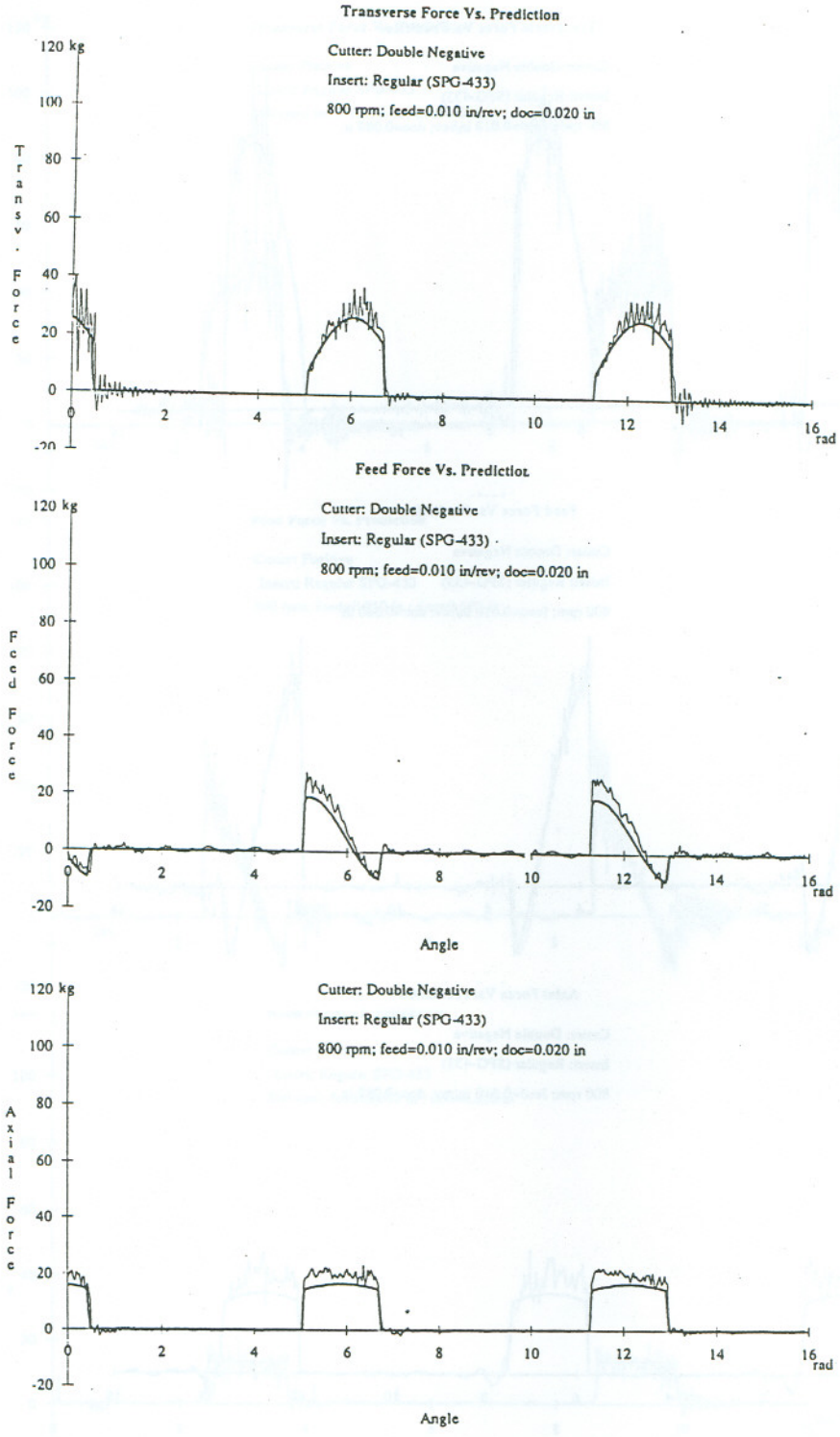

Fig C.5 Continuous Cut tests.Experiments vs Kt_Kc Prediction.
Double Negative Cutter. Regular Insert. 800 rpm; feed=0.010 in ;doc=0.020 in.

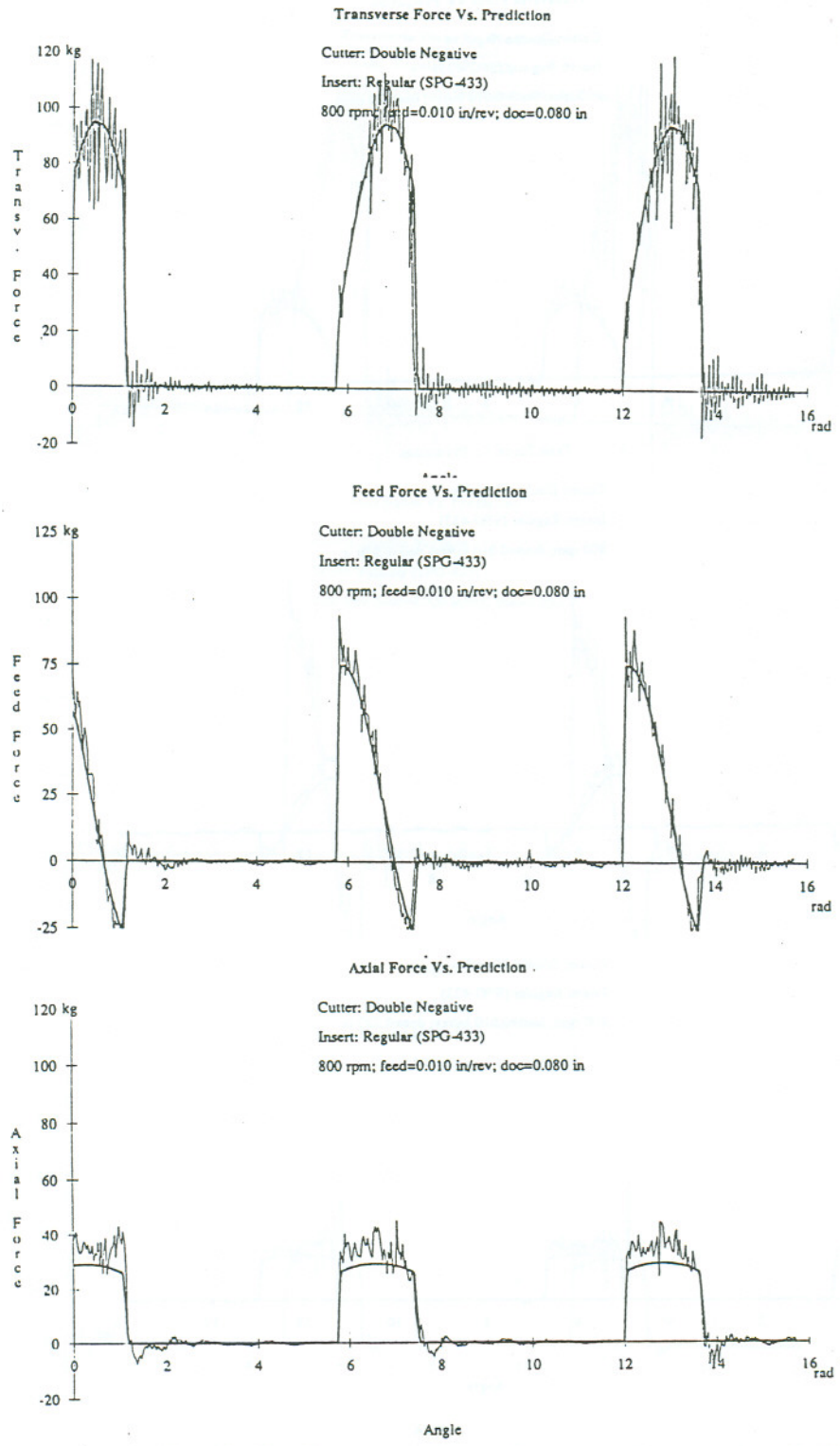

Fig C.6 Continuous Cut tests.Experiments vs Kt_Kc Prediction.
Double Negative Cutter. Regular Insert. 800 rpm; feed=0.010 in ;doc=0.080 in.

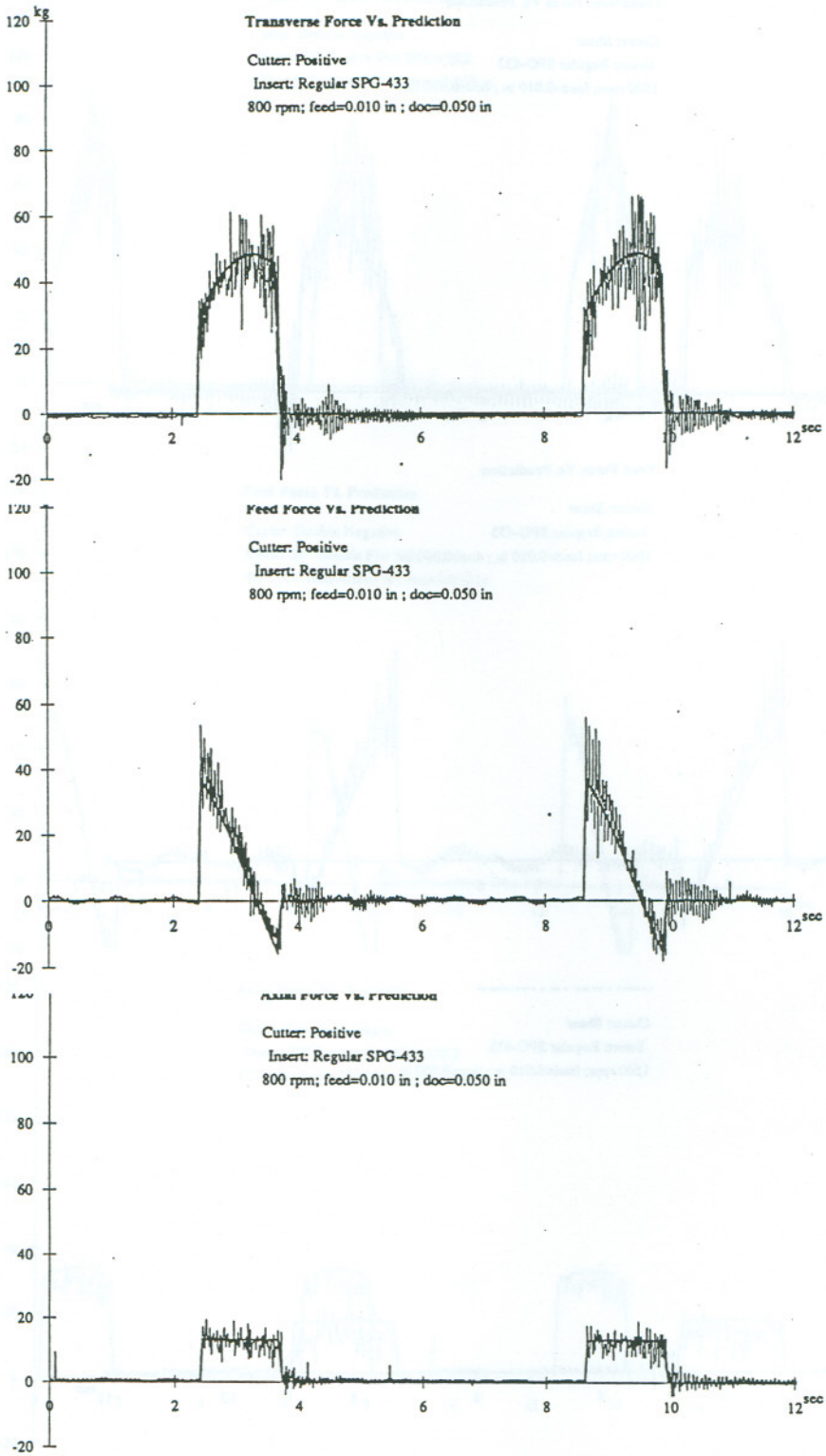

Fig C.7 Continuous Cut tests.Experiments vs Kt_Kc Prediction. Positive Cutter. Regular Insert. 800 rpm; feed=0.010 in ;doc=0.050 in.

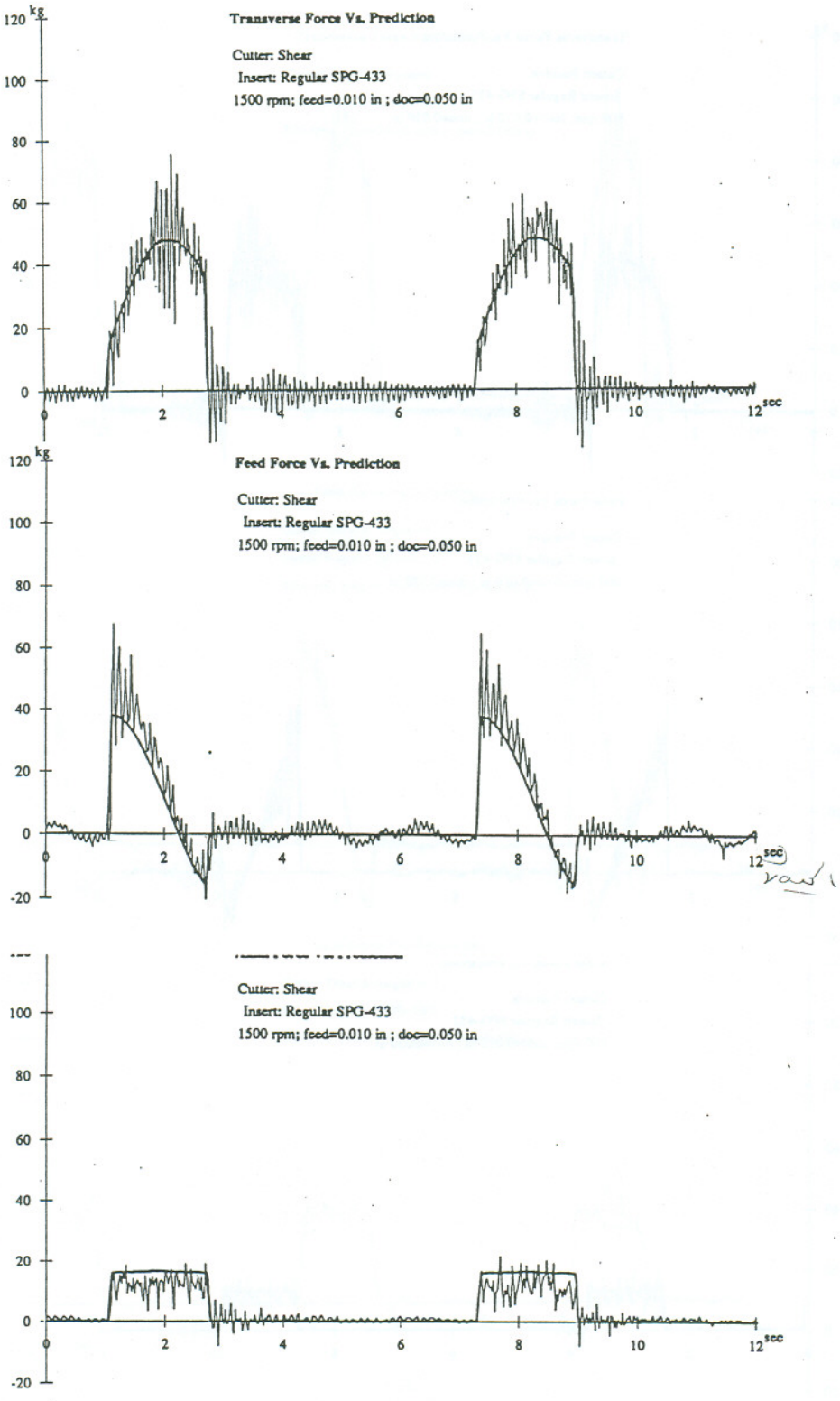

Fig C.8 Continuous Cut tests.Experiments vs Kt_Kc Prediction. Shear Cutter. Regular Insert. 1500 rpm; feed=0.010 in ;doc=0.050 in.

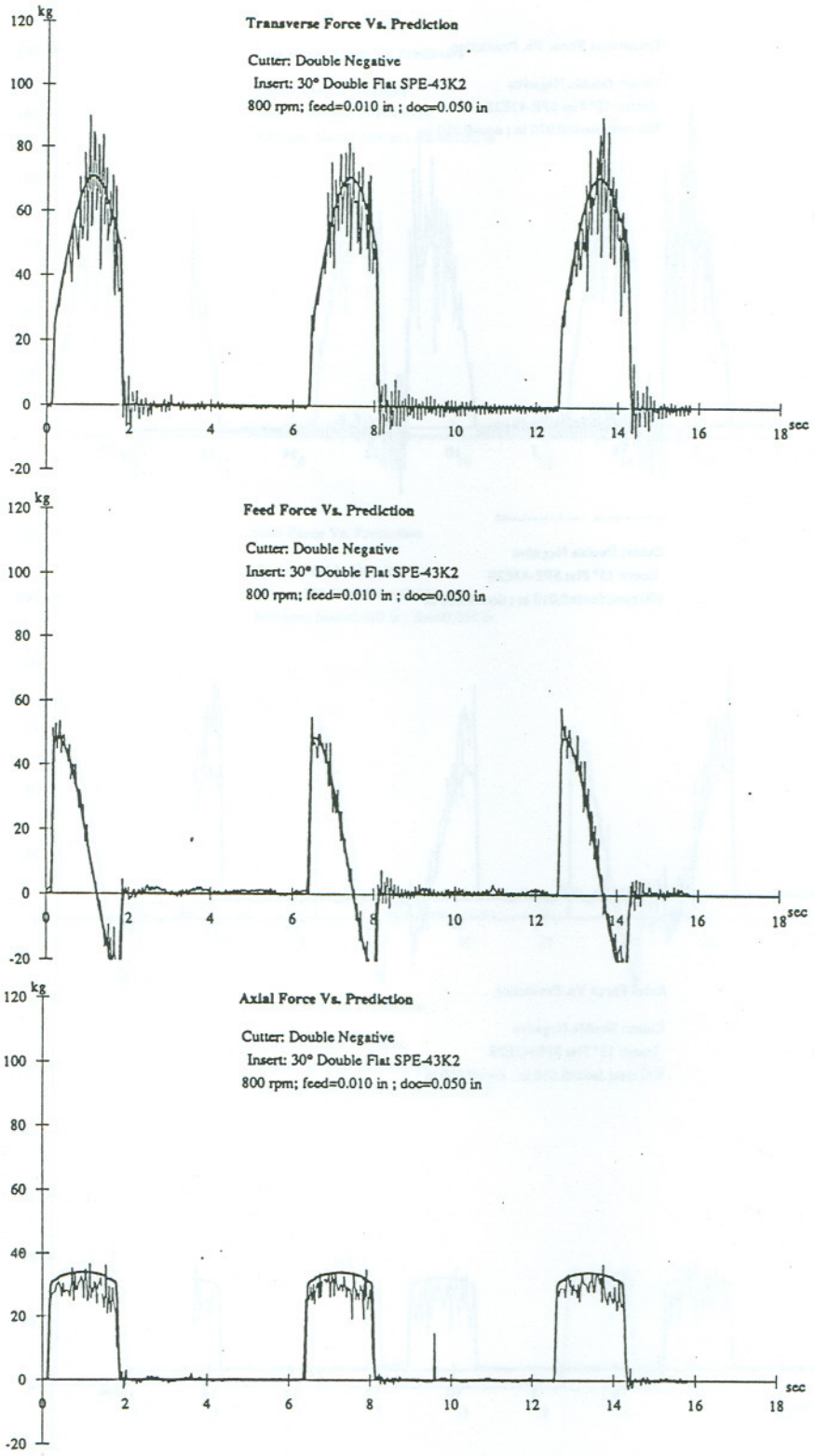

Fig C.9 Continuous Cut tests.Experiments vs Kt_Kc Prediction.
Double Negative Cutter. 30° Double Flat Insert. 800 rpm; feed=0.010 in ;doc=0.050 in.

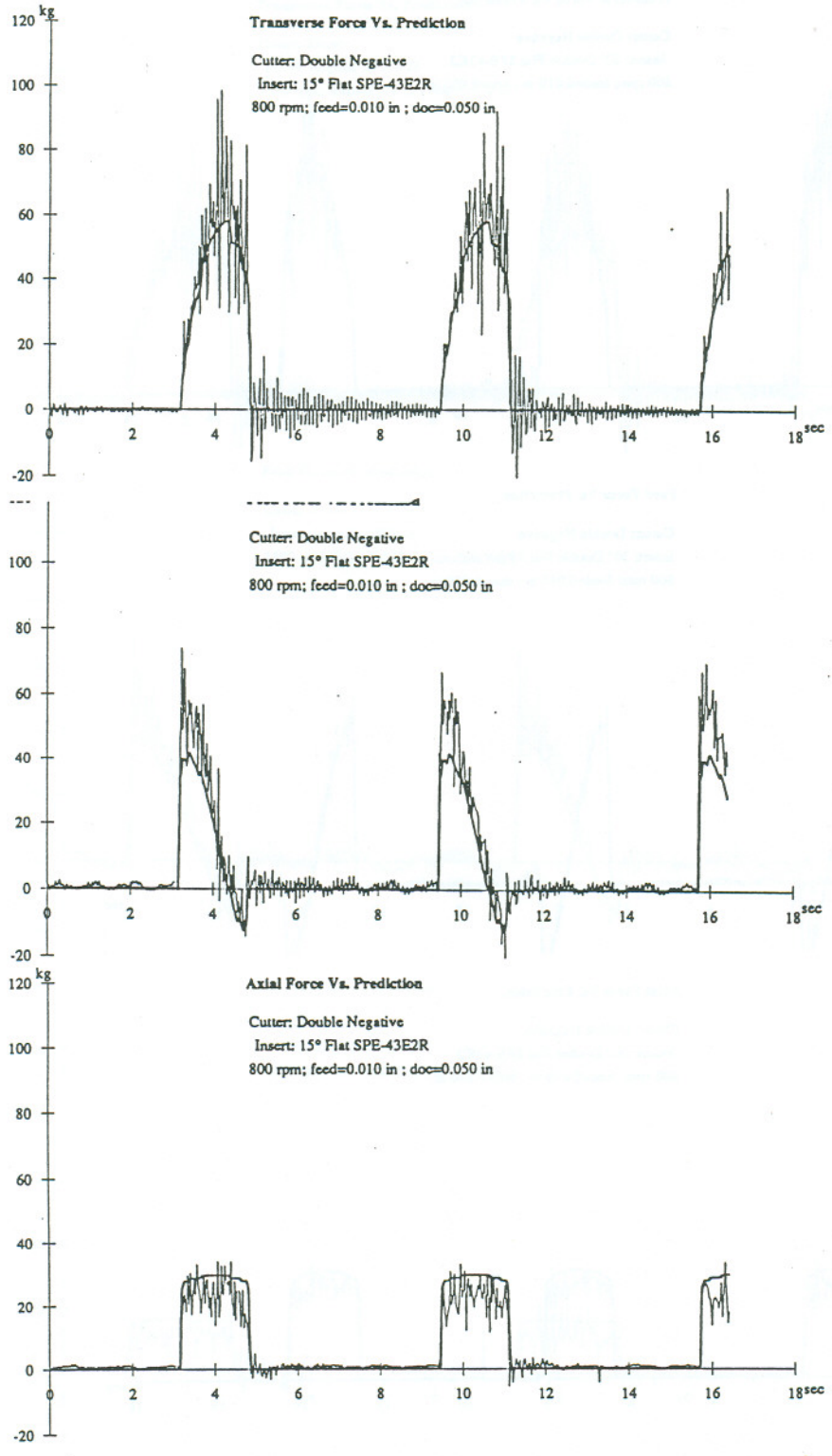

Fig C.10 Continuous Cut tests.Experiments vs Kt_Kc Prediction.
Double Negative Cutter. 30° Flat Insert. 800 rpm; feed=0.010 in ;doc=0.050 in.

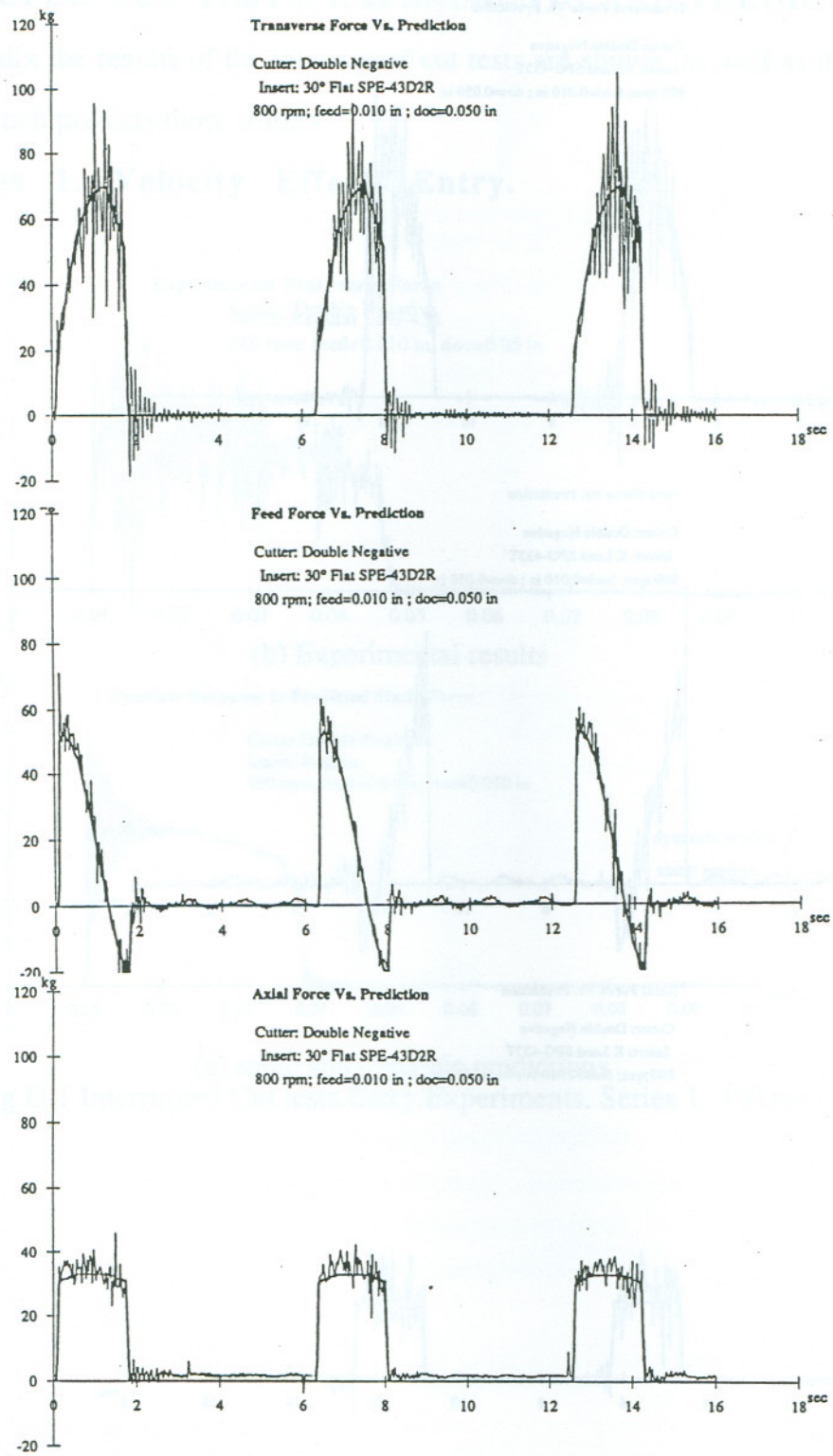

Fig C.11 Continuous Cut tests.Experiments vs Kt_Kc Prediction.
Double Negative Cutter. 15° Flat Insert. 800 rpm; feed=0.010 in ;doc=0.050 in.

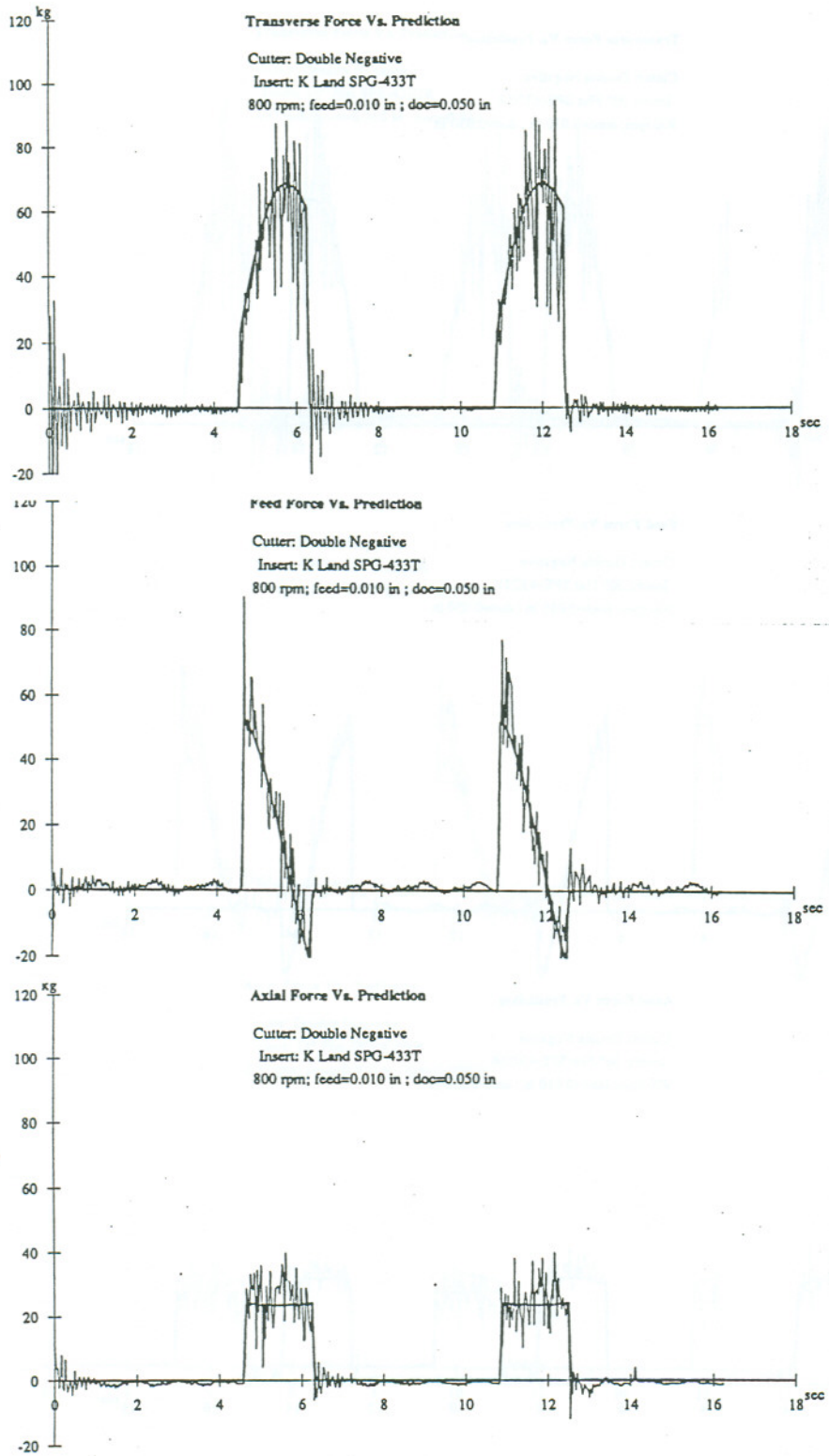

Fig C.12 Continuous Cut tests.Experiments vs Kt_Kc Prediction.
Double Negative Cutter. K land Insert. 800 rpm; feed=0.010 in ;doc=0.050 in.

APPENDIX D

INTERRUPED CUT TESTS. EXPERIMENTS AND PREDICTIONS.

In this appendix the results of the interrupted cut tests are shown; as well as the dynamic simulation which predicts those results.

D.1 Series 1. Velocity Effect. Entry.

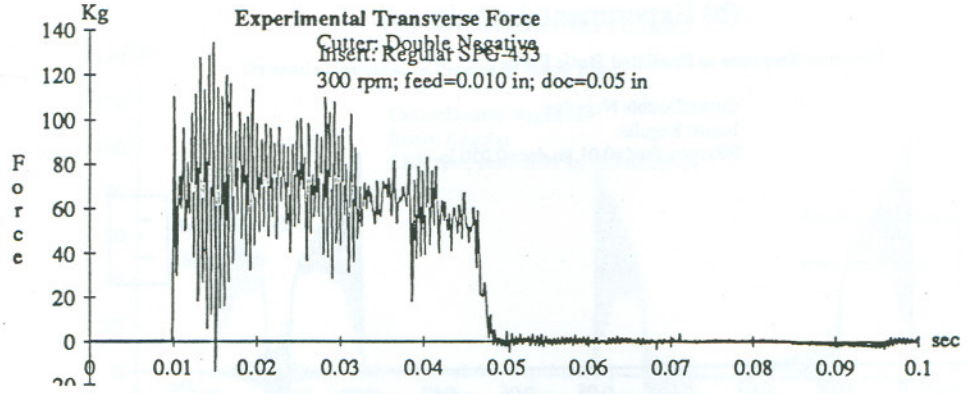

(b) Experimental results

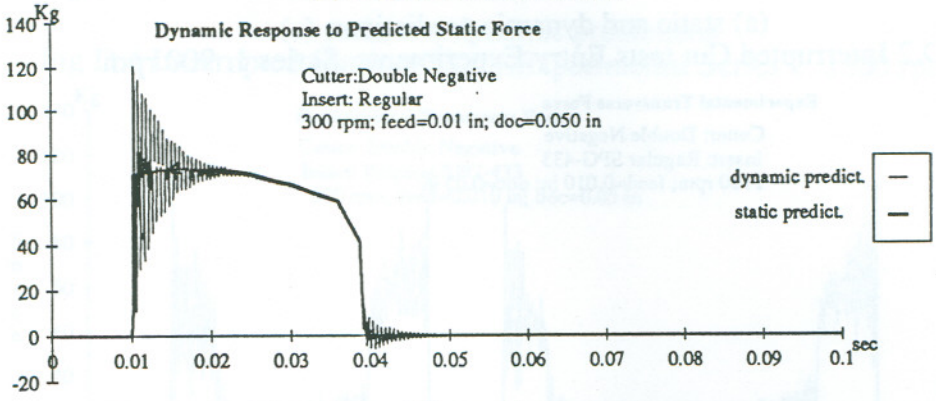

(a) static and dynamic predictions

Fig D.1 Interrupted Cut tests.Entry.Experiments. Series 1. 300 rpm

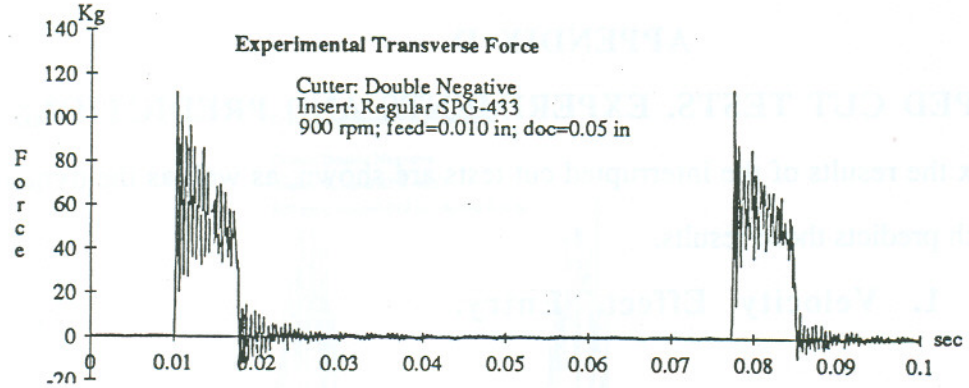

(b) Experimental results

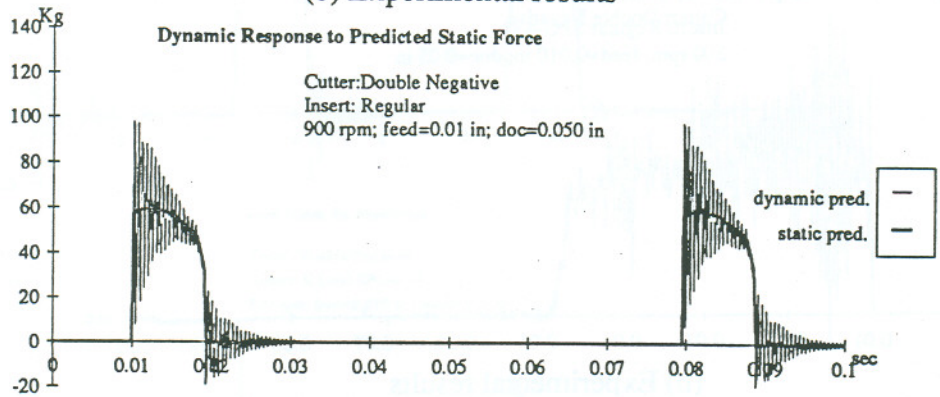

(a) static and dynamic predictions

Fig D.2 Interrupted Cut tests.Entry.Experiments. Series 1. 900 rpm

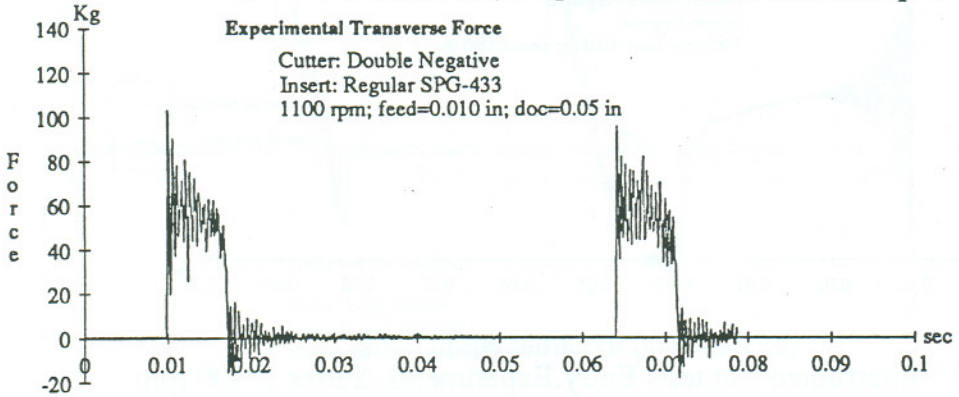

(b) Experimental results

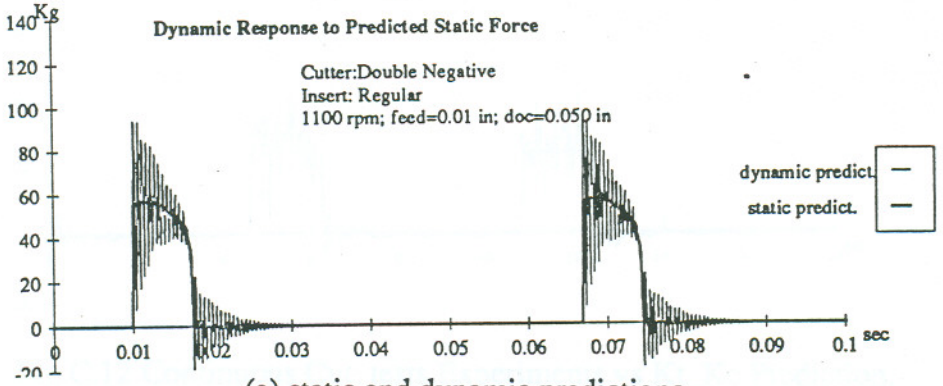

(a) static and dynamic predictions

Fig D.3 Interrupted Cut tests.Entry.Experiments. Series 1. 1100 rpm

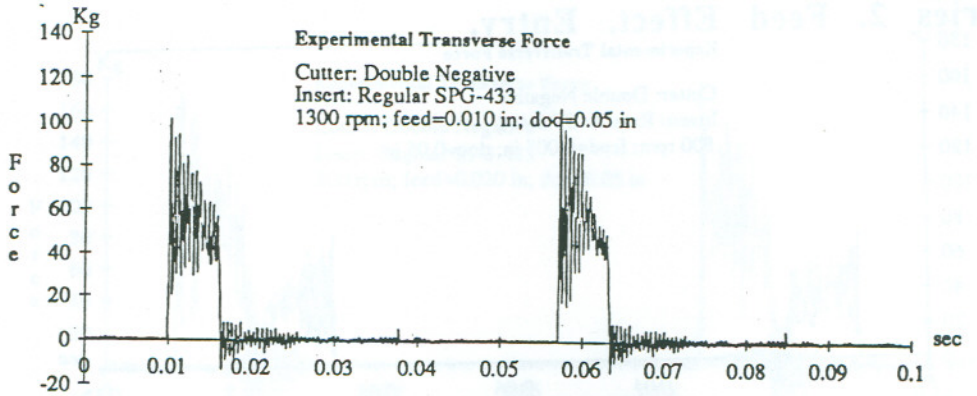

(b) Experimental results

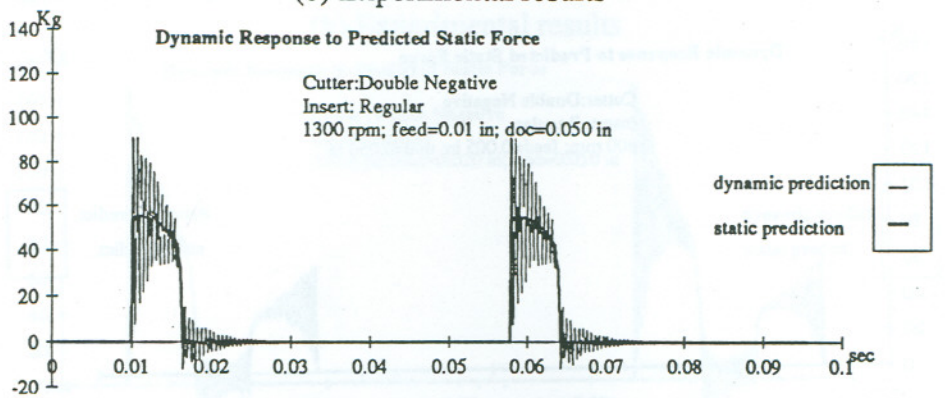

(a) static and dynamic predictions

Fig D.4 Interrupted Cut tests.Entry.Experiments. Series 1. 1300 rpm

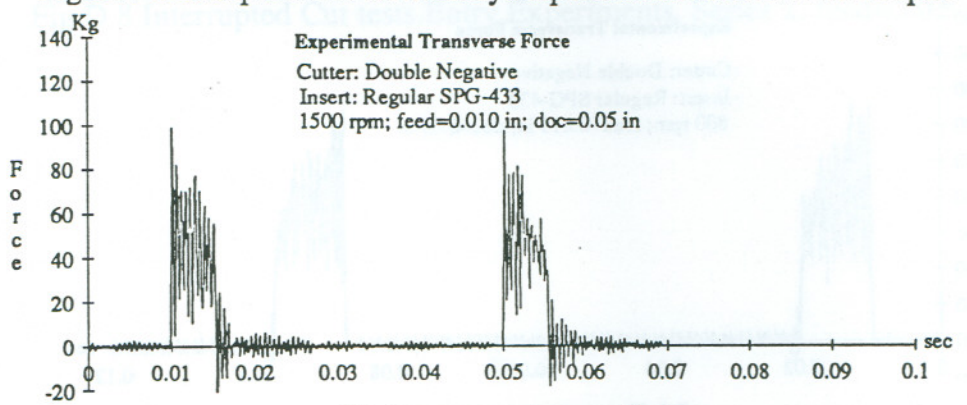

(b) Experimental results

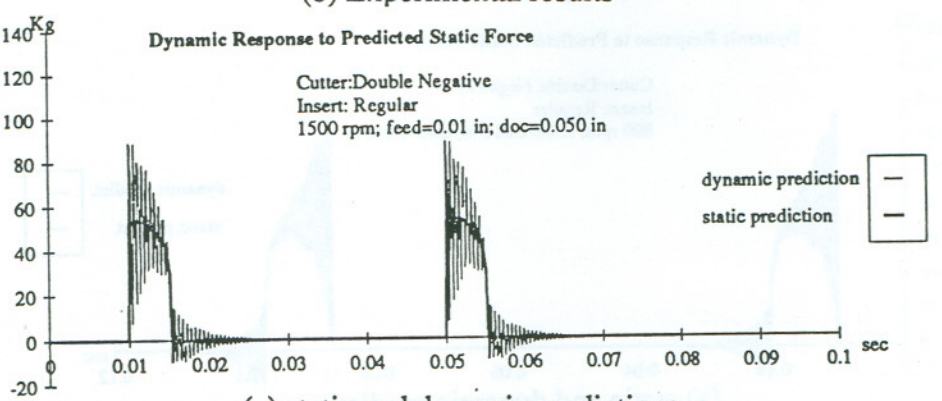

(a) static and dynamic predictions

Fig D.5 Interrupted Cut tests.Entry.Experiments. Series 1. 1500 rpm

D.2 Series 2. Feed Effect. Entry.

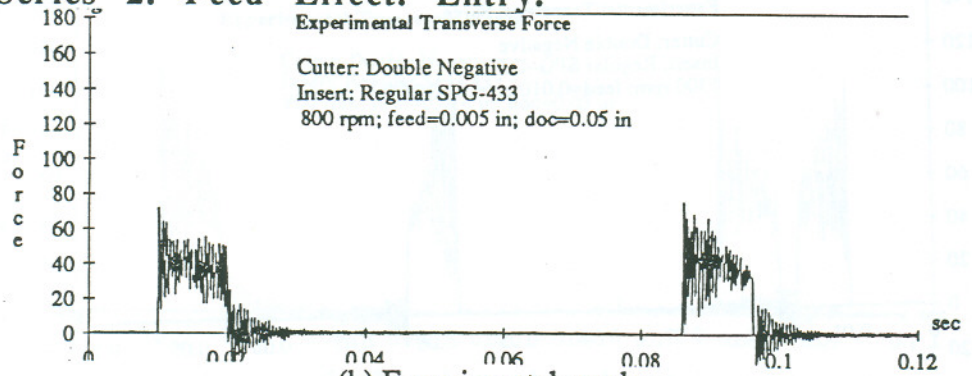

(b) Experimental results

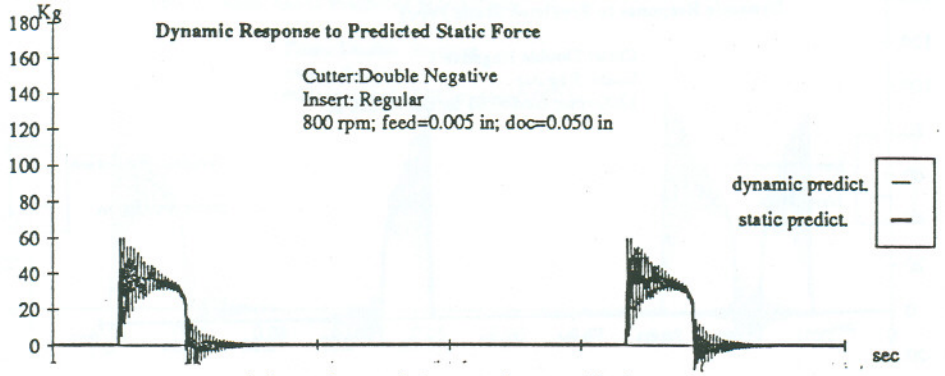

(a) static and dynamic predictions

Fig D.6 Interrupted Cut tests.Entry.Experiments. Series 2. feed=0.005 in

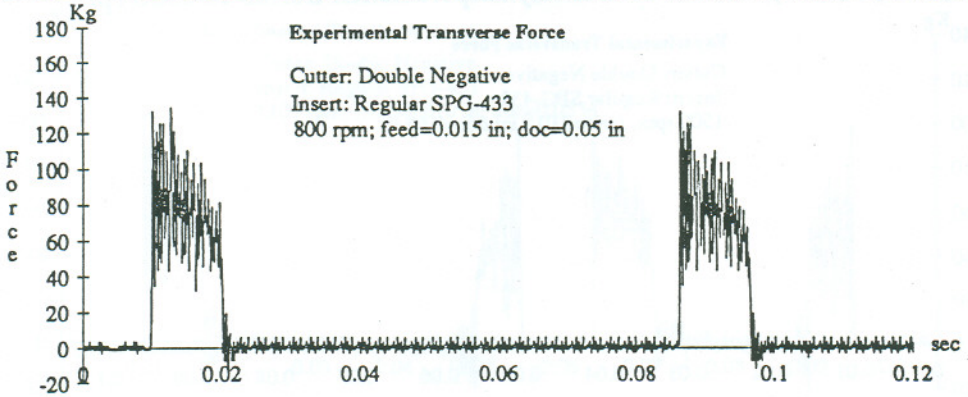

(b) Experimental results

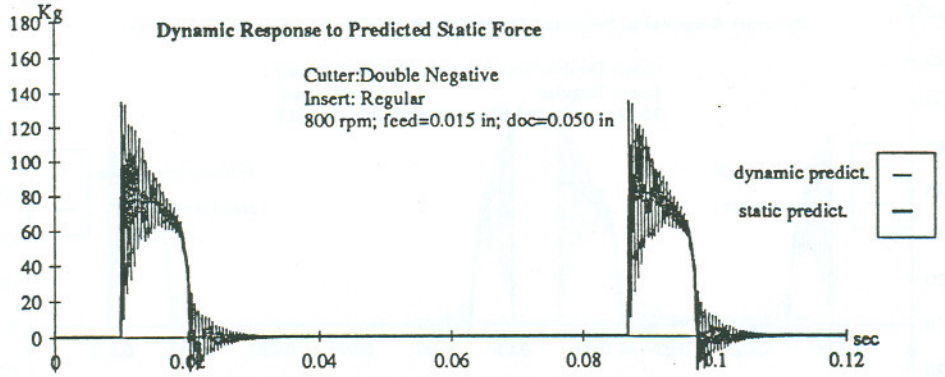

(a) static and dynamic predictions

Fig D.7 Interrupted Cut tests.Entry.Experiments. Series 2. feed=0.015 in

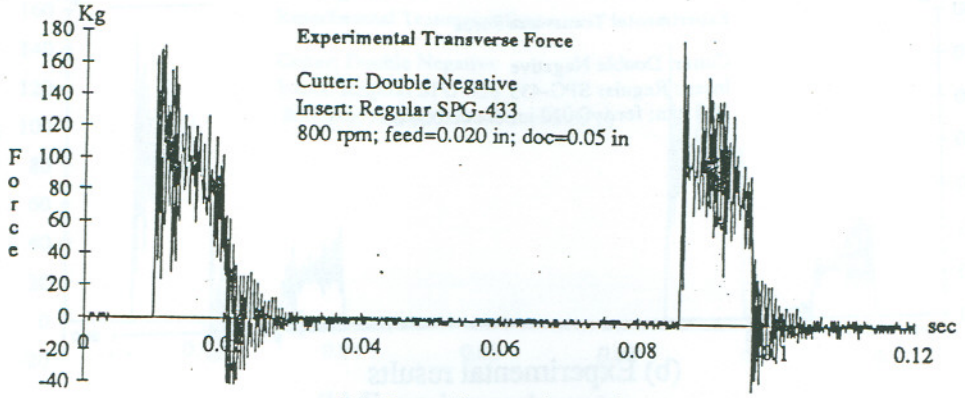

(b) Experimental results

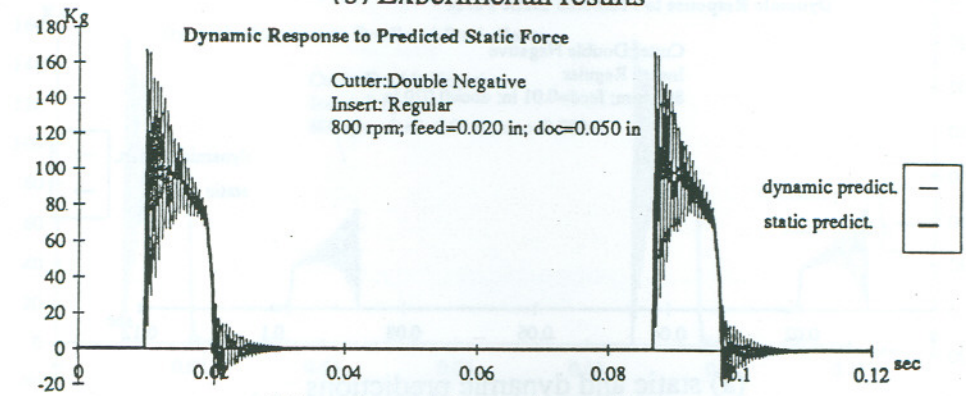

(a) static and dynamic predictions

Fig D.8 Interrupted Cut tests.Entry.Experiments. Series 2. feed=0.020 in

D.3 Series 3. Depth of Cut Effect. Entry.

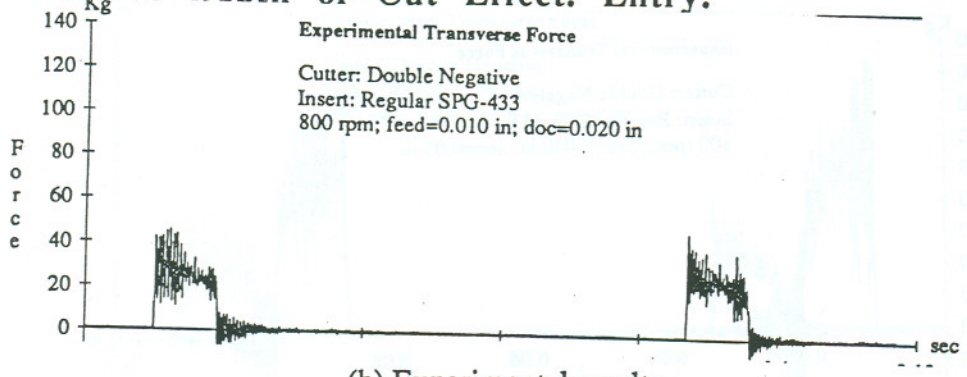

(b) Experimental results

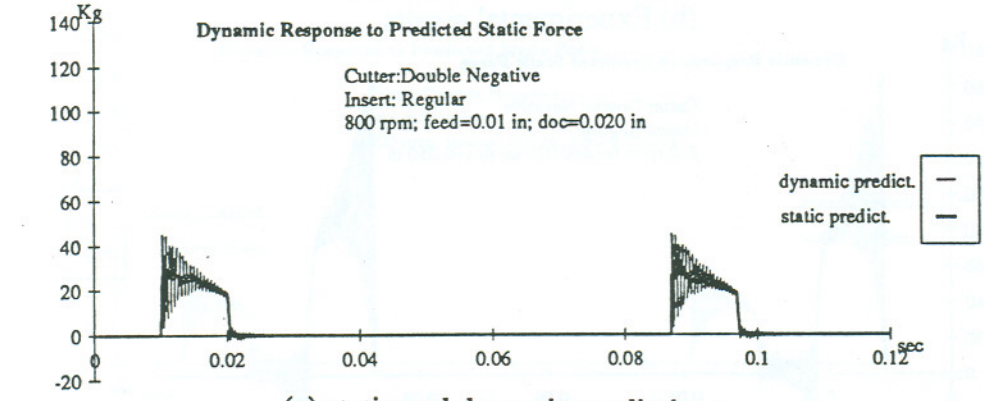

(a) static and dynamic predictions

Fig D.9 Interrupted Cut tests.Entry.Experiments. Series 3. doc=0.020 in

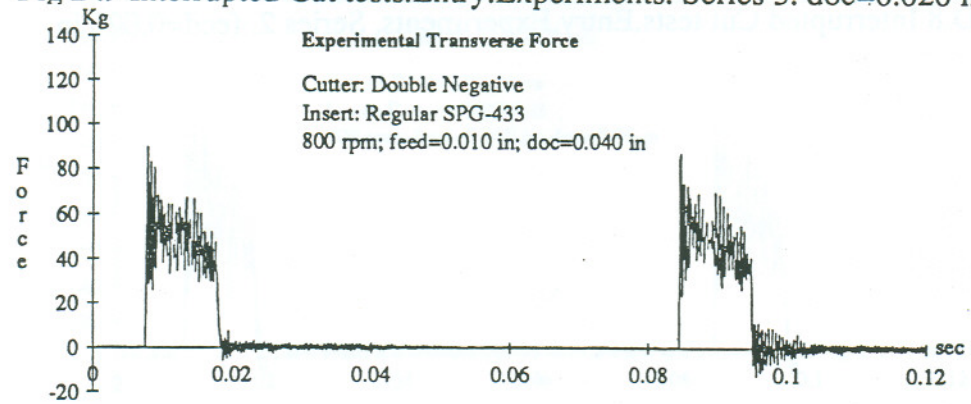

(b) Experimental results

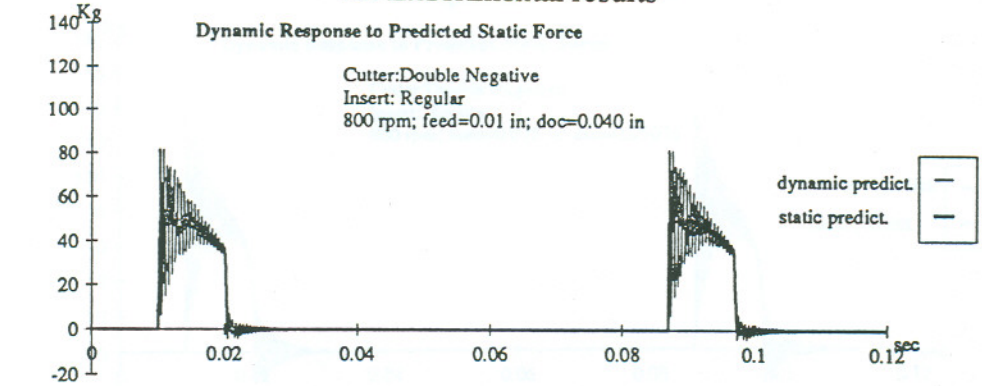

(a) static and dynamic predictions

Fig D.10 Interrupted Cut tests.Entry.Experiments. Series 3. doc=0.040 in

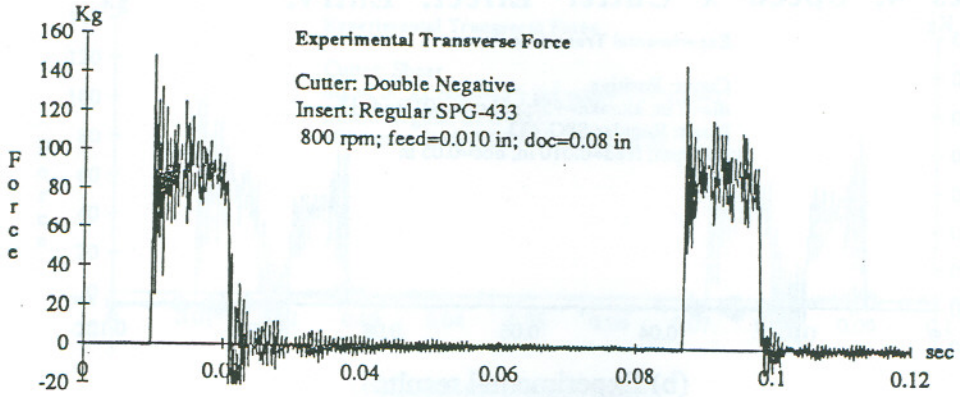

(b) Experimental results

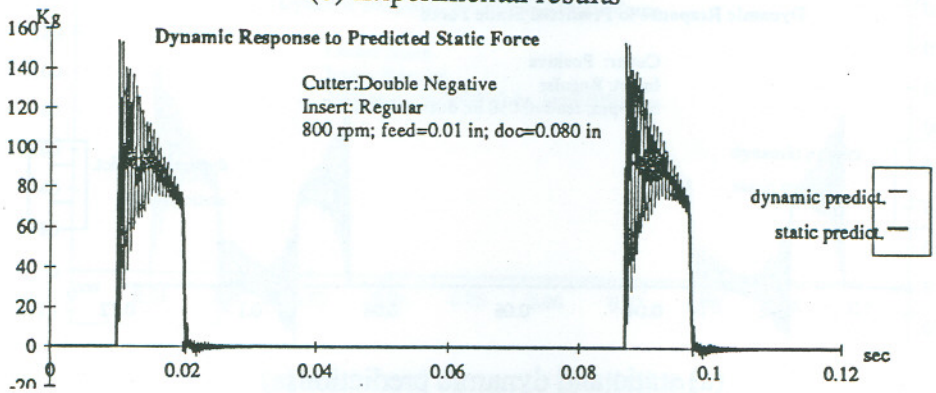

(a) static and dynamic predictions

Fig D.11 Interrupted Cut tests.Entry.Experiments. Series 3. doc=0.080 in

D.4 Series 4. Speed x Cutter Effect. Entry

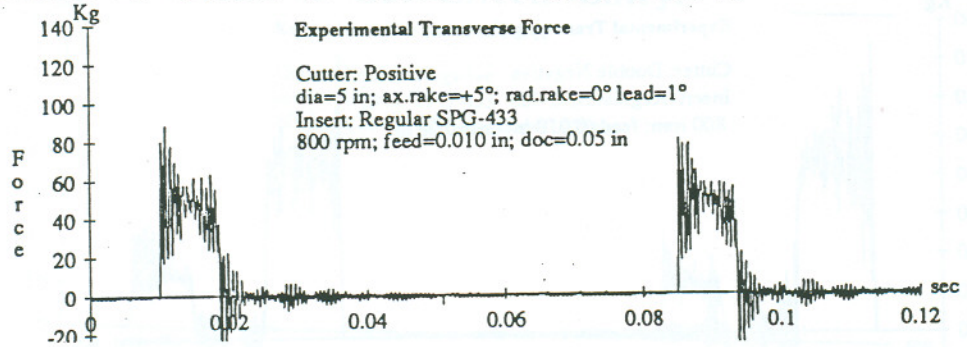

(b) Experimental results

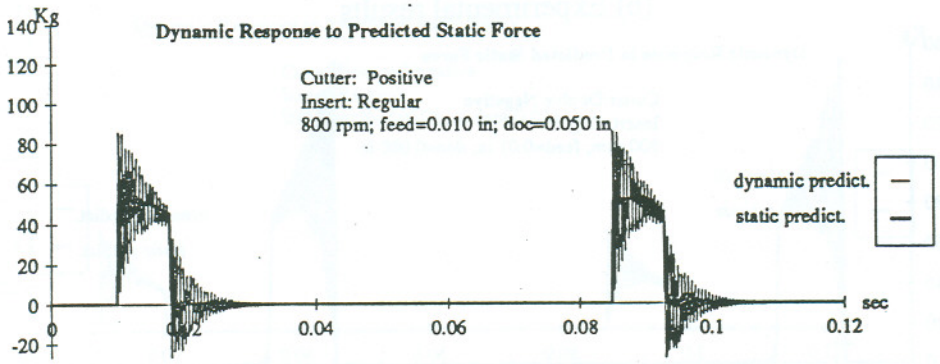

(a) static and dynamic predictions

Fig D.12 Interrupted Cut tests.Entry.Experiments. Series 4. Positive cutter, rpm=800

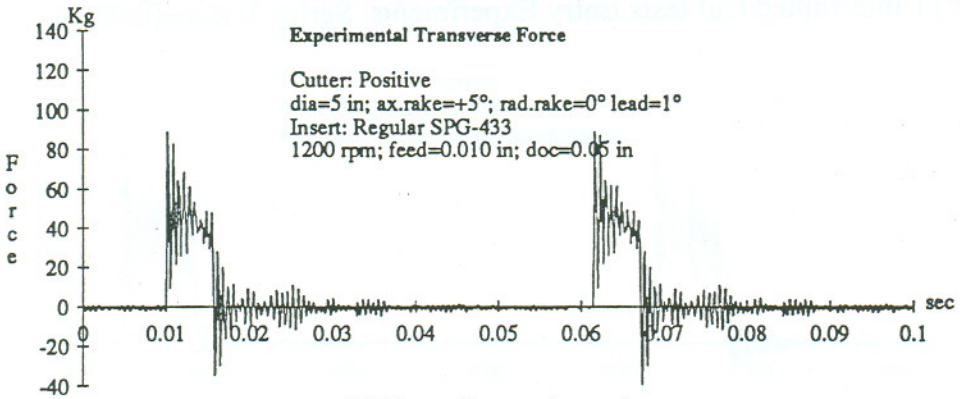

(b) Experimental results

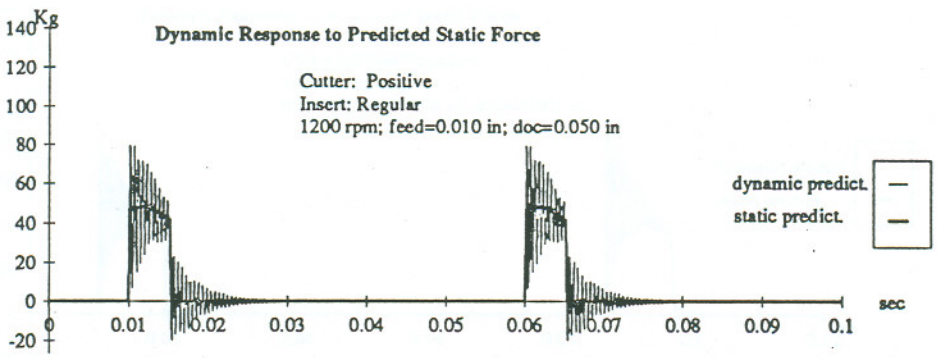

(a) static and dynamic predictions

Fig D.13 Interrupted Cut tests.Entry.Experiments. Series 4. Positive cutter, rpm=1200

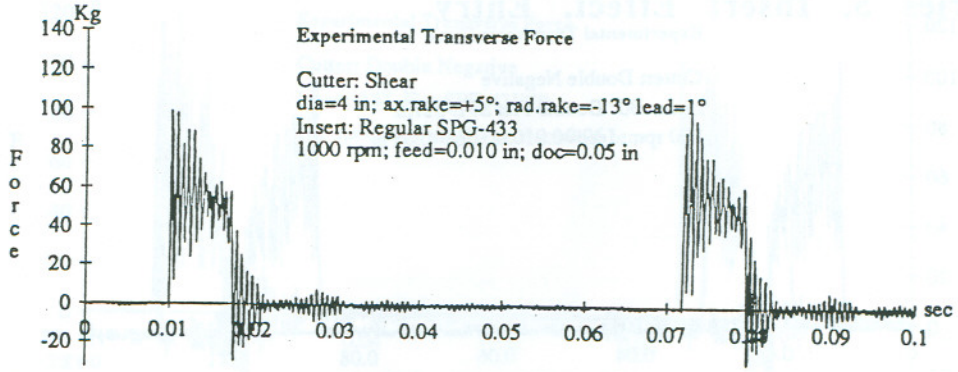

(b) Experimental results

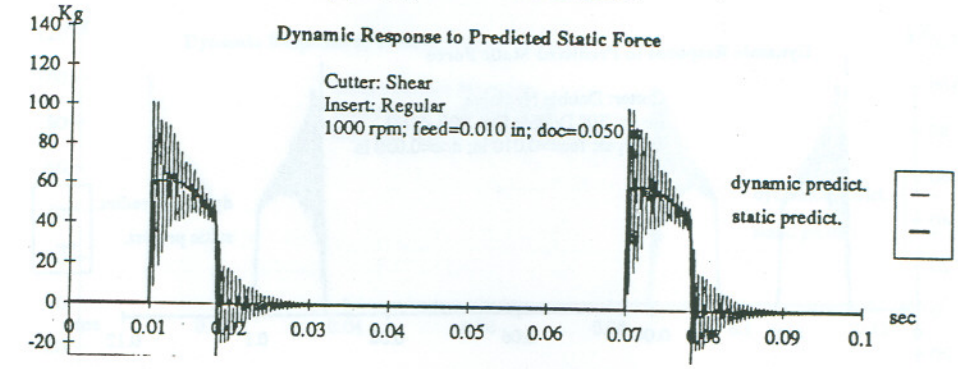

(a) static and dynamic predictions

Fig D.14 Interrupted Cut tests.Entry.Experiments. Series 4. Shear cutter, rpm=1000

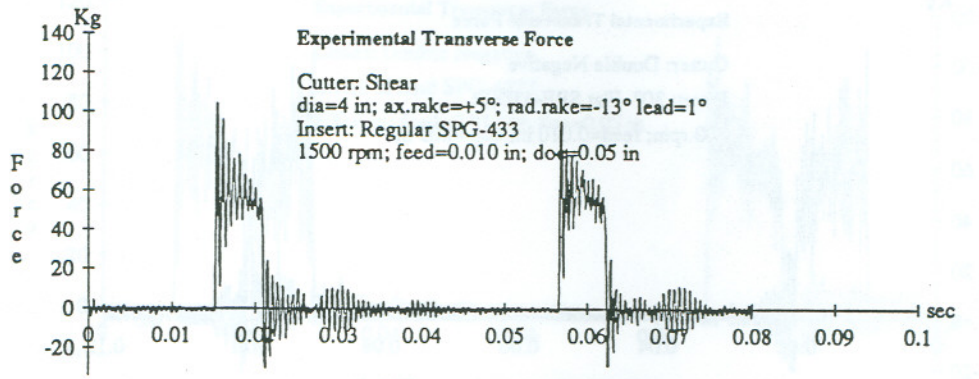

(b) Experimental results

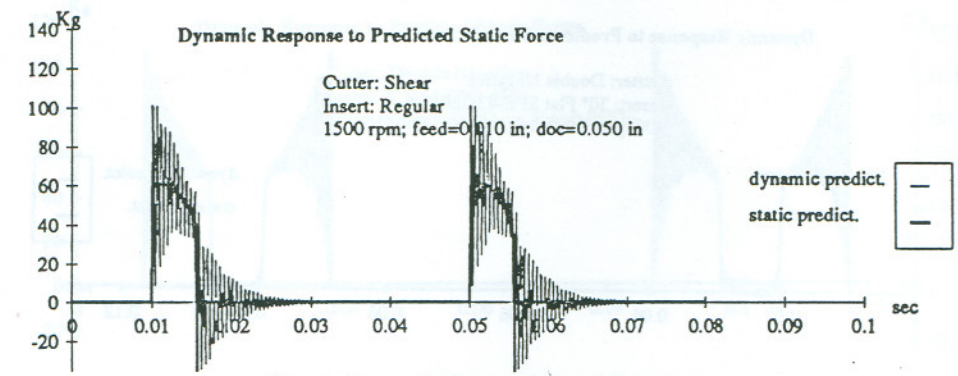

(a) static and dynamic predictions

Fig D.15 Interrupted Cut tests.Entry.Experiments. Series 4. Shear cutter, rpm=1500

D.5 Series 5. Insert Effect. Entry.

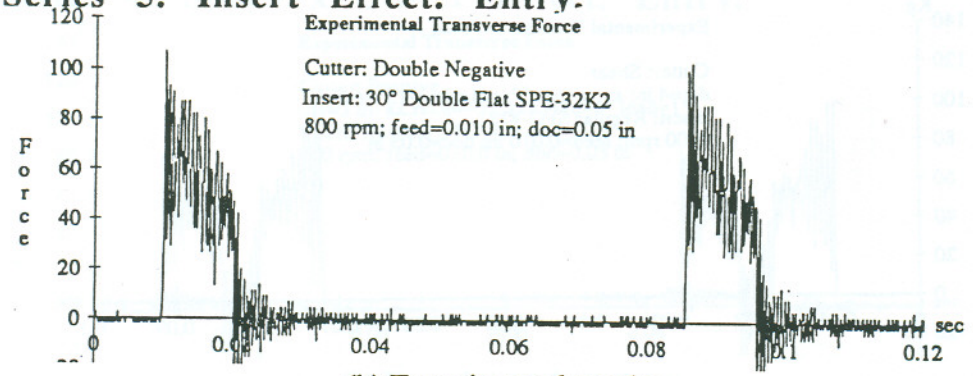

(b) Experimental results

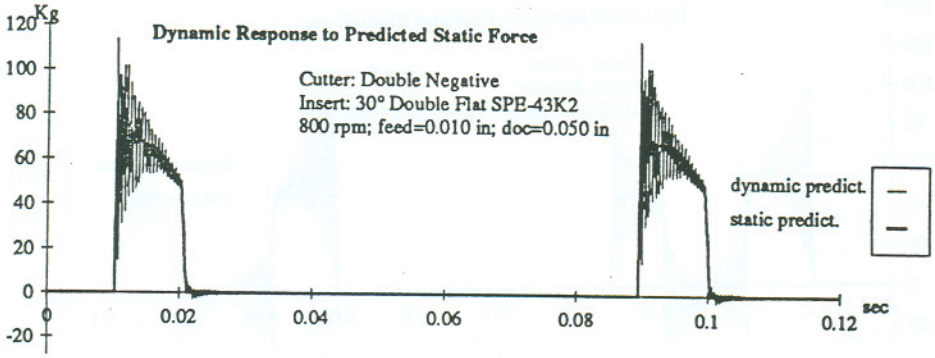

(a) static and dynamic predictions

Fig D.16 Interrupted Cut tests.Entry.Experiments. Series 5. Insert 30° Double Flatted.

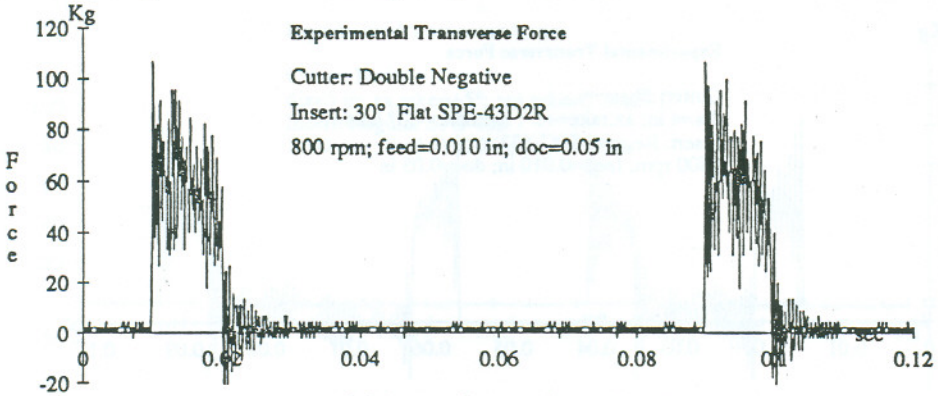

(b) Experimental results

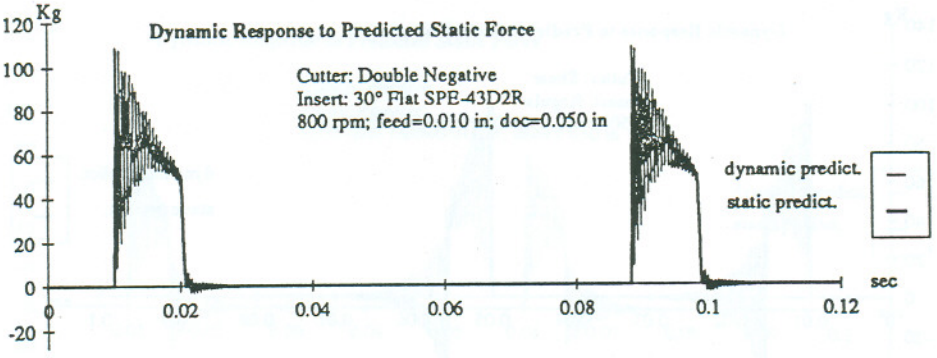

(a) static and dynamic predictions

Fig D.17 Interrupted Cut tests.Entry.Experiments. Series 5. Insert 30° Flatted.

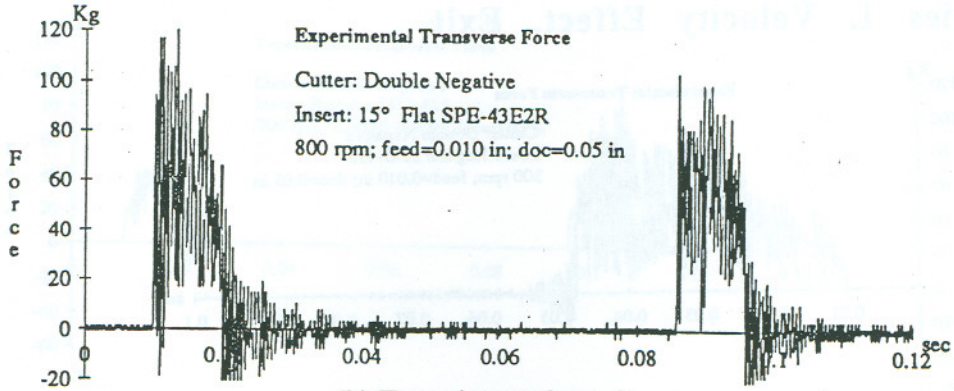

(b) Experimental results

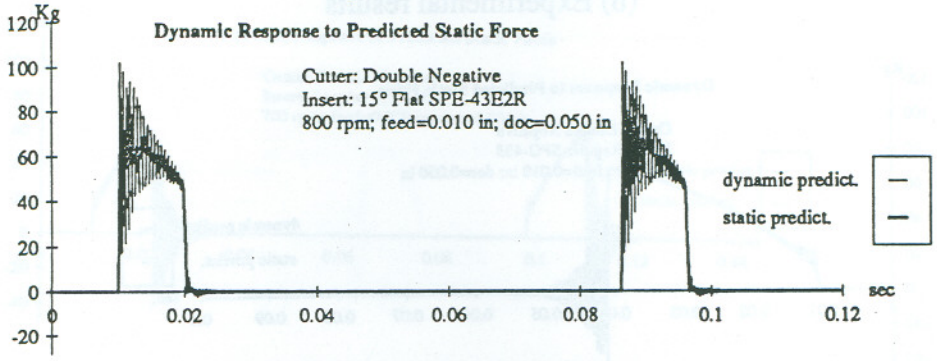

(a) static and dynamic predictions

Fig D.18 Interrupted Cut tests.Entry.Experiments. Series 5. Insert 15° Flatted.

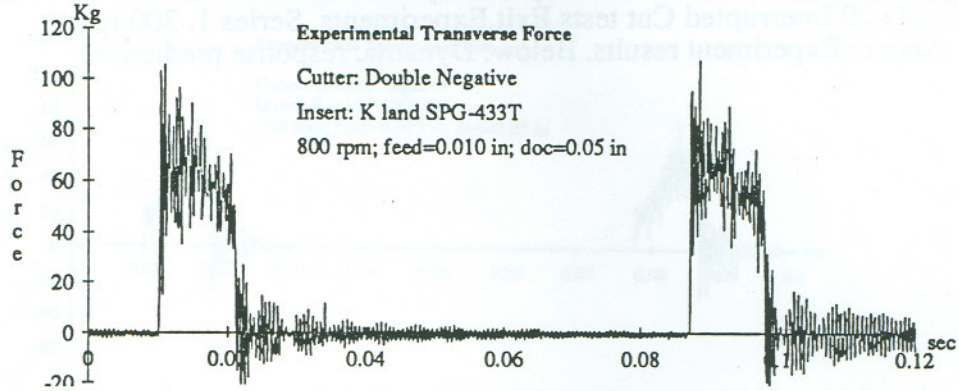

(b) Experimental results

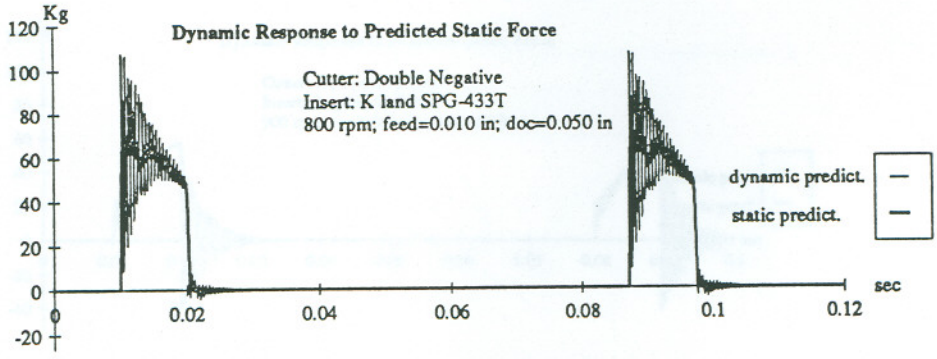

(a) static and dynamic predictions

Fig D.19 Interrupted Cut tests.Entry.Experiments. Series 5. Insert K land.

D.6 Series 1. Velocity Effect. Exit.

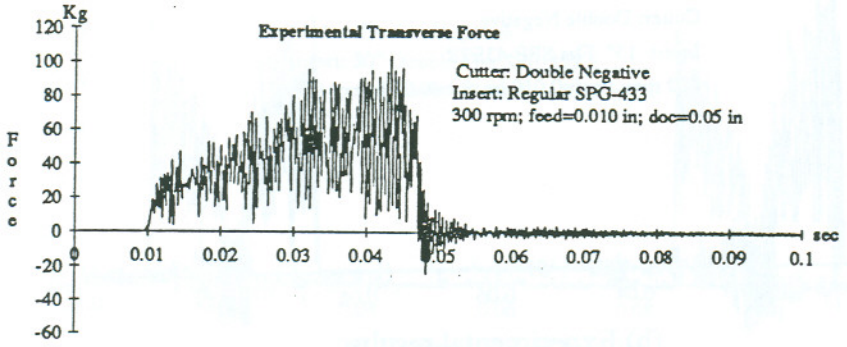

(b) Experimental results

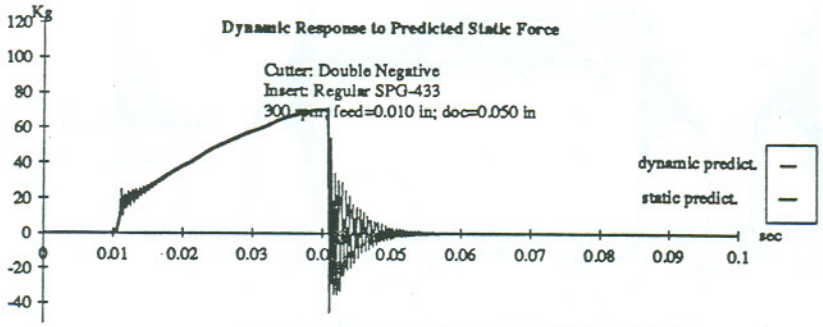

(a) static and dynamic predictions

Fig D.20 Interrupted Cut tests.Exit.Experiments. Series 1. 300 rpm
Above: Experiment results. Below: Dynamic response prediction.

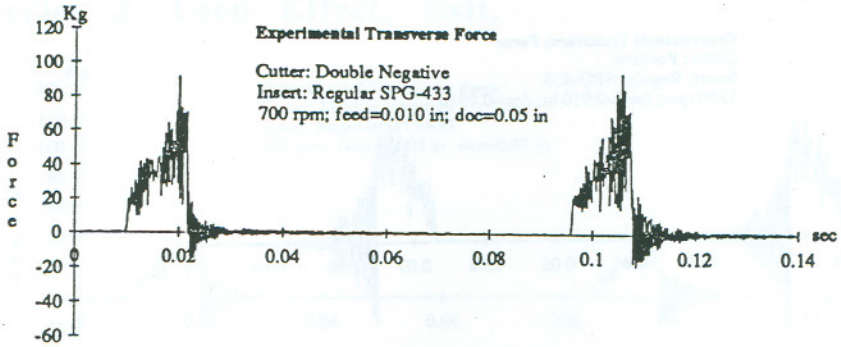

(b) Experimental results

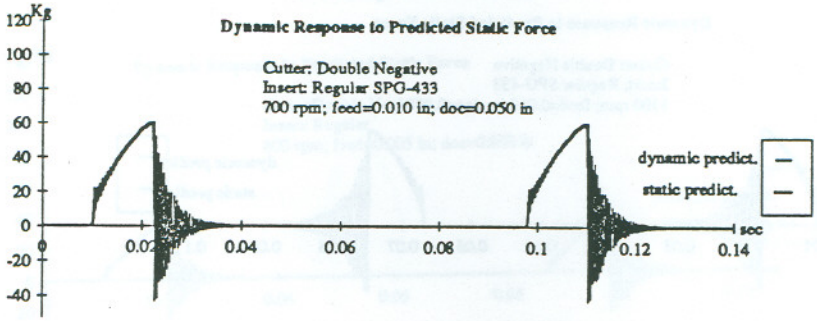

(a) static and dynamic predictions

Fig D.21 Interrupted Cut tests.Exit.Experiments. Series 1. 700 rpm

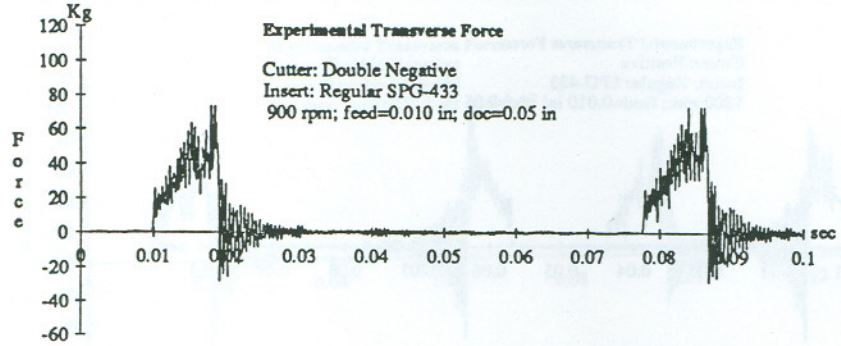

(b) Experimental results

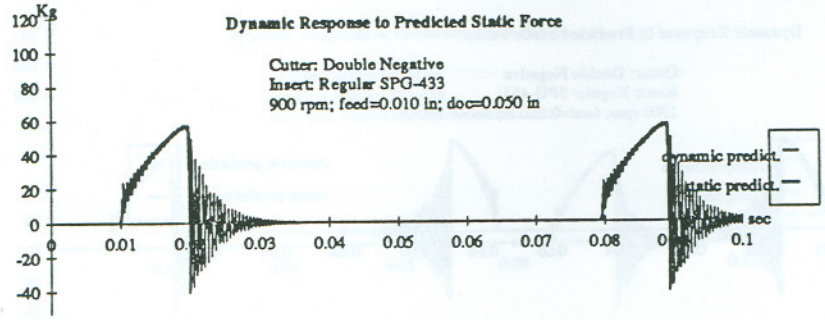

(a) static and dynamic predictions

Fig D.22 Interrupted Cut tests.Exit.Experiments. Series 1. 900 rpm

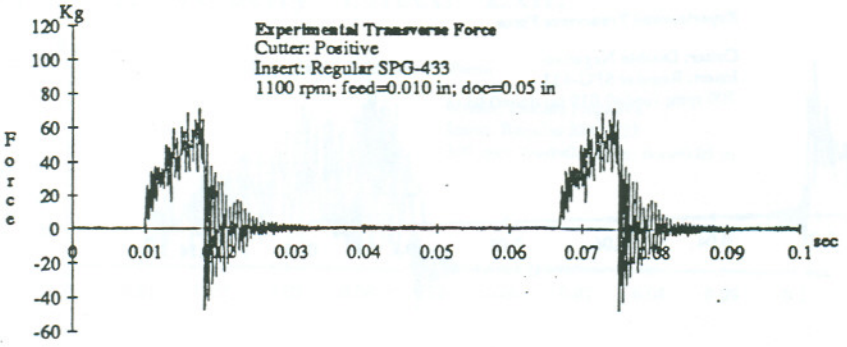

(b) Experimental results

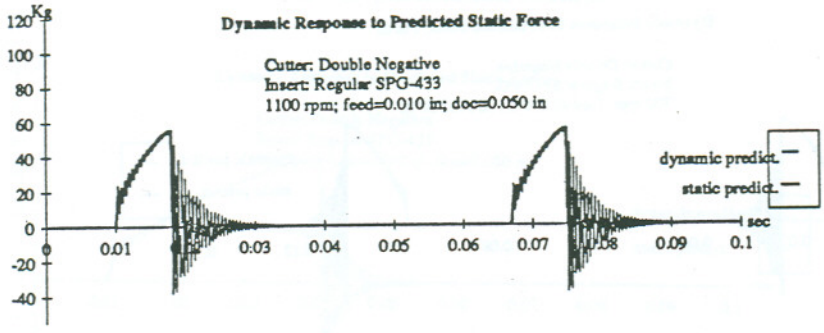

(a) static and dynamic predictions

Fig D.23 Interrupted Cut tests.Exit.Experiments. Series 1. 1100 rpm

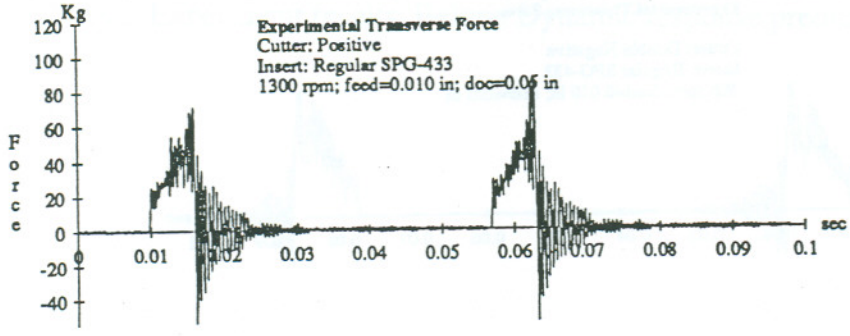

(b) Experimental results

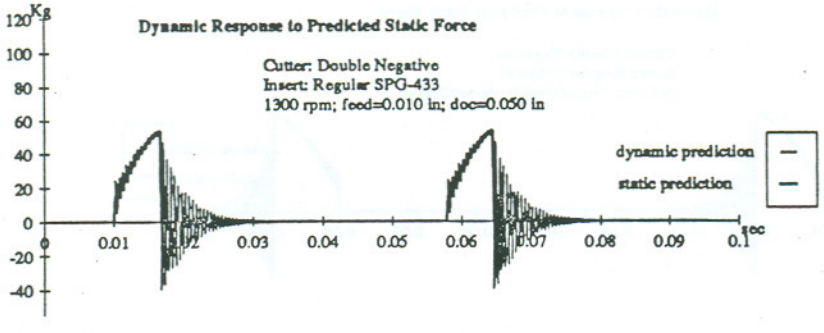

(a) static and dynamic predictions

Fig D.24 Interrupted Cut tests.Exit.Experiments. Series 1. 1300 rpm

D.7 Series 2. Feed Effect. Exit.

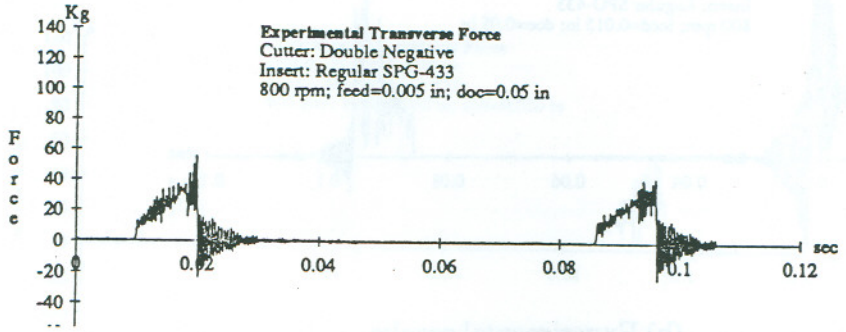

(b) Experimental results

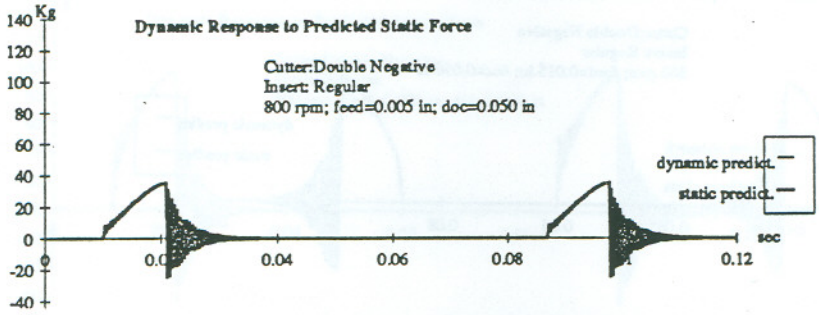

(a) static and dynamic predictions

Fig D.25 Interrupted Cut tests.Exit.Experiments. Series 2. feed=0.005in

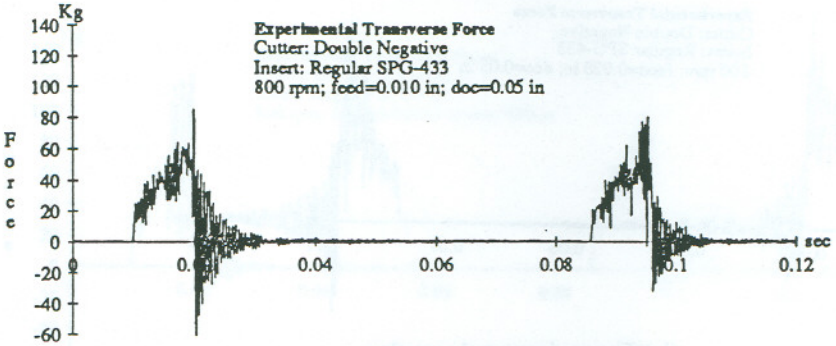

(b) Experimental results

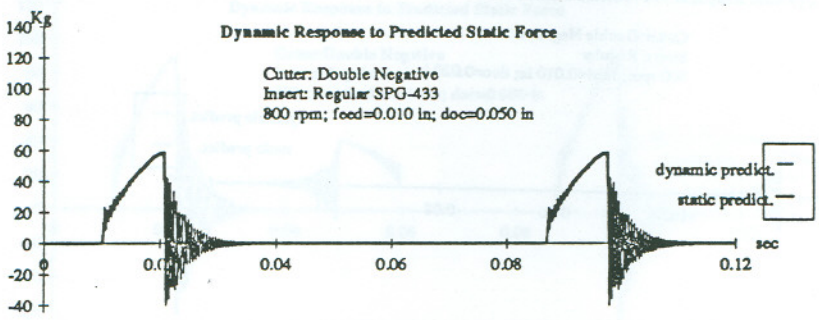

(a) static and dynamic predictions

Fig D.26 Interrupted Cut tests.Exit.Experiments. Series 2. feed=0.010 in

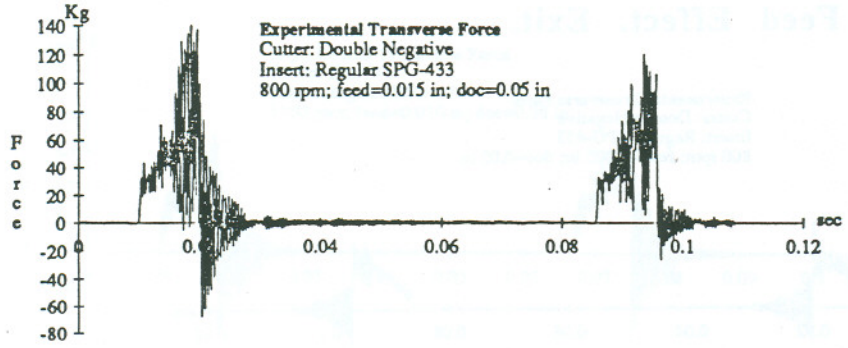

(b) Experimental results

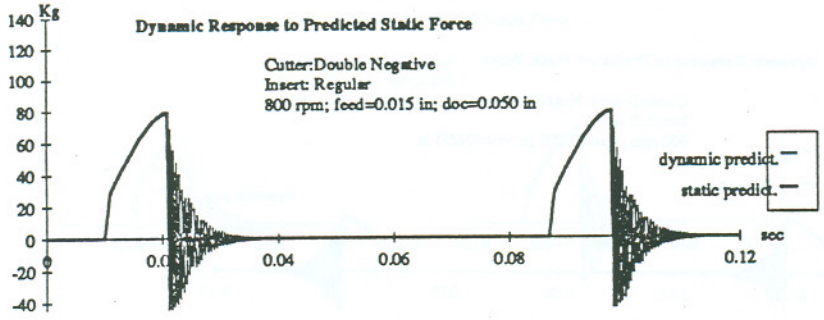

(a) static and dynamic predictions

Fig D.27 Interrupted Cut tests.Exit.Experiments. Series 1.feed=0.015in

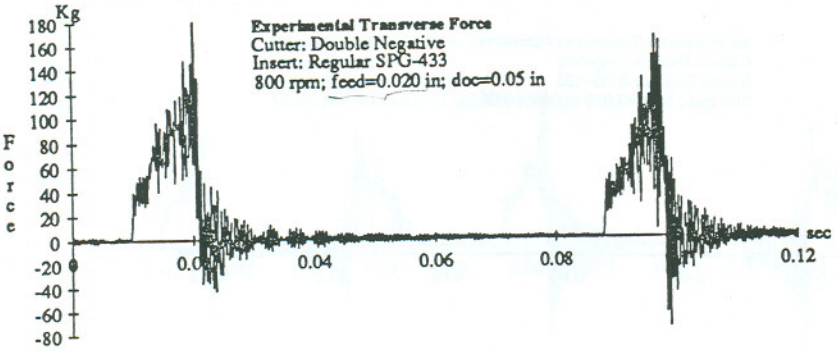

(b) Experimental results

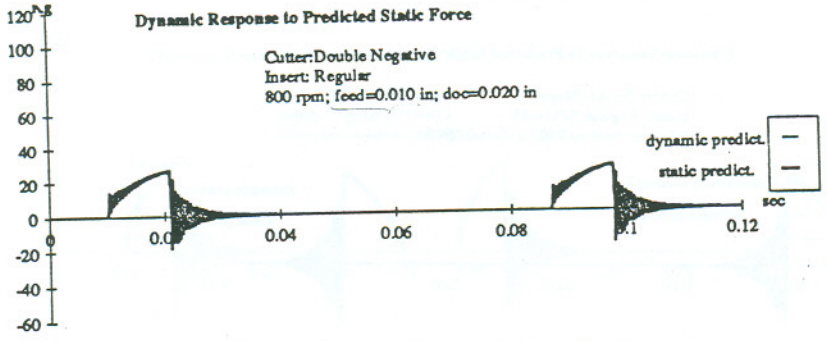

(a) static and dynamic predictions

Fig D.28 Interrupted Cut tests.Exit.Experiments. Series 2.feed=0.020 in

D.8 Series 3. Depth of Cut Effect. Exit.

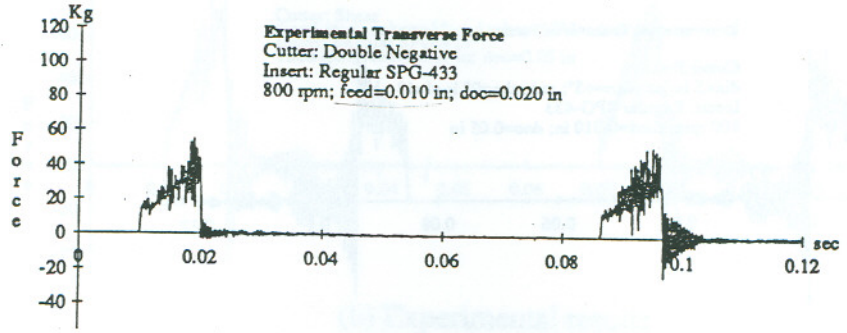

(b) Experimental results

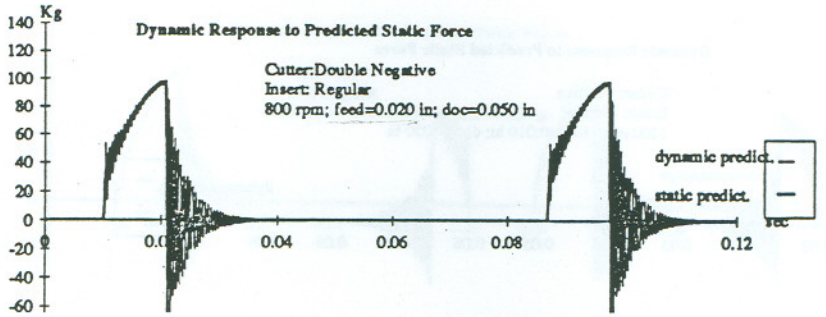

(a) static and dynamic predictions

Fig D.29 Interrupted Cut tests.Exit.Experiments. Series 3. doc=0.020 in

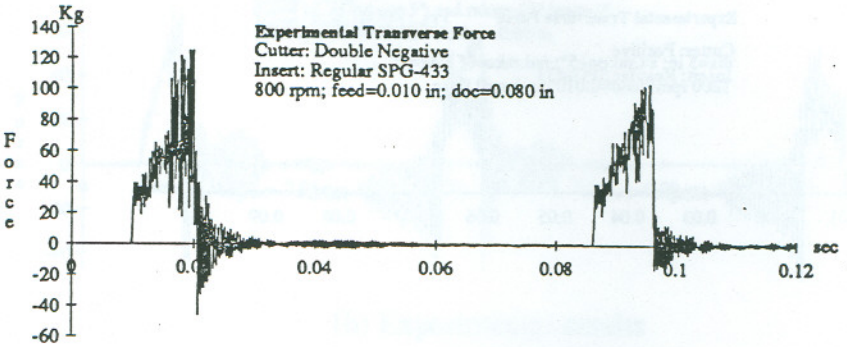

(b) Experimental results

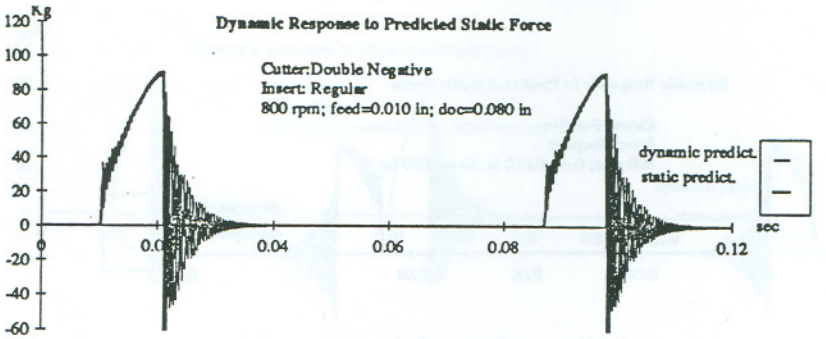

(a) static and dynamic predictions

Fig D.30 Interrupted Cut tests.Exit.Experiments. Series 3.doc=0.080 in

D.9 Series 4. Speed x Cutter Effect. Exit.

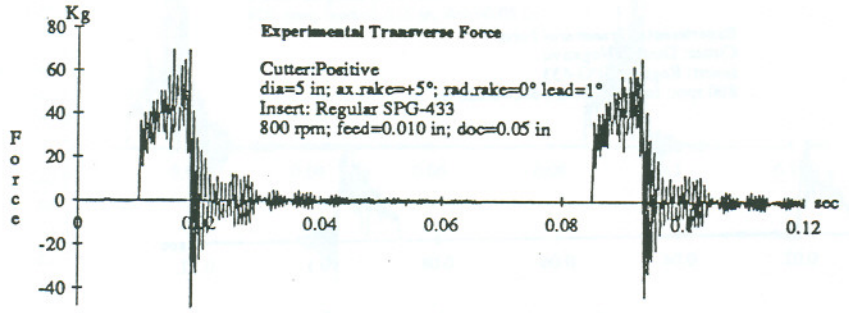

(b) Experimental results

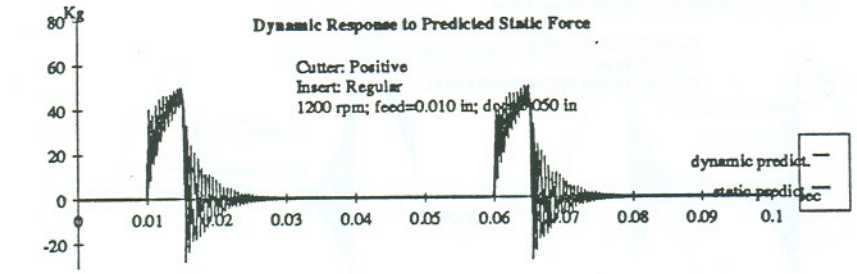

(a) static and dynamic predictions

Fig D.31 Interrupted Cut tests.Exit.Experiments. Series 4. Positive cutter, rpm=800

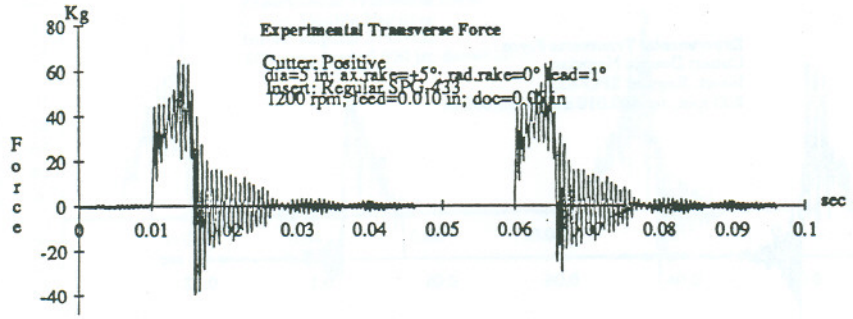

(b) Experimental results

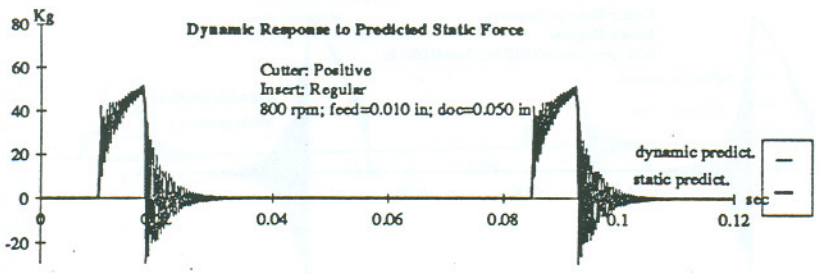

(a) static and dynamic predictions

Fig D.32 Interrupted Cut tests.Exit.Experiments. Series 4. Positive cutter, rpm=1200

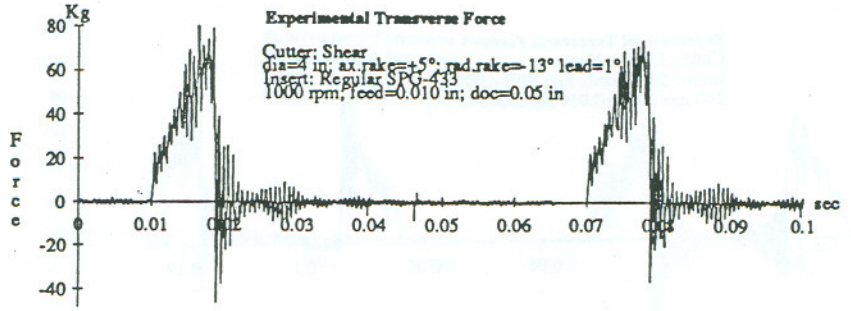

(b) Experimental results

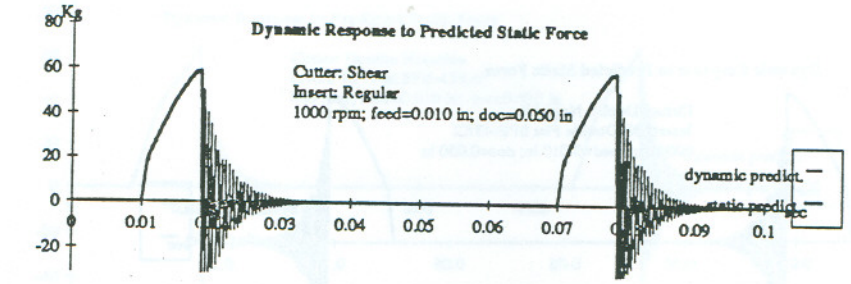

(a) static and dynamic predictions

Fig D.33 Interrupted Cut tests.Exit.Experiments. Series 4. Shear cutter, rpm=1000

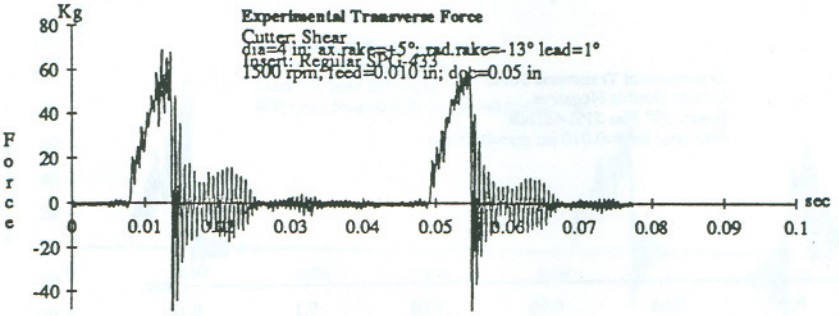

(b) Experimental results

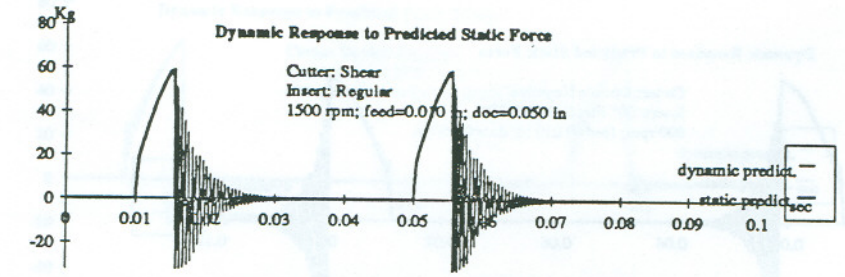

(a) static and dynamic predictions

Fig D.34 Interrupted Cut tests.Exit.Experiments. Series 4. Shear cutter, rpm=1500

D.10 Series 5. Insert Effect. Exit.

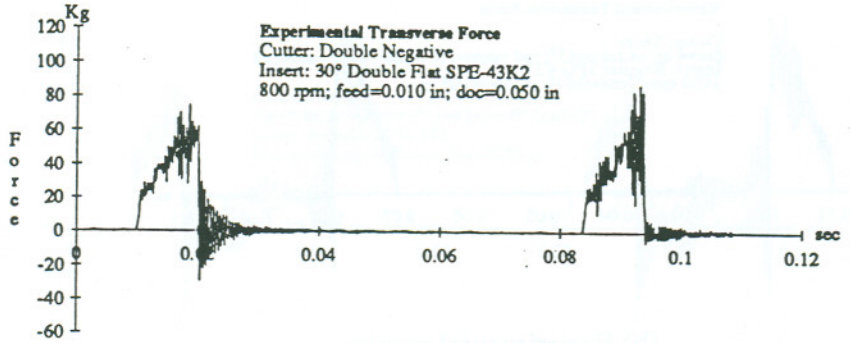

(b) Experimental results

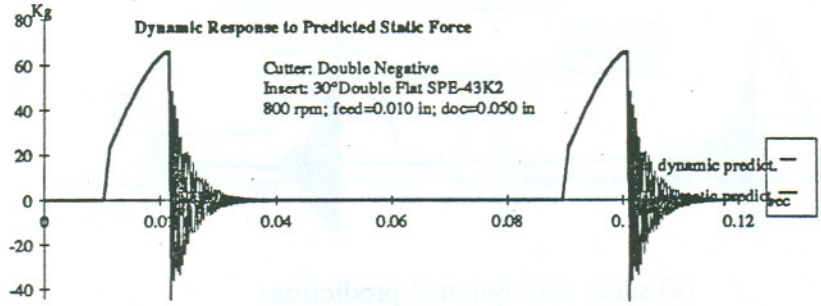

(a) static and dynamic predictions

Fig D.35 Interrupted Cut tests.Exit.Experiments. Series 5. Insert 30° Double Flatted.

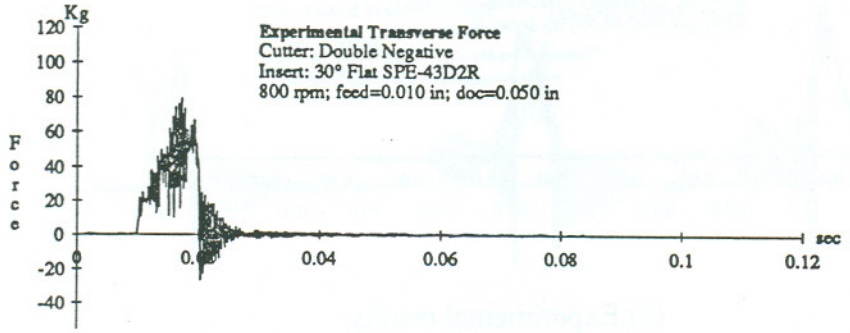

(b) Experimental results

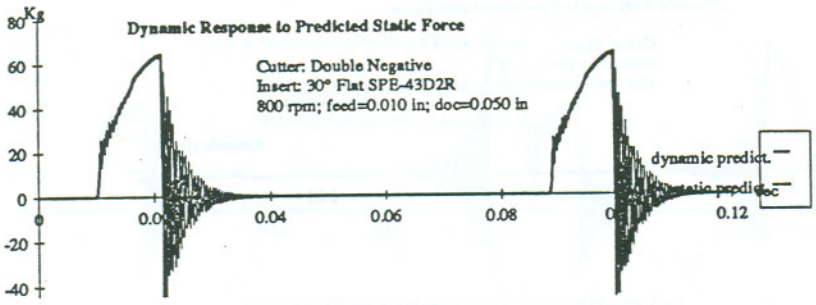

(a) static and dynamic predictions

Fig D.36 Interrupted Cut tests.Exit.Experiments. Series 5. Insert 30° Flatted.

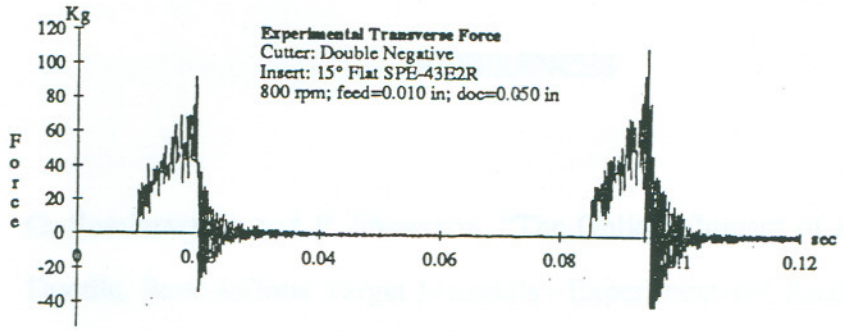

(b) Experimental results

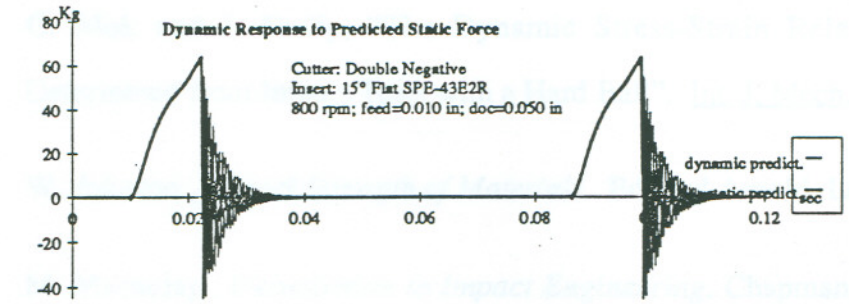

(a) static and dynamic predictions

Fig D.37 Interrupted Cut tests.Exit.Experiments. Series 5. Insert 15° Flatted.

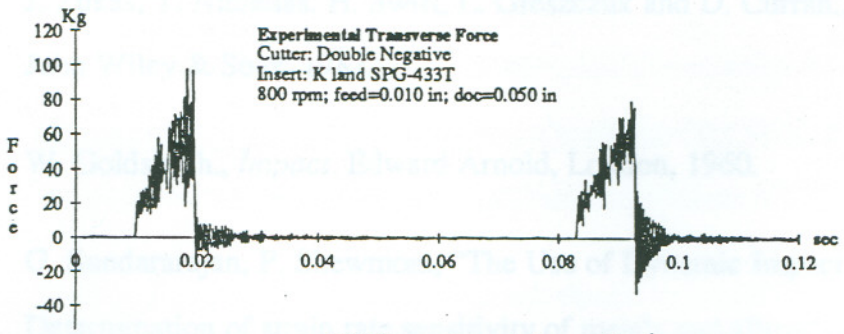

(b) Experimental results

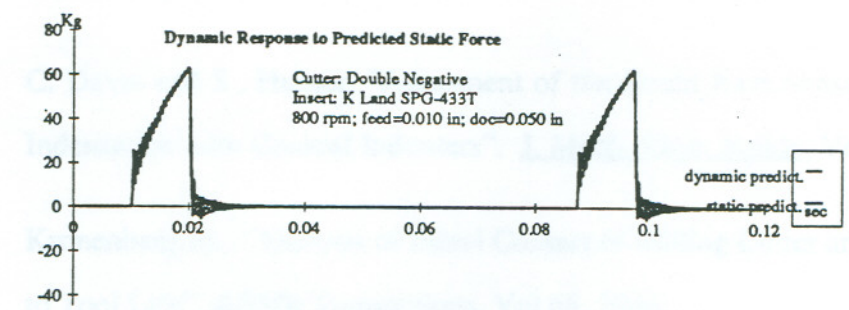

(a) static and dynamic predictions

Fig D.38 Interrupted Cut tests.Exit.Experiments. Series 5. Insert K land.

REFERENCES

[1] G. Sundararajan and P. Shewmon, "The Oblique Impact of a Hard Ball Against Ductile, Semi-infinite Target Materials - Experiment and Analysis". Int J. Impact Engng. Vol 6, No 1, 1987.

[2] C. Mok and J. Duffy, "The Dynamic Stress-Strain Relation of Metals as Determined from Impact Tests with a Hard Ball". Int. J. Mech. Sci. Vol. 7, 1965.

[3] W. Johnson., *Impact Strength of Materials*. Edward Arnold, London, 1972.

[4] M. Macaulay., *Introduction to Impact Engineering*. Chapman and Hall, London, 1987.

[5] J. Zukas, T. Nicholas. H. Swift, L. Greszczuk and D. Curran., *Impact Dynamics*. John Wiley & Sons. 1982.

[6] W. Goldsimth., *Impact*. Edward Arnold, London, 1960.

[7] G. Sundararajan, P. Shewmon., "The Use of Dynamic Impact Experiments in the Determination of strain rate sensitivity of metals and alloys". Acta Metallica. Vol 31, no101, 1983.

[8] C. Davis and S., Hunter, "Assesment of the Strain Rate Sensitivity of Metals by Indentation with Conical Indenters". J. Mech. Phys. Solids, Vol 8, 1960.

[9] Kronenberg M., "Analysis of Initial Contact of Milling Cutter and Work in Relation to Tool Life". ASME Transactions. Vol 68, 1946.

[10] Lehtihet E., Kane G., "Computer Aided Modelling of Tool/Work Contact in Interrupted Cutting". Integrated and Intelligent Manufacturing. Winter Annual Meeting of A.S.M.E. 1986. pp 309-320.

[11] T. Asai, S. Nakatani, A. Hara, Sumitomo Electric Industries, LTD. "Study of the Early Fracture of Carbide Tools". Annals of C.I.R.P, Vol 29, n 1, 1980.

[12] A. Pekelharing., TH Delft, Netherlands. "The Exit Failure in Interrupted Cutting". Annals of C.I.R.P. Vol 27, n1, 1978.

[13] A. Pekelharing., "Cutting Tool Damage in Interrupted Cutting".Wear, 62 (1980) 37-48

[14] P. Wallen, S Jacobson, S Hogmark. "Intermittent Metal Cutting at Small Cutting Depths". Int. J. Machine Tools and Manufacture. Vol 28; No 4; 1988 pp 515-528

[15] J. Ley., "Edge Preparation Relating to Physical Characteristics of Tool and Work Material". Intl. Conf. on Productivity Improvement through New Tools and Applications. IIT Research Institute. Chicago Illinois.1979.

[16] T. Loladze., "Nature of Brittle Failure of Cutting Tool". Annals of C.I.R.P, Vol 24, 1975.

[17] T. Shibasaka, H. Hasimoto, K. Ueda, Kanazawa University, K. Iwata, "Analysis of Brittle Failure of Cutting Tools Based on Fracture Mechanics". Annals of C.I.R.P, Vol 32, no1, 1983.

[18] S. Lo Casto, G. Passannanti. "On the Influence of the Radius between Face and Flank on the Tool Life of Sintered Carbides". Annals of C.I.R.P, Vol 34, no1, 1985.

[19] G. Galante, V. Grasso, V. Ruisi., "Tool Failure in Sequential Cutting of two Different Materials". Annals of C.I.R.P, Vol 34, no1, 1985.

[20] A. Ghani and G. Barrow., "Tool Failure at Exit During Interrupted Cutting". Annals of C.I.R.P Vol 34, no1, 1985.

[21] C. Youngdahl., "The Interaction Between Pulse Shape and Strain Hardening in Dynamic Plastic Response". Int J. of Impact Engng. Vol 7, no 1, 1988.

[22] G.M. Zhang, S., Yerramareddy, S. Lee and S.C. Lu. "Simulation of Intermitent Turning Process. Control Issues in Manufacturing Processes". Winter Anual Meeting of the ASME. San Francisco, California. Dec 10-15, 1989. DSC-Vol 18, pp1-9.

[23] Miyazawa S., Usui Y., "Measurement of Transient Cutting Force by means of Fourier Analyser". Precision Engineering . April 1985, Vol 7, No 2. pp 99-104.

[24] Van Brussel., "Comparative Assessment of Harmonic, Random, Swept Sine and Shock Excitation methods for the Identification of Machine Tool Structures with rotary Spindles". Annals of C.I.R.P Vol24/1/1975. pp 291-295.

[25] Jenkins G., Watts D., *Spectral Analysis and its Applications*. Holden-Day Inc. 1968.

[26] Ewins D., Modal Testing: *Theory and Practice*. Research Studies Press. 1984.

[27] Lee S., Kapoor S., DeVor R., "An Integrated Machinning Process Design Simulator for the Optimal Design of Face Milling Systems". Trans A.S.M.E. Journal of Engineering for Industry, Vol 107, No. 4, Nov 1985.

[28] Endres, W. J., "A Dynamic Model of the Cutting Force System in the Turning Process," M.S. Thesis, University of Illinois at Urbana - Champaign, 1990.

[29] Endres, W. J., J.W. Sutherland, and R.E. DeVor, "Quality Design Using a Computer-Based Dynamic Force Model for the Turning Process," Proc., of the ASME Symposium on Sensors and Controls for Manufacturing, (to be published).

[30] Fu, H. J., R. E. DeVor, and S. G. Kapoor, "A Mechanistic Model for the Prediction of the Force System in Face Milling Operations", Jour. of Eng. for Industry, Trans. ASME, Vol.106, No 1, 1984, pp.81-88.

[31] Merchant, M. E., "Basic Mechanics of the Metal-Cutting Process," Journal of Applied Mechanics, Sept. 1944, pp. A-168 to A-175.

[32] Subramani, G., S. G. Kapoor, R.E. DeVor, and R. Hayashida, "An Enhanced Model for Simulation of Face Milling Operations," Proc., 2nd Int. Conf on Computer -Aided Production Engr., 1987, pp.171-178.

[33] Radulescu.R. "Dynamic Modelling of Machining Processes using a Finit Element approach," M.S. Thesis, University of Illinois at Urbana - Champaign, 1991.

[34] H. Negishi, K. Aoki Mitsubishi Metal Co. and T. Sata University of Tokio. "Study on Tool Failure of Carbide Tools in Interrupted Turning". Annals of C.I.R.P, Vol 29, n 1, 1980.

[35] D. Bizeul, F. Le Maitre. E.N.S.M. Nantes, France. "Entrance Angle in Milling and Dynamic Stress Waves Propagation in the Tool". Annals of C.I.R.P, Vol 27, 1978.

[36] P. Black., *Theory of Metal Cutting*. McGraw-Hill, 1961.

[37] S. Ramalingam., "Plastic Deformation In Metal Cutting". PhD Thesis. University of Illinois at Urbana-Champaign, 1967.

[38] DeVries W., Evans M., "Computer Graphics Simulation of Metal Cutting". Annals of C.I.R.P. Vol.33/1/1984

[39] S. Nakamura, A. Yamamoto "Influence of Disengage Angle upon Initial Fracture of Tool Edge". Bull. Japa Soc. of Precision Engg. Vol 19, No. 3, Sept. 1985. pp 169-174.

[40] S. Ai., Z. Li "Study on Fracture of Cemented Carbide tool in Intermittent Turning". International Conference on Computer-Aided Production Engineering, Edinburg, April 1986.

[41] M. Hirao, J. Tlusty, R. Sowerby, G. Chandra. "Chip Formation with Chamfered Tools" Journal of Engineering for Industry, Vol. 104, Nov 1982, pp.339-342.

[42] K. Shintani, M. Ueki, Y. Fujimura. "Optimum Cutting Tool Geometry when Interrupted Cutting Carburized Steel by CBN Tool" Int. J. Machine Tools and Manufacture. Vol 29; No 3; 1989 pp 415-423.

[43] L. Lee, K. Lee, S. Gan. "On the Correlation between Dynamic Cutting Force and Tool Wear" Int. J. Machine Tools and Manufacture. Vol 29; No 3; 1989 pp 295-303.

[44] M. Dokainish, M. Elbestawi, U. Polat, B. Tole. Analysis of Stresses During Exit in Interrupted Cutting with Chamfered Tools. Int. J. Machine Tools and Manufacture. Vol 29; No 4; 1989 pp 519-534.

[45] E. Lenz, D. Moskowitz, J. Mayer, D. Stauffer. "Optimal Edge Geometry for Maximum Tool Life" A.S.M.E. Production Engineering Division. Vol 43, 1977.

[46] K. Ueda, T. Sugita, N. Taniguchi. "In-process proof testing of Cutting Tools in Interrupted Turning". International Institution for Production Engineering, Vol 37, 1988, pp 65-68.

[47] Fineberg Victoria K. "The use of Material Properties in the Analytical Prediction of Cutting Forces in Face Milling Operations" M.S. Thesis, University of Illinois at Urbana - Champaign, 1989.

[48] D. Stephenson, S. Wu, "Computer Models for the Mechanics of Three-Dimensional Cutting Process- Part II: Results for Oblique End Turning and Drilling." , Transactions of the A.S.M.E., Vol.110, Feb 1988. pp38-43

[49] T. Ramaraj, S. Santhanam, M. Shaw, "Tool Fracture at the End of a Cut-Part 1: Foot Formation" ,Journal of Engineering for Industry, Vol. 110, Nov 1988, pp.333-338.

[50] S. Pandit, S. Wu, *Time Series and System Analysis with Applications*. John Wiley & Sons Inc., 1983.

[51] *Physical and Engineering Properties of Cast Iron.* A.S.M. 1976

[52] PC-MATLAB for Personal Computers. The MathWorks, Inc. 1987